THE MECHANICAL PROPERTIES OF SPIDER SILK ARE DETERMINED BY THE GENETIC REGULATION OF FIBROIN PROTEINS AND CHEMICAL AND PHYSICAL PROCESSING DURING SPINNING.

by

Paul André Guerette

B.Sc. (Hons. Biology) Saint Francis Xavier University, 1990.

A THESIS SUBMITTED IN PARTIAL FULFILMENT OF THE REQUIREMENTS FOR THE DEGREE OF DOCTOR OF PHILOSOPHY

in

THE FACULTY OF GRADUATE STUDIES

Department of Zoology

We accept this thesis as conforming to the required standard

The University of British Columbia

August, 1997

In presenting this thesis in partial fulfilment of the requirements for an advanced degree at the University of British Columbia, I agree that the Library shall make it freely available for reference and study. I further agree that permission for extensive copying of this thesis for scholarly purposes may be granted by the head of my department or by his or her representatives. It is understood that copying or publication of this thesis for financial gain shall not be allowed without my written permission.

Department of Zoology

The University of British Columbia
Vancouver, Canada

Date Oct 20th, 1997

DE-6 (2/88)

ABSTRACT

Orb-web building spiders produce a functional variety of fibrous silks that exhibit a range in mechanical properties from Kevlar-like super fibers to rubber-like elastomeric fibers. The mechanisms of silk property control employed by the orb-spider were formerly not known, but were hypothesised to be related to the chemical sequence design of their fibers constituent fibroin proteins and the chemical and physical conditions of fiber spinning. The genome of the orb-spider *Araneus diadematus* was found to contain members of at least one fibroin gene family which encode proteins containing different proportions of crystal forming poly(alanine) domains and glycine rich amorphous domains. The fibroin genes were found to be expressed differentially in the spiders seven different gland types, indicating that transciptional regulation affords the spider the ability to produce a variety of gland-specific, compositionally distinct silk secretions that are predicted to have different crystallization potentials. Qualitative polarized light microscopy supports this prediction by showing that distinct glandular secretions crystallize differentially under identical shear conditions in the lab. The results therefore indicate that genetic regulation of fibroin genes affords the orb-spider the potential to modulate the mechanical properties of its large repertoire of silks.

Chemical micro-environment and physical draw processing conditions were also hypothesised to influence the mechanical properties of orb-spider silk. In the orb-web, the rubber-like native viscid (FL) silk is subject to a distinct chemical micro-environment provided by an inter-penetrating aqueous glue coating that contains water, salts, free amino acids and several water soluble Low Molecular Weight (LMW) compounds. The glue coating was removed by a water wash:dry process in the lab, and the processed FL fibers exhibited an increase in Birefringence and a change in mechanical properties indicative of the development increased supra-molecular order. The data indicate that a LMW plasticizer exists in the aqueous glue that functions either 1) by recruiting water

molecules from the atmosphere that in turn plasticize the FL network , 2) by interacting directly with the network and/or 3) by creating free volume to allow for additional mobility of the FL fibroins. The effects of physical draw processing were evaluated by subjecting the native FL fiber to water wash:draw:dry processing. Birefringence increased asymptotically with increased processing draw ratio indicating that an increase in supra-molecular organisation develops with draw. However, the optical data alone fail to reveal weather this new order arises from alignment of amorphous and pre-existing crystalline network components or from the creation of new crystal structure. A rudimentary comparison of Retardation values from draw processed FL fibers with published data from hydrated native FL silk at equivalent extensions supports the view that draw processing imparts new crystal structure. The mechanical properties of the native FL silk were also dramatically altered by physical processing, following the general trend of increased stiffness and ultimate strength, and decreased extensibility with increased processing draw ratio. It is suggested that the fibroins which comprise the native FL silk have the potential to strain crystallize and that this phenomenon may explain the exceptional breaking strength of the elastomeric viscid silk. Finally, the optical and mechanical data from processed FL fibers suggest that the orb-spider may employ specific processing regimes in the wild to tune the supra-molecular morphology and thus the mechanics of its variety of silks.

TABLE OF CONTENTS

LIST OF FIGURES

Chapter 1.

Chapter 2.

LIST OF TABLES

Chapter 1.

Chapter 2.

Chapter 3.

Chapter 4.

Appendix 2.

LIST OF SYMBOLS

1. Amino acids:

alanine: A
arginine: R
aspartate: D
asparagine: N
cysteine : C
glutamate: E
glutamine: Q
glycine: G
histidine: H
isoleucine: I
leucine: L
lysine: K
methionine: M
phenylalanine: F
proline: P
serine: S
threonine : T
valine: V
tryptophan: W
tyrosine: Y

2. Engineering Symbols:

σ: Stress
ϵ: Strain
E: Young's modulus of elasticity
$\cup$:Toughness

ACKNOWLEDEGMENTS

This thesis was communicated to me by aliens. Actually, first and foremost, I want to sincerely thank my supervisor, Dr. John Gosline, without whom this work would not have been possible. Thank you so much John, your clear view of science and your kind hearted nature make your lab an exceptionally fun, creative and exciting place. It is truly my pleasure to be a part of it all. The members of my supervisory committee, Bob Blake, Tom Grigliatti, Bill Milsom and Don Moermon, have all provided excellent advice that has helped me stay focused, and oppened my eyes to the many ins and outs of experimental work, writing and science policy. I would also like express my sincere gratitute to Drs. David Ginzinger and Bernhard Weber, both of whom have made enormous contributions towards helping me learn molecular biology and developing many of the ideas and experiments that form the basis for a large chunk of this thesis. I am also pleased to thank Dr. Ken Gardiner for giving me the opportunity to learn X-ray diffraction techniques in his lab at DuPont as well as for the very kind hospitality that he showed me while I was visiting Wilmington including a fantastic visit to the spider exhibit at the Smithsonian institute in Washington D.C. I also gratefully acknowledge the help and support of all my fellow lab mates, past and present, who have provided countless hours of insightful discussion, important lessons on how to avoid flying hockey pucks in the lab, and needless to say, many great laughs. My mother, father and brother also deserve a very large tip of the hat for the all the love, friendship, encouragement and support they have lent over my countless years of schooling. Finally, I want to thank my love Joanie Clarke, who's endearing friendship and brilliant sense of humor got me through the toughest part of this work-the writing.

CHAPTER 1

GENERAL INTRODUCTION

1. Introduction.

Silks are fibrous extracellular proteins that are produced in nature by arthropods. Silk producing insects use a single silk type during a specific stage in their life history to encase eggs or developing pupae to protect them from cold, predators, and desiccation. Orb-weaving spiders can produce up to seven mechanically distinct silk types that they use to make protective cocoons for offspring, as a safety dragline for locomotion and predator escapes, for ballooning locomotion, as adhesives to anchor other silks to each other and to substrates, and to provide their major source of nutrient uptake by entrapping airborne and terrestrial prey in intricately designed nets that function as complex mechanical systems (Vollrath, 1993).

Prior to this study, the mechanisms that allow orb-spiders to produce a variety of functionally and mechanically distinct silks were not known. Polymer scientists have recognised for decades that to control the physical properties of their synthetic materials, they required a detailed understanding of the factors that determine the hierarchical organization of those materials constituent polymer chains in three dimensional space. This 'supra-molecular' organization is what ultimately determines a polymers material properties. The major factors that govern supra-molecular organisation of both biological and synthetic polymers are presently recognised as 1) the chemical design of the polymers constituent chains and 2) the chemical and physical conditions that the polymer chains are subjected to when they are produced and processed into fibers. A detailed experimental investigation of the importance of these factors in the production of orb-spider silks should reveal the basic mechanisms that these spiders use to modulate the physical properties of their mechanically distinct silks.

I begin this chapter by introducing the reader to a variety spider taxa. Many of these spiders either hunt for prey by roaming the earth or catch prey in haphazardly constructed snares made from one or two silk types. In contrast, the use of many silk types by the orb-weavers reflects complexity

in both their life history patterns and in the mechanical design of their insect traps. I present the limited data available on the mechanical properties of orb-spider silks, and for comparative purposes the properties of several other biological and synthetic fibrous polymers are examined. A look at the factors known to determine supra-molecular organisation and physical properties in these other high performance fibers will clearly emphasise the impact that both polymer chain design and chemical/physical processing conditions can have on mechanical properties, and this will set the stage for an experimental investigation of the importance of these factors in the production of orb-spider silks.

2. Spiders in the field: web types, and silk types.

Spiders belong to the Order Aranea and with a few exceptions can be classified into two ecologically distinct groups based on general characteristics of their webs and silks. The first group are the more primitive wandering spiders. These ground dwelling species can produce at most two mechanically distinct silks that they use as draglines, to make egg cases, and to fortify their burrows. Wolf spiders (Suborder Labidognatha, Infra order Ecribillatae, Family Lycosidae) usually employ a sit and wait strategy to ambush their prey, while the more active jumping spiders (Suborder Labidognatha, Infra order Ecribillatae, Family Salticidae) stalk and pounce their prey by taking advantage of primary and secondary eyes for sharp images and accurate distance estimates. There are about 2500 wolf spider species and 4000 jumping spider species. The Tarantulas (Suborder Orthognatha, Family Theropsidae) and trap door spiders (Suborder Labidognatha, Family Ctenizidae) are primitive ground dwellers that ambush prey from burrows or from web sheets spun on the ground. There are about 800 species in the Theropsidae Family, and about 700 trap door spider species.

The second ecological group of spiders contains the sedentary web spiders, which spin four

basic web types; sheet webs, funnel webs, tangle webs, and orb-webs. Sheet weavers (Suborder Labidognatha, Infra order Ecribillatae, Family Linyphiidae) are considered slightly more advanced than the wandering spiders. Their webs are usually seen in grass and low bushes as a sheet of fine silk horizontal to the ground, with vertical threads projecting above the sheet (Fig. 1.1a). Prey impacts and becomes entangled in the vertical strands; the spider then shakes the entire web and the prey falls onto the sheet where the spider can attack it. There are about 3500 species in this Family. Funnel web spiders (Suborder Labidognatha, Infra order Ecribillatae, Family Agelenidae) spin sheet webs similar to the Linyphiidae but are more similar to the Lycosidae in their morphology and movements. They construct a funnel at the edge of their silk sheet and run out to attack prey that lands on it (Fig.1.1b). There are about 1000 species in this Family. Tangle-web spiders (Infra order Ecribillatae, Family Theridiidae) weave irregular silk networks in high bushes, trees and rocks. This family includes the black widow, *Latrodectus mactans,* which spins a tangled maze-like retreat with elastic sticky glue coated trap threads anchored to the ground (Fig. 1.1c). These threads dislodge from the substrate when prey fumbles into them, and their elastic recoil draws the prey into the web where it becomes entangled. This Family contains about 2500 species. The three dimensional sheet, funnel, and tangle webs are spun from relatively large quantities of one or two silks types, and the kinetic energy of impacting prey is usually dissipated through strand breakage. The orb-web is an elegant two dimensional design that requires much less silk protein in its construction, but its proper function depends on a precise mechanical coordination of several distinct silk types.

3. Orb-spiders and their silks.

While the first silk producing arachnids appeared in the middle Devonian period, about 385 million years ago (Shear et al. 1989), the fossil record indicates that the orb-weaving spiders probably

Figure 1.1.

Selected sedentary spider web architectures. a) Sheet web. b) Funnel web. c)Tangle web. d) Orb-web, with its major fibrous constituents; the MA silk frame and radii, and FL spiral silk.

a

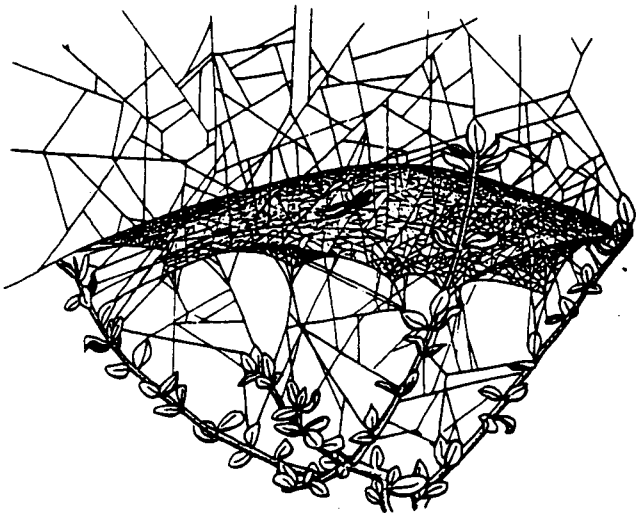

b

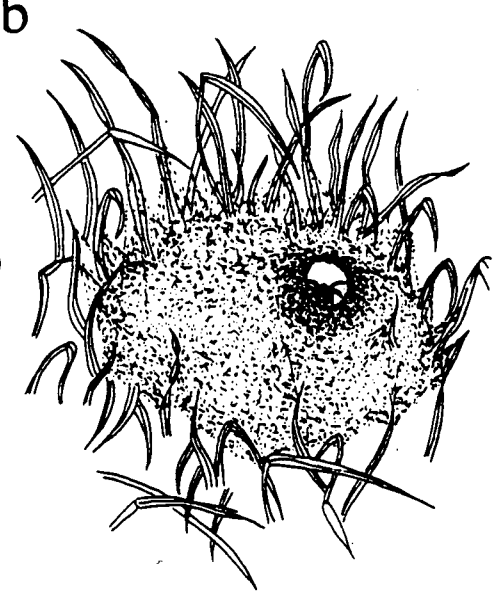

c

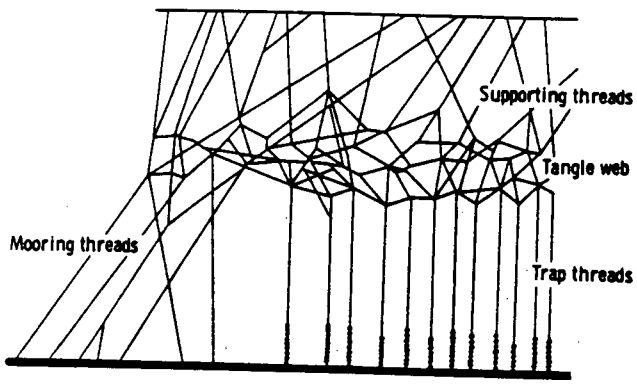
Supporting threads
Tangle web
Mooring threads
Trap threads

d

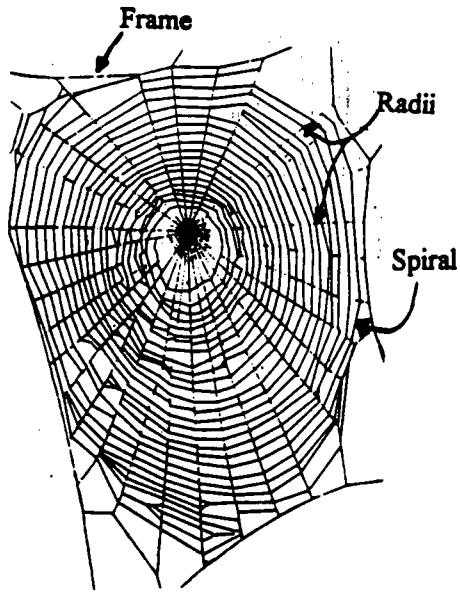
Frame
Radii
Spiral

did not emerge until the Jurassic period, about 180 million years ago (Sheldon et al. 1989). Present day orb-spiders belong to the Infra Orders Ecribillatae (ca. 3000 orb-spider species) and Cribillatae (ca. 1150 orb-spider species). Both groups create a circular, planar web design whose major fibrous constituents include the supporting frame and radii silk and the adhesive spiral catching silk (Fig. 1.1d). In order for this two dimensional web design to function as an efficient predatory trap, it must dissipate the kinetic energies of impacting prey while ensuring prey adhesion and entanglement for a period long enough to allow the spider to attack and wrap its dinner for subsequent consumption.

Cribillate spiders, like *Uloboris walckenaerius* (Family Uloboridae), make their orb-webs adhesive by hackling the spiral catching portion of their web with a mesh-work of fine sticky silk. They spin this silk by 'combing' it through a morphological structure called a cribellum located on their abdomen. The adhesive properties of the hackle threads were originally believed to arise from electrostatic charges generated by the combing action during spinning, or from the passive rubbing together of the thin hackle threads in the web (Peters, 1987), but it turns out that van der Waals attractions alone may explain their stickiness (Vollrath, 1994). The Cribillate orb-web catching silk consists of two core threads, two crimped threads and the extensive hackle silk mesh-work. These silks function together through strand elongation and multiple strand breakage to dissipate energy and entrap flying insects (Vollrath, 1994).

In contrast to Cribillate orb-spiders, Ecribillate orb-weavers make their webs sticky by coating a pair of core catching spiral silk fibers with viscous glue silk. Although the glue is not as sticky as the Cribillate hackled silk mesh-work, it appears to be less costly in terms of time and energy (Vollrath, 1993). While the Cribillate catching spiral functions by the mechanical coordination of several silk types, the Ecribillate glue coated core spiral silk dissipates energy because, as I will show, it is highly extensible and remarkably strong on its own.

4. Orb-spider silk mechanics.

Ecribillate orb-weavers produce as many as seven functionally and mechanically distinct silk types that each originate from different glands. Figure 1.2 and Table 1.1 show the orb-web design, glandular origin, and function of each of the silks produced by *Araneus diadematus* (Family Araneidae), the orb-spider that is the focus of this thesis work. For simplicity each silk type will be referred to by the two letter gland origin abbreviations given in Table 1.1. Published data on the mechanics of these or any other spider silks is sparse. The parameters that have been used to define the mechanical properties of fibrous silks include strength, stiffness, extensibility and toughness. For thin fibers these properties are usually determined from experiments that measure tensile force as a function of deformation, where the force is normalised to the fiber's initial cross-sectional area to generate a stress, with the S.I. units of N m^{-2} or Pa. The ultimate strength of a fiber is described as stress at failure. Strain describes the extensibility of the fiber in terms of the fractional increase in fiber length with respect to the original sample length; there are no units for this parameter. Stiffness, or Young's Modulus of Elasticity, describes the resistance of the fiber to tensile deformation and is determined from the slope of the stress strain curve, usually in the initial, linear, Hookean region. Young's Modulus of Elasticity carries the same units as stress. Toughness is the ability of a material to absorb work and is calculated by integrating the area under the stress strain-curve and dividing this value by the density of the material. The S.I. units for toughness are J Kg^{-1}.

Orb-spider silks exhibit a huge range in physical properties, from high ultimate strength, high modulus, relatively low extensibility fibers, to low modulus, high extensibility fibers that maintain reasonable ultimate strengths relative to other fibrous materials. A simple physical property classification scheme devised by Denny (1980) allows for straightforward comparisons of the mechanical properties of silks. These are categorised into three mechanical groups, A, B and C,

Figure 1.2.

Cartoon of the orb-spider *A. diadematus*. The silk glands contained within this spiders opithosoma (abdomen) are shown along with the different silks that each gland produces (from Vollrath, 1992).

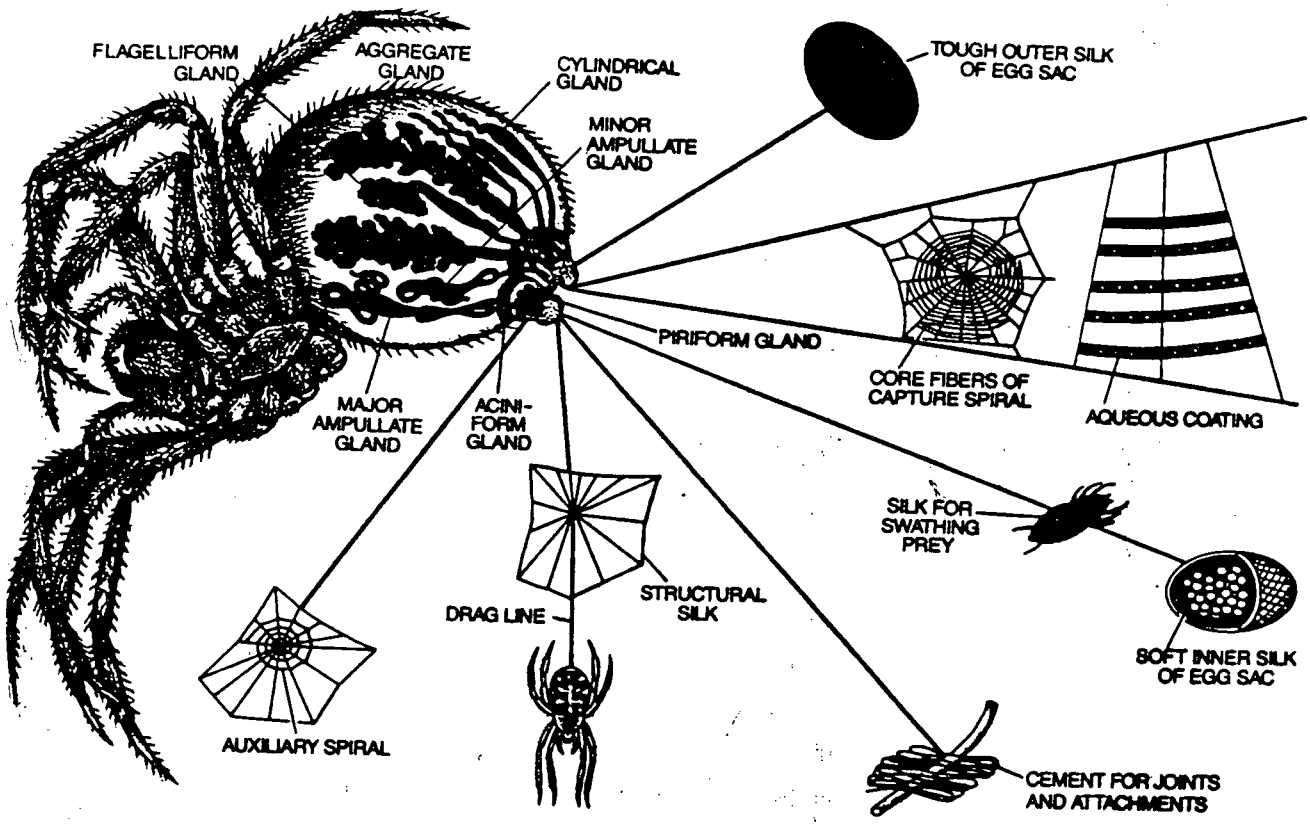
FLAGELLIFORM GLAND
AGGREGATE GLAND
CYLINDRICAL GLAND
MINOR AMPULLATE GLAND
TOUGH OUTER SILK OF EGG SAC
PIRIFORM GLAND
CORE FIBERS OF CAPTURE SPIRAL
AQUEOUS COATING
MAJOR AMPULLATE GLAND
ACINI-FORM GLAND
SILK FOR SWATHING PREY
STRUCTURAL SILK
DRAG LINE
SOFT INNER SILK OF EGG SAC
AUXILIARY SPIRAL
CEMENT FOR JOINTS AND ATTACHMENTS

Table 1.1. Glandular origin and function of all seven A. *diadematus* silks.

Gland.	**Gland Abbreviation.**	**Silk type.**	**Functional use of silk by the orb-spider.**
Major Ampullate	MA	frame, radii and dragline	structural support elements of the orb-web and locomotion.
Minor Ampullate	MI	accessory	support elements of the orb-web, ballooning locomotion ?
Flagelliform	FL	viscid	glue coated spiral, insect trapping portion of orb-web
Aggregate	AG	glue	glue coating of viscid silk, catching adhesive and FL plasticizer ?
Cylindrical	CY	cocoon	protective silk wrap for overwintering eggs.
Aciniform	AC	swathing	silk used to wrap prey for consumption.
Pyriform	PY	attachment	attachment silk, attaches silks to substrates and each other.

depending on their breaking strength and extensibility. The stress-strain plots of representative members from each mechanical group are presented in Figure 1.3, along with those of several other biological and synthetic fibres. Table 1.2 lists the physical properties of these fibers and a few other materials of comparative interest.

Mechanical Group-A and B silks usually show a high initial modulus followed by a yield, a point where polymer chain slippage and molecular reorganisation results in a decrease in modulus that gives rise to a 'plateau' behaviour with extension. The yield plateau is followed by an increase in modulus that is generally constant until failure. In some Group-A and B silks the plateau is imperceptible, and the stress-strain curve is basically linear. Group-C silks generally exhibit a very low initial modulus that is followed by a rise in stiffness until failure. When more silks are classified within this scheme, the mechanical properties of Group-A to C silks should actually constitute a continuum (Denny, 1980).

Group-A silks have high ultimate strengths, around 1 G Pa, high initial moduli, up to 15 G Pa, and relatively low extension at failure, between 10 and 35 %. Orb-spider MA and MI silks fall in this mechanical class. The MA silk of *A. diadematus* and that of another distantly related orb-weaver *Nephila clavipes* (Order Aranea, Family Tetragnathidae) are the strongest biological fibers known, and these materials retain ultimate failure stresses which approach those of the strongest man-made fibers, Kevlar and poly(ethylene) Spectra (Fig. 1.3, Table 1.2). MA silk's extensibility is considered low among silk fibers; however, it is high relative to high ultimate strength, high stiffness biological and synthetic fibers like Collagen, Cellulose, Kevlar and Spectra. This combination of high ultimate stress and moderate extensibility give the MA fiber a huge toughness (Table 1.2). While Kevlar is one of the strongest fibers known, its inability to deform gives it a relatively low toughness (Table 1.2), which would make it a less appropriate material in the design of an insect trap where the

Figure 1.3.

Stress-strain curves for selected silks and other biological and synthetic fibrous polymers that exhibit a broad range of mechanical properties. *A. diadematus* MA silk from Denny (1976), *A. diadematus* FL silk (personal data), *A. diadematus* CY , *B. mori*, *G. mellonella*, *A. mellifora* and *C. carnea* silks from Denny (1980). Spectra, Kevlar and drawn Nylon inferred from Schaefgen (1983). Bulk polymerized (BP) Nylon from Zimmerman (1988). BP-poly(ethylene) and Rubber from Andrews and Dawson (1988).

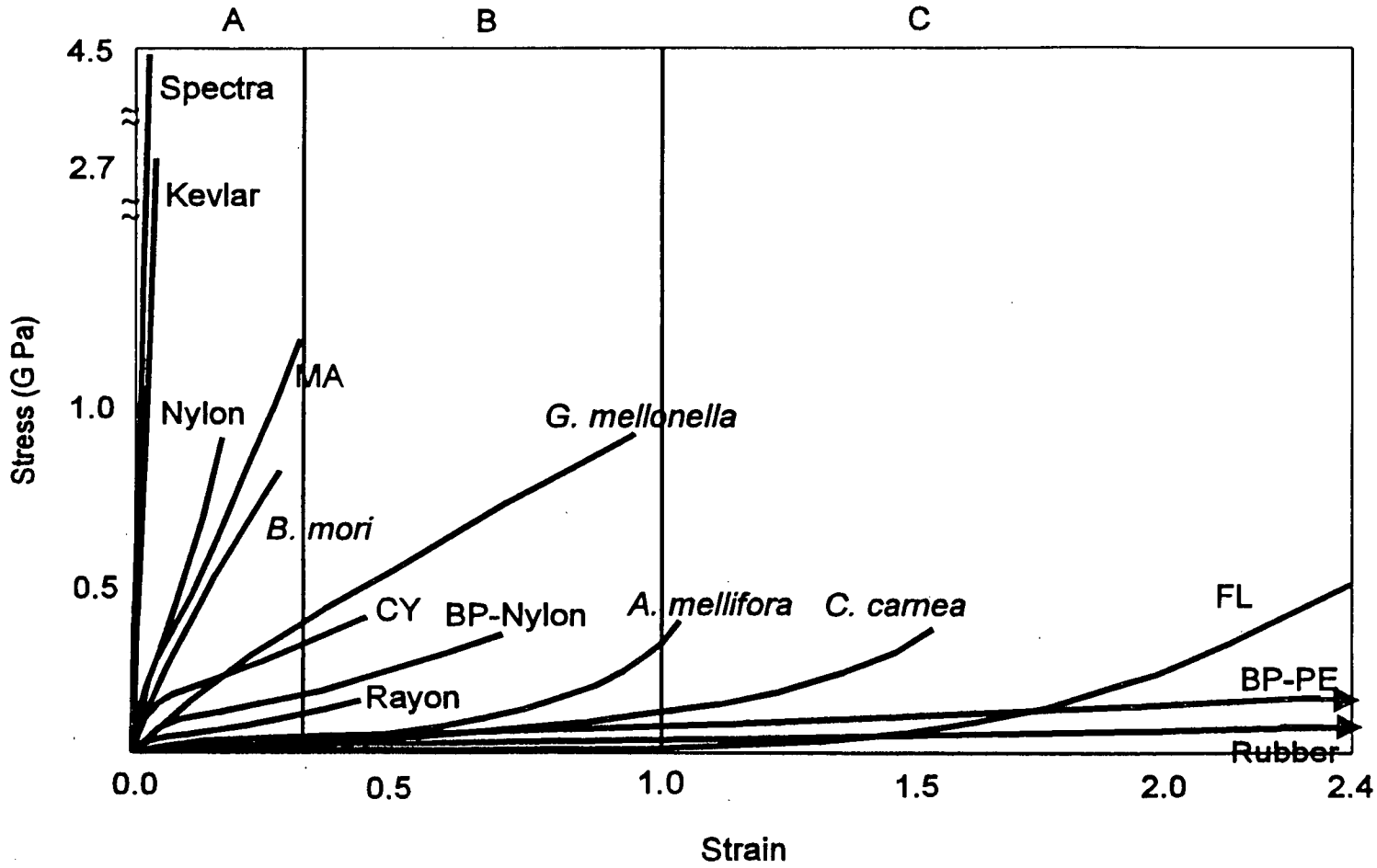
A
B
C
4.5
2.7
1.0
0.5
Stress (G Pa)
Spectra
Kevlar
Nylon
MA
B. mori
G. mellonella
CY
BP-Nylon
A. mellifora
C. carnea
FL
Rayon
BP-PE
Rubber
0.0
0.5
1.0
1.5
2.0
2.4
Strain

Table 1.2. Mechanical properties of a range of silks, high property fibers and high extensibility fibers and materials. References : 1. Denny, 1976; 2. Cunniff et al. 1994; 3. Wainwright et al., 1976; 4. Lucas ,1964; 5. Hepburn, 1979; 6. Schaefgen, 1983; 7. Oefstead, 1985; 8 Gosline et. al 1986. (BP=bulk polymerized).

	Modulus (Pa)	Strength (Pa)	Toughness (J/kg)	Failure ext. %	Mech. Group	Reference
MA (*A. diadematus*)	1.0×10^{10}	1.4×10^{9}	1.2×10^{5}	39	A	1
MA (*N. clavipes*)	2.2×10^{10}	1.1×10^{9}	$\sim 1.0 \times 10^{5}$	11	A	2
CY (*A. diadematus*)	2.2×10^{9}	5.4×10^{8}	$\sim 7.5 \times 10^{4}$	24	B	3
FL (*A. diadematus*)	3.0×10^{6}	5.0×10^{8}	1.0×10^{5}	200	C	personal
B. mori cocoon	1.0×10^{10}	8.0×10^{8}	$\sim 6.5 \times 10^{3}$	20	A	4
G. mellonella silk	$\sim 1.0 \times 10^{8}$	8.0×10^{8}	2.4×10^{5}	80	B	5
A. mellifera silk	$\sim 1.0 \times 10^{7}$	4.0×10^{8}	$\sim 7.0 \times 10^{3}$	105	C	5
C. carnea silk	$\sim 5.0 \times 10^{6}$	3.8×10^{8}	$\sim 1.0 \times 10^{4}$	150	C	5
Cellulose	3.0×10^{10}	8.0×10^{8}	9.0×10^{3}	2	A	3
Rayon	5.0×10^{9}	1.5×10^{8}	$\sim 1.0 \times 10^{5}$	20-30	B	3
Collagen	1.4×10^{9}	1.4×10^{8}	5.6×10^{3}	10	A	3
Kevlar-49	124×10^{9}	2.7×10^{9}	2.43×10^{4}	2.5	A	6
Spectra	119×10^{9}	4.7×10^{9}	1.22×10^{5}	5.2	A	6
BP-poly(ethylene)	5.0×10^{7}	2.5×10^{7}	$\sim 1.0 \times 10^{4}$	200 +	C	7
Nylon (highly drawn)	2.4×10^{9}	8.0×10^{8}	1.0×10^{5}	18	A	6
BP-Nylon	0.5×10^{9}	2.3×10^{8}	$\sim 1.0 \times 10^{4}$	65	B	7
High tensile steel	2.0×10^{11}	2×10^{9}	1.0×10^{3}	1	A	8
Glass	7.0×10^{10}	1×10^{7}	~ 1	1	A	7
Rubber	1.0×10^{6}	5×10^{8}	8×10^{4}	200 +	C	8

fibers must absorb large energies from out-of-plane loads imparted by the wind and by flying insects. Note that Cellulose, Collagen, Kevlar, Spectra and highly drawn Nylon all have mechanical Group-A type properties.

Group B silks have ultimate stresses around 0.5 G Pa, initial moduli of about 2-5 G Pa, and extensibilities ranging from 50 to 100%. High failure stress and large extensibility give these silks great toughness as well, and in the case of waxmoth *Galleria mellonella* (Class Insecta, Family Galleriidae) silk, this value is a remarkable 2.4×10^5 J Kg^{-1}. This toughness greatly exceeds that of any known natural or synthetic fibrous polymer and approaches that of some of the toughest materials known (Gilman, 1996). *A. diadematus* CY silk also falls in this group, but because of its lower ultimate strength, it is not as tough as the *G. mollonella* silk. Although they have yet to be characterised, orb-spider AC and PY silks likely fall in mechanical class A or B. Note that undrawn, bulk polymerised Nylon exhibits physical properties similar to *A. diadematus* CY silk.

Mechanical Group-C silks generally have lower ultimate strengths, around 300 M Pa, low initial moduli ranging from about 3 to 6 M Pa, and very high extensibilities ranging from 100 to 500 % (Denny, 1976; Kohler and Vollrath, 1995). *A. diadematus* FL silk, larval honey bee *Apis mellifora* (Class Insecta, Family Apidae) silk, and green lace wing fly *Chrysopa carnea* (Class Insecta, Family Chrysopidae) egg-stalk silk are examples of this mechanical class of highly extensible silks. *A. diadematus* FL silk has a high extensibility and a very respectable ultimate strength of 0.5 G Pa, and as such it may be likened to a high breaking strength rubber. High ultimate strength and high extensibility gives FL silk a toughness about equal to MA silk; so it can also function to absorb large amounts of kinetic energy in the orb-web. The aqueous glue that is produced by the AG gland of *A. diadematus* may be placed in this Group, but it actually flows under load and is better likened to a viscous fluid than a fiber. Undrawn bulk polymerised poly(ethylene), the type used in plastic

grocery bags also exhibits mechanical Group-C properties (Fig. 1.3, Table 1.2).

5. The molecular basis for the mechanical properties of fibrous materials.

It is clear that *A. diadematus* can spin silks that span the range from mechanical Group-A to Group-C fibers. The differences in properties must be linked to differences in supra-molecular organization of these silk's constituent polymer chains. Polymers can adopt both *Amorphous* and *Crystalline* supra-molecular morphologies, and these morphologies give rise to distinctly different mechanical properties.

5.1. Amorphous supra-molecular morphology.

Amorphous material contains no long range order, and its constituent polymer chains are disordered and possibly tangled (Fig. 1.4a). This type of supra-molecular morphology gives rise to deformable materials, since the application of a tensile load results in a change in shape of randomly coiled polymer chains that is resisted only by entropically based elasticity and polymer chain entanglements. Entanglements also prevent the chains from flowing past one another and disassociating. Rubber usually exhibits low initial modulus, low breaking strength and high extensibility at room temperature (see Fig. 1.2 and Table 1.2), and this is because its constituent polymer chains exist in the amorphous conformation and retain long range mobility under the appropriate conditions.

Strength and stiffness can arise from two additional factors in amorphous polymers. First, point cross-links can form between adjacent polymer chains that allow the amorphous material to resist long range deformation and to provide it with 'memory' that allows a deformed material can return to its original shape. An example is the elastomer used in automobile tires, which is a rubber

Figure 1.4.

Schematic models of polymeric supra-molecular morphology. a) Amorphous morphology b) Crystal morphology. c) Polymeric crystals (note that individual chains span several crystal and amorphous domains).

a)

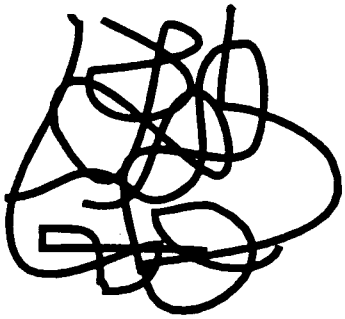

b)

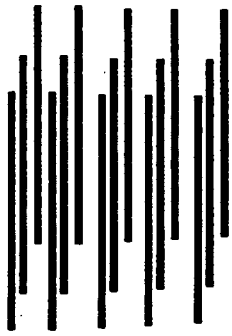

c)

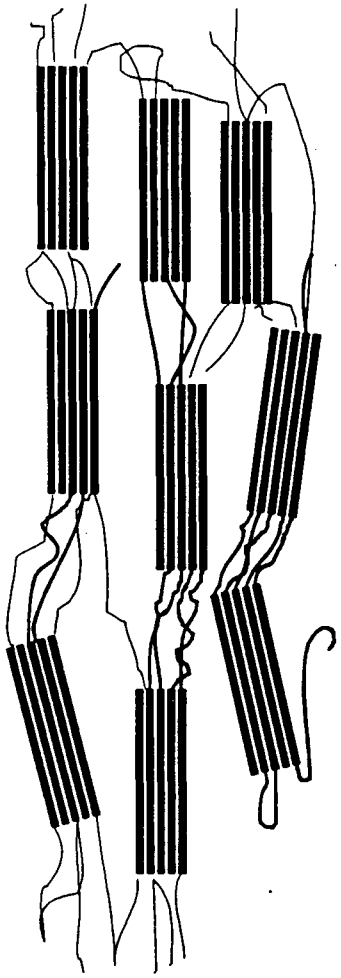

that has been cross-linked by a chemical reaction called vulcanisation. Second, the mobility of amorphous polymer chains depends on temperature, pressure or micro-environmental conditions. For example, the high extensibility behaviour described above for rubber occurs only when this material exists above its glass transition temperature, Tg. When the temperature is decreased below Tg, polymer chain motion and local molecular motions are drastically reduced, and the material becomes stiff and brittle and is considered 'glassy'. A polymer glass is an amorphous material that exists in a physical state below its glass transition. It is locked into the glassy state, and as a result it exhibits high initial modulus. However it develops stress concentrations quickly when placed under load, resulting in early failure and thus, low ultimate strength and low extensibility. Polymer chain micro-environment can also determine if a material exists in a glassy state or not. For example, under physiological conditions the biopolymer elastin behaves as a rubber. If this material is allowed to dehydrate, the water that imparts mobility to its polymer chains is lost, the polymer chains become essentially 'frozen' in space and the material becomes brittle and glassy.

5.2. Crystalline supra-molecular morphology.

Crystalline structure in polymeric materials forms from the stacking and/or folding of molecules into three dimensional arrays (Fig 1.4b). This molecular organisation can enhance stiffness and strength because 1) there is an increase in molecular density 2) inter-molecular stabilising interactions are established between adjacent chains and 3) the van der Waals radii of the densely packed atoms or molecules prevent slippage because of frictional resistance.

There is a key difference between molecular crystallites and the crystals formed from polymer chains. The molecular crystal forms a single crystal lattice, where the size of the crystal is very large relative to the size of the molecule, and the crystal lattice basically constitutes the entire material. This

is the case for inorganic or metallic crystals. Polymeric crystals are often much smaller than an individual molecule, so that the full length of a single polymer chain can actually extend through intervening amorphous structure to assemble into multiple, distinct micro-crystals. This allows many separate polymer chains to form continuous, extensively interconnected, semi-crystalline cross-linked networks (Fig. 1.4c). When a semi-crystalline polymer is subjected to a load, the cross-linking micro-crystals function co-operatively to resist load, enhancing both the stiffness and strength of the polymer. The proportion of micro-crystals in a polymer largely determines fiber properties. When more than 40 % crystal is present, polymeric fibers become significantly stiffer and stronger. High ultimate strength, high stiffness fibers like Cellulose, Kevlar, poly(ethylene) Spectra and Nylon are all considered highly crystalline, macromolecular composites. Polymers with less than 20 % crystal are considered lightly cross-linked rubbers, and they generally exhibit low initial moduli and low ultimate strength.

An examination of the supra-molecular organisation of two mechanically distinct orb-silks, the Group A-MA silk and the Group C-FL silk, reveals that the huge differences in fiber mechanics can be directly related to differences in both the mobility of amorphous network components and the degree of crystal structure present.

6. The supra-molecular morphology of two mechanically distinct orb-spider silks.

Molecular network models have recently been developed for the mechanically distinct *A. diadematus* Group-A MA and Group-C FL silks using non-Gaussian mechanical behaviour of these fibers when tested in their hydrated elastomeric state (Gosline et al. 1994). Most silks function in air at low relative humidity, where protein sequences in the amorphous conformation are locked in the glassy state. Both glassy and crystalline materials show high initial modulus behaviour, and as such,

it would be difficult to tease apart the contribution of the two components to the observed mechanical properties. Fortunately, spider MA silk super-contracts in water in the same way that wool does, where the fiber absorbs water, shrinks axially and swells laterally (Work, 1977). When the MA fiber is hydrated, it contracts to 0.6 its original length and swells to 2.4 times its original diameter. X-ray diffraction patterns on the hydrated MA silk indicate that it does not lose any of its crystals (ie. the crystals are stable in water) (Work and Morosoff 1982; Work, 1985). The water-swollen silk network exhibits conformational entropy elasticity that can be likened to the behaviour of a rubber (Gosline et al. 1984). Since the kinetically free amorphous chains contribute in large part to the observed physical properties of the swollen MA silk, it was possible to use The Kinetic Theory of Rubber Elasticity (Treolar, 1976) to evaluate its mechanical properties and to create a model of its supra-molecular morphology. Dry *A. diadematus* MA silk was predicted to contain network chains about 15 to 20 amino acid residues in length that are nearly fully extended in the direction of the fiber axis. They are locked into this extended conformation when the MA gland secretion is drawn from the spinneret and dried upon spinning. The cross-linking and reinforcing crystals were predicted to be rod-like with aspect ratios of 3 to 7. The crystal volume fraction was estimated to be between 20 and 31 % (Gosline, 1988; Gosline et al. 1993).

FL silk is coated and interpenetrated with the aqueous glue from the AG gland as it is spun. As a result, its peptide chains are never locked into the glassy state. When hydrated, the FL silk super-contracts slightly, and this likely reflects a small degree of molecular orientation in the native FL fibre. Non-Gaussian analysis of the FL silk suggests that it contains random-coiled chains about 40 amino acid residues long, and that the network is lightly cross-linked (Pollak, 1993). Pollak (1993) investigated the nature of the cross-links by subjecting a hydrated, native FL strand held under tension (at 75 % extension) to several drops of 6 M Guanidinium Hydrochloride (GuHCl), which is

known to disrupt weak inter-molecular forces but not covalent linkages. The axial retractive force originally maintained by the extended fiber decreased rapidly and steadily in less than 1 minute, indicating that the majority of cross-links present were non-covalent and could likely be accounted for by network entanglements and polymeric crystal structure. The crystals were predicted to have little if any preferred orientation and to occupy a very small volume fraction of less than 5 %. While the mirco-crystals cross-link the FL silk network, they are probably not present in sufficient quantity to reinforce it. The polymer network models for the semi-crystalline MA and the lightly cross-linked FL silks are shown for comparison in Figure 1.5.

In order to explain the way orb-spiders control the physical properties of their silks it is necessary to determine the factors that govern differential supra-molecular crystallization and amorphous network mobility in mechanically distinct silks. These factors may include both the chemical nature of the fibers constituent polymer chains and the chemical and physical conditions that these polymer chains are subjected to as they are processed into semi-crystalline fibers.

7. Polymer chain chemistry influences supra-molecular crystallization.

In order for crystalline supra-molecular morphology to arise in any polymer, the chemical structure of the polymer chains must meet several criteria : 1) the shape of chains must be *linear* to allow effective inter-molecular packing and interaction. Polymers with large side chains and branched 'dendritic' polymers will not crystallize. 2) The polymer chain must be *regular* in terms of stereo-chemical form and chemical composition. Irregular stereo-chemical form can arise from molecular configurations (eg. cis) that introduce kinks into the polymer main-chain. Polymer chains that are stereo-regular are called isotactic; those that are irregular are called atactic. A polymer with a regular chemical composition contains the same reiterated monomer along the entire length of its chains.

Figure 1.5.

Cartoon of the supra-molecular morphologies of the mechanically distinct a) Group-A MA and b) Group-C FL silks. Crystal structure is represented as black rectangles, amorphous structure is represented as individual peptide chains (from Gosline et al. 1994).

a)

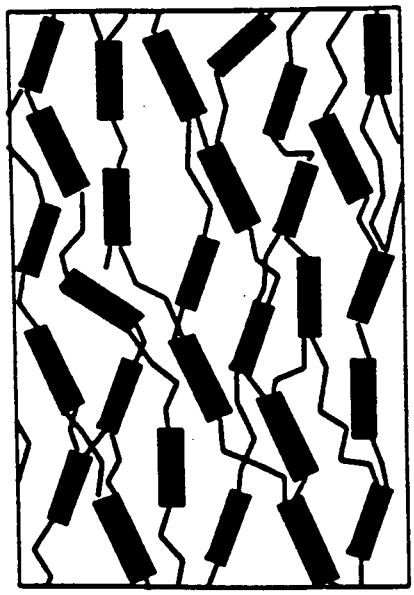

b)

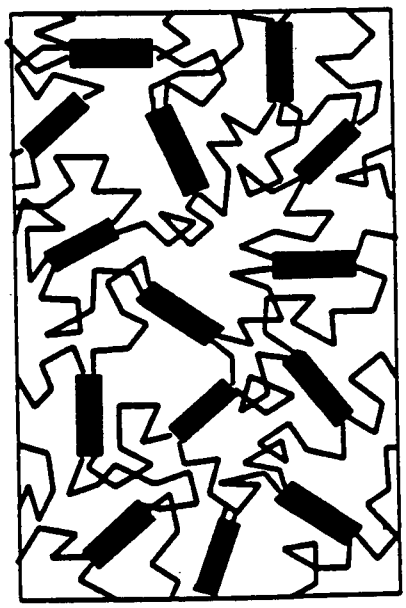

Irregularity in chemical composition arises from co-polymerisation, where the constituent monomers of a polymer are not reiterated sequentially but are random. In co-polymers crystallization can only occur if there is a significant stretch of repeated isotactic monomer sequence. 3) The *stiffness* of the polymer chain is also important in determining supra-molecular crystallinity. Rigid rod-like molecules pack and crystallise far more readily than flexible polymers. 4) The polymer chain *directionality* will also affect crystallization. Chain assembly can either be parallel or antiparallel, and this arrangement can determine the tightness of packing in a crystallite.

8. The conditions of fiber processing influence supra-molecular crystallization.

The combination of micro-environmental and physical conditions of fiber processing must also be appropriate for supra-molecular crystallisation to take place. Micro-environmental processing conditions refer to the specific environment that the polymer chains experience as they associate inter-molecularly; for example a specific solvent, temperature, pressure, or electrical charge may encourage inter-molecular aggregation of polymer chains into a crystal lattice, while others may inhibit this assembly.

Physical processing conditions refer to the physical forces and constraints that the polymer chains are subjected to as they associate during and/or after spinning. Spinning is the physical process of fiber production. Man-made fibers are spun by pumping the polymer in a liquid phase at the face of a spinneret; a metal disk containing many small holes. Small streams of polymer filaments emerge from the holes, are allowed to solidify by drying or cooling, and are wound together as solid semi-crystalline fibers. Physical draw can be imparted during or after spinning, and this is achieved by applying additional tensile deformation to the fiber, which aligns the polymer chains and encourages them to form inter-molecular crystals. In the absence of a physical draw, flexible

polymer chains have a tendency to fold back on themselves, resulting in less efficient molecular packing, a greater degree of amorphous structure, and materials that exhibit inferior mechanical properties. Spiders spin their fibers by drawing a concentrated aqueous silk protein through fine spigots located on spinnerets on their abdomens. Imposed draw combined with water loss on air exposure are believed to be key processes in the development of highly aligned, semi-crystalline, supra-molecular morphology known to be present in many silks (Tillinghast, 1984).

9. Crystalline structure in high ultimate strength, high stiffness fibers.

Under the appropriate processing conditions, linear, isotactic, stiff polymer chains form *extended-chain* polymer crystals. Extended-chain crystals are thermodynamically the most stable crystal type because they allow for a maximum number of non-covalent, stabilising, inter-molecular interactions. Figure 1.6a shows a schematic representation of an extended chain crystal. In many instances the polymer chains are non-linear, stereo-irregular, insufficiently rigid, or the processing conditions are simply inappropriate for extended chain crystallization to take place. The *folded-chain* crystal represents an energetic compromise, where lesser proportions of the polymer crystallize from the folding back of the chain on itself, and stretches of polymer that are unable to extend and crystallize are accommodated as amorphous structure in between the folded crystalline lamellae (Fig. 1.6b). Excess amorphous structure and folded-chain crystals can result in stress concentration on extension, and they generally result in materials with lower moduli and ultimate strengths.

To emphasise the importance of both polymer chain chemistry and processing in supra-molecular crystallization processes, several examples of polymer chemical designs and processing strategies used in the production of high ultimate strength, high modulus, low extensibility biological and synthetic fibers are considered here. Cellulose and Kevlar are discussed first because they

Figure 1.6.

Schematic representation of a) extended chain and b) folded chain supra-molecular morphologies (from Wainwright et al. 1976).

a)

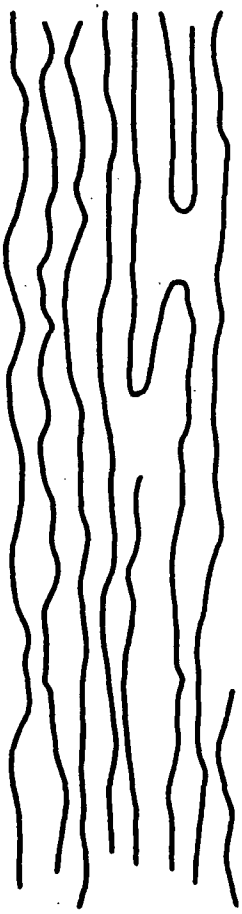

b)

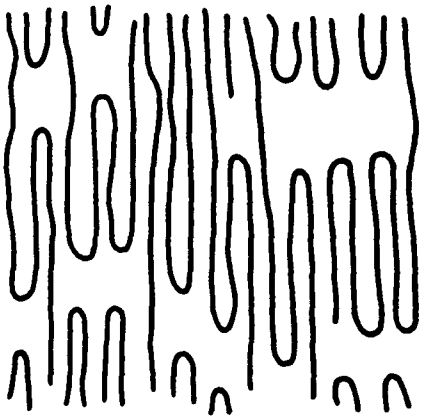

represent biological and synthetic high-property materials that are constructed from rigid polymer chains that have a great tendency to crystallize in the extended-chain conformation. They do, however, require very precise processing conditions. Poly(ethylene) Spectra and Nylon are synthetic polymers constructed from polymer chains that are much more flexible. As a result, it is necessary to subject these fibers to extensive physical draws, either during or after spinning, to achieve the extended chain crystal conformation. Nylon is of particular interest because its monomeric repeat bears likeness to natural protein sequences.

9.1. Cellulose : supra-molecular morphology and processing.

Cellulose, the principle polysaccharide in plant cell walls, is assembled from linear, isotactic chains of cellobiose monomers (Fig. 1.7a). Cellobiose is formed from the linkage of two β-glucopyranose residues via a β-(1→4) glycosidic bond, where each residue is rotated 180° relative to its neighbour. This orientation allows the ring oxygen to hydrogen bond with the C-3 OH group from the adjacent residue, keeping the cellobiose monomer in a rigid rod-like configuration that helps favour the formation of extended-chain crystals. When they are synthesised in plants, the cellobiose molecules string together with a high degree of polymerisation, about 2500 monomers, to form a linear cellulose molecule. Cellulose molecules can pack tightly in a staggered, antiparallel arrangement that brings the bridge oxygen of one chain in close proximity to the C-6 OH group from the adjacent chain, resulting in a large degree of inter-chain hydrogen bond stabilisation (Fig. 1.7b). This highly organised, hydrogen-bond stabilised structure is about 70 % crystalline, and the amorphous structure usually occurs where chain ends go out of register (Fig. 1.7c). The non-covalent, inter-chain hydrogen bonds co-operatively resist deformation, and failure of the elementary cellulose fibrils under tensile load actually takes place at the cellobiose bridge oxygen rather than from

Figure 1.7.

Molecular hierarchy of Cellulose. a) Cellobiose monomer (from Vincent, 1980). b) Cellulose unit cell structure including side view and view down chain axis. Unit cell dimensions : a = 0.835 nm, b = 0.785 c = 1.03 nm and nm (chain axis). c) Extended chain crystal structure of Cellulose, the elementary cellulose fibril is 3.5 nm in diameter and consists of about 36 rod-like antiparallel Cellulose chains (from Wainwright et al. 1976).

a)

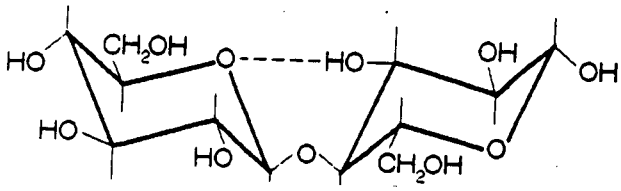
HO
CH2OH
O
HO
OH
OH
HO
HO
O
O
CH2OH
O

b)

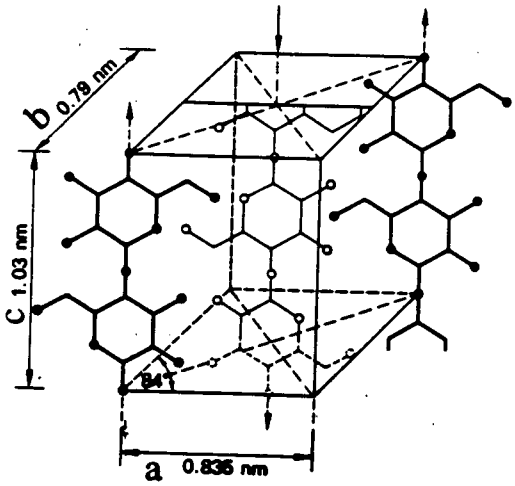
b 0.79 nm
c 1.03 nm
84°
a 0.835 nm

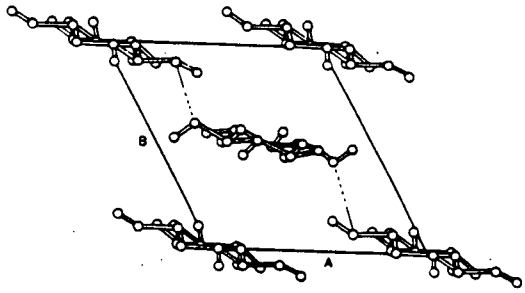
B
A

c)

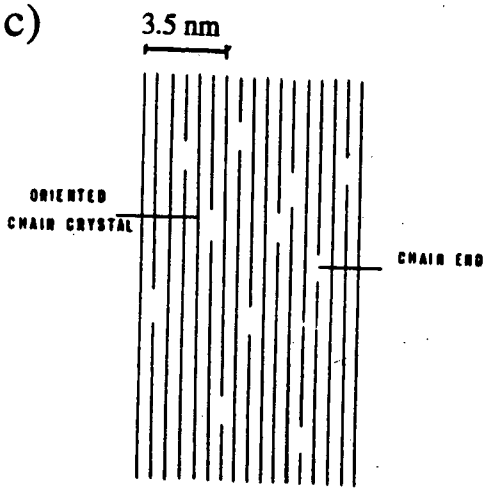
3.5 nm
ORIENTED
CHAIN CRYSTAL
CHAIN END

inter-chain slippage (Vincent, 1980).

The processing history of cellulose molecules is key in ensuring the formation of extended-chain crystal structure. While chains constructed from cellobiose monomer are quite rigid relative to other long chain polymers, if these chains are precipitated from solution they can develop the folded-chain crystal structure, where the parts of cellulose chains fold back on themselves to crystallize and other parts are left in amorphous conformations. This phenomenon is observed during the production of the related synthetic material Rayon. Rayon is produced by the *viscose* process, where cellulose xanthate purified from plants is reconstituted into cellulose and spun in an acid solution to induce crystallization and fiber formation. This process results in the formation of a degree of randomly-coiled chains that results in lower ultimate strength, lower modulus and higher extensibility (Fig. 1.3 and Table 1.2). Native, extended-chain cellulose crystals are produced via the UDP-glucose synthase pathway within the plasma membrane at the plant cell surface and are polymerised into a non-solvent medium (ie. H_2O) such that they are incorporated directly into the cellulose crystal lattice in the plant cell wall, and the molecules never have a chance to form folded chain crystals (Utlee, 1985). This unique combination of simultaneous polymer synthesis and crystal formation ensures that virtually all cellulose chains adopt the extended-chain crystal conformation, giving rise to the excellent physical properties shown in Figure 1.3 and Table 1.2.

9.2. Kevlar: supra-molecular morphology and processing.

The Kevlar fiber is an excellent example of a synthetic, high ultimate strength, high modulus, extended-chain crystalline polymer. Like Cellulose, Kevlar is assembled from long, rigid, linear isotactic polymer chains made of monomers containing six membered rings in their backbone. The molecular hierarchy of Kevlar in shown in Figure 1.8. Kevlar's basic building block is the aramid p-

Figure 1.8.

Molecular hierarchy of Kevlar. a) The PPT monomer. (Created by mixing terephthaloyl chloride in a solution of p-phenylenediamine in N-methylpyrolidine and hexamethyl phosphorictriamide) (from Northolt, 1973). b) Unit cell structure including side view and view down chain axis. Dimensions : a = 0.518 nm b = 0.787 nm, and c = 1.29 nm (chain axis) (from Northolt, 1973). c) Extended chain crystal structure (from Schaefgen, 1983) and d) Fibrillar morphology (from Schaefgen, 1983). Kevlar's elementary fibril is 600 nm in diameter and contains a 30 nm lamellar repeat defect zone. The liquid crystal PPT polymer is spun into Kevlar fibers with a dry jet or air gap spinning protocol (Jaffee, 1988).

a)

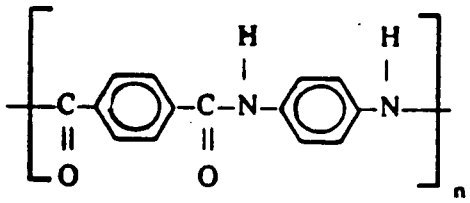
H
H
C
C
N
N
O
O
n

b)

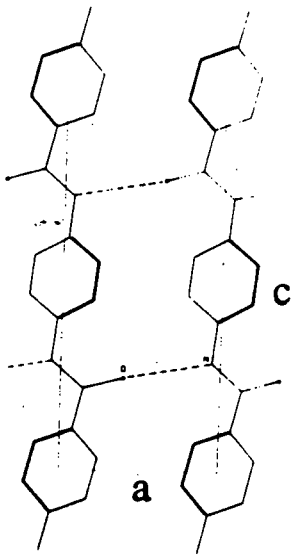
c
a

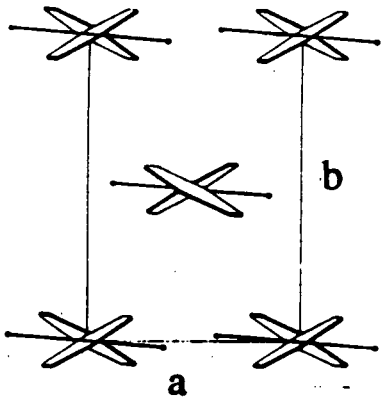
b
a

c)

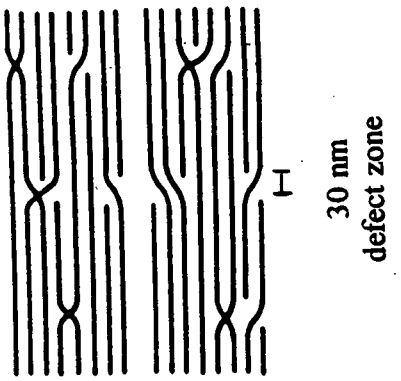
H
30 nm
defect zone

d)

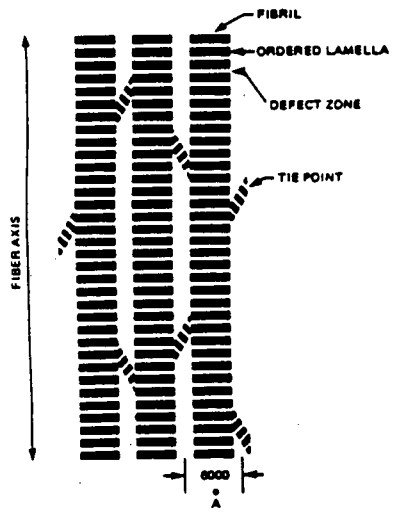
FIBRIL
ORDERED LAMELLA
DEFECT ZONE
TIE POINT
FIBER AXIS

phenyleneterephthalamide (PPT)(Fig. 1.8a). Chains of PPT monomers can pack tightly into parallel, extremely well oriented extended-chain lamellae, that are stabilised via inter-chain hydrogen bonds between a carboxyl oxygen of one chain and an amide hydrogen from an adjacent chain (Fig. 1.8b). Wide angle x-ray diffraction (WAXD) shows that the elementary fibrils contain a lamellar repeat that was determined by chemical degradation methods to be a defect zone (Schaefgen, 1983). Unlike conventional fibers that contain amorphous material between crystals, it is unlikely that any folds in the PPT chains exist. Instead, the bulk of the chains go right through the defect zone, but a significant fraction go out of register (Fig. 1.8c). It has been speculated that a larger population of chain ends than is expected statistically occur in this zone. The WAXD pattern also indicates a small proportion of randomly oriented crystal. This crystalline material loosely ties together many elementary fibrils into the single Kevlar fiber that is approximately 12 μm in diameter (Fig. 1.8d). One additional observation is that the fibrils in the centre of the fiber are less perfectly packed than those on the outside, giving rise to a skin core structure (Schaefgen, 1983).

Processing is key to ensure extended chain crystallization in Kevlar, because dilute isotropic solutions of aramids are known to form amorphous entanglements when they are spun. The preferred production method for Kevlar is to increase chain concentration so that entanglements fail to occur because of spontaneous, inter-molecular assembly of the rigid PPT chains into larger molecular aggregates. PPT chains assemble in 100 % sulfuric acid to form a white, cloudy, anisotropic, nematic liquid-crystalline phase. The liquid-crystalline phase is a physical state of matter between liquid and solid. Liquid-crystals have imperfect long-range orders of position and orientation and are made of rod-like molecular aggregations that tend to point along a common axis, the director. This quasi-oriented liquid-crystalline phase encourages global molecular alignment of the PPT chains during spinning and results in a high ultimate strength, high stiffness, virtually 100 % extended-chain crystal,

super-fibers, where no post spinning draw is required.

9.3. Poly(ethylene) : Supra-molecular morphology and processing.

Poly(ethylene) fibers provide a clear example of how different supra-molecular morphologies and physical properties can arise from the same polymer chains depending on the alignment induced by drawing during fiber formation. Poly(ethylene) is made from the linear, isotactic, reiterated carbon chain shown in figure 1.9a. These chains should have a large capacity to crystallize; however, they are much more flexible than Cellulose or PPT chains, so when they are bulk polymerised they have a tendency to fold back on themselves to form imperfect folded chain crystal lamellae (Fig. 1.9b). As a result, a large portion of the chains have to be accommodated as amorphous structure in inter-lamellar spaces. The folded-chain crystal morphology results in much lower ultimate properties (Fig. 1.3 and Table 1.2). To produce high ultimate strength, high modulus Spectra, the inherently flexible poly(ethylene) chains must be processed under very specific conditions to ensure that they are elongated and crystallized in the extended-chain form. Spectra is spun from dilute solutions (2 % wt) of long, very high molecular weight (300 K Da) poly(ethylene) chains in specific solvents that produce highly drawable gels. The gel forms because the high molecular weight of the chain results in sufficient polymer-polymer contact to produce a continuous structure that retains solvent even in very dilute concentrations (Schaeffgen, 1983). The dilute poly(ethylene) solution provides enough inter-chain contact to form structure but not enough to result in extensive entanglements of these coiled chains. When the gel is drawn, the inter-chain contacts keep the chains aligned, while the presence of the solvent keeps these chains from entangling or crystallizing. When the gel is super-drawn (ca. 2000 %), the chains can crystallize into a densely packed, highly oriented, extended-chain micro-fibrillar structures. The unit cell and the supra-molecular morphology of the

Figure 1.9.

Molecular hierarchy of poly(ethylene) a) The poly(ethylene) chain, usually polymerized using a Zeigler transition metal catalyst. b) Folded chain supra-molecular morphology of bulk polymerized poly(ethylene) (from Wainwright et al. 1976). c) Three dimensional unit cell structure of poly(ethylene) Spectra. Dimensions: a=0.736 nm, b=0.492, c=0.254 nm (chain axis). d) Extended chain crystal structure of Spectra. The crystals are 1.5 nm in diameter and 20 nm long (Andrews and Dawson, 1988).

a)

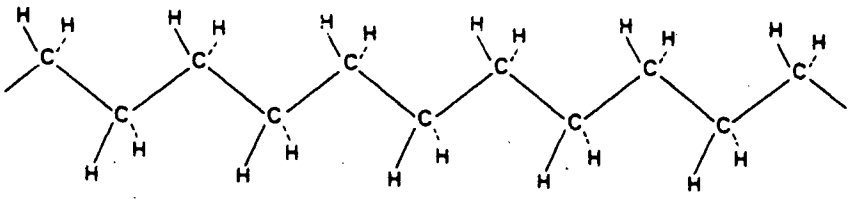

b)

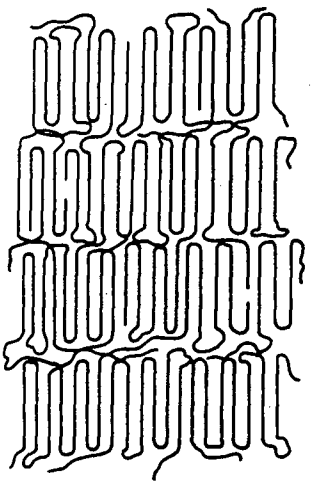

c)

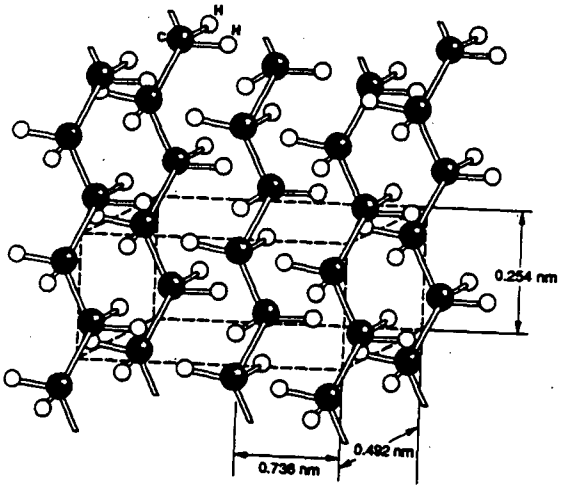

d)

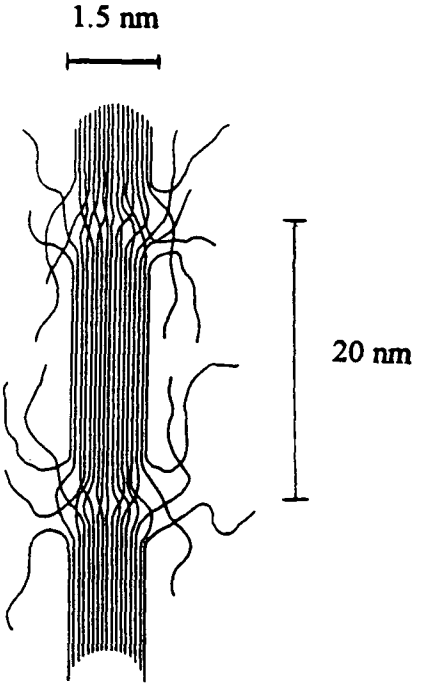

extended-chain micro-fibrils of Spectra are shown in Figures 1.9 c and d. The highly oriented elementary Spectra fibril is about 75 % crystal.

9.4. Nylon : supra-molecular morphology and processing.

Supra-molecular crystallinity and physical properties are also intimately related to the polymer chain chemistry and processing history of the synthetic, aliphatic polyamide, Nylon 6,6. The highly drawn Nylon 6,6 fiber is of particular interest to this study because it exhibits physical properties very similar to orb-spider MA silk, and it contains recurring amide groups as part of its polymer main chain sequence, as do protein sequences. Nylon 6,6 polymer chains are linear, stereo-regular molecules assembled from the reiterated monomer shown in Figure 1.10a. Nylon chains crystallize through inter-molecular hydrogen bonding and are stabilised by van der Waals interactions (Fig. 1.10b). The degree of crystallization depends on the imposed draw ratio following spinning. When the molten Nylon 6,6 polymer emerges from the spinneret and solidifies in filament form, it shows little molecular orientation and poor physical properties (see undrawn Nylon 6,6 in Fig. 1.3 and Table 1.2). The desired physical properties are achieved through a subsequent cold-draw process, where the fiber is drawn out to as much 600 % of its original length. This process aligns the Nylon 6,6 chains and encourages them to crystallize. Figure 1.10c shows the supra-molecular morphology of highly drawn Nylon 6,6 micro-fibrils. The stable crystals consist of stacked sheets assembled from adjacent hydrogen bonded chains that can adopt both extended-chain and folded-chain configurations. The elementary Nylon 6,6 micro-fibril also contains a substantial proportion of disordered amorphous domains as well as some extended chains that simply fail to crystallize. Highly drawn Poly(ethylene) Spectra and Nylon 6,6 fibers are clear examples of flexible-chain based polymers that must be processed by a high degree of physical draw to achieve high ultimate strength and stiffness.

Figure 1.10.

Molecular hierarchy of highly drawn Nylon. a) The Nylon 6, 6 monomer. (Formed from poly-condensation of hexamethylenediamine and adiptic acid or ϵ-caprolactam ring opening polymerization. b) Unit cell structure. Dimensions a=0.49 nm, b=0.54 nm and c=1.72 nm (chain axis). c) Supra-molecular morphology of Nylon 6,6, including extended and folded chain crystals and amorphous structure (Zimmerman, 1988).

a)

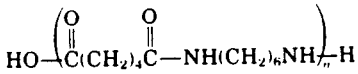

nylon-6.6

b)

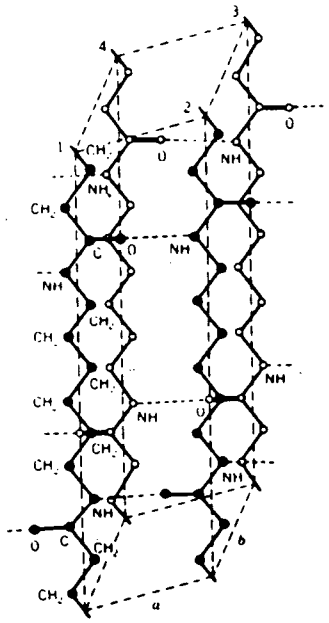

c)

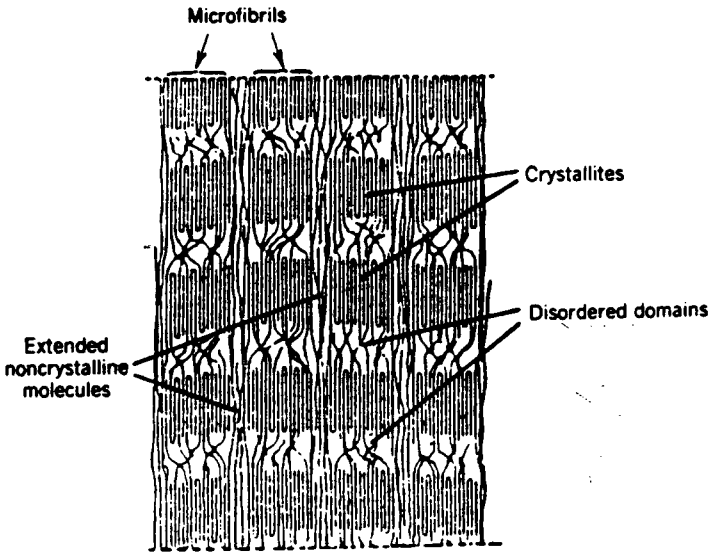
Microfibrils
Crystallites
Disordered domains
Extended
noncrystalline
molecules

10. The importance of fibroin sequence design in determining the supra-molecular organization of silks.

The examples of Cellulose, Kevlar, poly(ethylene) and Nylon 6,6 should emphasise the importance of both polymer chain chemical structure and processing history in determining supra-molecular crystallinity. An examination of these factors in spider silks should reveal the basic mechanisms governing differential crystallization and molecular mobility in mechanically distinct silks.

Silks in general are semi-crystalline fibers made from linear, isotactic, high molecular weight co-polymeric proteins called fibroins. (While these are considered strings of isotactic monomers since only L-amino acids occur in most proteins, some spiders have been shown to have the capcity to produce R-amino acids (note added in final proof (Dr. Waite, personal communication). Fibroins contain stretches of reiterated amino acid sequence blocks that can crystallize during spinning, and these crystal structures cross-link and reinforce the fibroin network, as was shown for *A. diadematus* MA and FL silks in Figure 1.5. Crystalline structure in most silks is based on β-pleated sheet secondary structure, but a few silks contain α-helical, poly(glycine)-II or Collagen-like secondary structure. The β-pleated sheet was first proposed by Pauling and Corey (1953a), where it was predicted that protein secondary structure could develop from parallel or antiparallel alignment of extended-chain amino acid sequences stabilised via multiple inter-chain hydrogen bonds between the carboxyl oxygens of one chain and amide hydrogens of an adjacent chain (Fig. 1.11a). To date, no examples of parallel-chain pleated sheet model have been confirmed experimentally in fibrous synthetic polypeptides or proteins. An extensive study by Marsh et al. (1955a) lead to the conclusion that *B. mori* silk contains anti-parallel β-pleated sheet secondary structure. X-ray crystallography predicts that multiple *B. mori* fibroin chains align in the anti-parallel fashion to form discrete β-sheet layers, where the fibroin chain axis is usually predominantly parallel to the fiber axis. These layers

Figure 1.11.

The molecular hierarchy of β-pleated sheet based micro-crystals. a) The β-sheet forms from alignment of poly-peptides in the extended chain conformation and inter-chain stabilization occurs via hydrogen bonding between the carboxyl oxygen from one chain and an amide hydrogen from an adjacent chain (from Fraser and MacRae, 1972). The hydrogen bonds are directed approximately perpendicular to the chain axis and in the plane of the sheet. (The anti-parallel β-sheet is a more stable form than the parallel β-sheet because the hydrogen bonding is more linear in the former instance). b) Micro-crystals form when β-pleated sheets stack in layers with amino acid side chains packing between sheets. This is a side view of a micro-crystal where the amino acid side chains are represented by hollow circles (from Wainwright et al. 1976). c) Schematic representation of the β-sheet micro-crystal structure known to exist in *B. mori* silk (from Denny, 1980).

a)

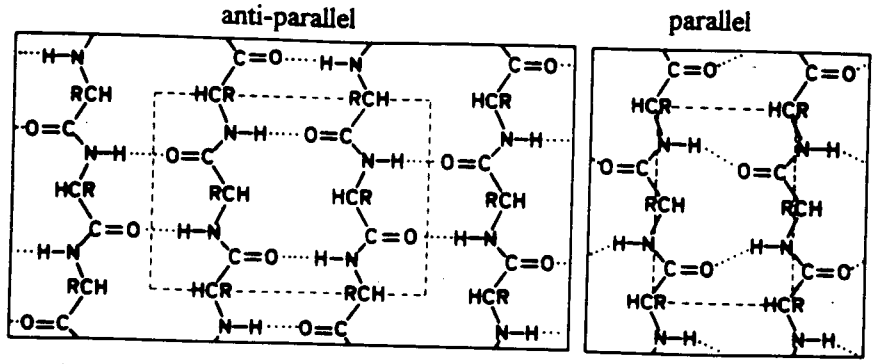
anti-parallel
parallel

b)

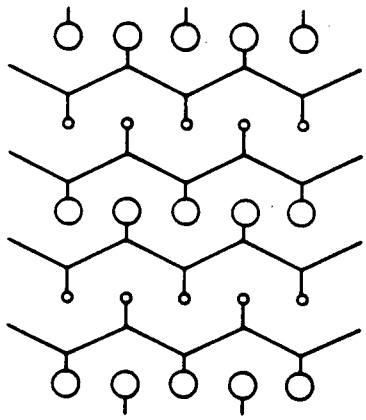

c)

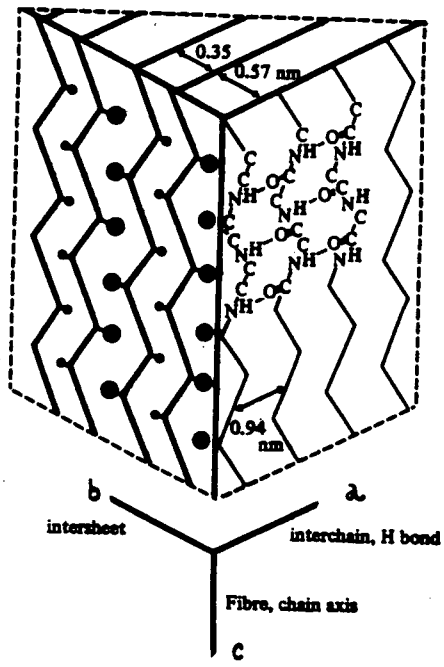
0.35
0.57 nm
0.94 nm
b
intersheet
a
interchain, H bond
Fibre, chain axis
c

pack tightly with alternating amino acid side chains projecting above and below the plain of the pleated sheets (Fig. 1.11b), forming fiber reinforcing micro-crystals (for example see Fig. 1.11c).

Warwicker (1960a), Lucas and Rudall (1968), and Rudall and Kenchington (1971) placed silk, β-pleated sheet based micro-crystals into five distinct groups that all have a common period of 0.944 nm in the hydrogen bonded a-direction and 0.695 nm along the fibroin chain axis c-direction. The micro-crystals are differentiated by their unit cell b-spacing, which describes the distance spanned by two β-pleated sheets. This inter-sheet spacing is a gauge of the tightness of packing of the sheets, which in turn, is a direct reflection of the size and charge of the side chains of the amino acid residues in the crystallized sequence block of the fibroin chain. Among the natural silks examined to date, this distance varies between 0.93 and 1.57 nm. Amino acid composition and sequence analysis combined with x-ray diffraction pattern interpretation can provide direct information on which fibroin sequence designs crystallize in silk fibers and how. The information available on micro-crystal types that have been observed by x-ray diffraction in natural silks is briefly summarized here.

10.1. Supra-molecular crystal structure in natural silks.

Group 1. This is the predominant crystal form in silkworm *Bombyx mori* silks. The unit cell b-dimension spacing is estimated at 0.92 nm, and it arises from the primary hexapeptide repeat GAGAGS (where G=glycine, A=alanine and S=serine) (Marsh et al. 1955a). Since alternating residues project above and below the plain of a β-pleated sheet, there is an alternating sheet packing arrangement where glycine packs with glycine residues at a spacing of 0.35 nm, and alanine and serine residues pack with themselves and each other at a spacing of 0.57 nm (Fig. 1.11c).

Group 2, a and b. Group 2a β-pleated sheet crystals assemble from reiterated -$[GAA]_n$ (n=4-6) sequence blocks at a b-spacing of 1.00 nm. *Anaphe infracta* (Class Insecta, Family

Thaumetopoeidae) silk contains this crystal class and has a composition that is almost entirely dominated by Glycine (31 %) and Alanine (57 %). Group 2b crystals also have a unit cell b-spacing of 1.00 nm and can only be differentiated from Group 2a crystal types by a lower x-ray equatorial reflection intensity. *Canefora asiatica* (Class Insecta, Family Psychidae) silk contains Group 2b crystals and is also rich in glycine (34%) and alanine (37%), but it contains a greater proportion of serine (11%) than *A. infracta*.

Group 3. Group 3 β-pleated sheet crystals assemble from reiterated poly(alanine) sequence blocks at a b-spacing of 1.06 nm. This x-ray class of crystal has been observed in the MA silk of the orb-spiders *N. clavipes* (Becker et. al 1994) and *N. madagascarensis* (Warwicker, 1960), in silks that contain only alanine, like that of *Antherae mylitta* (Class Insecta, Family Saturnidae), and in powders and crystallites formed from synthetic poly(L-alanine) sequences (Fraser and McRae, 1973). Group 3b crystals also have a unit cell b-spacing of 1.06 nm and like Group 2a and b silks, can only be differentiated from its Group 3a crystals by a lower x-ray equatorial reflection intensity. **The MA silk of *A. diadematus*, the orb-spider subject of this thesis, contains Group 3b poly(alanine) based β-sheet crystals (Work and Morosoff, 1982).**

Group 4. Group 4 β-pleated sheet crystals have a unit cell b-spacing dimension of 1.50 nm and assemble from sequences of amino acids containing bulky side chains. The South American sawfly produces silk that likely contains poly-dipeptide $(AQ)_n$ fibroin sequence (Q=glutamine). The appreciable proportion of bulky Glutamine residues likely prevents the tighter packing schemes observed in Group 1-3 crystals.

Group 5. These β-pleated sheet crystal types have a unit cell b-spacing of 1.57 nm and also assemble from fibroin sequences that contain bulky amino acids. The CY silk of the spider *N. senegalensis* contains 12 % Glycine, 29 % Alanine, 22 % Serine and 10 % bulky Glutamine, and its

x-ray pattern gives unit cell dimensions consistent with this crystal type.

In addition to the β-pleated sheet crystal types listed above, several other types of crystalline secondary structure have been observed in silks that bear reference.

Group 6, Cross-β Structure. This unique crystal structure forms from β-pleated sheets whose chain axis is perpendicular to the fiber axis and whose inter-sheet b-dimension is parallel to the fiber axis. This type of crystal is observed in lacewing fly *Chrysopa Flava* (Class Insecta, Family Chrysopidae) silk, which has a composition of 25% glycine, 21% alanine and 43% serine. In tension, Cross-β crystals unfold, and when the fiber is stretched to 5 or 6 times its original length a Cross-β→Group 3 crystal conformational transition occurs.

Group 7, α-Fibroin Structure. Several insect silks have been found to contain crystal structure with x-ray patterns that are similar to helical α-Keratins. The amino acid compositions of silks containing this structure differ from other silks in that there is a very low Glycine content and a higher proportion of charged residues. Hymenopteran bee, wasp, and ant larvae produce silks that have an x-ray diffraction pattern that fits a four stranded helical rope structural model.

Poly(glycine)-II structure. This structure is an extended chain helix with 3 amino acids per turn and a residue repeat distance of 0.31 nm. (Note that an α-helix contains 3.6 amino acids per turn and residue repeat distance of only 0.15 nm). This structure is observed in solomon seal sawfly *Phymatocera aterrima* (Class Insecta, Family Blennocampinae) silk, which contains 66% glycine and no other residue in excess of 8%. Long stretches of poly(glycine) sequences are likely to promote the formation of this PG-II structure. Synthetic poly(GGX) sequences can also crystallize into PG-II structure (Fraser and MacRae, 1973).

Group 0, Collagen Like-Structure. The Gooseberry sawfly *Nematus ribesii* (Class Insecta, Family Nematinae) produces a silk that contains 6-9% proline and 20-30% glycine and which has

an x-ray pattern that is collagen-like. Collagen structure is known to develop from the assembly of helical poly-tripeptide chains with the reiterated $(G\text{-}X\text{-}Y)_n$ amino acid sequence, (where X or Y is frequently proline) into higher order three-stranded ropes. *N. ribesii* collagen-like silk structure likely arises because of a similar reiterative placement of glycine in every third position of its silk fibroin sequence.

10.2. Supra-molecular organisation of orb-spider silks.

X-ray data on spider silks shows the presence of Group 3 poly(alanine) based β-pleated sheet crystals in the MA silks of the orb-spiders *A.diadematus*, *A. aurantia*, *A. marmoreus*, *N. clavipes*, *N.madagascarensis* and *Nephilengys cruentata* (Work and Morosoff, 1982 ; Fraser and MacRae, 1972). Solid state ^{13}C cross polarisation, magic-angle spinning nuclear magnetic resonance (CPMAS-NMR) and ^{2}H NMR spectra corroborate this evidence by showing that about 40 % of the *N. clavipes* MA fibroin alanine residues are immobile and exist as β-pleated sheet crystallites with a chain axis parallel to the fiber axis (Simmons et al. 1996). The ^{13}C CPMAS and ^{2}H NMR spectra also indicate a second motionally distinct population for alanine, and it has been estimated that about 60 % of the poly(alanine) fibroin sequence blocks are present as lesser oriented, less densely packed β-pleated sheet proto crystals. A schematic representation of the molecular hierarchy of the poly-(alanine) β-sheet based semi-crystalline MA silk is shown in Figure 1.12.

Although all silks contain micro-crystals, a fraction of the silk fibroins show no specific secondary structure by x-ray diffraction, as seen by a diffuse halo around the central x-ray beam stop. This amorphous protein morphology generally results from amino acid sequences that are non-repetitive, or from stretches of sequence that contain residues whose side chain conformation is not conducive to regular folding and packing. Local structure may be present in these amorphous regions

Figure 1.12.

The molecular hierarchy of orb-spider silk. a) The amino acid alanine. Reiterated poly(alanine) sequences are known to adopt β-sheet secondary structure in some orb-spider silks. b) The poly(alanine) β-sheet micro-crystal. Unit cell dimensions: a=0.944nm, b=1.06 nm, c=0.695 nm. c) Orb-spider silks contain both crystal and amorphous domains. Individual fibroin molecules span several different domains.

a)

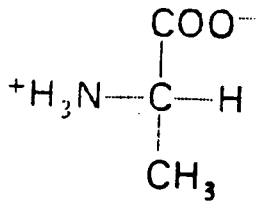

b)

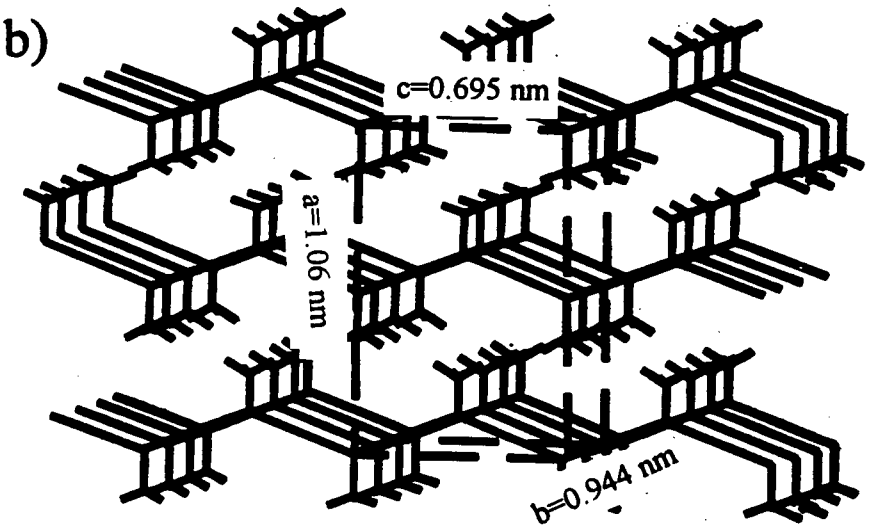

c)

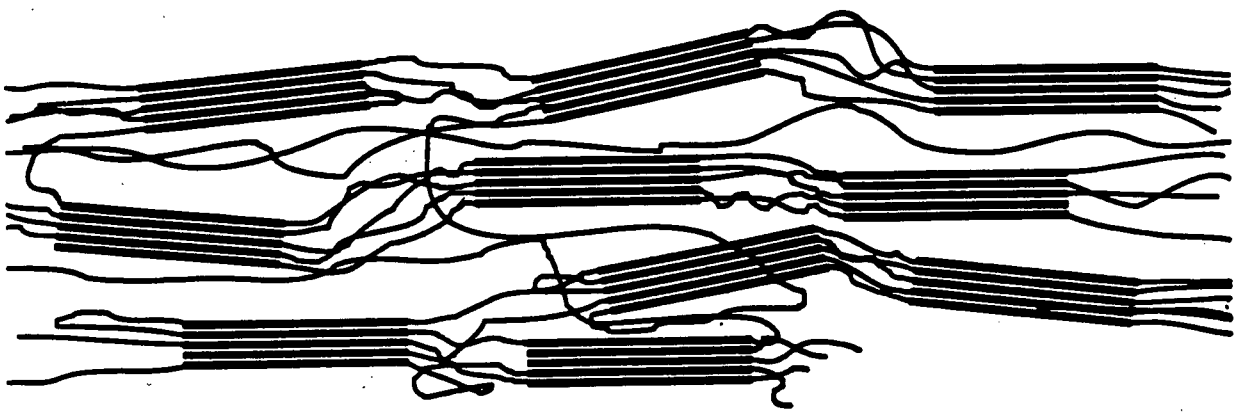

that fails to present a clear diffraction lattice to the x-ray beam, but that contributes to fiber mechanics none the less. Proton-driven, ^{13}C, 2-dimensional spin diffusion NMR spectra from the glycine-labelled fibroin of *N. madagascarensis* MA silk indicate that glycine rich MA fibroin sequences are ordered (Kummerlen et al. 1996). The simplest structural model that explains these data places glycine rich sequences is an extended-chain 3_1 helical conformation. This type of conformation is known to develop from natural and synthetic poly(glycine) sequences. The natural form is the PG-II structure cited above, and the synthetic form can develop from poly(A-G-G) and poly(L-A-G-G-G) sequences. Extended chain 3_1 helices have the potential to crystallize by forming multiple inter-molecular hydrogen bonds between the carboxyl oxygen of one chain and the amide hydrogen of an adjacent chain. The PG-II structural model proposed by Rich and Crick (1955) shows that a single 3_1 helix has the potential to bond with six of its neighbours in a hexagonal array (Fig. 1.13). It is not difficult to imagine that when individual fibroin molecules containing glycine rich sequences are drawn out and aligned, they may come into close contact with glycine rich sequences from an adjacent extended fibroin molecule to form crystal structure. In fact, Thiel et al. (1997) have recently presented empirical and theoretical evidence indicating that some of the glycine rich sequences present in *N. clavipes* MA fibroins can adopt the β-sheet conformation. However, these sequence stretches also contain other residues (eg. glutamine, tyrosine, leucine and proline) which could prevent the development of a perfect crystal packing scheme. The refined structural model for the micro-structure of *Nephila* MA silk employs the concept of non-periodic lattice (NPL) crystals. In NPL crystals the local composition, symmetry, and perfection of order are predicted to vary over distances that are small compared to the size of the entire NPL crystal (Thiel et al. 1997). In other words, the local structure of *N. clavipes* MA silk NPL crystals probably varies from perfectly crystalline domains, (based on poly(alanine) sequence runs), to aperiodic crystal structure whose organization

Figure 1.13.

Ball and stick diagram of the molecular structure of a 3_1 helix. a) Side view (from Kummerlen et al. 1996). b) View down chain axis (from Fraser and MacRae, 1972).

a)

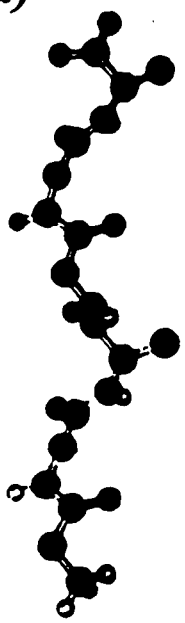

b)

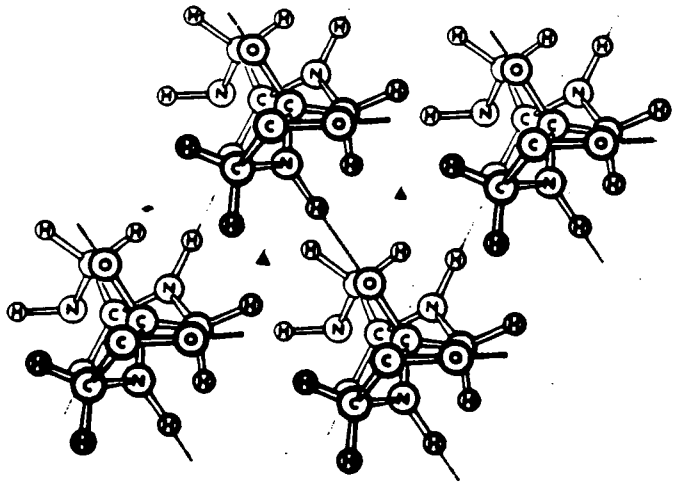

is determined by the sequence design of glycine rich sequences (Thiel et al. 1997).

11. The importance of fibroin sequence designs and amino acid composition in determining orb-spider silk mechanics.

While it is clear that the supra-molecular morphology of silk is intimately related to the primary sequence of its constituent fibroin(s), very little information is available on the primary peptide sequence designs present in spider silk fibroins. Prior to this study there where only two silk genes cloned from any spider. These were retrieved from the Ecribillate orb-spider *N. clavipes* and encode Spidroin-1 and 2, hereafter referred to as *N. clavipes* fibroins-1 and 2, (NCF-1 and 2). These spider fibroins contain reiterated modules with the peptide sequences shown in Figure 1.14. Both contain crystal-forming poly(alanine) sequences which likely give rise to many perfect crystallites, but the glycine rich sequences of NCF-1 and 2 are compositionally distinct, and likely give rise to distinct secondary structure in the MA fiber. That is, the GGX sequences (X= leucine, glutamine and tyrosine) of NCF-1 are beleived to develop aperiodic local crystal structure, while the glycine and proline rich sequences of NCF-2 likely give rise to the amorphous component of *N. clavipes* MA silk (Thiel et al. 1997).

NCF-1 and 2 were both cloned from the MA gland, and as such there was no information on the sequence designs present in fibroins from mechanically distinct spider silks. The amino acid composition of the silks from three different orb-weaving spider species are presented in Table 1.3. These data indicate that there are differences in the amino acid composition of equivalent silk types produced by the different orb-spider species. For example, while the MA silk of *A. diadematus*, *A. gemoides* and *N. clavipes* all contain similar proportions alanine, around 20 %, they each have distinct proline contents of 16 %, 10 % and 3.5 % respectively (please compare and contrast the

Figure 1.14.

Consensus amino acid sequence of the repeated *N. clavipes* fibroin 1 and 2 (NCF-1 and 2) (Hinman and Lewis, 1992). The consensus repeat of the *B. mori* heavy chain fibroin is included for comparison.

NCF-1
AGRGGLGGQGAGAAAAAAAGGAGQGGYGGLGSQG

NCF-2
GPGQQGPGGYGPGQQGP--SGPGSAAAAAAAAAA----GPGGYGPGQQGPGGY

B. mori **heavy chain**
GAGAGSGAAG[(SG(AG)$_2$]$_8$Y

Table 1.3.

The amino acid composition of the silks from three different orb-spider species. Symbols : - indicates only tace amounts are present; N/A indicates that data are not available for these silk types.

	A. diadematus							*A. gemoides*							*N. clavipes*						
	MA	MI	FL	AG	CY	AC	PY	MA	MI	FL	AG	CY	AC	PY	MA	MI	FL	AG	CY	AC	PY
Aspartate	1.0	1.9	2.7	9.2	6.3	8.6	10.5	2.4	1.2	N/A	N/A	5.9	N/A	N/A	1.2	2.8	N/A	N/A	3.6	N/A	N/A
Threonine	0.9	1.4	2.5	7.6	3.4	9.0	4.4	0.8	0.3	N/A	N/A	3.6	N/A	N/A	0.1	0.3	N/A	N/A	5.2	N/A	N/A
Serine	7.4	5.1	3.1	6.8	27.6	16.5	14.8	10.3	5.2	N/A	N/A	28.1	N/A	N/A	7.4	10.9	N/A	N/A	23.4	N/A	N/A
Glutamate	11.5	1.6	2.9	9.8	8.2	7.8	10.4	9.2	8.0	N/A	N/A	10.0	N/A	N/A	10.9	4.5	N/A	N/A	9.3	N/A	N/A
Proline	15.8	0.1	20.5	10.8	0.6	3.6	7.8	10.1	0.5	N/A	N/A	0.4	N/A	N/A	3.5	0.6	N/A	N/A	0.4	N/A	N/A
Glycine	37.2	42.8	44.2	14.5	8.6	13.2	7.8	42.0	51.6	N/A	N/A	9.3	N/A	N/A	45.8	42.6	N/A	N/A	7.3	N/A	N/A
Alanine	17.6	36.6	8.3	6.2	24.4	10.7	9.9	18.0	24.1	N/A	N/A	23.7	N/A	N/A	22.2	20.0	N/A	N/A	30.0	N/A	N/A
Valine	1.2	1.7	6.7	5.8	6.0	6.9	5.4	2.2	1.2	N/A	N/A	4.9	N/A	N/A	0.8	2.5	N/A	N/A	1.8	N/A	N/A
Cysteine	-	-	-	-	-	-	-	-	-	N/A	N/A	-	N/A	N/A	-	-	N/A	N/A	-	N/A	N/A
Methionine	-	-	-	-	-	-	-	-	-	N/A	N/A	-	N/A	N/A	-	-	N/A	N/A	-	N/A	N/A
Isoleucine	0.6	0.7	1.0	4.7	1.7	4.2	3.7	0.2	0.4	N/A	N/A	1.8	N/A	N/A	0.1	0.4	N/A	N/A	1.9	N/A	N/A
Leucine	1.3	1.0	1.4	5.5	5.7	8.2	5.4	1.5	1.5	N/A	N/A	6.6	N/A	N/A	3.5	2.2	N/A	N/A	6.9	N/A	N/A
Tyrosine	3.9	4.7	2.6	2.2	1.0	1.6	2.2	3.9	7.9	N/A	N/A	1.5	N/A	N/A	4.3	8.4	N/A	N/A	2.1	N/A	N/A
Phenylalanine	0.5	0.4	1.1	3.8	3.2	2.6	2.3	1.0	1.0	N/A	N/A	3.2	N/A	N/A	0.3	0.9	N/A	N/A	5.2	N/A	N/A
Lysine	0.5	0.4	1.4	7.4	1.8	2.6	9.0	0.5	0.5	N/A	N/A	2.0	N/A	N/A	0.3	0.5	N/A	N/A	1.0	N/A	N/A
Histidine	-	-	0.7	2.4	-	0.6	2.8	-	-	N/A	N/A	-	N/A	N/A	-	-	N/A	N/A	-	N/A	N/A
Arginine	0.6	1.7	1	3.4	1.5	4.0	3.6	1.9	2.8	N/A	N/A	1.7	N/A	N/A	1.7	2.9	N/A	N/A	3.2	N/A	N/A

proportions of other abundant residues for the same silk types produced by different spiders) . The data also show that most of the silk types produced by the same orb-spider species have distinct amino acid compositions. For example, the MI silk of *A. diadematus* contains almost no proline or glutamine, while the MA silk contains the aforementioned 16 % proline and about 11.5 % glutamine. (Please compare and contrast the amino acid compositions of different silk types produce by the same spider species). Distinctions in amino acid composition between mechanically distinct silk types produced by the same spider species likely indicates that there are differences in the sequence design of each silk's constituent fibroins, and possibly that compositionally and sequentially distinct fibroins produced in the different silk glands give rise to mechanically distinct fiber types. The experiments outlined in Chapters 2 and 3 of this thesis were designed to test the hypothesis :

"Orb-spiders control the supra-molecular morphology and mechanical properties of their silks through variations in the chemical sequence design of their silk's constituent fibroins".

This hypothesis was tested by cloning silk genes from of *A. diadematus*, examining the sequence designs of the different fibroins they encode, and by subsequently examining the gland-tissue expression localities of each of these genes using Northern analysis. The results will show that at least one spider fibroin gene family encodes proteins with variable proportions of crystal forming poly(alanine) sequences and amorphous glycine-rich sequences. By Northern analysis, each spider fibroin gene exhibits a distinct tissue specific expression pattern. It is deduced that silk gland specific expression of these fibroin genes affords the orb-spider the potential to produce compositionally distinct silk secretions that should maintain differential potential for crystallization when spun. This prediction was verified by testing the crystallization sensitivity of the silk secretions retrieved from

the MA, MI, FL and CY glands when sheared on a microscope slide in the lab, where each secretion exhibited a qualitatively distinct shear sensitivity when evaluated with polarized light microscopy.

Table 1.3 also indicates that mechanically distinct silks produced by the same orb-spider species can maintain similar amino acid compositions. For example the mechanical Group-A MA and Group-C FL fibers contain similar proportions of alanine, glycine and proline. While a detailed understanding of polymer chain chemistry is essential to understanding the basis for supra-molecular structure in silks, processing conditions of the different silk types must also be considered in order to explain how mechanical properties of silks are derived.

12. Structural evolution of fibroins during spinning.

As is the case for many semi-crystalline fibrous polymers, including Cellulose, Kevlar, poly(ethylene) Spectra and Nylon, supra-molecular crystallization in spider silk must also depend on the chemical and physical processing conditions that its constituent fibroins are subjected to as they move through the silk gland and are spun irreversibly into solid, semi-crystalline fibers. While the polymers literature provides a reasonable explanation of how simple reiterated polymer chains crystallize when spun, there is little indication as to how the more complex fibroin molecules may align and crystallise during silk production. The silk spinning process is particularly intriguing because fiber formation is accomplished without the extensive post-spinning draw required by other flexible chain based synthetic polymers, like Nylon 6,6, and under benign thermal and chemical conditions compared to high temperature and harsh solvent conditions required to convert liquid crystalline para-aramids into solid, high strength, high stiffness Kevlar fibers.

Recent studies indicate that the secretions from the *N.clavipes* MA and *B. mori* silk glands have the capacity to adopt liquid-crystalline organisation. When the contents of these silk glands were

allowed to dehydrate between microscope slide and cover slip and viewed under polarized light, they were found exhibit a micro-structure that was characteristic of the nematic liquid- crystalline phase (Magoshi et al. 1994; Kerkam et al. 1991). This result, taken togther with the previous observation that the silk gland secretions exibit low viscosity despite high polymer concentrations, a hallmark of some liquid-crystalline polymers, led researchers to deduce that the aqueous silk secretion could adopt nematic, liquid-crystalline organisation within the silk gland. It was not until very recently, however, that this prediction was born out. Willcox et al. (1996) examined the silk secretion micro-structure within the MA gland by cryogenic quenching of actively spinning *N. clavipes* subjects. The frozen animals were microtomed and the micro-structure of the glandular contents examined along the length of the glands using electron diffraction, atomic force microscopy (AFM) and transmission electron microscopy (TEM). Their results indicated the presence of a cholesteric, liquid-crystalline phase in the early duct portion of the gland, which is the thin conduit that leads through two convolutions to the spider's spinneret. The cholesteric, liquid-crystal phase is comprised of rod-like molecules, mesogens, that retain a chiral centre and produce inter-molecular forces that favor arrangement between super-posed rods at a slight angles to one another. The secretion within the early duct portion of the gland can be imagined as having a 'plywood-like' organisation made of a stack of very thin, 2-dimensional, nematic crystalline layers, with the director of each layer twisted relative to that above and below it. The major helical axis about which the cholesteric mesogens twist was predicted to be perpendicular to the glandular duct axis (Willcox et al. 1996).

Although many of the details remain to be elucidated, the schematic in Figure 1.15 summarizes the present view of the molecular organisation of the silk secretion as it moves from the proximal secretory tail portion of the gland, through the storage sac (which is also known to contain fibroin producing cells (Kovoor et al.1987)), into the long distal spinning duct, and is spun out under

Figure 1.15.

Cartoon of the evolution of supra-molecular structure of the orb-spider fibroin secretion in the MA gland of *N. clavipes*. a) Fibroin in the amorphous conformation. b) Cholesteric liquid crystalline phase, with schematic 'plywood' representation. c) Nematic liquid-crystalline phase. d) Semi-crystalline MA fiber.

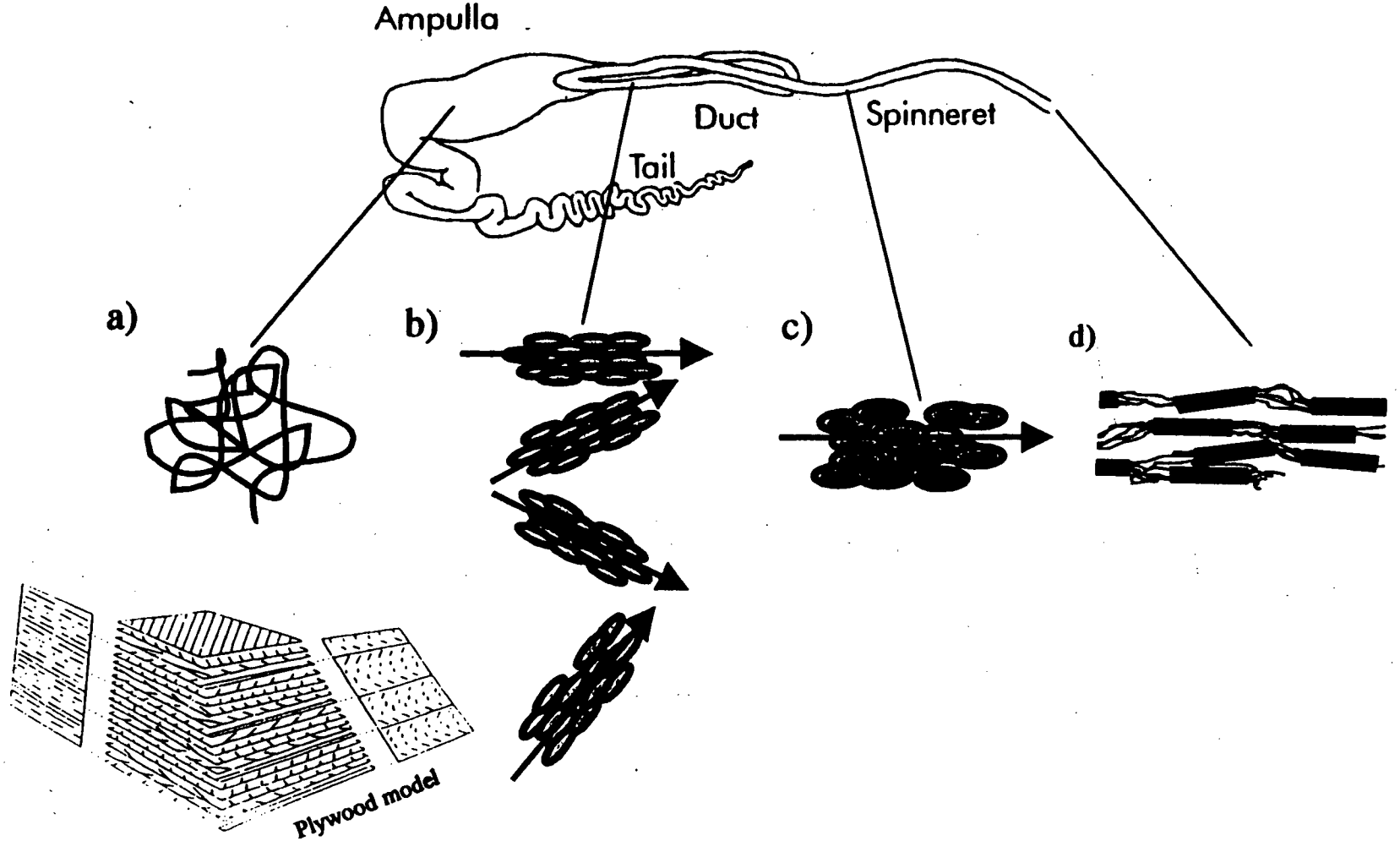
Ampulla
Duct
Spinneret
Tail
a)
b)
c)
d)
Plywood model

tension through the spider's spinneret as a solid, functional fiber. Native fibroin molecules are initially exported from cells in the tail and storage sac region into the glandular lumen. As additional fibroin is secreted into the lumen, the secretion is pushed forward and is stored in the sac region of the gland as a concentrated 20-30 % protein solution that likely maintains a predominantly random-coil conformation. At the point where the secretion enters the constricted duct region it undergoes a phase transition to the cholesteric liquid-crystal. The precise dimensions of individual rod-like mesogens are not known, but a 3 × 3 μm AFM scan of the frozen secretion in the early duct portion of the gland shows a sinusoidal periodicity of 270 nm with a depth of 13 nm, indicating that the width and height respectively should fall inside this size range. These size predictions indicate that the rod like-mesogens are comprised of many fibroin molecules, and because aggregates of random-coils do not acheive orientation on the molecular or segmental level, it is predicted that the cholesteric phase develops from anisotropic secondary or tertiary structure of aggregates of several fibroin molecules (Willcox et al. 1996). It has not been possible to obtain micro-structural information from the secretion as it moves further into the spinning duct, however, it has been predicted that the chiral nematic structure with its helical axis perpendicular to the duct axis would easily be converted to the nematic phase under the flow field that must develop during fiber spinning (Willcox et al. 1996). When the secretion acheives the nematic phase, all the mesogens are beleived to be be oriented along a common director, parallelel to the duct axis. At this stage the mesogens are likely to be highly amenable to shear crystallisation, and their common orientation promotes global molecular orientation of the fibroins during spinning.

Spiders spin their threads out under tension, either by pulling with one appendage (usually the fourth), or by affixing one end of the thread to a substrate or another silk and physically moving away from the attachment site. As the secretion is drawn through the spigot orifice during spinning, inter-

molecular, viscous drag resistance must become high at some point along the thin duct, and the fibroin molecules cease to flow past one another and align to form crystallisation nucleation sites which grow into the stable semi-β-crystalline fibrous form with continued spinning. The spinning process may also involve active removal of water from the silk secretion in the gland duct (Tillinghast, 1984) or passive expulsion as the fibroin molecules begin to associate inter-molecularly, and water is simply squeezed out of the crystallized network and evaporates at the air-spigot interface.

There are a few more details available on the processes of supra-molecular organisation and crystallization in the fibroin secretion produced by the silkworm, and these details may provide insights into fiber formation processes of spider silks. X-ray diffraction, infrared spectroscopy and viscometry data show that the *B. mori* fibroin secretion undergoes a series of secondary structural transitions along the length of the silk gland (Magoshi et al. 1994; Magoshi et al. 1985; Iizuka, 1985). Fibroin molecules are synthesized predominantly in the posterior tail region of the *B. mori* silk gland and are exported into the glandular lumen in the random-coil conformation. As more protein is synthesised, the secretion moves forward into the middle storage sac of the gland as an aqueous, 12 % fibroin gel that has a random-coiled conformation with a small proportion of crankshaft (silk I) β-sheet structure (Magoshi et al. 1994; Fraser and MacRae, 1972). Gelation is believed to be induced by the formation of chelate-type junctions between ionized fibroin $-COO^-$ side groups and Ca^{2+} ions derived from the silkworms mulberry leaf diet. Further into the storage sac, increased Ca^{2+} concentration, a gradient decrease in pH from 6.5 to 4.9, and a gradual expulsion of water results in an increase in silk I structure and an increase in the aqueous fibroin gel concentration to about 25 % by the time it enters distal thin duct portion of the gland. The viscosity of the gel in the storage sac decreases as it approaches and enters this anterior duct, which likely indicates a transition to the liquid crystalline phase (Magoshi et al. 1994).

Like spider silk, the fiber formation mechanism for *B. mori* silk is believed to involve a shear and elongational load-induced phase transition from the nematic liquid-crystalline state to the well oriented semi-β-crystalline solid fiber (Silk II). A silkworm's silk glands are located near its mouth, and during spinning it attaches one end of a viscous progenitor fiber pair to a substrate and then uses a repeated figure of eight motion to pull the silk secretion into a fiber at a draw ratio of about three times its initial length by moving its head away from the attachment site at an approximate velocity of 4 to 15 mm/sec. The coagulation of the liquid-crystalline silk is enhanced by a morphological structure located in the thin silk gland duct, called a silk press, which acts as a fulcrum during drawing. Clearly, precise processing conditions have evolved for both spider and silkworm fiber spinning which are conducive to the formation of highly oriented, crystallized fibroins.

12. The importance of chemical and physical processing conditions in determining orb-spider silk mechanics.

Prior to this study, there was little hard data available related to the importance of micro-environment or physical draw in determining supra-molecular crystallinity and physical properties of any silks. The experiments outlined in Chapter 4 of this thesis were designed to test the hypothesis:

"Orb-spiders control the supra-molecular organization and mechanical properties of their silks through specific chemical and/or physical processing strategies".

Ecribillate *A. diadematus* FL silk is a unique material that has allowed for the experimental evaluation of the importance of both chemical and physical processing conditions in the lab.

12.1. The influence of chemical micro-environment on the supra-molecular organization and physical properties of the FL silk.

In the orb-web, the FL fibroin network is subject to a distinct chemical micro-environment provided by an interpenetrating glue coating that contains water, glycoproteins, free amino acids and several water soluble low molecular weight (LMW) compounds (Vollrath et al. 1990). ^{13}C NMR spectroscopy has been used to demonstrate that the mobility of the FL silk fibroins depends on the presence of water (Bonthrone et al. 1992). When FL silk is subjected to dessicating conditions, the fibroins appear to become locked in the glassy state. These data strongly support the prediction that FL fibroin network micro-environment influences its supra-molecular organization and mechanical properties. I chose to examine the effects of removing the aqueous glue coating from the FL silk by using a simple water wash\dry process. The results will show that processed FL fibers exhibit a change in optical properties that is indicative of an increase in supra-molecular organization and possibly an increase in crystallinity. The mechanical properties of the Group-C native FL silk were also dramatically altered by processing to a material that shows high initial modulus, lower extensibility behavior. The high initial modulus indicates that either that the mobility of amorphous FL network component is dramatically reduced as it underwent a glass-phase transition on drying, and/or that new supra-molecular crystal structure develops with the processing manipulation. The fibroin sequences present in the FL fibroin network were predicted to retain an amorphous conformation and a high degree of mobility in the native state because of the presence of a micro-environmental 'plasticizer' that may function either by 1) recruiting water molecules from the atmosphere which in turn hydrate the FL silk network, 2) by interacting directly with the network and/or 3) by creating free volume to permit mobility of the native FL networks fibroin constituents.

12.2. The influence of physical draw on the supra-molecular organization and physical properties of the FL silk.

To test the hypothesis that, like many other flexible chain polymers, supra-molecular crystallinity and mechanical properties of orb-spider silk depends on specific physical draw processing conditions, the native FL silk was subjected to water wash\draw\dry manipulations using several processing draw-ratios. The optical properties of the processed FL fibers indicate an increase in supra-molecular organization that suggests either an increase in alignment of amorphous sequences along the fiber axis, alignment of pre-existing crystal structure along the fiber axis and/or the creation of new crystal structure with increased processing draw ratio. The mechanical properties of the native FL silk fibers were also dramatically altered by draw processing, following the general trend of increased ultimate strength, increased stiffness and decreased extensibility with increased draw processing. It is suggested that orb-spiders may use specific draw processing regimes in the wild to tune the properties of their silks.

13. Concluding remarks.

This thesis provides, for the first time, clear experimental evidence for the importance of both 1) the genetic control of the chemical composition and sequence designs present in orb-spider silks and 2) the importance of processing conditions in determining supra-molecular organization and/or network mobility. Both of these factors are apparently key to determining the physical properties of the orb-spiders rich repertoire of mechanically distinct silks.

CHAPTER 2

ARANEUS DIADEMATUS SILK GENES ARE PART OF AT LEAST ONE FIBROIN GENE FAMILY.

INTRODUCTION

Prior to this study there were only two silk fibroin genes cloned from any spider. These are partial cDNAs from the Golden Orb Weaver *Nephila clavipes* which encode reiterated modules with the peptide sequences that were shown in Figure 1.14 of Chapter 1. The signature of these spider silk fibroins are reiterated modules that contain crystal forming poly(alanine) blocks 8-10 residues long and amorphous glycine rich blocks ~ 25-40 residues long. The reiterated NCF-1 module contains a crystal forming poly(alanine) block 7 residues long and a glycine rich repeat with the sequence GGAGQGGYGGLGSQGAGRGGLGGQG. The reiterated NCF-2 module contains a poly(alanine) domain 8-10 residues long and a glycine rich domain that is also rich in proline and glutamine. The modules shown in Figure 1.14 are reiterated throughout the known protein sequence with only minor substitutions or deletions up to a 78-100 residue non-silklike COOH-terminal domain.

Both ncf genes were cloned from the MA gland of *N. clavipes*, and as such there was no information available on the sequence designs of fibroins from different glands which give rise to mechanically distinct silks (please note that, by convention, the lower case fibroin name, eg. ncf, is used to refer to is used to the fibroin gene while the upper case, eg. NCF, is used to refer to the fibroin protein. Table 1.3 showed that different silks from the same spider species have very different amino acid compositions, and this indicates that distinctions in their basic peptide designs occur, which could explain, at least in part, the differences in physical properties for different silks. To test this hypothesis I chose to examine the peptide sequences present in three silks whose mechanical properties span the spectrum of those observed for the orb-weaving spider *Araneus diadematus.* cDNA libraries were constructed from the MA, CY and FL glands. To date I have cloned 5 distinct partial fibroin cDNAs. All 5 *A. diadematus* genes and both *N. clavipes* genes were found to encode large modules of silk-like sequences which contain variable proportions of crystal forming domains and amorphous glycine-

rich domains. Four of the five encoded *A. diadematus* fibroins, both *N. clavipes* fibroins and protein sequence encoded from a small polymerase chain reaction product from the related orb-weaver *Araneus bicentenareus* were also found to contain a non-silk-like 78-108 residue COOH-terminal homology domain. The similarity in the internal modular organization of the encoded spider silk sequences and the occurrence of a COOH-terminal homology domain in 7 of the 8 known spider fibroins indicates that many of the fibroin genes maintain a common phylogenetic ancestor and are therefore part of a fibroin gene family. This chapter documents the structural organisation of the newly revealed *A. diadematus* fibroin genes and the proteins they encode. With the limited data available, possibilities for the molecular phylogenetic origins of the spider fibroin genes are discussed.

The proteins that the spider fibroin genes encode have similar peptide repeat motifs, however, there appeared to exist sufficient variation in the proportion crystal forming blocks that silk gland-specific expression could afford the orb-spider the potential to modulate the degree of crystallinity in its different silk types. Chapter 3 is a direct continuation of this chapter, where the tissue expression localities of the 5 genes cloned in this study are examined. In that chapter it is concluded that the physical properties of *A. diadematus* silks are determined at least in part through gland-specific regulation of the fibroin genes.

MATERIALS AND METHODS

1. Silk gland dissections.

Orb-weaving *A. diadematus* spiders were collected from the U.B.C. endowment lands and sacrificed in the lab by severing the cephalothorax with a scalpel. The abdomen was then held in place on plasticine in a petri dish with insect pins. A circular incision was made around the spinnerets, the whole abdomen was immersed in spider Ringers solution (Work, 1977), and one sagittal incision and two medial incisions were then made on the spider's ventral side. The entire gland-spinneret complex was then teased away from the abdominal tissue and floated intact in the spider Ringers solution. Glands were identified, isolated, and immediately placed in a 0.5 ml microfuge tube and frozen in liquid nitrogen for subsequent RNA extraction.

2. cDNA Library Construction and Screening.

5μg poly-A+ RNA was purified separately from 100 MA, FL and CY glands with the Micro-Fast Track™ mRNA isolation kit (Invitrogen). cDNA libraries from MA, FL and CY glands were generated with Stratagene's ZAP-cDNA® synthesis kit according to the manufacturers instructions. cDNAs were ligated into the UNI-ZAP™ XR vector and packaged and propagated in Gigapack® II Gold phage. The libraries had an mRNA transcript representation of ~ 10^6 plaques per μl of phage. They were then amplified by plating 2 x 10^5 plaques on 10 40× 40 cm square NZY plates (Maniatis, 1983). The plaques were grown to the size of a pin head, then 10 ml of SM phage dilution buffer (Maniatis, 1983) was poured on top of the plates. These were incubated overnight at 4 °C with gentle shaking, and the amplified library was retrieved in the SM solution and stored at - 70 °C with 10 % DMSO (Maniatis, 1983).

The cDNA libraries were screened in three separate rounds, each to the tertiary level at low

stringency (42°C, 0.01 % SDS, 1 × SSC), with α^{32}-P-dCTP random labeled oligonucleotides. In the first round, MA and FL libraries were screened with 3 oligonucleotides whose design was based on NCF-1 and 2 crystalline and amorphous domains (Table 2.1). In the second round, the FL library was screened with a probe encoding a GGPGGPGG module predicted to occur in FL silk simply based its heavy amino acid bias of 44% glycine and 21% proline (see Tables 1.3 and 2.1). In the third round, the CY library was screened simultaneously with the NCF-1 crystalline domain probe and a synthetic oligonucleotide probe designed to target a highly conserved sequence block found to occur within the COOH-terminal domain of ADF-2 to 4, NCF-1 and 2 and ABF-1 (see Results and Table 2.1).

In addition to the three specific screening rounds, 20 phage plaques from the MA library and 12 phage plaques from the FL library were selected at random, and their plasmids were isolated and sequenced. This was done to obtain a general estimate of the representation of silk clones in the amplified libraries with respect to all other cDNAs present.

Putative silk clones were cored from tertiary screening plates and pBluescript® phagemids containing cDNA inserts were excised *in vivo* from the UNI-ZAP™ XR vector into *E. coli* SOLR™ cells with the filamentous Exassist™ helper phage (Stratagene). The pBluescript plasmids were purified from SOLR™ cultures with the Qiagen™ miniprep DNA purification system. Because the silk genes are so repetitive, DNA sequence walking was not possible. Complete sequence from each of the selected partial cDNAs was therefore obtained by generating nested deletions (Promega erase-a-base system™) and sequencing a single strand of the appropriate sized fragments with the automated Applied Biosystems nucleic acid sequencer (Nucleic Acids Processing System, U.B.C.). The sequences were then linked into continuous, partial cDNA sequences.

Table 2.1.

Sequences of synthetic oligonucleotide probes used to screen *A. diadematus* MA, FL and CY gland cDNA libraries (lower case). The amino acid sequences these probes would encode are listed below each oligonucleotide sequence (upper case).

NCF-1

gca	gca	gca	gca	gca	gca	gca
A	A	A	A	A	A	A

NCF-1

gga	gga	gca	gga	caa	gga	gga	tat
G	G	A	G	Q	G	G	Y

NCF-2

gga	gga	tat	gga	cca	gga	caa	caa
G	G	Y	G	P	G	Q	Q

Putative ADF-FL silklike repeat

gca	gca	cca	gca	gca	cca	gca	gca
G	G	P	G	G	P	G	G

COOH-terminal Identity Sequence Block

tct	gga	tgt	gat	gca	ctt	gtt	caa
S	**G**	**C**	**D**	**A**	**L**	**V**	**Q**

3. Sequence analysis.

Sequence alignment, restriction mapping, codon usage predictions (see Appendix 2), amino acid composition, and protein hydrophilicity indices were obtained using the MacVector genetic manipulations program.

RESULTS

The results presented here describe the gene and protein sequence of five distinct *A. diadematus* silk fibroins. The criteria used to initially qualify a cDNA as a spider silk fibroin gene prior to complete sequencing were: 1) encoded proteins with poly(alanine) and/or glycine rich silklike repeat sequences and 2) expression of these genes in only silk gland tissues, as determined by Northern analysis. For convenience the gene and protein structural analysis in this chapter have been separated from the expression analysis in Chapter 3. It is noted, however, that the work was simultaneous, such that all five *A. diadematus* genes discussed below are, in fact, expressed in silk gland tissue and not in a control spider visceral tissue.

1. A. diadematus fibroin genes.

In the first screening round the NCF probes identified approximately one in twenty plaques as putative silk clones in each of the MA and FL libraries (~2% of plaques). Twenty clones from each library were sequenced from 5' and 3' ends and four unique partial *A. diadematus* fibroin (adf) cDNAs were identified. adf-1 is a 1.2 kb fragment which appeared only in the MA library screen, adf-2 is a 1.0 kb fragment which appeared in the MA library, adf-3 is a 2.0 kb fragment which appeared in both MA and FL libraries and adf-4 was a 1.4 kb fragment which also appeared only in the MA library. Nested deletions were generated for adf-1 to 4, and appropriate sized deletions were sequenced and linked.

Of the twenty random clones selected from the MA library no silk-like sequences were observed. 16 of the clones encoded what were classified as 'housekeeping' proteins and 4 clones were classified as junk sequence with no discernable open reading frame.

In the second screening round the 'GGPGGPGG' probe revealed a single silk-like cDNA, adf-

5, from the FL library (0.95 kb). Sequence from 12 randomly picked clones from the FL library revealed the same cDNA species 2 more times. 8 of the randomly selected clones were classified as housekeeping proteins and 2 as junk sequence. Complete sequence from the small adf-5 clone was obtained simply by linking extended 5' and 3' sequencing runs.

The third screening round on the CY library revealed adf-2 and two additional distinct partial cDNAs, which were tentatively named adf-6 and 7. The protein sequences that these two cDNA fragments encode are presented in Appendix 1. Complete sequencing and expression analysis of these putative fibroin genes will be performed at a later date.

The 5 distinct, partial, *A. diadematus* silk cDNA sequences are presented in figures 2.1 to 2.5. (The sequences are all from the 3' end of the genes because the first strand cDNA synthesis was primed with an oligo-dt primer). The clones contain characteristic Guanine and Cytosine rich repeats that encode corresponding silk-like amino acid repeat modules, at least one translational stop site (caps, bold italics), a poly-adenylation signal (bold underlined), distinct UTRs ~100 to 130 nucleotides long, and poly-A tails of lengths varying from 15 to 19 nucleotides.

2. Encoded A. diadematus fibroins.

The proteins encoded by adf-1 to adf-5 were named ADF-1 to ADF-5. The silk-like sequences for these fibroins are presented in figures 2.6 to 2.10. In general, these proteins consist of reiterated modules 9 to 68 amino acid residues long which contain crystal forming poly(alanine) and/or poly(alanine-glycine) domains in addition to amorphous glycine-rich domains. It is noted that secondary structural modelling of fibrous peptide repeats with programmes designed mainly for globular proteins provides limited and possibly confusing results, and it remains unclear at this point what secondary structure, if any, the glycine rich regions adopt. Throughout this thesis the glycine-

Figure 2.1.

Complete nucleotide sequence from the partial 1.2 kb adf-1 cDNA.

```
   1 gcacgagtct agttatgctg ctgctatggc tgcatctacg agaaattcag actttatccg
  61 aaacatgtct tatcaaatgg gaagactgtt atcgaatgcc ggtgcgatta ctgaaagtac
 121 tgcctcgtct gctgcgtcca gtgcctcttc tacagtaact gaaagtataa gaacttatgg
 181 acctgccgca atctttagtg gagctggagc aggagccggt gtgggtgtag gaggtgctgg
 241 cggatacggc caaggctacg gggctggagc tggtgctggg gcaggtgcag gtgcaggagc
 301 aggtggtgct ggaggatatg gccaaggcta tggtgccgga gctgcagcag cggctggtgc
 361 tggagctgga gctgcaggag gatatggagg cggcagtggt gctggagctg gaggtgccgg
 421 tggatatggc caaggctacg gogctggatc tggagcaggc gcaggagctg ctgcagcggc
 481 tggtgctagt gctggagctg caggaggata tggaggagga gctggtgtag gcgcgggagc
 541 aggagcaggt gctgcaggtg gatatggcca aagctacggc tctggagctg gagctggagc
 601 aggtgccggg gctgcagcag cggctggcgc aggagcaaga gctgcaggtg gatatggagg
 661 aggctacggt gctggagctg gtgcaggagc tggcgcagcg gctagtgctg gagcttcagg
 721 aggatatgga ggaggatatg gaggaggagc tggtgcaggt gccgtcgcag gagcttcagc
 781 cggttcatat ggaggtgctg tcaatcgctt gtctagtgct ggagctgcaa gtagagtatc
 841 ttctaatgtt gcagctattg cctctgctgg tgccgccgcc cttcccaatg taatttcaaa
 901 tatttactca ggtgtcctta gttcgggtgt ttcttctagt gaagctctga ttcaagctct
 961 gttggaagtg atttctgcac ttattcatgt attaggcagt gcctctatcg gtaatgttag
1021 ctcagtagga gtaaacagtg cattgaatgc tgttcagaat gcagttggcg catatgcagg
1081 gTAAttcaga TGActctgta agaatataaa ttggaccttt tttagaTAAc tgctatattt
1141 ttatgaatat atctatTAAt tccaaataaa ttttgcatgt cttgaaaaaa aaaaaaaaa
```

Figure 2.2.

Complete nucleotide sequence from the partial 1.0 kb adf-2 cDNA.

```
  1 ggttcccaag gagctggtgg agccggacaa ggtggatatg gagctggagg aggaggtgcc
 61 gcagcagccg cagcggcagc cgtaggagca ggaggcggag gacaaggagg cttgggttct
121 ggtggtgccg gacaaggata cggtgccgga ttaggtggac aaggtggagc ttctgcagcc
181 gcagcagcag ccggtggaca aggaggtcaa ggaggtcaag gcggatatgg aggattaggt
241 tcccaaggag ctggtggagc aggacaatta ggatatggag ctggacaaga aagtgccgca
301 gcagccgcag cggcagccgg aggagcagga ggcggaggac aaggaggctt gggtgctggt
361 ggtgccggac aaggatacgg tgccgccgga ttgggtggac aaggaggagc aggacaaggt
421 ggaggttctg gagccgcagc agcagccggt ggacaaggag gacaaggcgg atatggagga
481 ttaggtcccc aaggagctgg tggagccgga caaggaggat atggaggagg tagtttgcaa
541 tatggtggac aaggtcaagc acaagctgca gcagcctctg ccgcagcatc gcgcctttct
601 tctccaagtg ctgctgctag ggtctcatct gccgtatctt tggtatctaa tggtggacca
661 actagtcctg cagctttatc aagttctatt agcaatgttg tttctcaaat tagcgctagt
721 aaccctggtc tttcgggatg tgacattctt gttcaagcat tacttgaaat tatttccgcc
781 ttggtacaca ttcttggatc tgctaatatt ggtccagtta actctagttc ggctggtcag
841 tcagcttcaa ttgtcgggca gtctgtatac cgagctttgt ctTAAgaaac ttattcaatc
901 tctcttttgt taatttcttt aattcagatg ttcagtataa tttctttgaa ataaaatttt
961 gcatgattga aaaaaaaaaa aaaa
```

Figure 2.3.

Complete nucleotide sequence from the partial 2.0 kb adf-3 cDNA.

```
   1 gcacgagccg gatctggaca acaaggaccc ggacaacaag gacccggaca acaaggaccc
  61 ggacaacaag gaccatatgg acccggtgca tccgccgcag cagcagccgc tggaggttat
 121 ggacccggat ctggacaaca aggacccagc caacaaggac ctggccaaca aggacccggt
 181 ggtcaaggac catatggacc cggtgcatcc gccgccgcag cagccgctgg tggatatgga
 241 cccggttccg gacaacaagg accaggaggt caaggaccat atggacctgg ttcatccgct
 301 gccgcagcag ccgctggagg taatggaccc ggatctggac aacaaggggc cggtcaacaa
 361 ggtcctggac aacaaggacc cggtgcatcc gccgccgcag cagccgctgg aggatacgga
 421 cccggatctg gacaacaagg acccggacaa caaggaccag gaggtcaagg accatatgga
 481 cctggtgcat ccgccgctgc agcagccgct ggaggatacg gacccggatc tggacaagga
 541 cccggacaac aaggaccagg aggtcaagga ccatatggac ccggtgcatc cgctgcagca
 601 gcagccgctg gaggttatgg acccggatct ggacaacaag gacccggaca acaaggacct
 661 ggacaacaag gacccggtgg tcaaggacca tatggacccg gtgcatccgc cgccgcagca
 721 gccgctggag gatacggacc cggttatgga cagcaaggac caggacaaca aggaccagga
 781 ggtcaaggac catatggacc tggtgcatcc gccgcctcag cagcctctgg aggatacgga
 841 cccggatctg gacaacaagg acccggacaa caaggacctg gaggtcaagg accatatgga
 901 cctggtgcat ccgccgcagc agcagccgct ggaggttatg gacccggatc tggacaacaa
 961 ggaccaggcc aacaaggacc cggtcaacaa ggacctggac aacaaggacc cggtggtcaa
1021 ggaccatatg gacctggtgc atccgccgca gcagcagccg ctggaggtta tggacccgga
1081 tctggacaac aaggacccgg tcaacaagga cccggtcaac aaggacccgg tcaacaagga
1141 cccggtcaac aaggacccgg ccaacaagga cccggtcaac aaggacccgg ccaacaagga
1201 cctggtcaac aaggtcccgg tggtcaaggg gcatatggac ctggtgcatc cgccgcagca
1261 ggagccgctg gaggttatgg acccggatct ggacaacaag gacccggaca acaaggaccc
1321 ggacaacaag gacccggaca acaaggaccc ggacaacaag gacccggaca acaaggaccc
1381 ggacaacaag gacccggaca acaaggacca tatggacctg gtgcatccgc cgcagcagca
1441 gccgctggag gttatggacc cggatctgga caacaaggac ccggccaaca aggacctgga
1501 caacaaggac ccggtggtca aggaccatat ggacctggtg cggcttctgc agctgtatct
1561 gttggaggat atggaccaca aagctcctcg gttcctgttg catcagcagt cgcttctcgc
1621 ctttcttctc cagcggccag ttctagagtt tcatcggctg tatcatcttt ggtatctagt
1681 ggacctacta agcatgctgc actttctaat actatcagta gcgttgtatc gcaagttagt
1741 gcaagtaatc ctggtctttc tggttgcgat gtacttgttc aagcattgct cgaagttgta
1801 tcggccctgg tatctatcct tggatcttct agtatcgggc aaattaacta tggtgcctct
1861 gctcagtaca cccaaatggt aggtcaatct gtagctcaag cccttgctTA AtaccgtTAA
1921 atgattTGAa aattcttttc aatattaata tgacatattt gcatatttgt aatctttctc
1981 aataaattgt gaagcatatt aaaaaaaaaa aaaaaaaaa
```

Figure 2.4.

Complete nucleotide sequence from the partial 1.4 kb adf-4 cDNA.

```
   1 gcaggatctt cagcagcagc ggccgcggca gcaagtggat ctggaggata cggacctgaa
  61 aaccaaggac catctggacc tgtagcatat ggacctggtg gacccgtatc ttcagctgca
 121 gcagcagccg ctgcaggaag tggacctggt ggatacggac ctgaaaacca aggaccatct
 181 ggacccggag gatatggacc tggtggttcc ggatcttcag cagcagcagc agccgctgca
 241 gcaagtggac ctggaggata tggacctgga agccaaggac catctggacc tggtggatcc
 301 ggaggatatg gtcccggaag ccaaggggca tctggacctg gtgggcctgg tgcatctgcg
 361 gcagcagcag cagcagccgc tgcagcaagt ggacctggag gatatggacc tggaagccaa
 421 ggaccatctg gacctggagc atatggacct ggtggacccg gatcttcagc tgcagcagca
 481 gccgctgcag caagtggacc tggaggatat ggacctggaa gccaaggacc atctggacct
 541 ggagtatatg gacctggtgg acccggatct tcagctgcag cagcagccgc tgcaggaagt
 601 ggacctggtg gatacggacc tgaaaaccaa ggaccatctg gacccggagg atatggacct
 661 ggtggttccg gatcttcagc agcagcagca gccgctgcag caagtggacc tggaggatat
 721 ggacctggaa gccaaggacc atctggacct ggtggatccg gaggatatgg tcccggaagc
 781 caaggggggat ctggacctgg tgcatctgcg gcagcagcag ccgctgcagc aagtggacct
 841 ggaggatatg gacctggaag ccaaggacca tctggacctg gatatcaagg ccctagtggt
 901 cctggagcat atggcccatc tccttctgct tccgcatccg ttgcagcctc tgtttatctt
 961 cgcctgcagc ctcgtctaga ggtgtcttcc gctgtatcgt ctttagtgtc tagcggacct
1021 acgaatggtg ctgctgtttc tggagctttg aatagtttag tatctcagat tagtgcaagt
1081 aatccaggtt tatcgggatg tgatgctctt gtgcaggcat tattggaatt agtgtctgct
1141 cttgtggcaa ttctttcatc tgcaagtatt ggccaagtca acgtcagctc tgttagtcag
1201 tcaactcaaa tgattagcca agctctttca taaacacttg gtaaaatata gtcgtcTAGt
1261 tcaaatgagt ttgtattgaa attcatttgt aatttttatT GAaatgtatt cccaagtatg
1321 aatttaataa attgttgatt gcaagtttaa aaaaaaaaaa aaaaa
```

Figure 2.5.

Complete nucleotide sequence from the partial 0.9 kb adf-5 cDNA.

```
  1 ggaccaggtg gtgccggacc ttatggacca ggtggtgccg gcccttatgg accaggcggt
 61 gtaggaccag gtggagccgg accttatgga ccaggaggag aaggtggcgc aggaccaggt
121 ggagccggac cttatggacc aggcggagca ggagttggtc caggaggagc acctggatct
181 ccaggaggtc caggtggacc aggaggacca ggcggaccag gaggagctgg gccttatgga
241 ccaggcggag taggacccgg tggagccgga acttatggac caggcggagt aggaccaggt
301 ggagctggac cttttggacc aggaggacca ggtggaccag gtggcgcagg accggaagaa
361 ggagagggtc ccgtaacagt agacgtcgaa gtaaatgttg gaggttcacc aggaggagga
421 ccagttggcg taggaccagg cggagtagga ccaggaggag taggaccagg tggagctgga
481 ccttatggac caggcggtgt aggaccagga ggagccggac cttatggacc aggcggagca
541 ggagtctcca gcggcgctgg tggaatccgt ggtggacaaa catacggtgg atcatctagg
601 cttccatctt tggtgaacgg actgatgggc tctatgcaac aatccggatt taattatcag
661 aacttcggaa atgttatgtc tcagtacgcc acagggtccg gaacatgcaa cagtaacgat
721 gtgaatctgc tgatggacgc gcttatggcg gctttgcact gcctgtctta cggatccggt
781 tctgttccgc ctactccgac ttattctgcg atgtctgcct acaaccagtc tatccgtaga
841 atgtttgcat atTAAggctc tcttctgtac ctgaattatg atataaaatt ccttatgttg
961 ttaaatgtaa ttgcaatcaa taaagtgtga aatataaaaa aaaaaaaaaa a
```

Figure 2.6.
Predicted silk-like amino acid sequence of the ADF-1 protein.

[1]GGYGQGYGAGAGAGAGAGAGGA[24]
[25]GGYGQGYGAGAAAAAGAGAGAA[46]
[47]GGYGGGSGAGAGGA[60]
[61]GGYGQGYGAGSGAGAGAAAAAGASAGAA[88]
[89]GGYGGGAGVGAGAGAA[104]
[105]GGYGQSYGSGAGAGAGAGAAAAAGAGARAA[134]
[135]GGYGGGYGAGAGAGAGAAASAGAS[158]
[159]GGYGGGYGGGAGAGAVAGASAGSYGGAVN[187]

Figure 2.7.

Predicted silk-like amino acid sequence of the ADF-2 protein.

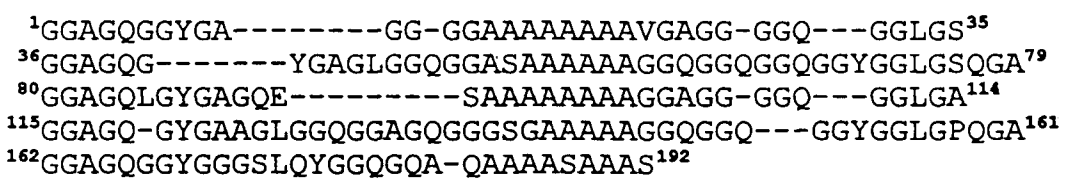
1GGAGQGGYGA--------GG-GGAAAAAAAAVGAGG-GGQ---GGLGS35
36GGAGQG-------YGAGLGGQGGASAAAAAAGGQGGQGGQGGYGGLGSQGA79
80GGAGQLGYGAGQE---------SAAAAAAAAGGAGG-GGQ---GGLGA114
115GGAGQ-GYGAAGLGGQGGAGQGGGSGAAAAAGGQGGQ---GGYGGLGPQGA161
162GGAGQGGYGGGSLQYGGQGQA-QAAAASAAAS192

Figure 2.8.

Predicted silk-like amino acid sequence of the ADF-3 protein.

[1]GPGQQGPYGPGASAAAAAAGGYGPGSGQQGPSQQGPGQQ[39]
[40]GPGGQGPYGPGASAAAAAAGGYGPGSGQQ[68]
[69]GPGGQGPYGPGSSAAAAAAGGNGPGSGQQGAGQQGPGQQ[107]
------[108]GPGASAAAAAAGGYGPGSGQQGPGQQ[133]
[134]GPGGQGPYGPGASAAAAAAGGYGPGSGQ-GPGQQ[166]
[167]GPGGQGPYGPGASAAAAAAGGYGPGSGQQGPGQQGPGQQ[205]
[206]GPGGQGPYGPGASAAAAAAGGYGPGYGQQGPGQQ[239]
[240]GPGGQGPYGPGASAASAASGGYGPGSGQQGPGQQ[273]
[274]GPGGQGPYGPGASAAAAAAGGYGPGSGQQGPGQQGPGQQGPGQQ[319]
[320]GPGGQGPYGPGASAAAAAAGGYGPGSGQQGPGQQGPGQQGPGQQGPGQQGPGQQGPGQQGPGQQGPGQQ[388]
[389]GPGGQGAYGPGASAAAGAAGGYGPGSGQQGPGQQGPGQQGPGQQGPGQQGPGQQGPGQQGPGQQGPGQQ[452]
[453]GP-----YGPGASAAAAAAGGYGPGSGQQGPGQQGPGQQ[486]
[487]GPGGQGPYGPGAASAAVSVGGYGPQS[512]

Figure 2.9.
Predicted silk-like amino acid sequence of the ADF-4 protein

[1]GSSAAAAAAAA--SGSGGYGPENQGPSGPVAYGPGGP[35]
[36]VSSAAAAAAA--GSGPGGYGPENQGPSGPGGYGPGGS[70]
[71]GSSAAAAAAAA--SGPGGYGPGSQGPSGPGGSGGYGPGSQGASGPGGP[116]
[117]GASAAAAAAAAAASGPGGYGPGSQGPSGPGAYGPGGP[153]
[154]GSSAAAAAAAA--SGPGGYGPGSQGPSGPGVYGPGGP[188]
[189]GSSAAAAAAA--GSGPGGYGPENQGPSGPGGYGPGGS[223]
[224]GSSAAAAAAAA--SGPGGYGPGSQGPSGPGGSGGYGPGSQGGSGP[266]
[267]GASAAAAAAAA--SGPGGYGPGSQGPSGPGYQGPSGP[301]

Figure 2.10.
Predicted silklike amino acid sequence of the ADF-5 protein.

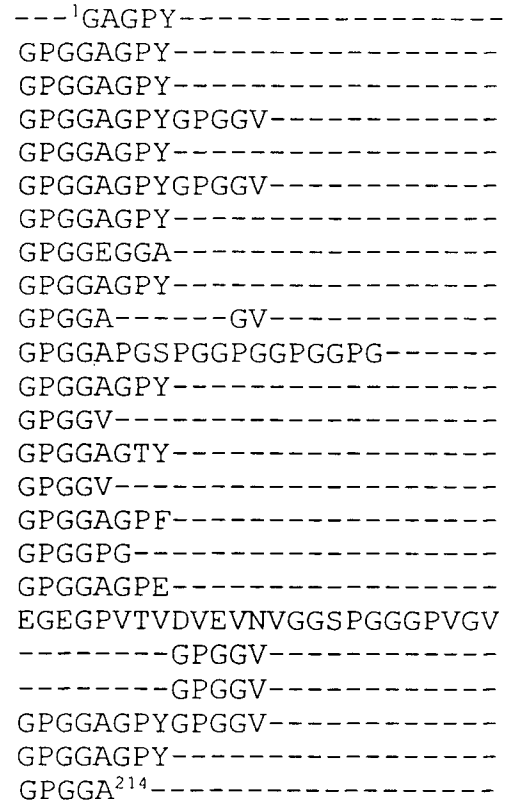
---[1]GAGPY----------
GPGGAGPY----------
GPGGAGPY----------
GPGGAGPYGPGGV----------
GPGGAGPY----------
GPGGAGPYGPGGV----------
GPGGAGPY----------
GPGGEGGA----------
GPGGAGPY----------
GPGGA------GV----------
GPGGAPGSPGGPGGPGGPG------
GPGGAGPY----------
GPGGV----------
GPGGAGTY----------
GPGGV----------
GPGGAGPF----------
GPGGPG----------
GPGGAGPE----------
EGEGPVTVDVEVNVGGSPGGGPVGV
--------GPGGV----------
--------GPGGV----------
GPGGAGPYGPGGV----------
GPGGAGPY----------
GPGGA[214]----------

rich sequence blocks will be referred to as amorphous components, although solid state chemistry may soon reveal that many of the glycine-rich sequences present in spider silk fibroins actually direct the formation of helices, β-turns or other secondary structures.

The conserved silk-like modules are reiterated throughout the known sequence of the fibroins up to 78-108 residues before the COOH-terminal end of each protein. Figure 2.6 shows that ADF-1 is comprised of reiterated modules with crystal forming poly(alanine) blocks 5 residues long, crystal forming poly$(GA)_n$ (n=2-7) blocks similar to those crystal forming GAGAGS blocks in *B. mori* silk, and glycine rich amorphous blocks consisting of GGYGQGY or GGYGGGY heptapeptides. Figure 2.7 shows that ADF-2 is comprised of reiterated modules that contain crystal forming poly(alanine) blocks 4-8 residues long and amorphous glycine rich GGAGGQGGY and GGQGGQGGQGGYGGLGSQGA sequences. ADF-3 is comprised of reiterated modules that contain crystal forming poly(alanine) blocks 8-10 residues long and amorphous repeat blocks of GPGGQGPYGPG, GGYGPGS $(GPGQQ)_n$ (n= 1 to 8) (Fig. 2.8). ADF-4 is comprised of reiterated modules that contain crystal forming ASAAAAAA blocks and amorphous repeat blocks of GPGSQGPS and GPGGY (Fig. 2.9). ADF-5 is very distinct from the other cloned spider fibroins. It contains no crystal forming poly(alanine) sequences and is comprised almost entirely of amorphous GPGGAGPY and GPGGAGPYGPGGV sequences (Fig. 2.10).

3. The COOH-terminal homology domain of spider fibroins.

The COOH-terminal sequences from ADF-1 to ADF-5, NCF-1 and 2 and ABF-1 are aligned and compared in Figure 2.11. It is clear that a high degree of identity is maintained between 7 of the 8 known spider COOH-terminal fibroin sequences (ADF-1 to 4, NCF-1 and 2 and ABF-1). Table 2.2 is an identity matrix for the same domain with strict identity represented in the lower left half of the

Figure 2.11.

COOH-terminal domain identity for the known spider fibroins. The COOH-terminal amino acid sequences of ADF-1 to 5, NCF-1 and 2, and ABF-1 are aligned and compared. Asterisks denote amino acids that are conserved in at least six of the eight sequences. The conserved cysteines are shown in bold type.

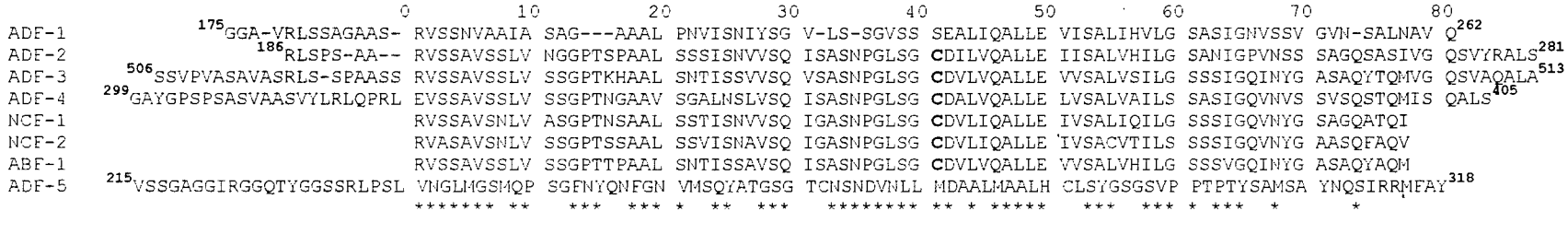
0 10 20 30 40 50 60 70 80
ADF-1 175GGA-VRLSSAGAAS- RVSSNVAAIA SAG---AAAL PNVISNIYSG V-LS-SGVSS SEALIQALLE VISALIHVLG SASIGNVSSV GVN-SALNAV Q262
ADF-2 186RLSPS-AA-- RVSSAVSSLV NGGPTSPAAL SSSISNVVSQ ISASNPGLSG CDILVQALLE IISALVHILG SANIGPVNSS SAGQSASIVG QSVYRALS281
ADF-3 506SSVPVASAVASRLS-SPAASS RVSSAVSSLV SSGPTKHAAL SNTISSVVSQ VSASNPGLSG CDVLVQALLE VVSALVSILG SSSIGQINYG ASAQYTQMVG QSVAQALA513
ADF-4 299GAYGPSPSASVAASVYLRLQPRL EVSSAVSSLV SSGPTNGAAV SGALNSLVSQ ISASNPGLSG CDALVQALLE LVSALVAILS SASIGQVNVS SVSQSTQMIS QALS405
NCF-1 RVSSAVSNLV ASGPTNSAAL SSTISNVVSQ IGASNPGLSG CDVLIQALLE IVSALIQILG SSSIGQVNYG SAGQATQI
NCF-2 RVASAVSNLV SSGPTSSAAL SSVISNAVSQ IGASNPGLSG CDVLIQALLE IVSACVTILS SSSIGQVNYG AASQFAQV
ABF-1 RVSSAVSSLV SSGPTTPAAL SNTISSAVSQ ISASNPGLSG CDVLVQALLE VVSALVHILG SSSVGQINYG ASAQYAQM
ADF-5 215VSSGAGGIRGGQTYGGSSRLPSL VNGLMGSMQP SGFNYQNFGN VMSQYATGSG TCNSNDVNLL MDAALMAALH CLSYGSGSVP PTPTYSAMSA YNQSIRRMFAY318

Table 2.2.

COOH-terminal identity matrix for the spider fibroins. Identity was calculated over a 78 residue sequence identity stretch in the COOH-terminal domain of the spider fibroins. The COOH-terminal domain of the ADF-5 fibroin had no identity with any of the other spider fibroin COOH-terminal sequences and so it is excluded from the identity matrix. The stippled portion of the matrix denotes strict identity, the remainder show functional identity with conservative amino acid substitutions.

	ADF-1	ADF-2	ADF-3	ADF-4	NCF-1	NCF-2	ABF-1
ADF-1		69	63	65	63	65	65
ADF-2	47		81	83	85	79	86
ADF-3	44	68		82	87	85	95
ADF-4	40	68	72		82	82	82
NCF-1	44	74	78	70		87	87
NCF-2	42	69	73	67	81		86
ABF-1	44	71	91	71	74	76	

matrix and conservative amino acid substitution identity represented in the upper right portion of the matrix. These data can provide a crude index of the phylogenetic relatedness of these fibroins. Of the COOH-terminal domains compared, between 40 and 91 % strict identity and 63 to 95 % functional identity exists (ADF-5 is not included in the matrix since its COOH-terminal domain was found to maintain no homology with any other known spider fibroins). The ADF-1 COOH-terminal domain is the most distinct of those compared in Table 2.2, showing 40 to 47 % strict identity and 63 to 67 % functional identity with the other spider fibroins. The ADF-3 COOH-terminal domain shows a very high identity with the ABF-1 COOH-terminal domain, with 91 % strict identity and 95 % functional identity in this region.

The function of this COOH-terminal homology domain is not known at this time. Interestingly, 6 of the 8 COOH-domains contain a highly conserved cysteine residue (Fig. 2.11 :**bold**). This may represent an inter and or intra-fibroin disulfide linkage site. Figures 2.12 and 2.13 are hydrophilicity plots for the COOH-terminal domains of ADF-1 to 5, NCF -1 and 2 and ABF-1. All except ADF-5 exhibit near identical charge profiles. This may indicate that certain regions of this domain are potentially important for cell signalling or for protein-protein interactions. These possibilities will be addressed in the Discussion section of this chapter.

Figure 2.12.

Hydrophilicity plots of the COOH-terminal domain of ADF-1 to 4. (The charge scale is Kyte -Doolittle).

ADF-1

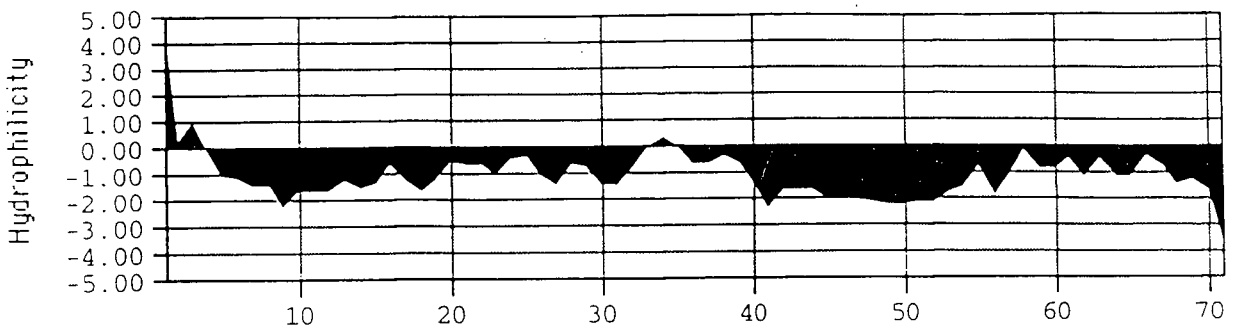

ADF-2

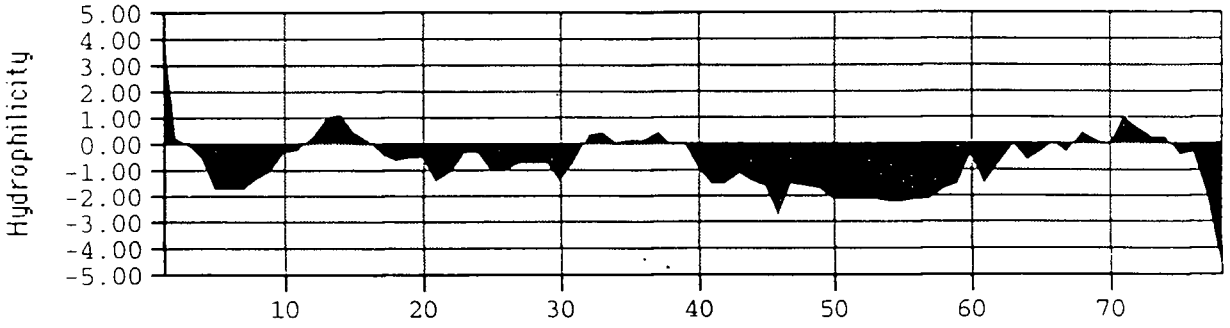

ADF-3

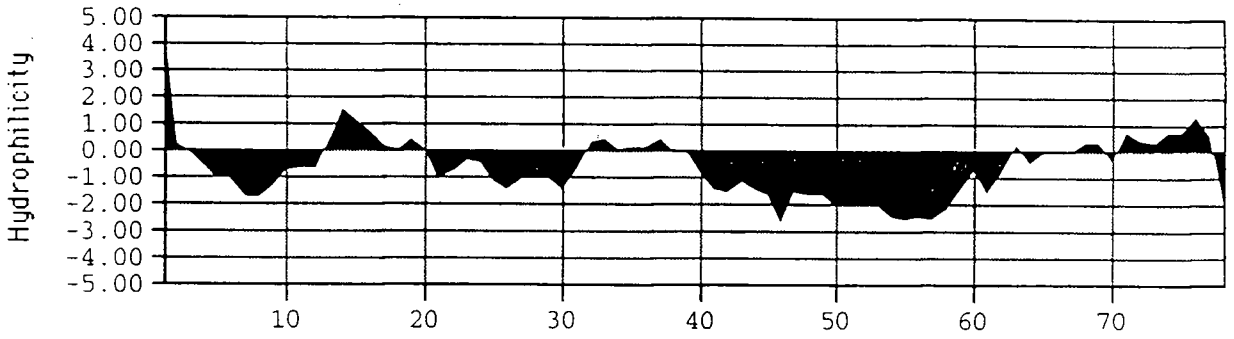

ADF-4

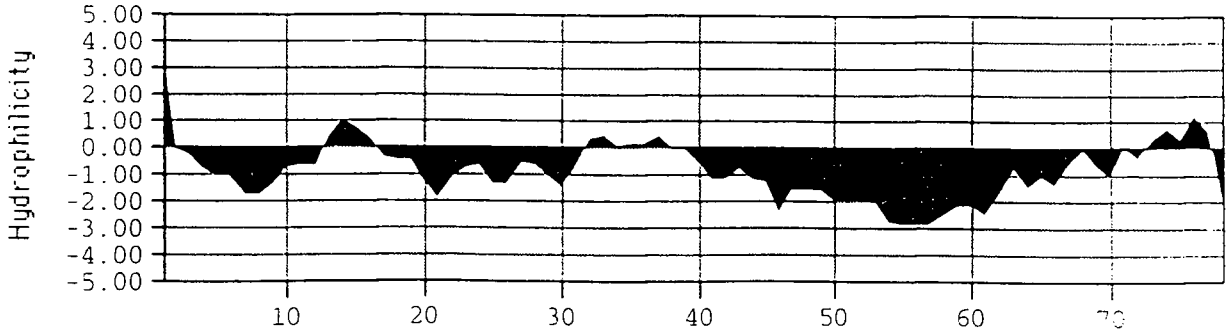

Figure 2.13.
Hydrophilicity plots of the COOH-terminal domain of ADF-5, NCF-1 and 2 and ABF-1.

ADF-5

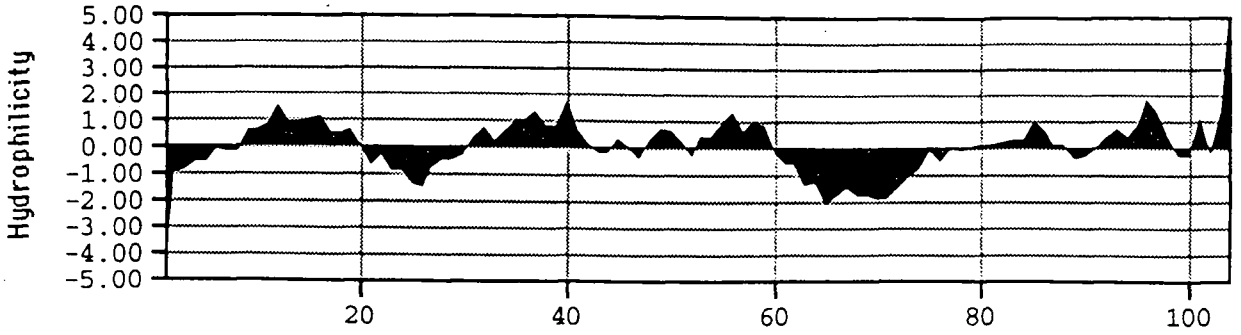

NCF-1

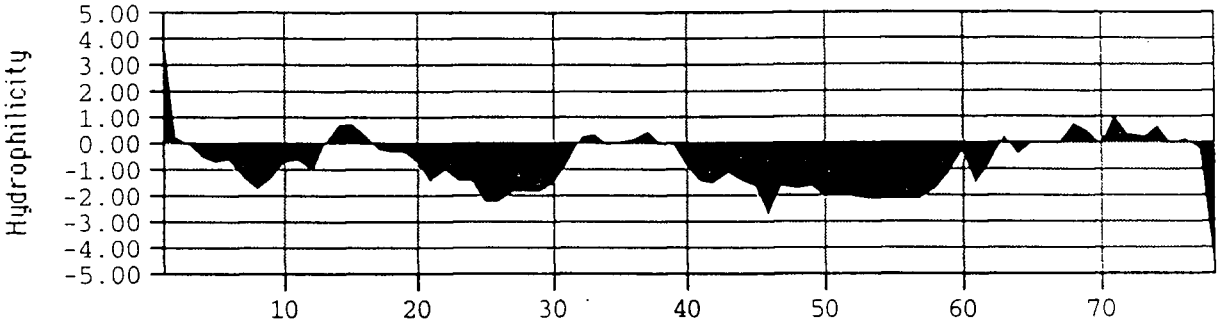

NCF-2

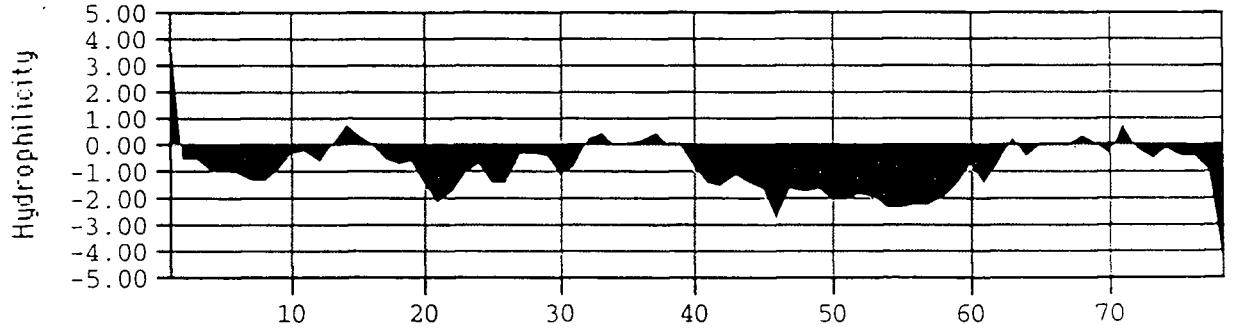

ABF-1

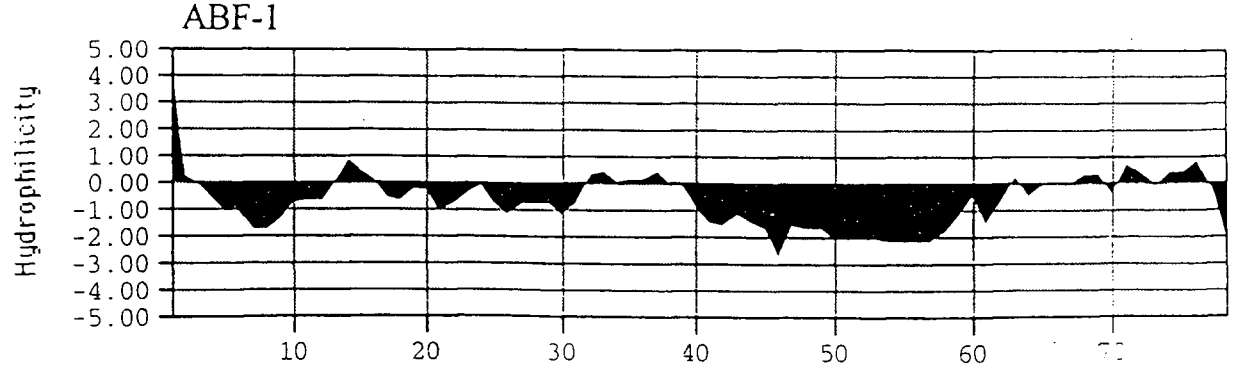

DISCUSSION

1. 7 of the 8 known spider fibroin genes are part of a gene family.

The Results section of this chapter included data on the isolation of five partial silk cDNA clones from the spider *A. diadematus*. These genes and 2 other spider fibroin genes from *N. clavipes* all encode similar reiterated modules which contain sequences of both crystal forming poly(alanine) and/or poly(alanine-glycine) blocks, and/or amorphous glycine-rich blocks. With the exception of ADF-5, all of the known spider fibroins contain a COOH-terminal homology domain. Together these results indicate that at least 7 of the 8 known spider silk fibroins are part of a gene family.

adf-2 to 4, ncf-1 and 2 and abf-1 appear to be closely related. This conclusion is based on the similarities in the modular arrangement of crystal forming and amorphous blocks they encode, and at least 67 % direct homology in their encoded COOH-terminal domains. Due to the limited amount of data available at this time, it is difficult to make detailed inferences on the inter or intra-species relatedness of these seven spider fibroin genes. This difficulty is compounded by the fact that there are several parameters from which relatedness may be inferred. These include the structural organisation of the encoded proteins, the degree of identity between their COOH-terminal domains, and the use of very specific amino acids within the glycine rich domains.

adf-3 and 4 and ncf-2 appear to be more closely related to one another than to the other spider fibroin genes because the fibroins they encode contain similar sized crystal and amorphous domains, they have high COOH-terminal domain identity, and their glycine rich sequence blocks contain proline, a residue which is absent from the other known fibroins with the exception of ADF-5.

While adf-3 and ncf-2 appear to be closely related, particularly based on the proline content of their encoded proteins, ADF-3 actually has higher COOH-identity with NCF-1 than NCF-2, so it is clear that the criteria available to establish fibroin gene relationships may be contradicting. The only

sequence available from ABF-1 is from its COOH-terminal domain. It maintains very high identity with the COOH-terminal domain of ADF-3, and this may indicate that these fibroins are species homologues.

adf-2 and ncf-1 appear to be closely related. Their encoded proteins have similar sized crystal and amorphous blocks, high COOH-terminal domain identity, and their glycine-rich regions are both devoid of proline, but contain leucine, a residue absent from the other known spider fibroins.

adf-1 is very distinct from the other fibroin genes. It encodes crystal forming sequences which are more similar to the *B. mori* heavy chain fibroin than to all the spider fibroins, and its COOH-terminal domain has at best 47 % direct identity with all the other known fibroins.

The most distinct of all the known spider fibroins genes is adf-5. The COOH-terminal domain it encodes maintains no identity with the other fibroins, and the hydrophilicity profile of this domain is distinctly different from all the other fibroins (Fig. 2.13). In addition, its encoded silk-like sequences are completely devoid of crystal forming poly(alanine) or poly(alanine-glycine) blocks. The GPGGAGPYGPGGV repeat bears similarity to the amorphous sequences which comprise the elastomeric structural protein elastin. It will be demonstrated in Chapter 3 that the adf-5 transcript is expressed to detectible levels in only the FL gland, which produces the elastomeric viscid silk. The fact that there are large distinctions between ADF-5 and all of the other known spider fibroins suggests that adf-5 represents the first member of novel and distinct elastomeric fibroin gene family. In the future, the COOH-terminal domain from ADF-5 may be used as a probe to retrieve other related members from this second putative gene family.

The conclusions drawn above regarding the relatedness of the spider fibroins are based on preliminary data. More precise molecular phylogenetic clades will only become available when genomic sequencing reveals potential similarities in regulatory sequences and intron-exon organisation

of the known spider fibroins, and additional efforts are made to obtain fibroin gene sequences from both related and more distant spider species.

In addition to the major conclusion that 7 of the 8 known fibroin genes are part of the same gene family, detailed study of the peptide design of the COOH-terminal domain, the modular organisation of the fibroin genes and proteins, and codon usage patterns within the fibroin genes may provide insights into the cellular mechanisms important in silk synthesis and possibly clues on the molecular origin of the first silk gene.

2. The COOH-terminal homology domain of the spider fibroins.

The function of the highly conserved spider fibroin COOH-terminal homology domain is presently not known. It is possible that the highly conserved cysteine residue, which occurs in ADF-2, 3 and 4 as well as NCF-1 and 2 and ABF-1, is important for inter or intra-fibroin disulfide cross-linking. It has recently been demonstrated that the major protein constituent of *N. Clavipes* dragline is broken down from a ~ 700 k Da fragment to two ~ 320 k Da bands under reducing conditions (O'Brien, personal communication). (Also, the transcript sizes revealed from Northern blot analysis in Chapter 3 predict individual fibroins in the 300 k Da range). The amino acid composition of the *N. clavipes* dragline silk indicates that only trace amounts of cysteine are present. Taken together, this information suggests that the cysteine residue within the COOH-domain may be involved in linking two fibroin molecules together. It may be speculated that sequences flanking the cysteine residue create a molecular stalk which makes the sulfide of the cysteine side chain accessible for cross-linking with other cysteine side chains. Another intriguing possibility is that the conserved hydrophobic sequences that flank the cysteine residue are a BiP or Disulfide isomerase binding domains. These proteins may assist in the formation of the disulfide linkage. In the future it may be possible to address

this question with *in vitro* Yeast 2 hybrid system and Immunoprecipitation experiments.

3. Modular organisation of fibroins.

Six of the seven available fibroin genes and the *B. mori* heavy chain fibroin genes are now known to contain nucleotide repeats which encode one or two highly conserved reiterated modules. How did this modular gene structure arise? One possibility is that fibroin gene structure arose through exon shuffling. In contrast with ancient protein genes, there is unquestionable evidence for a major role of exon-shuffling in the modular assembly of many proteins, a process which is now known to be unique to animals and widely used in the creation of multi-domain proteins (Patthy, 1994). The modular assembly of many structural proteins, including to name a few, collagen types V , VI, VII, IX, XI, XII, and XIV, fibrillin, twitchin and titin, has previously been demonstrated (Patthy, 1994; Labeit and Kolmerer, 1995) . The genomic sequence of these modular proteins can betray their mode of construction by showing intron-exon boundaries which match protein domain boundaries. However, since the exon-intron pattern of modular protein genes is a result of a continuous interplay between intron insertion and removal, the genomic organisation may not necessarily reflect the pattern that existed at the time of assembly. Therefore, it may be erroneous to look at introns as assembly points.

The phase distribution of the intronic splice sites can provide additional clues on the origins of a protein's modular assembly. Modular proteins that develop through exon shuffling must have identical intronic splice sites in order that the module be placed in frame with its adjacent module. Interestingly, most modular proteins and almost all extracellular modular proteins contain phase 1-1 intronic splice sites. That is, the introns at both 5' and 3' boundaries always split the reading frame between the first and second nucleotides of a codon. More accurate predictions on the evolutionary

assembly processes of silk fibroin genes will soon be possible when genomic sequencing reveals the specifics of the intron/exon organisation and the location of their intronic splice sites.

The silk fibroin genes all contain repetitive elements very similar to Alu and microsatellite sequences which occur throughout the eukaryotic genome. It is possible that the primordial silk gene arose from a translocation or retro-transposition event that brought these nucleotide repeat sequences into a coding region. These sequences are similar to recombination hot spots observed for many other genes (MacDonald et al. 1994) so that the repetitive super-structure of the fibroins genes may have arisen by continual unequal cross over events (gene slippage) or by duplication, tandem duplication, insertion and/or deletion of a primordial repetitive fibroin gene sequence over time (Mita et al. 1988).

4. Codon usage and codon pattern bias.

A detailed examination all of the available fibroin genes indicates that codon usage is skewed for the high abundance amino acids of each of the fibroins. The data also indicates that codon usage patterns are conserved between modules of the same fibroin. This information may offer important insights into the molecular mechanics behind the rapid and efficient synthesis of the fibroin products by the silk glands. Appendix 2 includes all the codon usage data and a preliminary prediction that an observed pattern of codon bias may determine mRNA structure which could in turn regulate the translational pausing observed during *N. clavipes* and *B. mori* fibroin synthesis (Candelas et al. 1983). This issue is worth addressing since translational pauses have been predicted to be important for fibroin folding and processing in the cell.

5. Concluding remarks.

Four of the five spider fibroin genes cloned in this study and three others from different orb spider species were found to be members of the same gene family. The proteins they encode contain variable proportions of crystal forming poly(alanine) and/or poly(glycine-alanine) blocks, such that tissue specific regulation of expression of these genes could offer the spider the potential to control the physical properties of its different silks. In Chapter 3 I proceed with Northern expression analysis in order to test this hypothesis.

CHAPTER 3

THE MECHANICAL PROPERTIES OF *A. DIADEMATUS* SILKS ARE DETERMINED BY GLAND-SPECIFIC EXPRESSION OF MEMBERS FROM AT LEAST ONE ORB-SPIDER FIBROIN GENE FAMILY.

INTRODUCTION

Chapter 2 presented strong evidence for the existence of at least one *A. diadematus* fibroin gene family. The genes I have isolated all encode reiterated modules containing different proportions of crystal forming poly(alanine) and/or poly(glycine-alanine) domains. The fibroin composition and hence crystal forming domain content of each silk secretion were formerly not known. However, it was hypothesized that silk gland-specific expression of the fibroin genes would offer the orb-spider the potential to modulate fiber crystallinity by controlling the precise fibroin composition of distinct glandular secretions. This hypothesis was tested by probing a Northern blot containing total RNA isolated from each of the seven *A. diadematus* silk glands with unique probes created from restriction fragments from each of the adf cDNAs. The results presented in this chapter demonstrate the occurrence of gland-specific expression patterns for each of the five fibroin genes isolated in this study. By combining the new data on the tissue specific expression localities of the adf genes and the amino acid composition of the silk-like repeats they encode with the published amino acid composition of *A. diadematus* silks, it was then possible to generate preliminary predictions of the fibroin composition and crystal forming domain content of MA, MI and FL silks. (This approach also provides partial information on the fibroin composition of the AG and CY silks). These preliminary predictions suggest that there is a large degree of variability in the crystal forming domain content between the different orb-spider silk gland secretions. However, the potential for these different secretions to crystallize under identical processing conditions has not been examined. Therefore, I determined the relative crystallization potential of the MA, MI, FL and CY secretions by subjecting them to identical shear conditions and then qualitatively evaluating the crystallinity of the shear products using polarized light microscopy. All four silk secretions were found to be differentially shear sensitive, and the degree to which each secretion shear crystallizes appears to correspond

roughly to the proportion of crystal forming poly(alanine) and\or poly(glycine-alanine) domains predicted to be present in each secretion type.

MATERIALS AND METHODS

1. Northern expression analysis of the adf transcripts .

Ten final instar *A. diadematus* spiders were collected from the U. B. C. endowment lands during September and October 1994, and the seven silk gland types were dissected from each spider according to the Methods outlined in Chapter 2. Total RNA was extracted separately from each gland type and a control visceral tissue according to the methods of Chomezynski (1986), using a micro-tissue homogeniser (Pierce Co.). 13±3μg (A_{260}) total RNA from each tissue type and a Gibco RNA ladder were electrophoresed in nine separate lanes. The ladder was then cut off and stained with ethidium bromide, and the rest of the gel was blotted, hybridized with a single adf probe, and washed at high stringency (0.01 × SSC, 0.01 × SDS, 65 °C) according to standard methods (Maniatis, 1983). The Northern blot was then autoradiographed for 24 hours at -70°C and developed. Prior to re-probing, the blot was stripped and exposed for 3 days to ensure complete removal of previous probes. Probes were obtained from the 3' most 180-250 nucleotides of the adf-1 to adf-5 clones by excising these fragments from the pBluescript plasmid with clone-specific restriction digests, and purifying the fragments from low melt agarose with the GeneClean™ DNA purification system. adf-1 and adf-2 were digested with SSP1 and Xho1, adf-3 with Xba and Xho1, adf-4 with DDE1 and Xho1, and adf-5 with Spe1 and Xho1. The purified fragments were random hexamer labeled with α- ^{32}P d-CTP. The nucleotide sequences of the probes generated are indicated in figures 2.2 to 2.7 (Chapter 2) in bold, these regions were chosen to include the 'unique' UTR sequence to minimize cross-hybridization to transcripts from related fibroin gene family members.

2. Shear crystallization experiments.

MA, MI, FL and CY glands were dissected from final instar *A. diadematus* spiders as is

described in the Methods section of Chapter 2. Glands were then placed on a microscope slide and washed with distilled water. Most of the water was then poured off by tilting the slide, and the remainder was dried from the ouside of the gland with a Kimwipe™. An incision was then made along one side of the gland to allow the aqueous silk secretion to flow onto the slide, after which the gland tissue was removed and discarded. Care was taken not to place the contents of the gland under load to avoid shear crystallizing the silk secretion prior to initiating the shear experiment.

The isolated secretions from MA, MI, FL and CY glands were subjected to a simple shear manipulation where a microscope cover slip was placed on top of the secretion and was sheared by pushing it along the slide with one finger. While the precise forces applied were not controlled, the experimentor was well practised at this push technique, and consistent results were obtained for each secretion type. The slide was then examined under plane polarised light, and the crystallinity of the sheared product was qualitatively evaluated, based simply on the brightness of the sample, which provided an indication of the birefringence of the sample sheared product and hence its relative crystal content. The texture of the shear product was also evaluated qualitatively.

RESULTS

1. Northern expression analysis of the adf transcripts and molecular weight predictions for their encoded proteins.

The Northern blot with lanes containing total RNA from each of the seven silk glands and a control spider visceral tissue was probed separately with the unique UTR sequence from each of adf-1 to adf-5 clones (Figs. 3.1-3.5). Gland-specific expression patterns are observed for all five of the adf transcripts tested. In several cases multiple bands appeared on the Northern blots upon probing with the adf UTR sequences. It is important to recognize that band multiplicity could reflect 1) expression of the same gene in different tissue types, 2) the occurrence of splicing variants of the same fibroin gene, 3) the occurrence of alternative transcriptional start sites in the cases where band doublets appear close together in the same lane or 4) cross-hybridization to closely related fibroin genes.

The molecular weights of the encoded full length ADFs were predicted by subtracting the 3' UTR sequence from the transcript sizes revealed in the Northern blots, and by using an average molecular weight of the amino acids contained in the predicted silk-like repeats of each partial ADF, assuming that like most other structural proteins these reiterated sequences occur throughout the entire length of the protein. The molecular weight of the COOH-terminal domain was calculated separately for each ADF and added to the predicted molecular weight of the silk-like protein sequence. The molecular weight predictions represent only very crude estimates. They were obtained to provide general estimates of the newly revealed fibroins and to emphasise that the fibroins are some of the largest proteins in all of biology. (Note that in the cases where multiple bands occur the predictions will obviously not hold if the additional bands represent cross-hybridization to different fibroin species with distinct amino acid composition).

Figure 3.1.

Northern blot containing 13 ± 3 μg total RNA from all seven *A. diadematus* silk glands and a control visceral tissue probed with the 3' restriction fragment of adf-3. b) the same blot probed with a control 1.4 kb *Caenorhabditis elegans* β-actin cDNA.

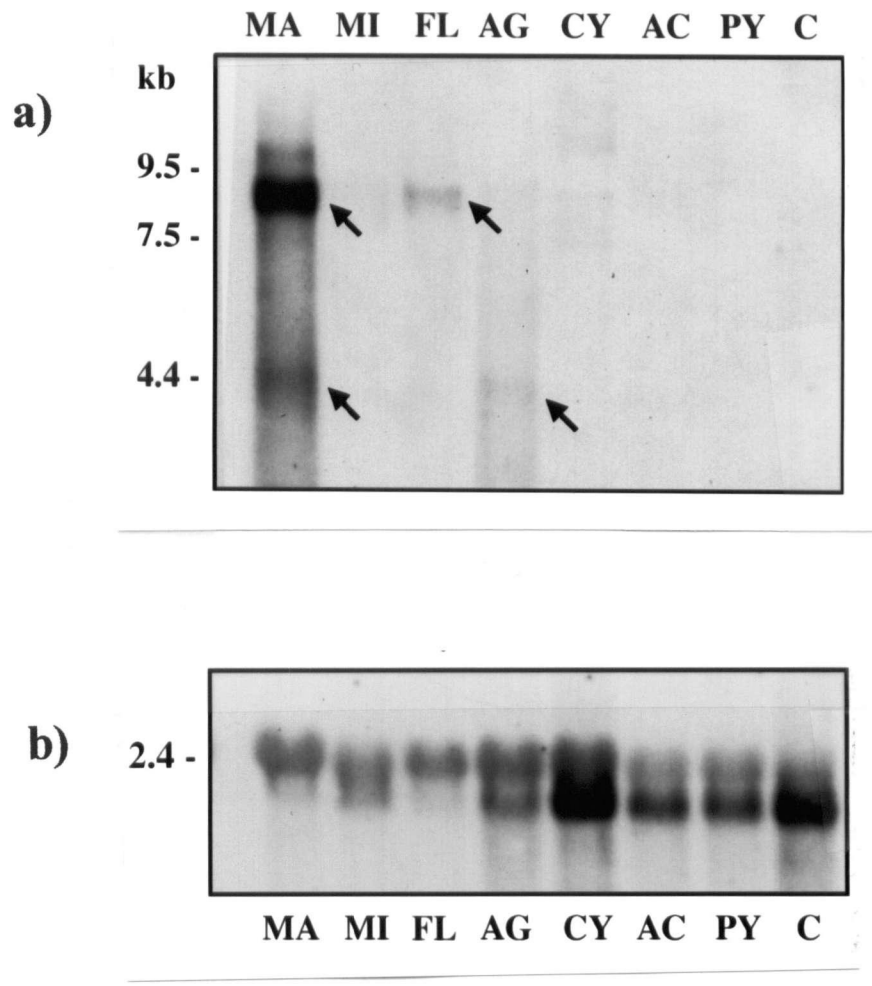
a)
MA MI FL AG CY AC PY C
kb
9.5 -
7.5 -
4.4 -
b)
2.4 -
MA MI FL AG CY AC PY C

Figure 3.2.

Northern blot containing 13 ± 3 μg total RNA from all seven *A. diadematus* silk glands and a control visceral tissue probed with the 3' restriction fragment of adf-4.

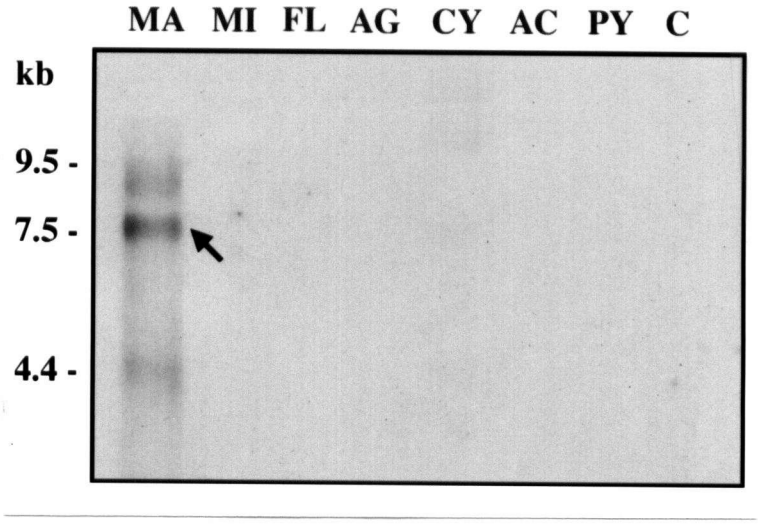
MA MI FL AG CY AC PY C
kb
9.5 -
7.5 -
4.4 -

Figure 3.3.

Northern blot containing 13 ± 3 μg total RNA from all seven *A. diadematus* silk glands and a control visceral tissue probed with the 3' restriction fragment of adf-1.

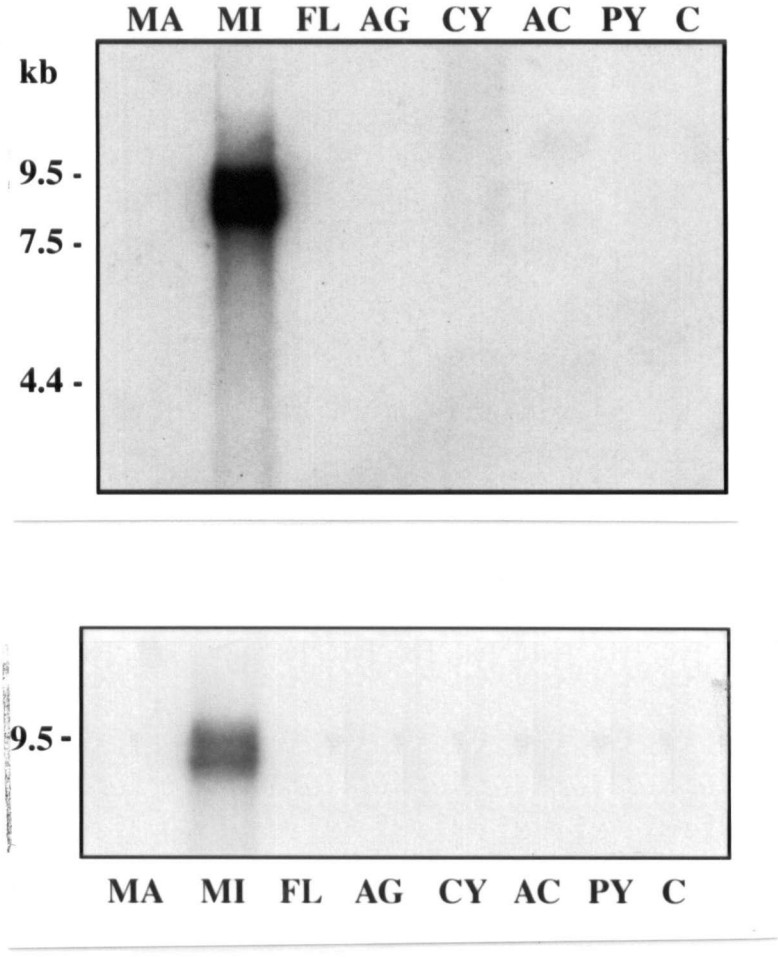
MA MI FL AG CY AC PY C
kb
9.5 -
7.5 -
4.4 -
9.5 -
MA MI FL AG CY AC PY C

Figure 3.4.

Northern blot containing 13 ± 3 μg total RNA from all seven *A. diadematus* silk glands and a control visceral tissue probed with the 3' restriction fragment of adf-2.

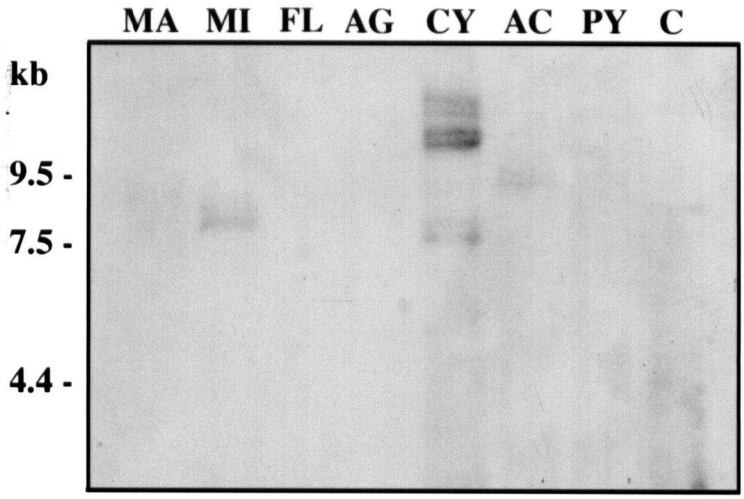
MA MI FL AG CY AC PY C
kb
9.5 -
7.5 -
4.4 -

Figure 3.5.

Northern blot containing 13 ± 3 μg total RNA from all seven *A. diadematus* silk glands and a control visceral tissue probed with the 3' restriction fragment of adf-5.

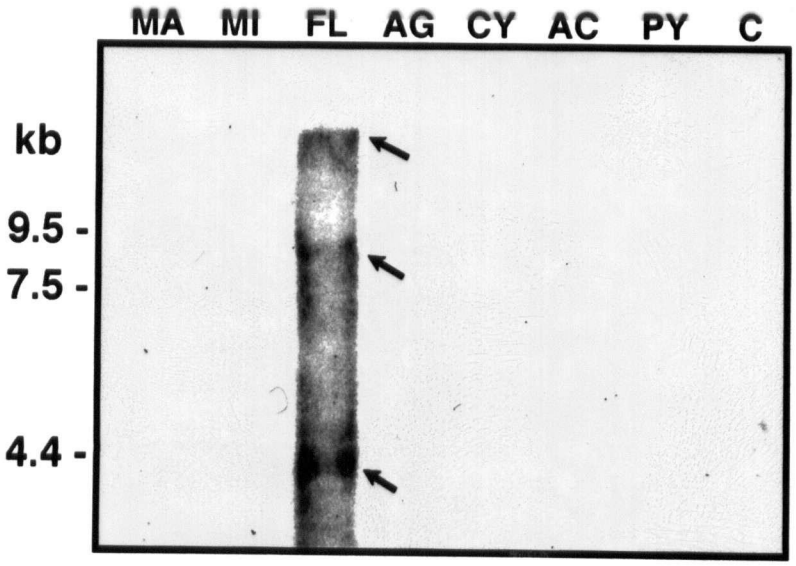
MA
MI
FL
AG
CY
AC
PY
C
kb
9.5 -
7.5 -
4.4 -

1.1. *Major Ampullate gland.*

Two of the five adf genes showed high levels of expression in the MA gland. Very high transcript levels occur for adf-3 at ~ 4.4 and ~ 9.5 kb (Fig 3.1a). (The same blot was probed with a control *C. elegans* β-actin cDNA to verify that similar amounts of total RNA were loaded in each lane Fig. 3.1b). The two adf-3 messages would translate into proteins about 1400 and 3000 amino acids long with predicted molecular weights of 150 kD and 310 kD respectively. adf-4 was also expressed at high levels in the MA gland, with a single transcript at ~ 7.5 kb (Fig. 3.2). The two bands at 4.4 and 9.5 kb are believed to result from cross-hybridization to the closely related adf-3 transcript. The ~ 7.5 kb transcript would encode a protein about 2500 amino acids long, with a predicted molecular weight of 240 kD.

1.2. Minor Ampullate gland.

Only one of the five adf genes was expressed in the MI gland. Very high transcript levels occur for adf-1 in the 9.0 to 9.5 kb range (Fig. 3.3a), and a short exposure of the same blot revealed two discrete bands at ~ 9 and ~ 9.5 kb (Fig. 3b). The adf-1 transcripts would encode proteins about 2800 and 3100 amino acids long with predicted molecular weights of 270 kD and 300 kD respectively.

1.3. Flagelliform gland.

Two of the five adf genes were found to be expressed in the FL gland (Figs. 3.1 and 3.4). adf-3 was expressed at low levels with a transcript at ~ 9.5 kb (Fig. 3.1). This message was also expressed in the MA gland, and its predicted length and size are listed above. adf-5 was expressed at high levels in the FL gland with transcripts at ~ 4.4, ~ 7.5 and ~ 11 kb. These transcripts would

encode proteins about 1500, 2500 and 3800 amino acids long with predicted molecular weights of 140, 290 and 360 kD respectively.

1.4. Aggregate gland.

Only one of the five adf genes isolated was expressed in the AG gland. adf-3 was expressed at low levels, with a transcript size of ~ 4.4 kb (Fig. 3.1). This message was also expressed in the MA and FL glands, and its encoded fibroin length and weight are predicted above.

1.5. Cylindrical gland.

Only one of the five adf genes isolated was expressed in the CY gland. adf-2 was expressed at moderate levels with three transcript doublets occurring at ~ 7, ~ 8, and ~ 9.5 kb (Fig. 3.5). These messages would encode proteins approximately 2500, 3900 and 4500 amino acids long with predicted molecular weights of 250 kD, 380 kD and 440 kD respectively.

1.6. Aciniform and Pyriform glands.

None of the adf probes hybridized in the AC or PY lanes.

1.7. Control.

None of the the adf probes hybridized to the control RNA purified from visceral tissue.

2. Shear crystallization experiments.

The shear crystallization sensitivity of four different silk gland secretions was examined. Figure 3.6 shows plane-polarized light pictures of shear crystallized MA, MI, FL and CY silk secretions. Photographs were taken at equal exposure times of 1/4 second (unless otherwise specified in the figure legend) to allow for a direct qualitative comparison of birefringence (brightness), and hence degree of crystal formation of the shear products. Each secretion type showed a qualitatively distinct shear crystallization sensitivity and shear product "texture".

2.1. Major Ampullate secretion.

The sheared MA silk secretion was moderate to highly crystalline, as indicated by its high brightness under plane-polarized light (Fig. 3.6a). It is much more crystalline than the FL shear product but less so than the MI and CY shear products. The sheared MA secretion had the most fibrous texture of the four tested, and the size of the observed fibers is similar to the MA fibers (spun by *A. diadematus* (ca. 1-2 μm)) .

2.2. Minor Ampullate secretion.

The MI shear product was highly crystalline (Fig. 3.6b). It was much more crystalline than the FL shear product, slightly more so than the MA shear product, and of roughly similar crystallinity to the CY shear product. This sheared secretion had a granular texture with some fibrous structure.

2.3. Flagelliform secretion.

The FL secretion was negligibly crystalline, as is indicated by a virtually black image when

Figure 3.6.

Shear crystallization sensitivity of a) MA, b) MI, c) FL (short exposure), d) FL (long exposure), e) FL (bright field), and f) CY silk secretions. (Scale bars ~5μm). All secretions were viewed under plane polarized light except e. Arrow=shear direction. All photographs were taken at an equal exposure time of 8 minutes except for d) which was at 8 minutes.

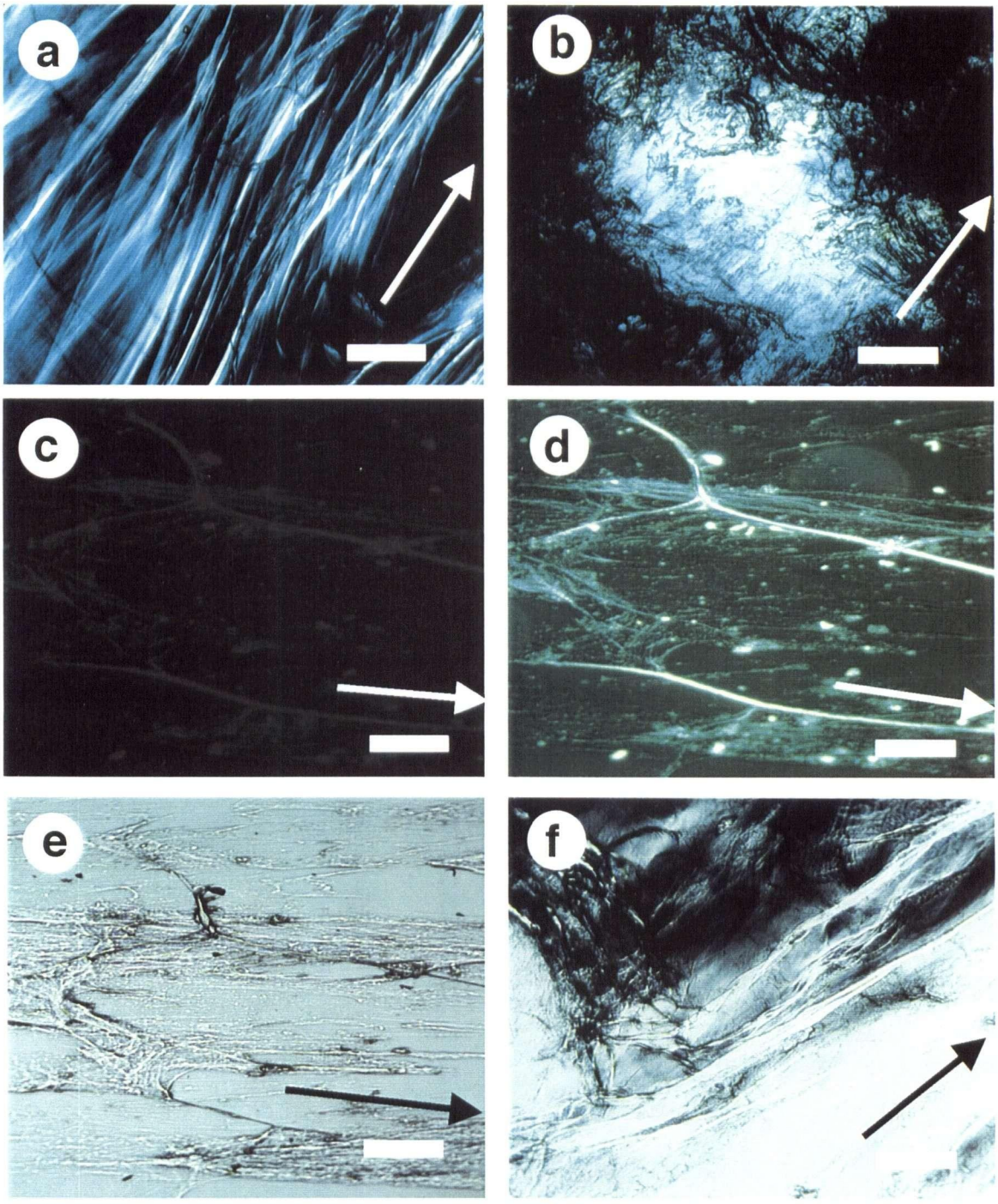
a
b
c
d
e
f

viewed with plane polarized light (Fig. 3.6c). A small amount of mildly crystalline fibrous material can be seen when this sheared product was photographed with a very long exposure time of 8 minutes (Fig. 3.6d). Figure 3.6e is a picture the same sheared FL product under bright field, showing that a substantial amount of the FL secretion was present in this experiment, but that it simply failed to shear crystallize.

2.4. Cylindrical secretion.

The CY shear product was highly crystalline (Fig. 3.6f). It had a comparable crystallinity to the MI shear product, it was more crystalline than the MA shear product, and much more so than the FL shear product. The CY sheared product had a smooth texture, with some fibrous structure.

DISCUSSION

Northern analysis demonstrated that silk gland-specific expression occurs for each of the five the adf genes isolated in this study. These results indicate that transcriptional regulation affords *A. diadematus* the capacity to produce a variety of gland-specific, compositionally distinct silk secretions with distinct supra-molecular crystallization potentials.

1. Transcriptional regulation of fibroin synthesis.

The molecular circuitry that regulates the spatio-temporal expression of spider fibroins remains to be elucidated, and this will only begin to be possible when genomic sequence including the promotor and its up and downstream sequence elements become available from several spider fibroin genes. Research on the molecular mechanisms of transcriptional regulation of the *B. mori* heavy chain fibroin gene is somewhat more advanced. Several sequence elements are known to be involved in expression enhancement of that silkworm silk gene. A sequence element located in the 5' flanking region from -238 to -73, called enhancer I (En I), is essential for tissue specific expression (Suzuki et al. 1986; Hui et al. 1989; Suzuki et al 1991). This sequence contains two octamer motifs, one at -202 to -194 and one at -191 to -183, that are very similar to some *Drosophila* homeodomain sequences. These sequence elements are bound by a 125 kD protein named fibroin factor 1 (FF1) in the presence of a second protein called fibroin factor 2 (FF2). If these octamer sequence elements are synthetically altered, binding of the FF1 protein fails to occur. There are two possibilities for the binding properties of the FF1 protein. The first is that FF1 contains a homeodomain in its amino acid sequence and binds to the octamer motifs (Suzuki et al. 1991). Homeobox proteins can act as potent transcriptional activators and may play a role in the activation of silk genes. The second possibility is that FF1 does not contain a homeodomain. FF1 has a molecular weight that is larger than other

known homeobox proteins, and it requires the cooperative binding of FF2 to act as a positive transcriptional activator, a characteristic not seen for other homeobox proteins studied. FF1 may in fact compete with homeobox proteins which could act as negative transcriptional regulators by binding the octamer motifs in En 1. *Drosophila* even-skipped protein is known to be a negative transcriptional regulator, and it binds the En 1 sequence. Therefore, there may exist as yet unidentified negative transcriptional regulators similar to the even-skipped protein in *B. mori* and in spider silk gland tissues.

Interestingly, octamer motifs are also found in the En II element that occurs between +156 and +454 in the first intron of the *B. mori* heavy chain fibroin gene. It has been hypothesised that if FF1 also binds in this region, a protein bridge could be created through an FF1-FF2-FF1 complex (Suzuki et al. 1991). Such a bridge, created through non-DNA binding of the FF2 protein could cause a torsion induced conformational change in the DNA surrounding the TATA box and initiation site, possibly rendering this region accessible to the transcription initiation complex.

While the formation of the En I-FF1-F2 complex has been shown to be specific to posterior silk gland tissues for *B. mori* (Susuki et al. 1991), the FF1 molecule occurs in other *B. mori* tissues. It may be that FF1 is specifically modified in silk gland tissues, allowing it to bind FF2. A cellular mechanism for silk-gland specific FF1 modification may be phosphorylation by a silk tissue specific kinase, which could itself be activated via a second messenger like cAMP.

There are probably several different cell signalling pathways that activate fibroin gene transcription in different orb-spider gland types. First, expression and spinning of some silks, like spider and silkworm cocoon silk, occurs at a very specific life history stage, and therefore the transduction signals that regulate the expression in the CY gland are likely instar-specific and hormonal. Second, there may be timing signals between cells of different spider silk glands during

web spinning. For example, it may be necessary to temporally couple the synthesis of FL and AG fibroins with MA fibroin production so that the former secretions are available to be spun at the time of completion of the frame and radii of the web. The MA and FL glands are in direct contact with one another and are at most three cell layers thick each, so that inter-glandular signalling may be possible. Thirdly, Candelas et al. (1990) have demonstrated that MA fibroin synthesis can be stimulated mechanically. When excessive amounts of the MA fiber are mechanically drawn from the orb-spider in the lab, *de novo* MA fibroin synthesis occurs. Candelas et al. (1990) predict that there are stretch receptors in the glandular epithelium, and when resting glandular tension becomes low, a signal transduction cascade is triggered to initiate the synthesis of additional MA fibroins. Conversely, when the CY silk is mechanically drawn, only a small amount of new CY fibroin synthesis is observed. The stretch receptor mechanism may therefore be essential to ensure that MA dragline silk is available to the spider at all times, while the regulation of the fibroin volume in the CY gland is apparently not as stringently coupled to volume based stretch receptors.

2. Differential splicing as a putative mechanism for fiber property control.

The adf-1, adf-2, adf-3 and adf-5 transcripts all exhibit at least two band sizes on hybridization with the probes from their respective 3' sequences. It may be hypothesized that an additional level of complexity of fiber property control exists through transcriptional splicing. The elastic PEVK element in the giant muscle protein titin is known to be differentially spliced in various tissues. This mechanism is believed to result in tissue specific mechanical properties (Swindell, 1996). In order to approach this question for orb-spider silks, it will be necessary to obtain adf genomic sequences to directly compare the intron\exon organisation with full length cDNA sequences obtained for the different transcript sizes.

3. Crystal forming domain content and shear crystallization of A. diadematus silks.

The predicted silk-like fibroin sequences from the partial adf-1 to 5 cDNAs constitute only about one tenth to one fifth of the very large full length fibroins. If however, it is assumed that these spider fibroins, like virtually all other fibrous proteins, contain similar structural motifs that are reiterated throughout virtually the entire length of the protein, then it is possible to combine preliminary ADF compositional data, Northern analysis expression data, and the published amino acid compositional data on the orb-spider silks to make predictions on the fibroin composition of several silks. Here, some of the major fibroin constituents of the MA, MI and FL silks are accounted for, and the proportion of crystal forming domains present in each of these silks is estimated.

The shear crystallization sensitivity of each of the secretions from the MA, MI, FL and CY glands appears to correspond roughly with the predicted crystal forming capacity of each of these secretion types. It is important to recognize, however, that the shear experiments represent only very preliminary findings. While the applied shear was likely equivalent in all cases, the chemical micro-environments of each secretion type may differ. As a result, the crystallization potential of each secretion type may not only be determined by crystal forming domain content of its constituent fibroins but also by the presence of other, as yet unidentified compounds.

3.1. Major Ampullate silk (Dragline).

adf-3 and 4 are both expressed at high levels in the MA gland (Figs 3.1 and 3.2). ADF-3 contains 21 % crystal forming, ASAAAAAA domains, and 79 % amorphous GPGGQGPYGPG, GGYGPGS and $(GPGQQ)_n$, (n = 1 to 8) domains. ADF-4 contains 27 % crystal forming SSAAAAAAAA domains, and 73 % amorphous GPGSQGPS and GPGGY blocks. Table 3.1 shows the amino acid composition data that was presented in Table 1.3 along with the compositions of the

Table 3.1

The amino acid composition of *A.didematus* silks (Andersen, 1970), and ADF-1 to ADF-5.

	MA	MI	FL	AG	CY	AC	PY	ADF-1	ADF-2	ADF-3	ADF-4	ADF-5
Aspartate	1	2	3	9	6	8	11	0	0	0	1	1
Threonine	1	1	2	8	3	10	4	0	0	0	0	2
Serine	7	5	3	7	28	16	15	5	4	6	17	6
Glutamate	11	2	3	10	8	8	10	2	11	18	3	0
Proline	16	-	21	11	1	3	8	0	1	15	16	17
Glycine	37	43	44	14	9	14	8	46	47	38	34	47
Alanine	18	37	8	6	24	11	10	37	27	17	22	9
Valine	1	2	7	6	6	7	5	1	1	1	1	6
Cysteine	-	-	-	-	-	-	-	0	0	0	0	0
Methionine	-	-	-	-	-	-	-	0	0	0	0	0
Isoleucine	1	1	1	5	2	4	4	0	0	0	0	1
Leucine	1	1	1	6	6	9	5	0	4	0	0	2
Tyrosine	4	5	3	2	1	2	2	9	4	5	5	5
Ph-ala	0	0	1	4	3	2	2	0	0	0	0	1
Lysine	1	0	1	7	2	2	9	0	0	0	0	0
Histidine	0	0	1	2	-	1	3	0	0	0	0	1
Arginine	1	2	1	3	1	4	4	1	0	0	0	1

silk-like sequences of each of the predicted partial ADFs. Individually, ADF-3 and ADF-4 fail to account for the known composition of MA dragline silk, however, an ADF-3:ADF-4 ratio of 3:2 matches the composition of the MA silk very closely. The combination of these two fibroins in a 3:2 ratio would give a material containing 25 % crystal forming domains. This value is consistent with the crystal content predicted for *A. diadematus* MA silk based on network models (Gosline et al. 1993) and is in agreement with the crystal content predicted from X-ray and NMR for *N. clavipes* (see Chapter 1). While it is possible that other, as yet uncloned adf genes encode additional dragline fibroins, the relatively extensive screen of the MA library yielded only the adf-3 and 4 genes.

The MA secretion shear product is highly crystalline but less so than the MI and CY secretions (Fig. 3.6). This qualitative result appears somewhat consistent with a material containing about 1/4 crystal forming domains compared to the MI and CY silks that both may contain as much as 3/4 crystal domains. Note that the shear product texture appears similar to the MA silk fibers spun by A. *diadematus*, and the dimensions of these fibers very closely matches that of the orb-spiders dragline.

3.2. Minor Ampullate silk (accessory fiber).

The 3' adf-1 fragment was the only probe that hybridized in the MI RNA lane. 68% of the silk-like sequence of ADF-1 occurs as crystal forming poly(alanine) domains 5 residues in length and $(GA)_n$ domains, where n =2-7. The remaining 32% of ADF-1 is occupied by amorphous GGYGQGY repeats. The composition of ADF-1 is almost a direct match with the known composition of the MI silk (Table 3.1). Therefore, ADF-1 is likely a major constituent of the MI fiber, and the MI secretion probably contains close to 70 % crystal forming sequence elements. *N. clavipes* MI silk may contain 2 fibroins that are similar in composition and sequence design to ADF-1 (Lewis, 1992). It is therefore

possible that other fibroins are present in the *A. diadematus* MI silk, but if they are to be major constituents, they must have a similar amino acid composition to ADF-1.

The sheared MI secretion appears to be more crystalline than the MA shear product and about equal to the CY shear product. This qualitative result seems consistent for a secretion whose major fibroin constituent contains a very high proportion (69%) of poly(alanine) and poly(glycine-alanine) crystal forming domains. The MI secretion crystallizes almost immediately, in the first 1-2 mm of the applied shear, and on further shearing the crystallised MI secretion 'blob' fails to draw into a fiber but instead rolls onto itself to give the granular texture seen in Figure 3.6.

3.3. Flagelliform silk (viscid silk).

adf-3 was expressed at low levels and adf-5 at high levels in the FL gland. As listed above for the MA gland, ADF-3 contains 21 % crystal domains and 79 % amorphous repeats. ADF-5 contains no crystal domains, with 100 % of the silk-like sequence present as blocks of glycine, proline and valine rich repeats that are similar to elastic protein sequence motifs seen in elastin (Rosenbloom et al. 1993). Table 3.1 shows that the composition of ADF-5 alone very closely approximates the known composition of the FL silk, indicating that ADF-5 is likely a major constituent of this silk. The sequence motifs present in ADF-5 may have a low capacity for β-sheet crystallization because of the predominance of proline, whose side chain reduces the linearity of the fibroin chain because its side chain links back to the main chain and creates kinks in the peptide backbone. Regularly placed prolines can allow for crystallization in structural proteins, as is the case of the three stranded collagen rope, however the ADF-5 prolines are not regularly spaced, and they likely impede crystal formation to some degree.

The sheared FL secretion was negligibly crystalline. This qualitative result is consistent for

a secretion with a major fibroin constituent that contains almost no crystal forming poly(alanine) or poly(glycine-alanine) domains. Some crystalline fibers can be observed for the sheared FL product with a very long photographic exposure (Fig. 3.6d), indicating that some of the fibroin sequences present in the FL secretion can crystallize to a small degree. The FL secretion may have a mild propensity to crystallize because of the presence of poly(alanine) domains of ADF-3 or other as yet unrevealed crystal forming fibroin sequences, but because of the close match of ADF-5 to the known FL composition, these must only be present in small proportions.

3.4. Aggregate silk (viscid silk glue).

AG silk is viscous and coats the core FL silk fibers in the orb-web, appearing as glue droplets on their surface. adf-3 was found to be expressed at very low levels in the AG gland, but the composition of ADF-3 does not match the composition of the AG silk (Table 3.1), and it is therefore likely that other AG fibroin genes remain to be cloned. In Chapter 4 additional chemical and physical factors that may influence crystallisation of the FL silk are investigated. It will become clear that the non-fibrous AG glue plays a key role in determining the mechanical properties of the fibrous FL silk.

3.5. Cylindrical silk (Cocoon Silk).

adf-2 is expressed at relatively high levels in the CY gland alone. The silklike repeats contain 19 % crystal-forming poly(alanine) blocks ~ 8 residues long and 81% amorphous GGAGQGGY and GGQGGQGGYGGLGSQGA sequence blocks that are similar to the sequences found in the elastomeric proteins elastin (Rosenbloom et al. 1993). The composition of ADF-2 alone fails to account for the known composition of *A. diadematus* CY silk, and it is likely that there remain other

CY proteins to be discovered. The multiplicity of bands observed in the expression analysis indicates either 1) that there are alternative transcriptional start cites for adf-2, 2) that adf-2 is alternatively spliced or 3) that cross-hybridisation to very closely related CY specific adf transcripts that have not yet been uncovered by the library screens. While the expression analysis of adf-6 and 7 remains to be done, they are candidates for constituents of the CY silk (see Appendix 1).

The sheared CY secretion appears more crystalline than the MA and FL shear products and somewhat similar to the MI shear product. This qualitative result indicates that the CY secretion contains fibroins with large proportions of crystal forming domains, as was shown to be the case for the MI secretion. The Northern expression analysis showed that adf-2 was expressed at moderate levels in the CY gland, but it only contains 19 % crystal forming domains and fails to account for the known CY silk composition. The ADF-6 protein shown in Appendix 1 contains as much as 70 % crystal forming AGAGAG and AAAA sequences and remains a candidate for a major fibroin constituent of the CY fiber. However, this sequence appears not to have enough serine in its composition to match the known composition of the CY fiber. Though it remains to be isolated, I predict that the major fibroin constituent of the CY silk will contain crystal forming AAAAAA, ASASAS and/or SSSSSS sequences, and that orb-spider cocoon silk contains β-sheet crystals containing a large proportion of serine residues.

The CY shear product differs from the MI shear product in that it has a smooth rather than granular texture. Apparently the CY secretion remains in the aqueous or liquid crystalline phase longer than the MI secretion, so that while under shear it spreads out smoothly rather than coagulating immediately. This may either be a result of differing constituent fibroin chain sequences or possibly different micro-environmental conditions that occur in the different gland types.

3.6. Aciniform and Pyriform silks (Swathing and Attachment silks).

None of the adf probes hybridized in the AC and PY lanes, indicating that other as yet unidentified adf genes remain to be cloned to account for the amino acid compositions of these two silks. It should be noted that with very long exposures of 1-2 weeks the adf-2 probe hybridized very weakly in both the AC and PY lanes, showing band doublets in the 9-10 kb range. These bands are likely a result of cross-hybridization to related adf transcripts with low identity. These provide a good starting point for cloning the AC and PY fibroins. These glands are very small, and it will likely be necessary to use genomic DNA or PCR based approaches to clone the fibroin genes from these tissues.

Concluding Remarks.

It is important to emphasize that the preliminary predictions on the fibroin composition of individual silk types provided above are inferred from genetic data. As such, it must be recognized that direct proof of the presence of specific fibroins within individual silk types is not possible at this time. While it would likely be extremely difficult and time consuming, it may possible to obtain more direct evidence by 1) dissolving individual silk types in harsh solvents (eg. hexafluoroisopropanol) 2) isolating specific fibroins under reducing conditions on a western blot, and 3) undertaking a peptide sequencing project. Given the limitations imposed by the peptide sequencing technology presently available, as well as the grave difficulty that will arise from sequencing through repetitive fibroin sequences, this approach appears to be unreasonable at this time. The conclusions, summarized below, are therefore drawn with the apparently reasonable assumption that if a specific fibroin gene is expressed in a specific gland tissue type, the protein it encodes likely comprises part of the fiber spun from that gland.

Northern blot expression analysis showed silk gland-specific expression patterns for all of the adf genes tested, and it was deduced that gland-specific transcriptional regulation determines distinct fibroin compositions for each *A. diadematus* silk secretion. It was possible to reasonably account for the fibroin composition of the MA, MI and FL silks, and to partially account for the fibroin composition of the AG and CY silks. Each secretion type was predicted to be of a different fibroin composition and crystal domain content and therefore to maintain a different shear crystallization potential under similar processing regimes. This prediction was supported by shear crystallization experiments which indicate that each secretion type tested was differentially shear sensitive and that the propensity towards crystallization corresponded roughly with the predicted crystal domain content of each secretion type.

Transcriptional regulation, therefore, provides the orb-spider with the potential to express and spin a variety of mechanically distinct silks. There remains much to be learned about the spider fibroin genes, the molecular mechanics of their regulation, and the precise fibroin composition of each distinct silk type. Possible experimental approaches to address these issues are offered in the Future Directions section of Chapter 5.

CHAPTER 4

SUPRA-MOLECULAR ORGANIZATION AND MECHANICAL PROPERTIES OF *A. DIADEMATUS* FL SILK ARE INFLUENCED BY CONDITIONS OF FIBER PROCESSING.

INTRODUCTION

Chapters 2 and 3 showed that, as is the case for high property semi-crystalline fibers like Cellulose, Kevlar, Spectra and Nylon, supra-molecular crystallization of spider silk depends intimately on the chemical sequence design of its constituent polymer chains. Orb-spiders express at least one family of fibroin genes differentially in their seven silk glands, allowing them to produce a variety of compositionally distinct glandular secretions that each have different crystallization potentials. Transcriptional regulation of genes encoding fibroins with different polymer chain chemistries, therefore, affords the orb-spider the potential to produce a variety of mechanically and functionally distinct silk types.

It was explained in Chapter 1 that the supra-molecular crystallinity, and hence the mechanical properties of fibrous polymers, depends on both polymer chain chemistry and the chemical and physical conditions to which the polymers constituent molecular chains are subjected when they are spun. In this chapter the effects of processing conditions on the supra-molecular crystallinity and mechanical properties of *A. diadematus* FL silk are investigated. This introduction summarizes the information presently available on the physical properties, supra-molecular organization, fibroin composition and the chemical micro-environment of the FL silk. It should become clear that FL silk is an exceptional material with characteristics that are ideal for investigating both chemical and physical factors that may influence supra-molecular crystallization during spinning.

1. The physical properties of MA and FL silks.

A comparative look at the mechanical properties of the MA and FL silks clearly indicates that these two fibers have very distinct mechanical properties. Figure 4.1a shows typical engineering stress-strain plots for *A. diadematus* MA and FL silks, and Table 4.1 lists the published values for

Figure 4.1.
a) Engineering and b) True stress strain plots of MA and FL silks.

a)

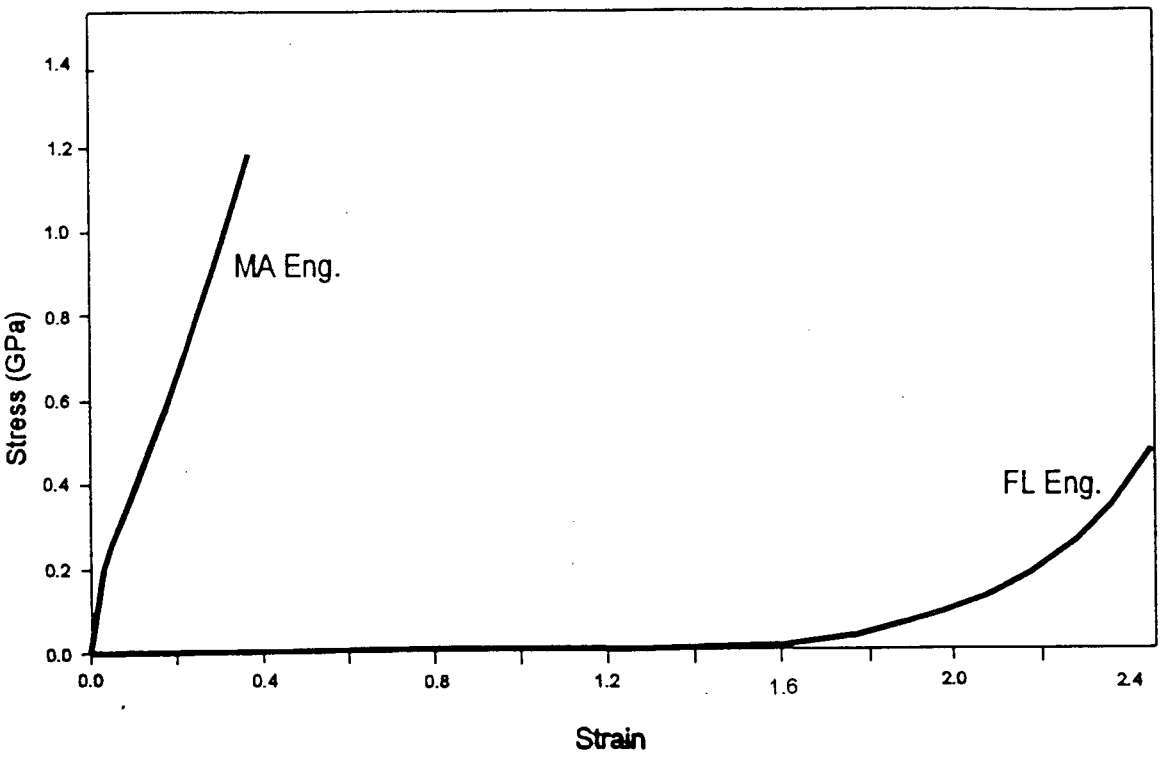
MA Eng.
FL Eng.
Stress (GPa)
Strain
0.0
0.2
0.4
0.6
0.8
1.0
1.2
1.4
0.0
0.4
0.8
1.2
1.6
2.0
2.4

b)

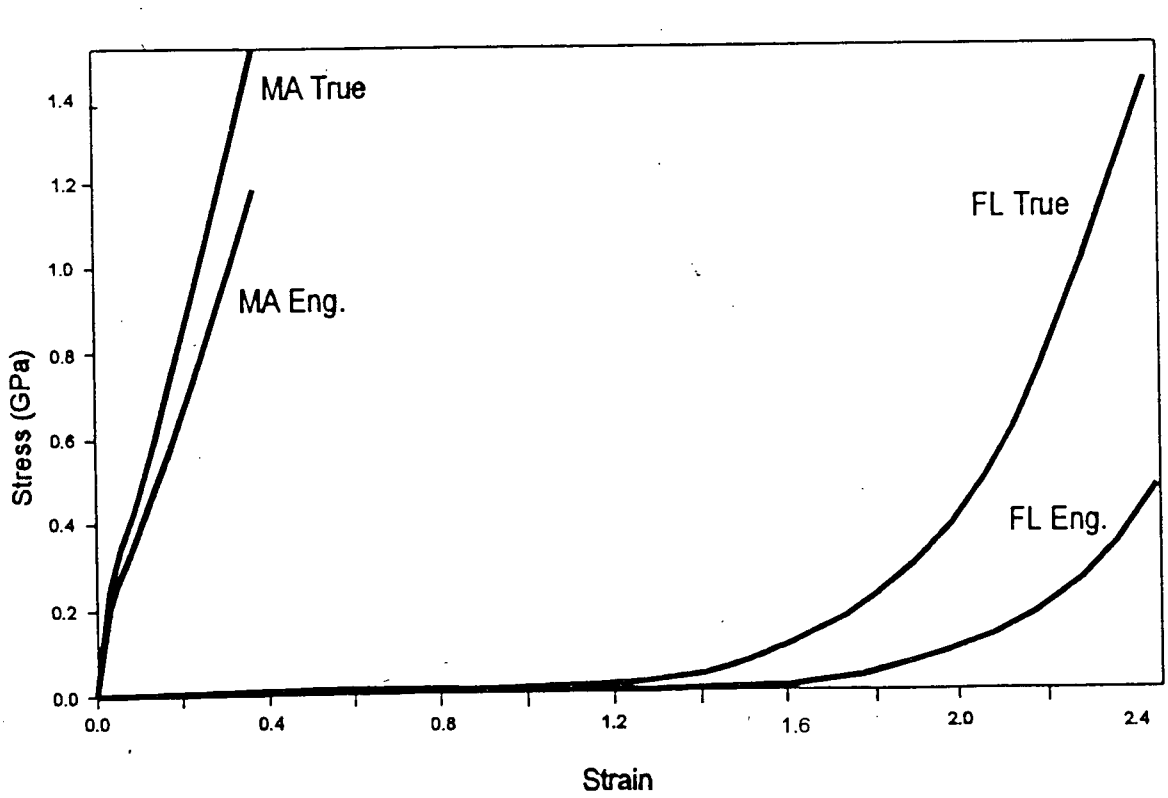
MA True
MA Eng.
FL True
FL Eng.
Stress (GPa)
Strain
0.0
0.2
0.4
0.6
0.8
1.0
1.2
1.4
0.0
0.4
0.8
1.2
1.6
2.0
2.4

Table 4.1.

Published mechanical property values of MA and FL silk from two different *Araneus* orb-spider species. References : 1. Lucas, 1964. 2. Kohler and Vollrath, 1995. 3. Denny, 1976.

Silk Type.	σ_{Fail} Eng. (G Pa)	σ_{Fail} True (G Pa)	ϵ_{Fail}	$E_{Initial}$ (G Pa)	E_{Final} (G Pa)	$\cup \times 10^5$ (J Kg^{-1})	Strain Rate (Sec^{-1})	Ref.
MA, Drag. (*A.diadematus)*	1.42	1.85	0.30	-----	4.70	------	------	1
MA, Radial. *(A.diadematus)*	1.15	1.60	0.39	8.0	4.10	1.62	0.6	2
MA Frame. (*A. sericatus*)	1.42	1.80	0.27	20.5	4.07	1.32	0.01	3
FL (*A. diadematus*)	1.34	7.72	4.76	-----	0.28	------	0.6	2
FL (*A. sericatus)*	0.76	1.54	2.03	0.003	0.49	1.18	0.07	3

ultimate strength, initial and final moduli, and breaking energy for the same two fiber types for two different *Araneus* species, *A. diadematus* and *A. sericatus*. Recall that the MA silk constitutes the orb-web frame and radii as well as the spider's dragline silk, so the MA silk sample citation is included for the data from each different reference source. Also, the mechanics of silk exhibit a strain rate dependence, so the tensile test strain rates are included in Table 4.1. Strain rate is expressed as the change in length of the fiber (ΔL) divided by the initial length (L_0) per second, $\Delta L/L_0$ sec^{-1}. The strain rate reported for MA radial and FL silks by Koeler and Vollrath (1995) may be confounding. The value they reported, which is included in Table 4.1, is apparently the cross-head speed incurred by the speed of their motor (0.6 mm sec^{-1}). When this data is corrected using the mean L_0 reported in that paper (5.1 mm), the actual strain rate equals 0.12 sec^{-1}. This value is close to the strain rate of 0.1 sec^{-1}. used in this study (see Methods).

A. diadematus MA silk can be considered a Group-A fiber. Its characteristic stress-strain profile follows a very high initial slope that leads into a very small yield plateau, followed by rise in slope up to a very large failure stress at around 30 to 40 % extension. The mean ultimate engineering stress values reported for *Araneus* MA silk are exceptional, ranging from 1.15 to 1.42 G Pa. The mean initial moduli reported for MA silk range from 8.0 to 20.5 G Pa, and the mean final moduli are all around 4 G Pa.

In contrast to the high stiffness, high strength, Nylon-like MA silk, *Araneus* FL silk is classified as a Group-C fiber. It exhibits a low initial modulus of around 3 M Pa and great extensibility, with reported breaking extension values of up to 500 % (Koeler and Vollrath, 1995). FL silk is, however, unique among the Group-C materials since its breaking strength is competitive with the ultimate strengths of Group A fibers like MA silk, Cellulose, Nylon and *B. mori* cocoon silk (Table 4.1, also see Table 1.2 and Fig. 1.3). With its high ultimate strength and high extensibility, FL

silk may be likened to a high ultimate strength rubber. In fact, the breaking strength of the FL fiber should be considered as more pronounced than is indicated by the stress strain plot in figure 4.1a, and the ultimate engineering strength values reported in Table 4.1 because engineering stress is calculated by dividing force values obtained in a force-extension record by the initial cross-sectional area of the fiber. This is a standard protocol used in engineering, when the materials tested are rigid and do not undergo large scale deformation, and the initial cross sectional area is not significantly different from the cross sectional area at failure. This is clearly not the case for highly extensible materials like the FL silk. Since it stretches to about 3 or 4 times its original length before breaking, it must neck down to a much smaller cross sectional area at failure. For elastomeric materials, like rubbers and the FL silk, stress values are therefore more usefully computed as *true* stresses. True stress is calculated using instantaneous cross-sectional areas, where the area at a specific strain is determined by assuming that the fiber maintains a constant volume throughout its tensile deformation. Both engineering and true stress vs. strain plots for the MA and FL silk are included in Figure 4.1b for comparison, and Table 4.1 includes true ultimate stress values. The true stress estimates range between a very respectable 1.54 G Pa and an unbelievable value of 7.72 G Pa. Even the lowest ultimate true stress estimate of 1.54 GPa surpasses MA silks reported exceptional ultimate engineering stress. This value is almost identical to MA silks ultimate true stress of 1.6 to 1.85 G Pa. While FL silk has been likened to a rubber, the highest performance rubbers achieve true breaking stresses at least an order of magnitude lower than this (Saltman, 1977). In this context, FL silk is indeed the most exceptional rubber known. A re-visitation of the supra-molecular network organization and fibroin composition of the FL silk provides insights into the molecular basis for its exceptional physical properties.

2. Supra-molecular organization and fibroin composition of A. diadematus FL silk.

It was explained in Chapter 1 that mechanical characterization was coupled with molecular network theory to generate a picture of the supra-molecular organization of both the MA and FL silk fibroin networks (Gosline et al. 1994; Pollack, 1993). FL silk was modeled as a rubber that is lightly cross-linked and reinforced by randomly oriented micro-crystals. The crystals were predicted to occupy less than 5% of the fiber volume and to cross-link a predominantly amorphous network containing random-coiled peptide chains between 20 and 60 amino acid residues long. The results in Chapter 3 demonstrated that a major fibroin constituent of FL silk was ADF-5, and a minor fibroin constituent was ADF-3. The large amorphous component of the FL silk network likely arises from the elastomeric glycine, proline valine and tyrosine rich sequences contained in ADF-5, and the amorphous glycine rich sequences of ADF-3.

It is not possible, however, to explain the elastomeric properties of FL silk based only on its fibroin composition and network organization. Chapter 1 explained that the amorphous sequences of MA silk achieve a glassy state when they are exposed to air on spinning, and the lack of mobility of the amorphous sequences confers stiffness to the fiber. If the amorphous sequences of ADF-5 and ADF-3 were exposed to air, these kinetically free chains would likely be shifted beyond their glass transition and locked into the glassy state, and the FL fiber would not exhibit the elastomeric properties that it does (Vollrath et al. 1989; Bonthrone et al. 1992). The FL fibroin chains remain mobile because they are never allowed to dry. They are subject to a very precise chemical micro-environment as they are spun and while they function in the orb-web.

3. The FL silk micro-environment.

As they are spun, FL fibers are coated and interpenetrated by an all enveloping aqueous glue that is produced in the separate aggregate gland (AG). While the AG product is considered a silk, its amino acid composition is very distinct from the other orb-web silks (see Table 1.3). It is non-fibrous, and it exhibits Newtonian flow characteristics that result in the arrangement of the liquid glue into many stable droplets that stud the FL fibers. Examination of the individual droplets with phase contrast microscopy shows that glycoproteins self-assemble to form a 'doughnut-like' core within individual droplets, where the FL fiber passes through the center of the doughnut (Vollrath and Tillinghast, 1991). NMR analysis of water wash offs of the *A. diadematus* orb-web show that the aqueous glue coating also contains a surprisingly large, water-soluble, non-protein Low Molecular Weight (LMW) fraction that is formed from a concentrated solution of hygroscopic substances related to neurotransmitters (Vollrath et al. 1990). Table 4.2 lists these LMW components and their respective concentrations for 4 different orb-spider species. A small proportion of free amino acids and inorganic salts were also present in the wash offs, and these data are included in Table 4.2. Together, water, glycoproteins, LMW compounds, amino acids and inorganic salts form an aqueous glue with several possible functions. Most importantly for this study, these compounds may influence the supra-molecular organization of FL silks constituent fibroins as they are spun and while they function.

The first part of this chapter examines the effects of altering FL silk's fibroin network micro-environment by subjecting the FL fiber to a simple water wash\dry processing manipulation. The results will show that this manipulation results in a significant increase in optical anisotropy of the FL fibroin network and a dramatic change in mechanical properties to a high initial modulus, lower extensibility material. It is deduced that the wash\dry process removes a water soluble 'plasticizer'

Table 4.2.

Concentrations of the water soluble LMW components of the orb-web of four different orb-spider species (Vollrath, 1990). A. d. is *Araneus diadematus*, A. c. is *Araneus cavaticus*, A. a. is *Argiope aurantia* and A. t. is *Argiope trifasciata*.

		A.d.	A.c.	A.a.	A.t.
<u>High abundance compounds</u>					
Choline	$(CH_3)_3{}^+NCH_2CH_2OH$	1.5 M	12 %	20 %	16 %
Betaine	$(CH_3)_3{}^+NCH_2COO^-$	0.2 M	2 %	3%	3 %
Isethionic acid	$HOCH_2CH_2SO_3^-$	1.1 M	23 %	6 %	21 %
N-acetyltaurine	$CH_3CONHCH_2CH_2SO_3^-$	0.3 M	6 %	17 %	5 %
GABamide	$^+NH_3CH_2CH_2CONH_2$	1.9 M	45 %	48 %	6 %
<u>Low Abundance Compounds</u>					
Cysteic acid	2 %				
Lysine	2 %				
Serine	2 %				
Glycine	1%				
Potatssium Nitrate 7 %					
Potassium dihydrogenphosphate 3%					
Glycoproteins [??]					

that acts either by recruiting water molecules from the atmosphere that in turn hydrate the FL network, or by directly interacting with the network. When this plasticizer is removed with the water wash\dry manipulation, amorphous sequences may crystallize and/or the mobility of the amorphous fibroin sequences may be drastically reduced as they undergo a glass transition, giving rise to a high initial modulus, lower extensibility material. The results, therefore, provide additional evidence that the fibroin network of at least one orb-spider silk requires a precise chemical micro-environment to maintain functionally important mechanical properties.

Because the FL silk is spun in an aqueous micro-environment, its constituent fibroins have not been aligned and encouraged to crystallize on drying, as is the case for the MA silk. The second part of this Chapter examines the influence of physical draw on supra-molecular organization and mechanical properties by subjecting native FL fibers to a water wash\draw\dry processing manipulation. Optical anisotropy was found to increase asymptotically with increased processing draw, and the mechanical properties of the native Group-C fiber were altered to those more similar to a Group-A material. These results indicate that new supra-molecular organization is imparted to the FL fiber with draw processing, and a preliminary comparison of retardation values of the draw processed and hydrated native FL silk at equivalent extensions suggests that some new crystal structure develops from draw processing. Based on this observation, I suggest that the exceptional ultimate strength of the native FL silk results from strain crystallization of the FL fibroins at high extensions.

The results demonstrate for the first time that supra-molecular organization and mechanical properties of FL silk depends on the chemical and physical conditions of processing. Orb-spiders may use these processing strategies to tune the mechanical properties of their many silks.

MATERIALS AND METHODS

FL silk fibers were processed under specific conditions in the lab in order to examine the influence of micro-environment and physical draw on FL fibroin network. Molecular organization was determined using quantitative polarized light microscopy, and mechanical properties were determined from tensile testing. This section describes the methods of sample acquisition, fiber manipulation, and molecular and mechanical characterization of the processed FL silk fibers.

1. FL silk sample acquisition.

Orb-webs from final instar *A. diadematus* spiders were collected from the historic overlook adjacent the U.B.C. campus by taping the webs to empty wooden frames 45 cm × 45 cm. Several frames containing individual orb-webs were placed in wooden boxes 50 × 50 × 50 cm and stored in the lab at room temperature. Experiments were performed on silk strands from stored webs that were at most two weeks old. FL fibers occur as pairs in the orb-web, so individual experiments were performed on FL fiber pairs. Accordingly, all force measurements were adjusted to give physical properties for a single fiber.

2. FL fiber processing.

2.1. The influence of network micro-environment on supra-molecular organization and mechanical properties of the FL silk-The wash\dry manipulation.

A water wash\dry manipulation was used to remove any water soluble compounds that could interact with the FL fibroin chains to influence their network organization and ultimately the physical properties of the FL fiber. FL fiber pairs were plucked from stored orb-webs by tethering them across caliper tips covered with two-sided sticky tape. The spacing between the calipers was reduced

about 2 mm to bring the fibers to their estimated resting slack length (ie. zero tension) without allowing the surface tension of the glue droplets to reel in the core FL fiber. The sample pair was then secured to the calipers with an additional layer of tape, washed by immersing the caliper ends in a large petri dish containing distilled water adjusted to pH 7 with dilute HCl, and then dried by removing the mount from the water and exposing the fibers to air. Samples were removed from water by supporting them on a glass slide coated with parafilm, so that the fiber pair was contained in a bubble of water on the slide. The fibers were then slid horizontally through the water meniscus and exposed to air to dry. This protocol was used in order to minimize a potential water surface tension load that might influence fibroin chain alignment and crystallinity of the fibers. The unavoidable uncertainties in manipulating a fiber that is only a micron in diameter likely contributes to the variability in the physical properties of processed FL samples. The processed fibers were mounted on a microscope slide for quantitative polarized light microscopy or into the tensile testing apparatus for mechanical characterization. 10 fiber pairs, 5 from each of two separate orb webs were subjected to the wash\dry process and then characterized optically. Similarly, 10 fiber pairs, 5 from each of the same two orb-webs, were wash\dry processed and subjected to tensile testing.

2.2. The effects of physical draw on the supra-molecular organization and mechanical properties of the FL silk-The wash\draw\dry manipulation.

A water wash\draw\dry protocol was designed to extend and align the FL fibroin chains in the hydrated state prior to removal from water and drying, to determine if crystallization and ultimately the physical properties of the FL silk are influenced by increased processing draw ratio. FL fiber pairs were subjected to the same processing protocol as was described for the wash\dry manipulation above, with the exception that the calipers were drawn to extensions of 60%, 120% or

180% of the original fiber pair length while they were immersed in water. The processed fiber pair was then removed from the water, allowed to air dry, and mounted for optical and mechanical characterization. In total, 10 processed fiber pairs (5 fiber pairs from each of the same two separate orb-webs used for the wash\dry experiments) were characterized optically for each of the 60%, 120% and 180% draw ratio manipulations. Similarly, 10 processed fiber pairs (5 from each of the same two webs) were characterized mechanically for each of the 60%, 120% and 180% draw ratio manipulations

3. Birefringence theory and measurements .

Polarized light microscopy provides the capability to reveal and quantify sub-microscopic molecular order. The partial alignment of molecular bonds or sub-microscopic particles renders a material birefringent, which alters the state of polarized light passing through it. When plane polarized light is directed through a material, the light wave is considered to split into two orthogonal waves that will each experience refractive indices (RI's) specific to the plane of atomic structure through which their electric fields oscillate. Consider two light waves, one oscillating in the YZ plane and the other in the XY plane. If the waves reach their maximum and minimum at the same point, they are in phase, and their sum at corresponding points leads to one wave, linearly polarized at 45° , as is shown in figure 4.2a. If the two waves are 180° out of phase, the resultant wave is linearly polarized at 45° in the opposite sense, as is shown in figure 4.2b. If the waves are 90° out of phase, the resultant wave is circularly polarized, where the electric field vector rotates around the origin as the wave propagates. In an isotropic material, there is no difference in the RI that the two orthogonal waves experience, and the wave that emerges will be polarized at 45°. On the other hand, waves with electric fields that fluctuate parallel and perpendicular to the aligned axis of an anisotropic

Figure 4.2.

Schematic of the motion of polarized light rays. a) Two orthogonal in phase waves-the resultant wave oscillates at 45°. b) Two orthogonal waves 180° out of phase-the resultant wave oscillates at 45° in the opposite sense. c) The resultant of two orthogonal waves that are 90° out of phase is circularly polarized.

a)

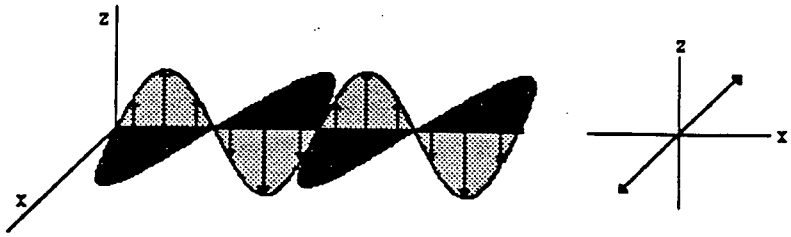

b)

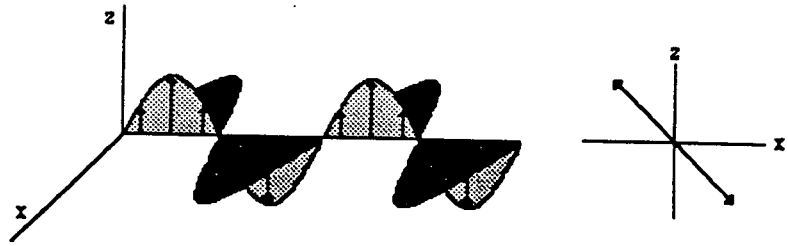

c)

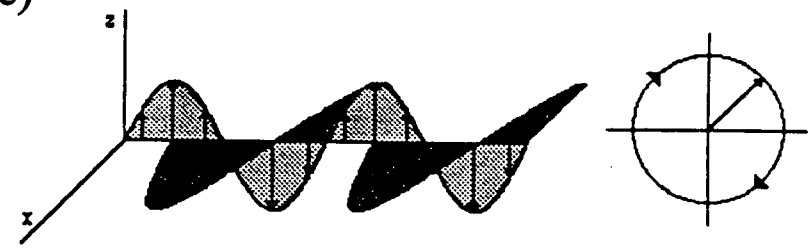

material experience different RI's, where the waves oscillating parallel to the oriented molecular plane are considered to slip through faster than interrupted rays oscillating perpendicular to it. As a result, the emergent wave is elliptically polarized, and the material exhibits birefringence.

When plane polarized light is directed at a 45° angle to a silk fiber, the rays oscillating parallel to the low RI fiber axis emerge faster than those rays oscillating perpendicular to this axis which experience a larger RI. It is possible to calculate the optical retardation of the material from the angle at which the two ray components are out of phase. This is done practically by visualizing an optimally bright fiber oriented at 45° to the cross polarizers (with the optimally black isotropic background of the slide mount) and rotating an optical compensator through the fibers extinction minimum where the fiber becomes maximally dark. The angle of compensator rotation, θ, is then easily converted to the phase difference (in nanometers) between the two wave components, or retardation Γ, by implementing a simple cosine relation that is compensator specific (see below). Birefringence, the measure of optical anisotropy of a material, is obtained by normalizing the retardation to the path length that the light rays must travel through the fiber, as:

$$\beta=\Gamma/\text{diameter} \qquad (1)$$

where β=birefringence. In this study the diameter of the fiber was measured with a Wild filar micrometer eyepeice to ± 0.2 μm. Diameter measurements on FL fiber pairs using light microscopy by Pollack (1993) and the scanning electron microscope (SEM) FL fiber diameter measurements obtained during the course of this study indicate that individual FL fibers are elliptical in cross section. Figure 4.3 shows a typical top and side view of an FL fiber pair. In the case where the retardation measurement was obtained from two adjacent FL fibers clearly in view, the path length used to

Figure 4.3

SEM Polaroid photograph of a typical FL silk strand as viewed from the top and side showing the elliptical shape of these FL fibres.

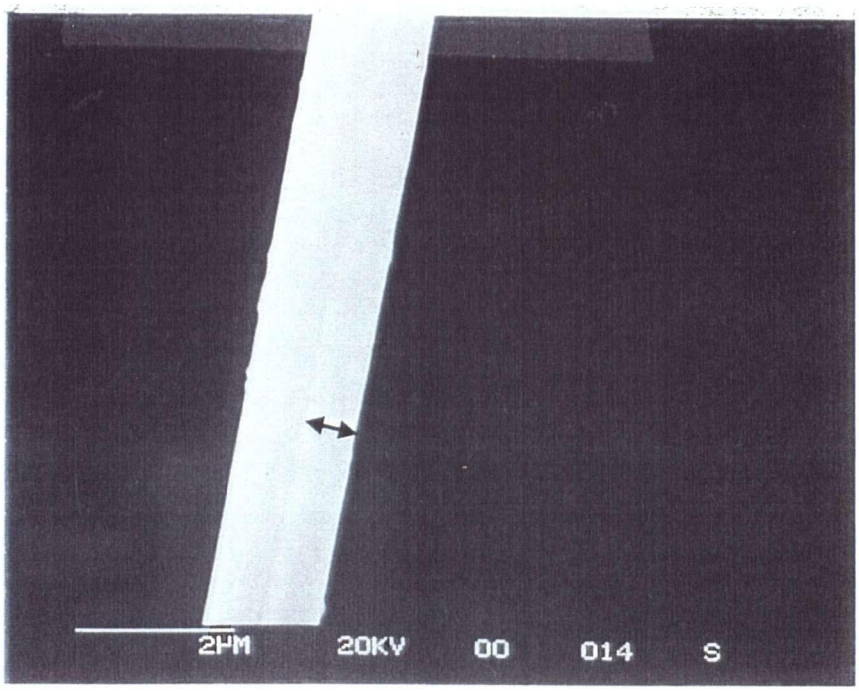
2HM
20KV
00
014
S

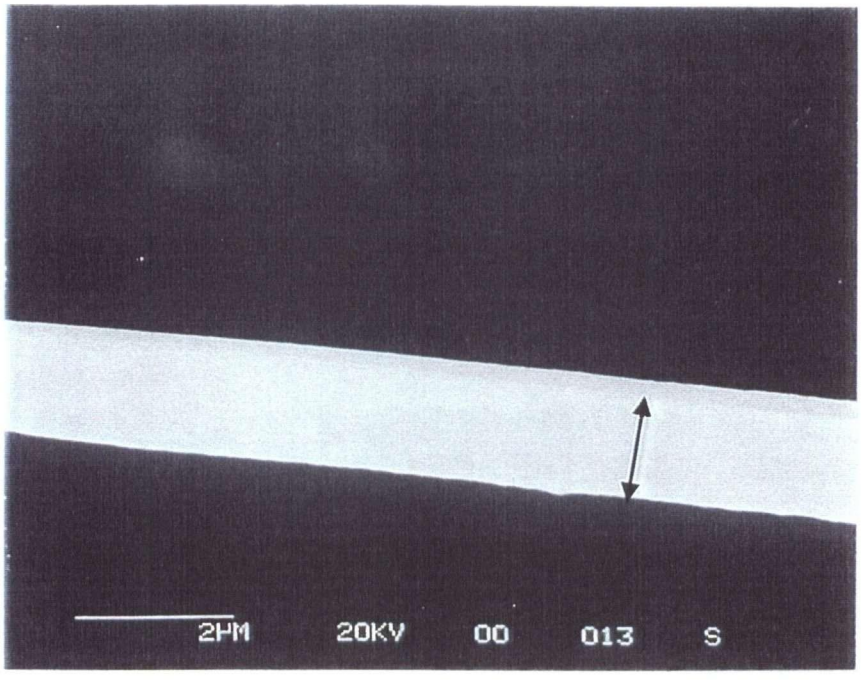
2HM
20KV
00
013
S

normalize retardation to rirefringence was the long axis diameter of the fiber ellipse. When the fiber pair was stacked, the retardation value obtained was actually for two fibers, so this value was divided by two and then normalized to birefringence using the fiber's short axis diameter as the path length value.

FL silk samples from the same two orb-webs used for the tensile tests where processed (wash\dry or wash\draw\dry) and mounted on microscope slides, tethered between two-sided sticky tape. Each sample was immersed in microscope immersion oil (optical refraction index n_D=1.51), mounted on a Wild M-21 polarizing light microscope and viewed with a 100 × oil immersion Wild lens. The sample was set at extinction, where the fiber was maximally dark, and then rotated 45° from this extinction state. At this point the fiber was maximally bright. A compensator was then rotated through its extinction minima and the retardation value used in equation 1 to determine birefringence. It is noted that the assignment of the extinction minimum is relatively subjective and requires a trained eye that has been accommodated to the dark for no less than 20 minutes. The data was therefore accumulated with the assistance of an additional experimenter, Mr. Ken Savage. Retardation values were obtained by both myself and Mr. Savage at each sample site, and the values were averaged prior to normalization by path-length. For high birefringence fibers a 1/4λ plate (λ=456nm) was used and the compensator was rotated through a single minimum. Here, the angular rotation of the compensator was converted to the phase difference of the two orthogonal waves (retardation) with the relation $\Gamma_{nm}=3.03\theta$. For low Birefringence fibers it was necessary to use a 1/30λ Berek compensator (λ=456nm). Here the compensator was rotated through four minima, and the four Retardation values averaged for each sample. With this compensator, angular rotation was converted to retardation with the relation $\Gamma_{nm}=17.2\cos\theta$.

4. Mechanical characterization of FL silk.

4.1 The tensile testing apparatus.

A tensile testing apparatus was constructed to measure the physical properties of silks (Fig. 4.4). An ultra-sensitive force transducer (Fig. 4.4a) designed to measure forces in the 50 to 5000 milli-Newton range was built by bonding two silicon strain gauges (BLH electronics) to a 5 × 10 mm piece of stainless steel shim stock with a thickness of 0.01 inches. The gauges were wired to form a ½ Wheatstone bridge configuration, and the transducer was mounted on the end of a Precision Screw-Travel Stage mechanism (Edmunds Scientific, Fig 4.4b), with an independently mobile stage (Fig. 4.4c) that was driven by a 72 RPM synchronous step motor (Figure 4.4d). 22 gauge syringe needles were glued vertically to the transducer and to the mobile stage (Fig.4.4e's), and individual silk fiber samples were mounted between these two 'posts' with 5 minute Epoxy. The apparatus was inserted into an enclosed chamber (Fig. 4.4f) that allowed for control of temperature and humidity.

The motor drove the movement of the mobile stage at an extension rate of ~ 1 mm sec^{-1}, placing the fiber under tensile load. Since the motor speed was not easily controlled, care was taken to mount samples at a starting length L_o of close to 10 mm in order to maintain a constant strain rate. In fact, the mean starting sample length was 9.99±0.06 (standard error). As a result, the strain rate used in this study was determined to be very close to 0.1 sec^{-1}. Voltage deflections from the transducer were recorded through a pre-amplifier connected on-line to a PC data acquisition system (Labtech Notebook™). The transducer had an inherent resonance of 900 Hz and the motor generated noise at 60 Hz. In order that the data be collected away from the confounding noise and transducer resonence, the transducer output was filtered using a low pass 10 Hz anti-alias analogue filter and was digitized at 200 Hz. The digital record was then filtered with a second order, low pass, 30 Hz digital Butterworth filter to virtually eliminate all noise. The transducer was calibrated by measuring

Figure 4.4.

Photograph of silk tensile testing apparatus. a) transducer, b) screw travel apparatus, c) mobile stage, d) motor, e) silk mount posts, f) environmental control chamber.

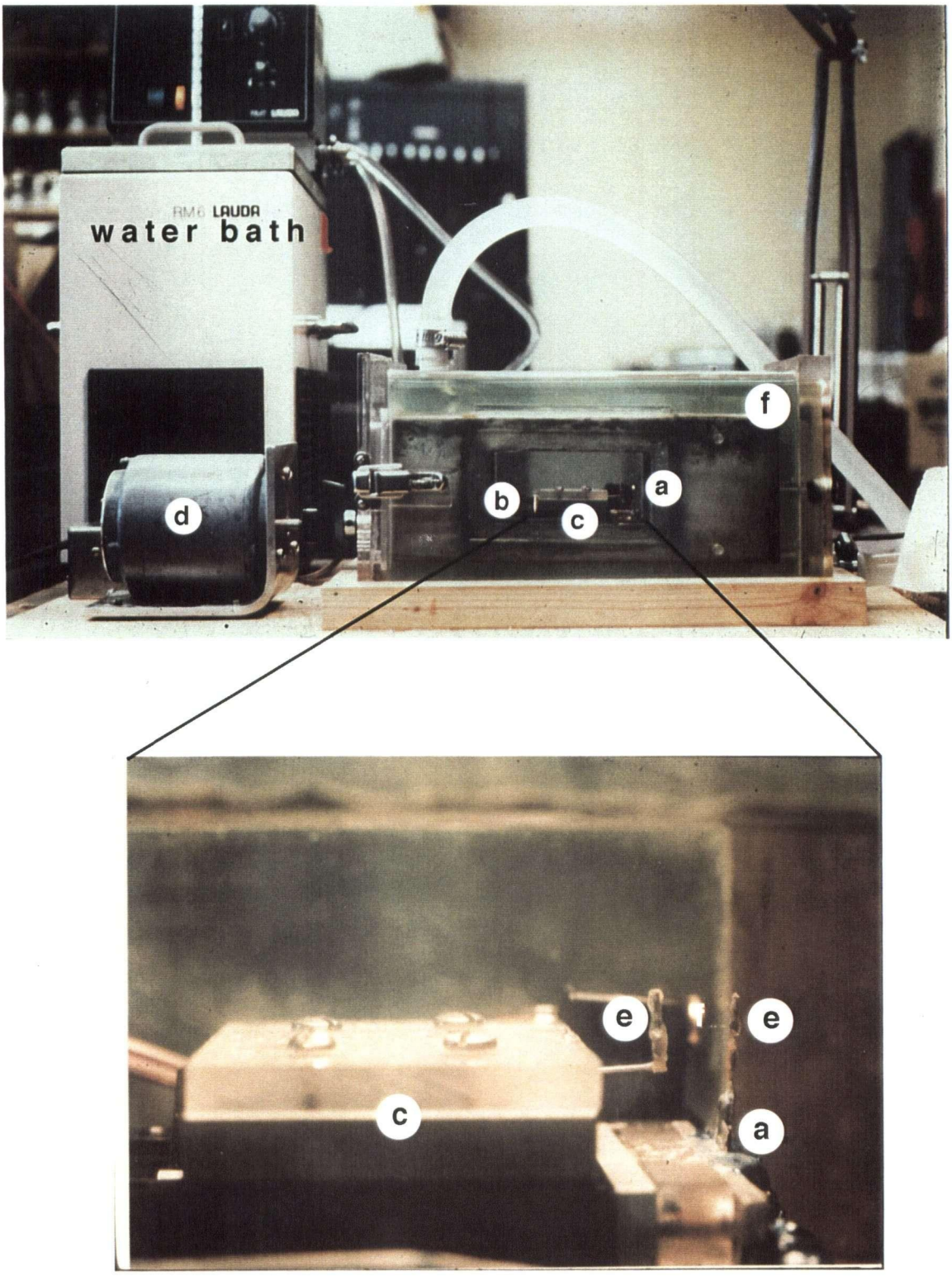
RM6 LAUDA
water bath
f
a
b
c
d
e
e
c
a

the voltage deflections achieved when suspending small plasticine balls of known weights ranging between 100 mg and 2000 mg from the transducer. The calibration regression was linear in this mass range. The compliance of the transducer beam and stage mount beam (Fig. 4.4e) were quantified by mounting a rigid paper clip between these two posts and then recording the voltage deflections incurred by 0.125 mm movements of the mobile stage. A single 0.125 mm movement incurred close to a 0.6 volt deflection on the same pre-amplifier gain setting used in the tensile tests. Assuming linearity in voltage vs. distance relation and examining high modulus measurements for which compliance should have the most profound effects, it was determined that system beam bending resulted in about a 1-4 % underestimate of initial modulus. The compliance of the system was therefore considered to be negligible, particularly when compared to the much larger degree of inter-sample variation.

4.2. Tensile tests.

One half of each FL fiber pair was mounted in the tensile testing apparatus using 5 minute Epoxy, and the other half was simultaneously mounted on an SEM stub covered with two sided sticky tape. The SEM stub was held in place next to the transducer with a custom designed holder attached to a ring stand. During mounting the fiber was delicately cut between the transducer post and the SEM stub. The SEM stub was then stored under ambient lab conditions. Once the glue had dried (10 minutes were allotted) the portion of the FL fiber mounted in the tensile testing apparatus was brought to its resting slack length by decreasing the distance between the transducer and stage posts manually. The resting slack length was defined as the point were the fiber maintained negligible resting tension but was not sagging. The length of the tensile test fiber pair sample was then measured with calipers to ± 0.02 mm, and the silk mount, together with the mobile stage apparatus, were placed

in the environmental control water jacket. The motor was then attached to the screw travel mechanism, and the experiment initiated by turning on the motor. All the tensile tests were done at ambient lab humidity and 22 °C, since a pilot study indicated that below 50 °C humidity dependant variation in physical properties were negligible (data not shown).

Ten processed fibers were tested for each of the wash\ 0, 60, 120 and 180 % draw\dry manipulations, 5 from each of two different orb-webs. The physical properties of the native FL silk were also determined from 7 samples from each of two additional orb-webs (14 samples total).

4.3 Fiber diameter measurements .

Processed FL fiber pairs mounted on SEM stubs were gold sputter coated with the Nanotech SEM Prep II sputter coater for 3.2 minutes under vacuum. Each stub was then placed in the SEM and photographed at 2000 × magnification. A grid containing 2680 etches per mm was photographed at the same magnification to calibrate the measurements obtained. The SEM photographs were taken as quickly as possible to avoid heating and melting the fibers under the concentrated electron beam, which results in necking down of the fiber and a misrepresentation of its actual diameter.

The thickness of the gold sputter coat was determined by sequentially coating a small metal notch on an SEM stub. Each coating was estimated to increase the notch thickness by 22 nm (11 nm per side). 22 nm was therefore subtracted from each silk diameter to refine the accuracy of diameter measurements.

Pollack (1993) has shown that *A. diadematus* FL fibers are elliptical in cross section, with an ellipticity ratio of close to 1.5 (diameter of long axis/diameter of short axis). SEM photographs of FL fibers pairs were therefore taken from top and side angles, and both long and short axis diameters calculated for each fiber. The data again indicates that the FL fibers are elliptical in cross-section

with an ellipticity ratio of close 1.54 (data not shown). The cross-sectional area of each fiber ellipse was determined with the relation $\Pi(ab)$ where a and b are the long and short radii of the elliptical FL fiber respectively.

Individual cross-sectional area values were initially matched up with force data from respective fiber pair samples to calculate stress. It became clear, however, that a relatively large variability between fiber diameter measurements from the same web resulted in fairly large variability in initial moduli, the parameter that should be most sensitive to diameter variability. The variability in diameter measurements may have been introduced through deformation of the FL fiber pair during the delicate manipulation of gluing one half of the silk FL fiber pair to the transducer and mobile stage posts while simultaneously attaching the other half to the SEM stub. Also, while the SEM photographs were taken as quickly as possible to avoid heating and melting the fibers under the concentrated electron beam, this process may have resulted in a degree of misrepresentation of the actual fiber diameter. The mean diameter values from each of the two webs at each draw processed length, n=5 top and side in each case, were therefore used to calculate stresses using the original complementary force extension data from each sample.

Native FL fiber diameter measurements were obtained from the light microscope using a Leitz Filar micrometer because it was predicted that desiccating conditions used for the SEM would result in a dramatic reduction of the diameter of the aqueous glue coated native fiber. Measurements were obtained from samples plucked from a location in the orb-web just adjacent the site where a corresponding native FL fiber was sampled for tensile testing, where it was assumed that the fiber diameter of the two adjacent FL fibers was identical.

5. Dialysis of the FL secretion

Birefringence and mechanical data from the wash\dry experiments indicate that the aqueous FL silk glue contains a water soluble plasticizer of the FL silk network (see Results). It was unclear whether the plasticizer was produced in the FL and/or the AG gland. The FL secretion was shown to shear crystallize to only a nominal degree when retrieved directly from the FL gland (see Fig. 3.6), possibly indicating that a plasticizer exists within the FL gland. The FL secretion was therefore dialyzed against water in an attempt to remove any plastisizing agent(s). The FL secretion was isolated on a microscope slide, as described in the Methods section of Chapter 3, a dialysis membrane with a 10 kD molecular weight cutoff was then placed on top of the secretion, and a drop of distilled water added to the top of the membrane. The entire mount was left to dialyze for 30 minutes, after which the dialysate was removed and stored at -20 °C in an Eppendorf tube. The control protocol involved placing the dialysis membrane on top of the isolated FL secretion in the absence of water (ie. dialysis against air alone). The dialysis membrane was then removed and the dialyzed FL secretion was subjected to the same shear manipulation detailed in the Methods section of Chapter 3. The crystallinity of the dialyzed sheared FL secretion was qualitatively evaluated based on its brightness under polarized light.

The plastisizing capacity of the FL dialysate on the MA secretions was also examined. This was done by placing a drop of the FL dialysate on the isolated MA secretion and qualitatively evaluating the crystallinity of the secretion following drying or following shear manipulation. The parallel control for these experiments involved placing a drop of distilled water (pH 7) on the secretion rather than a dialysate drop.

RESULTS

The results demonstrate that the supra-molecular organization and physical properties of *A. diadematus* FL silk can be precisely controlled in the lab with specific processing manipulations. These observations indicate that, like many other high performance fibrous polymers, the mechanical properties of one and probably many other natural silks depends on specific chemical and physical conditions that govern supra-molecular organization.

1. The influence of FL silks micro-environment on its supra-molecular organization and physical properties.

1.1 Optical characterization of the wash\dry FL silk.

Table 4.3 documents the mean optical properties obtained from the native (Pollack, 1993), wash\dry, and wash\draw\dry FL fiber sample sets. The mean birefringence of the wash\dry processed FL samples was 0.0105 greater than that of the native FL fibers. In comparatively assessing the difference in birefringence between these two sample sets, it is important to consider that the diameter of the glue coated native FL silk was between 1.86 and 2.19 times greater than that of the washed fiber, so that when birefringence is calculated, the difference in diameter amplifies the apparent difference between the native and wash\dry processed states by a factor of about of about 2. To the exclusion of path length, the processed fibers showed a significant mean retardation increase of about 10 nm relative to that of the native FL fiber. This observation indicates that an increase in supra-molecular order develops with the wash\dry manipulation, but it remains to be determined whether this new order arises from alignment of amorphous sequences along the fiber axis, alignment of pre-existing crystals along the fiber axis and/or from the creation of new crystal structure.

Table 4.3.

Macromolecular order of native and processed FL silks as assayed by birefringence. retardation values are included for comparative purposes (see text). n=sample number.

State of FL silk	Birefringence	Retardation (nm)	n
native (with glue)	0.0014 ± 0.0007	3.10 ±0.90	4
wash\dried	0.0119 ± 0.0021	12.78 ± 2.74	10
wash\60% drawn\dried	0.0163 ± 0.0022	14.33 ± 3.03	10
wash\120% drawn\dried	0.0230 ± 0.0030	16.82 ± 3.16	10
wash\180% drawn\dried	0.0218 ± 0.0017	14.07 ± 2.00	10

1.2. Mechanical properties of native and wash\dry processed FL silk.

Due to the sparsity in available data on the mechanics of *Araneus* threads, the mechanical properties of *A. diadematus* native FL silk were initially characterized. The full complement of native FL silk physical properties are documented as part of Table 4.4 as means ± 95 % C. I.'s. The native FL silk had a mean ultimate engineering stress of 0.47 G Pa, a mean true stress of 1.6 G Pa , a mean failure strain of 2.48, a mean final modulus of 0.55 G Pa and an a mean energy to break of 1.18×10^5 J Kg^{-1}.

Figure 4.5 and Table 4.4 show that wash\dry processing of the FL fiber results in a dramatic change in mechanical properties from the low initial modulus, high extensibility behavior of the native fiber, to one with a 1530 fold greater initial modulus with a 2.67 fold lower extensibility. The processed FL fiber has a very distinctive stress strain profile. A very high initial modulus is followed by a sharp yield into a long, low modulus plateau region that ends with a small rise in modulus and finally, specimen failure. Both the optical and mechanical properties of the processed fibers suggest that the fibroins that constitute FL the fiber have a capacity to adopt order and physical properties that are not permitted by their functional micro-environment in the orb-web. A water soluble component of the aqueous glue coating of the native FL fiber must be implicated as an FL fibroin network 'plasticizer'.

2. Dialysis shear experiments.

It remains unclear if the FL network 'plasticizer' is produced in the AG and/or FL glands. Chapter 2 showed that the shear product of the FL secretion was minimally crystalline compared to the other silk secretion shear products, and this may indicate that the plasticizer occurs within the FL gland proper. The FL secretion was therefore dialyzed against distilled water in order to to remove

Figure 4.5.
Engineering stress strain plot of FL silk and wash\dry FL silk.

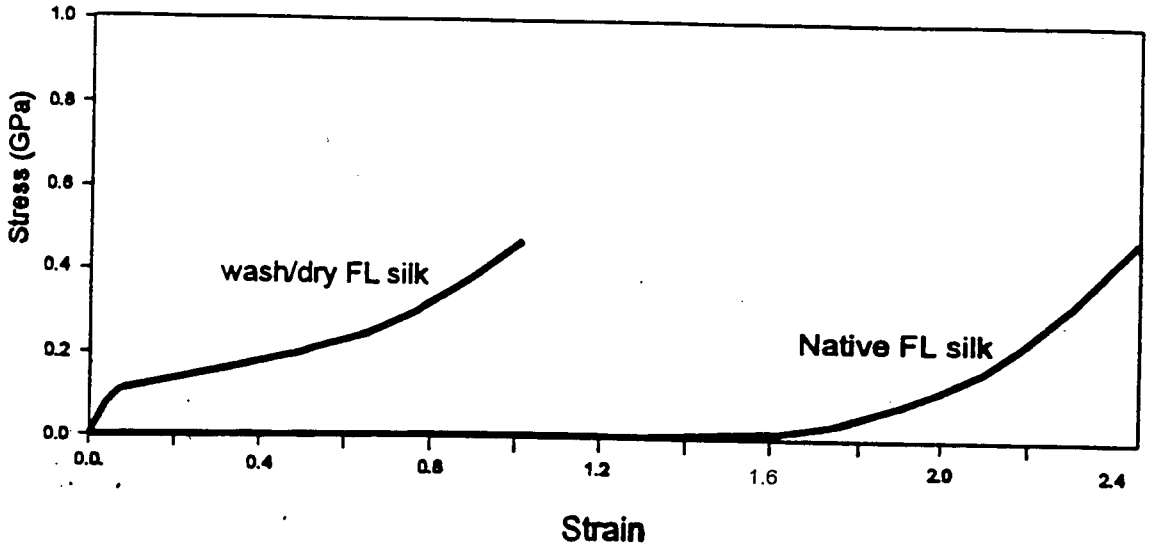
1.0
0.8
0.6
0.4
0.2
0.0
Stress (GPa)
wash/dry FL silk
Native FL silk
0.0
0.4
0.8
1.2
1.6
2.0
2.4
Strain

Table 4.4.

The mechanical properties of *A. sericatus* MA, *A. diadematus* native FL, and *A. diadematus* wash\dry and wash\ % draw\dry processed FL fibers. Symbols: σ is Stress: ϵ is Strain; E is Modulus, ∪ is Toughness. 1 : From Denny, 1976. All other data are reported as means ± 95 % Confidence Intervals. N/A = not available.

	Eng. σ_{Fail} (G Pa)	Trueσ_{Fail} (G Pa)	σ_{Yield} (G Pa)	ϵ_{Fail}	ϵ_{yeild}	$E_{Initial}$ (G Pa)	$E_{Failure}$ (G Pa)	$\cup \times 10^5$ (J Kg^{-1})
MA [1]	1.42	1.80	N/A	0.27	N/A	20.50	4.07	~ 1.3
FL	0.44 ± 0.11	1.53	-------	2.48 ± 0.29	--------	0.03 ± 0.01	0.55 ± 0.18	1.91 ± 0.45
0%	0.47 ± 0.11	0.91	0.08 ± 0.02	0.93 ± 0.41	0.02 ± 0.01	4.59 ± 1.30	0.69 ± 0.44	1.18 ± 0.37
60%	0.73 ± 0.16	1.22	0.11 ± 0.02	0.67 ± 0.28	0.02 ± 0.01	5.38 ± 0.77	1.20 ± 0.54	1.64 ± 0.56
120 %	1.21 ± 0.28	1.92	0.16 ± 0.03	0.59 ± 0.15	0.03 ± 0.01	7.15 ± 1.24	1.97 ± 0.44	2.79 ± 0.64
180 %	1.10 ± 0.23	1.49	0.17 ± 0.03	0.35 ± 0.06	0.03 ± 0.01	7.59 ± 1.21	2.40 ± 0.67	1.67 ± 0.57

any LMW plasticisers. The dialyzed FL secretion was then sheared and its crystallinity evaluated qualitatively. When the dialyzed FL secretion is sheared a network of luminous structures develops (Fig. 4.6a). This pattern was not observed for the control dialyzed secretion which exhibits a shear product basically identical to the sheared FL secretion shown in Figure 3.6c. (data not shown). This result would indicate that a LMW plasticizer produced in the FL gland has been removed from the FL secretion, and in its absence the FL fibroins can crystallize under shear. However, when the same dialyzed\sheared FL secretion is placed in immersion oil and viewed under plane polarized light, the apparent crystalline regions disappear, showing that the luminous network results from polymer microscope-slide glass-surface interface reflections. A closer look between those interfaces does reveal some stable crystal structures that are not seen in the control sheared FL product (Figure 4.6b), suggesting that a plasticizer exists within the FL gland. However, the crystals occur on only a very fine scale and are present in much lower quantities than the crystal structures of MA, MI and CY secretion shear products.

To test the possible crystal inhibiting effects of the dialysate from the FL secretion on the on other silk secretions, a drop of dialysate was introduced to the MA secretion on a microscope slide, and the preparation was allowed to dry in air. A parallel control MA secretion was placed on a microscope slide in a drop of distilled water and allowed to air dry. Figure 4.6 c and d shows that there was a qualitative decrease in the brightness of the sample that was dried in dialysate compared to that dried in water alone. When the same experiment was done to include the shear, however, the shear product of the MA secretion was not discernable from the control shear products (secretion introduced to a drop of water and sheared), or from the crystalline shear products shown in Figure 3.6 (data not shown). Together, these results suggest that a water soluble plasticizer produced in the FL gland can have a mild inhibitory effect on the crystallization of the fibroins of other silks, but that

Figure 4.6.

Crystallinity of silk secretions viewed under polarized light. a) 40 × magnification of the FL secretion sheared following dialysis against distilled water pH 7 (scale bar ~ 5μm). b) 100 ×magnification of a (scale bar ~ 2 μm). c) 40 × magnification of the MA secretion dried in a drop of distilled water pH 7 (scale bar ~ 5μm). d) 40 × magnification of the MA secretion dried in the FL secretion dialysate (scale bar ~ 5μm). All photgraphs were taken at 1/4 second exposure time.

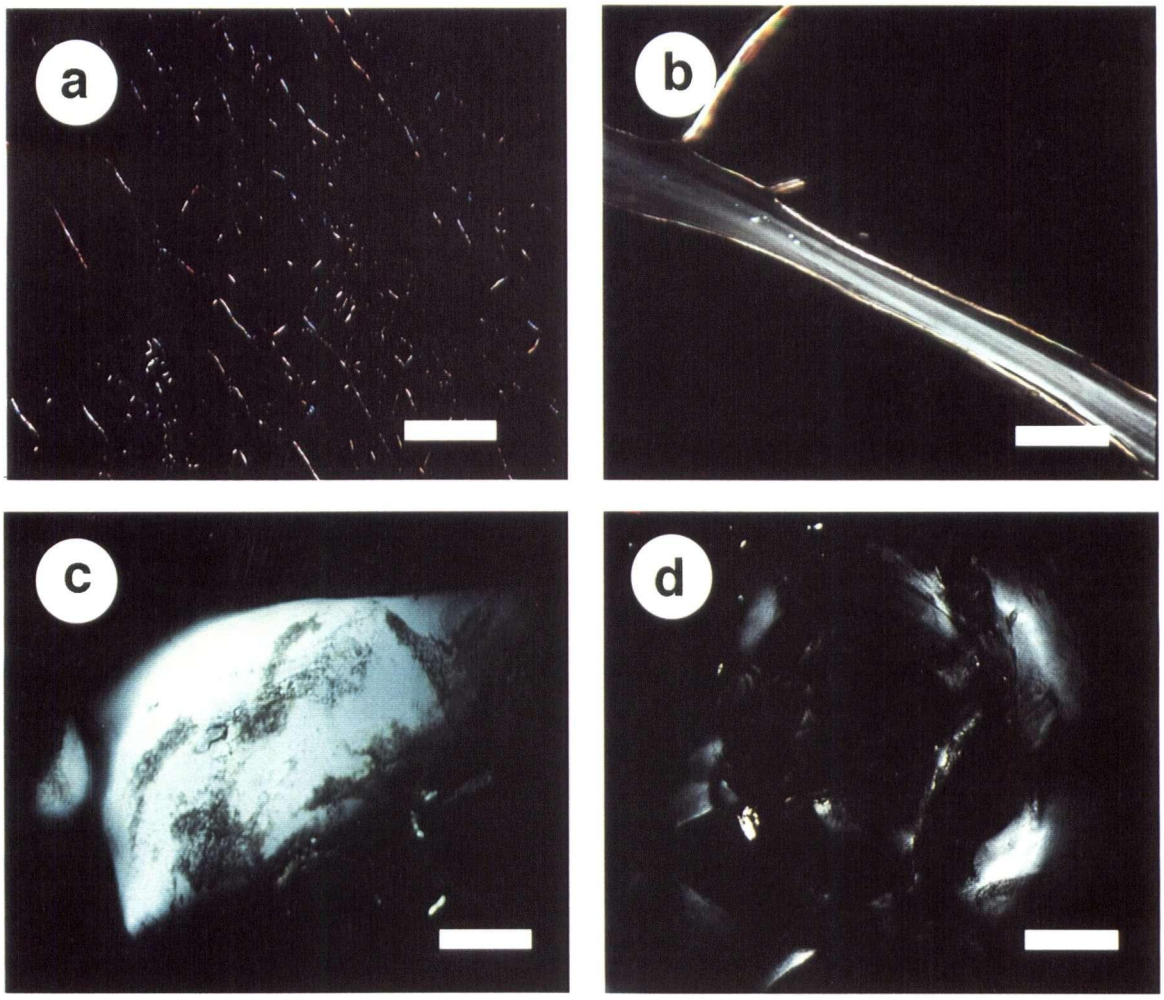
a
b
c
d

primary peptide designs which contain a high proportion of crystal forming domains can not be inhibited under shear with any water soluble LMW compounds extracted from the FL secretion. It remains to be determined whether other plasticizers that may be derived from the AG gland can function as more potent crystal inhibitors for all silks.

The plasticizing capacity of each of the of the high abundance LMW compounds listed in Table 4.2 was tested on each of the MA, MI, and CY secretions by obtaining these compounds in synthetic form from Sigma corporation. No plasticizing effects were observed for any of these compounds, whether they were assayed independently or in a solution that incorporated all of them at *in vivo* concentrations (data not shown). It is noted, however, that two of the major LMW constituents, GABamide and Isethionic acid were not commercially available and that GABA and Isothiocyanate were used in their place.

3. The influence of physical draw processing on the supra-molecular organization and mechanical properties of A. diadematus FL silk.

3.1. Optical characterization of the wash\draw\dry processed FL fibers.

Table 4.3 and Figure 4.7 show that the birefringence of the draw processed FL fibers increased asymptotically with draw processing, reaching a plateau at 120 % draw. Analysis of Variance (ANOVA) indicates significant differences between mean birefringences from the different draw treatments ($P<0.001$, $F=20.5$, $DF=38$), and the Student Newman Keules method indicates that only the mean birefringences from 120 % and 180 % draw processed sample sets are statistically similar ($P>0.05$). The 120 % drawn FL fibers had a mean birefringence of 0.0230, which approaches MA silks birefringence of 0.035. The draw processed fibers may develop increased birefringence through alignment of amorphous sequences along the fiber axis, alignment of the pre-existing crystals

Figure 4.7.

Plot of mean birefringence ± 95 % C.I. vs. draw percent for wash\draw\dry processed FL silk. The mean birefringence of MA and native FL silk are included for comparison.

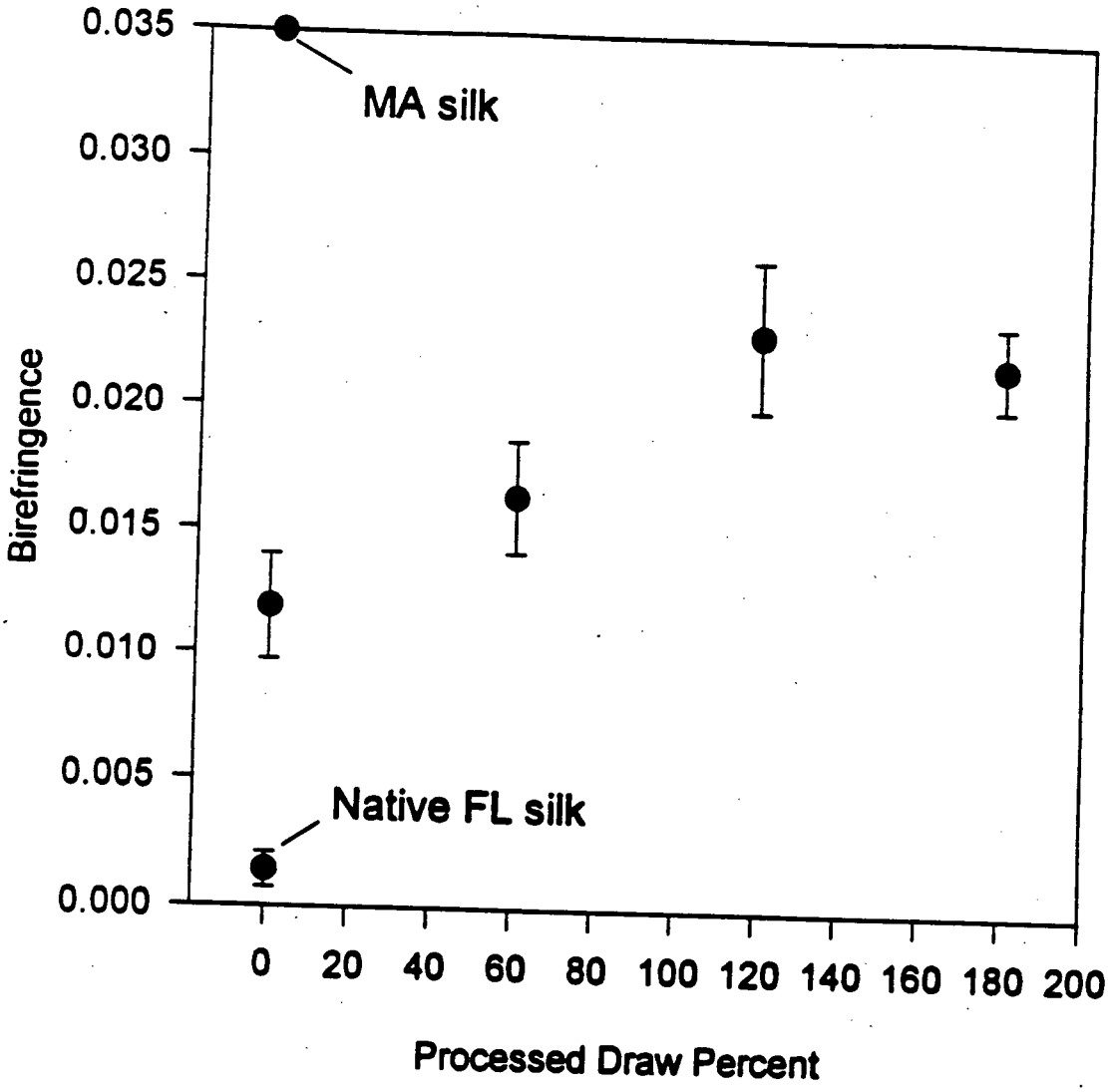
0.035
0.030
0.025
0.020
0.015
0.010
0.005
0.000
Birefringence
MA silk
Native FL silk
0
20
40
60
80
100
120
140
160
180
200
Processed Draw Percent

along the fiber axis, and/or from the formation of new crystal structure. It is of particular interest to determine if the processing draw resulted in the formation of new crystal structure. Therefore, in an attempt to tease apart the contribution that alignment of amorphous and previously existing crystals make to birefringence, the Discussion section of this Chapter compares the optical properties of the draw processed FL fibers to previously published data from the hydrated native FL silk at equivalent extensions.

3.2. Mechanical characterization of the wash\draw\dry processed fibers.

The mechanical properties of the FL silk were dramatically altered by draw processing. Ultimate and yield engineering stresses, initial and final moduli and toughness all increased significantly with increased draw, while extensibility decreased. Figure 4.8 shows the range of stress stain behaviors that the draw processed fibers exhibit, and the full complement of physical parameters from the tensile testing experiments are summarized in Table 4.4. The change in each physical parameter with draw are presented for visual appraisal in Figures 4.9 to 4.15 as mean values ± 95 % C. I.'s.

Figure 4.9 shows that ultimate engineering stress increased asymptotically with increased processing draw, reaching a plateau at 120 % draw. Analysis of Variance (ANOVA) indicated significant differences between mean failure stresses from the different treatments ($P < 0.0001$, $F = 27.5$, $DF = 38$), and the Student Newman Keules (SNK) method showed that statistical similarity occurs only between the mean failure stresses at 120 % and 180 % processed draw ($P > 0.05$). The ultimate stress of the 120 % processed fiber was truly exceptional. With a mean value of 1.21 G Pa, it at least equals the breaking strength of Group-A MA silk and approaches some of the strongest fibers known (see Table 1.2). Table 4.3 also includes the predicted true ultimate stress values for

Figure 4.8.
The full range of engineering-stress strain behaviour exhibited by draw processed FL silk.

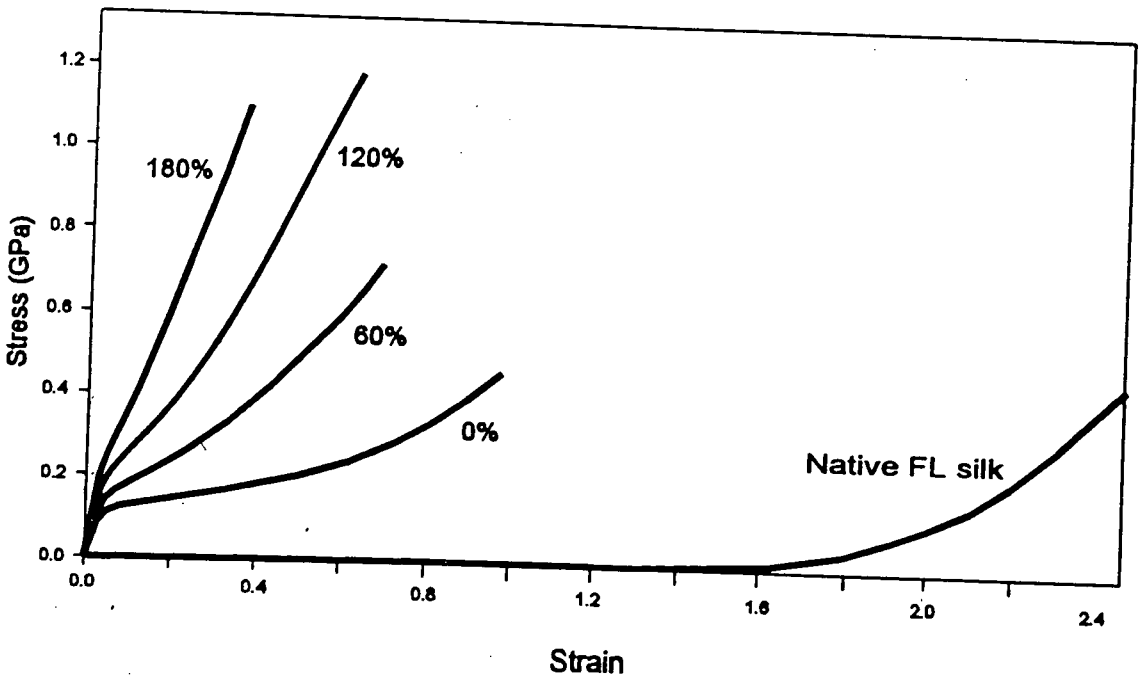
Stress (GPa)
1.2
1.0
0.8
0.6
0.4
0.2
0.0
180%
120%
60%
0%
Native FL silk
0.0
0.4
0.8
1.2
1.6
2.0
2.4
Strain

Figure 4.9.
Plot of mean ultimate stress ± 95 % C.I. vs. processed draw percent for FL silk.

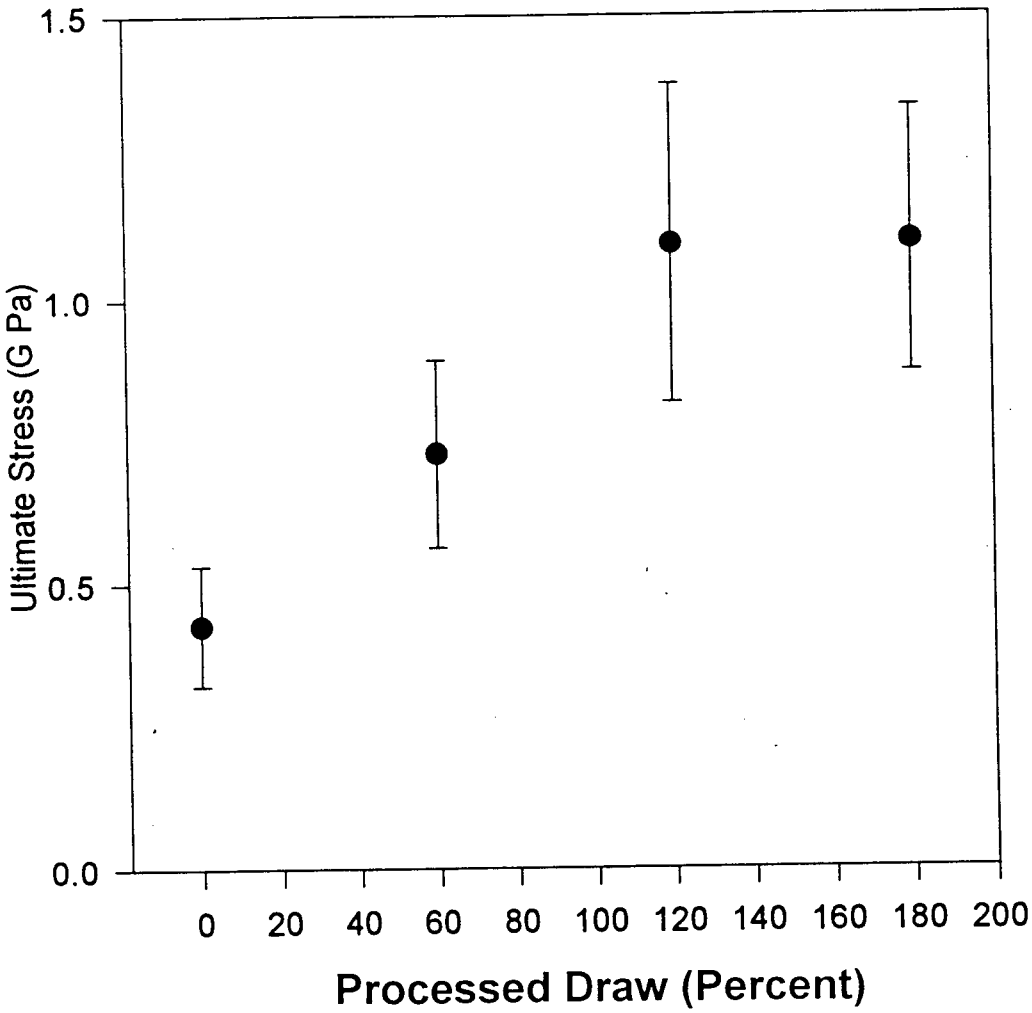
1.5
1.0
0.5
0.0
Ultimate Stress (G Pa)
0
20
40
60
80
100
120
140
160
180
200
Processed Draw (Percent)

Figure 4.10.
Plot of mean yield stress ± 95 % C.I. vs. processed draw percent for FL silk.

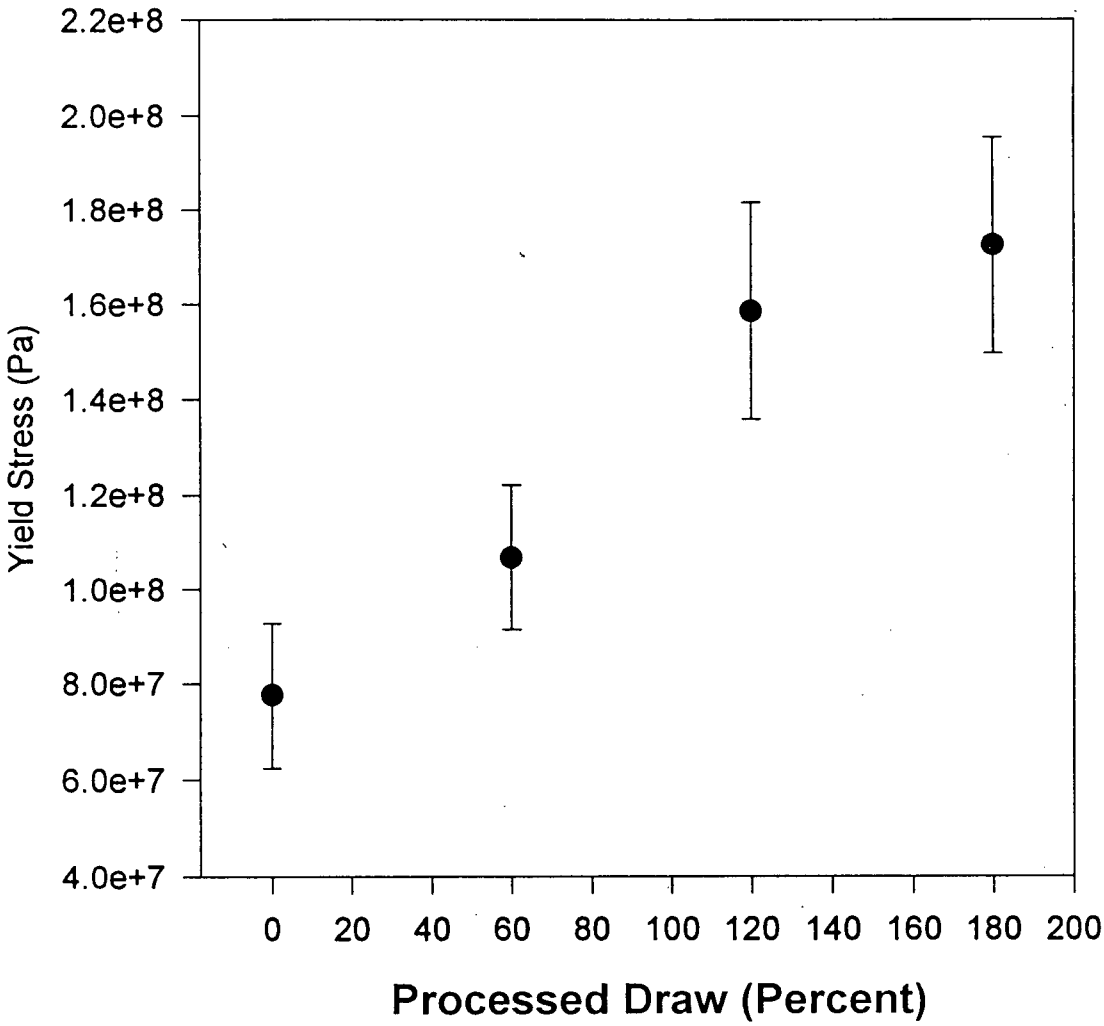
2.2e+8
2.0e+8
1.8e+8
1.6e+8
1.4e+8
1.2e+8
1.0e+8
8.0e+7
6.0e+7
4.0e+7
Yield Stress (Pa)
0
20
40
60
80
100
120
140
160
180
200
Processed Draw (Percent)

Figure 4.11.
Plot of mean failure strain ± 95 % C.I. vs. processed draw percent for FL silk.

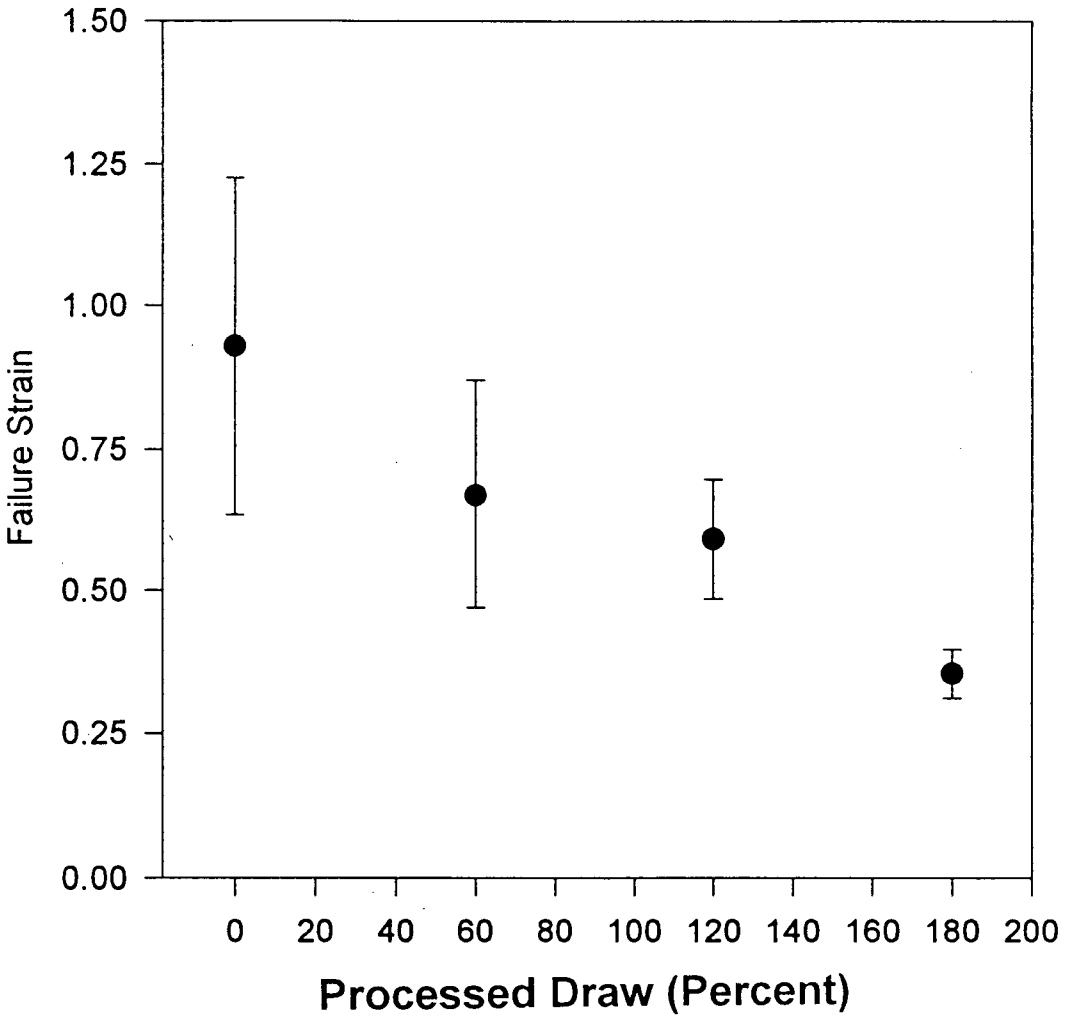
1.50
1.25
1.00
0.75
0.50
0.25
0.00
Failure Strain
0
20
40
60
80
100
120
140
160
180
200
Processed Draw (Percent)

Figure 4.12.
Plot of mean yield strain ± 95 % C.I. vs. processed draw percent for FL silk.

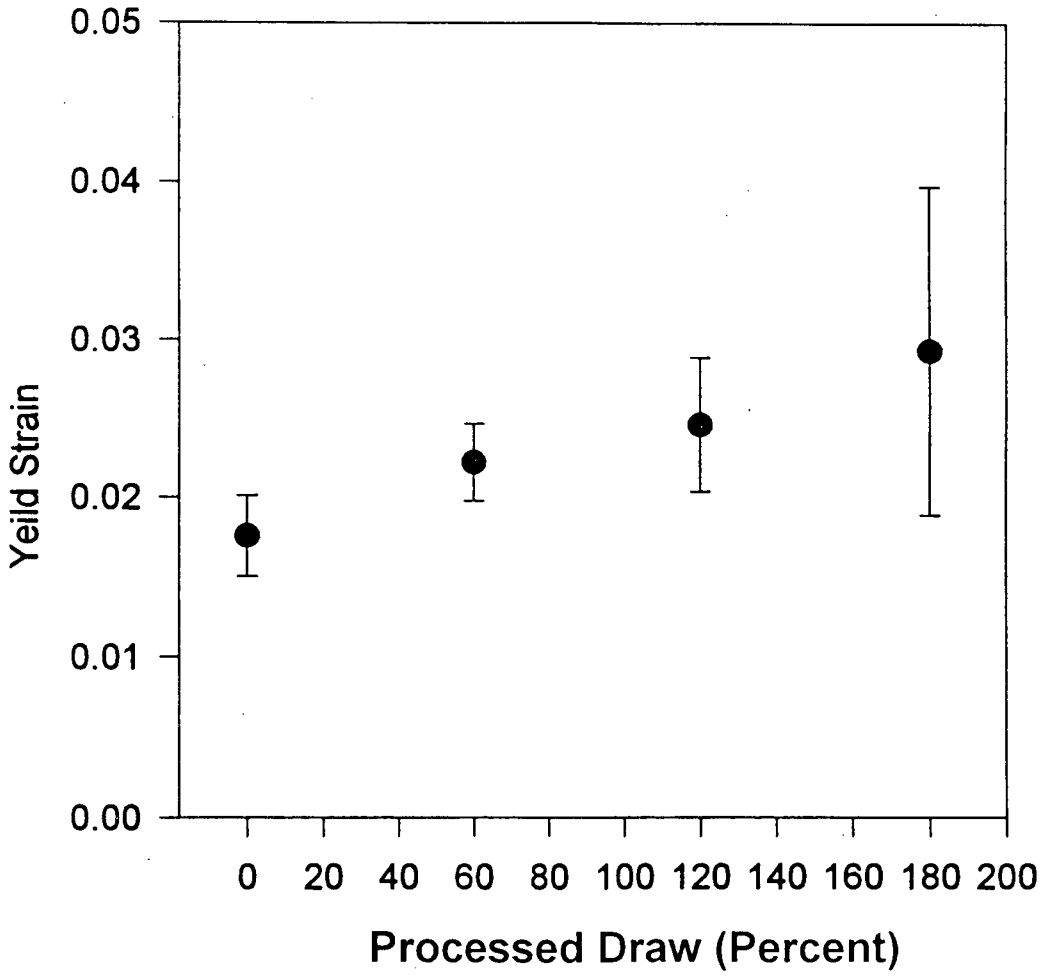
0.05
0.04
0.03
0.02
0.01
0.00
Yeild Strain
0
20
40
60
80
100
120
140
160
180
200
Processed Draw (Percent)

Figure 4.13.
Plot of mean initial modulus ± 95 % C.I. vs. processed draw ratio for FL silk.

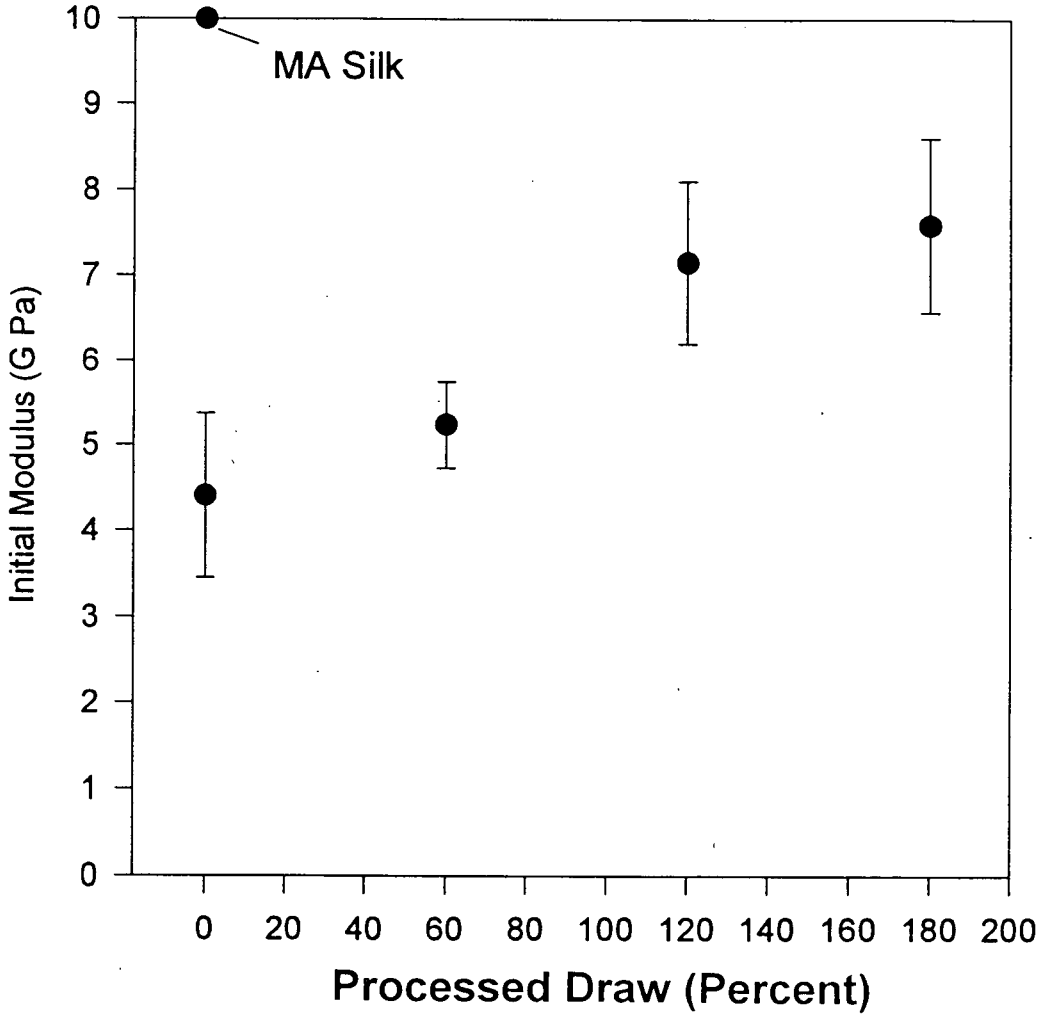
MA Silk
Initial Modulus (G Pa)
Processed Draw (Percent)
0
1
2
3
4
5
6
7
8
9
10
0
20
40
60
80
100
120
140
160
180
200

Figure 4.14.
Plot of mean final modulus ± 95 % C.I. vs. processed draw percent for FL silk.

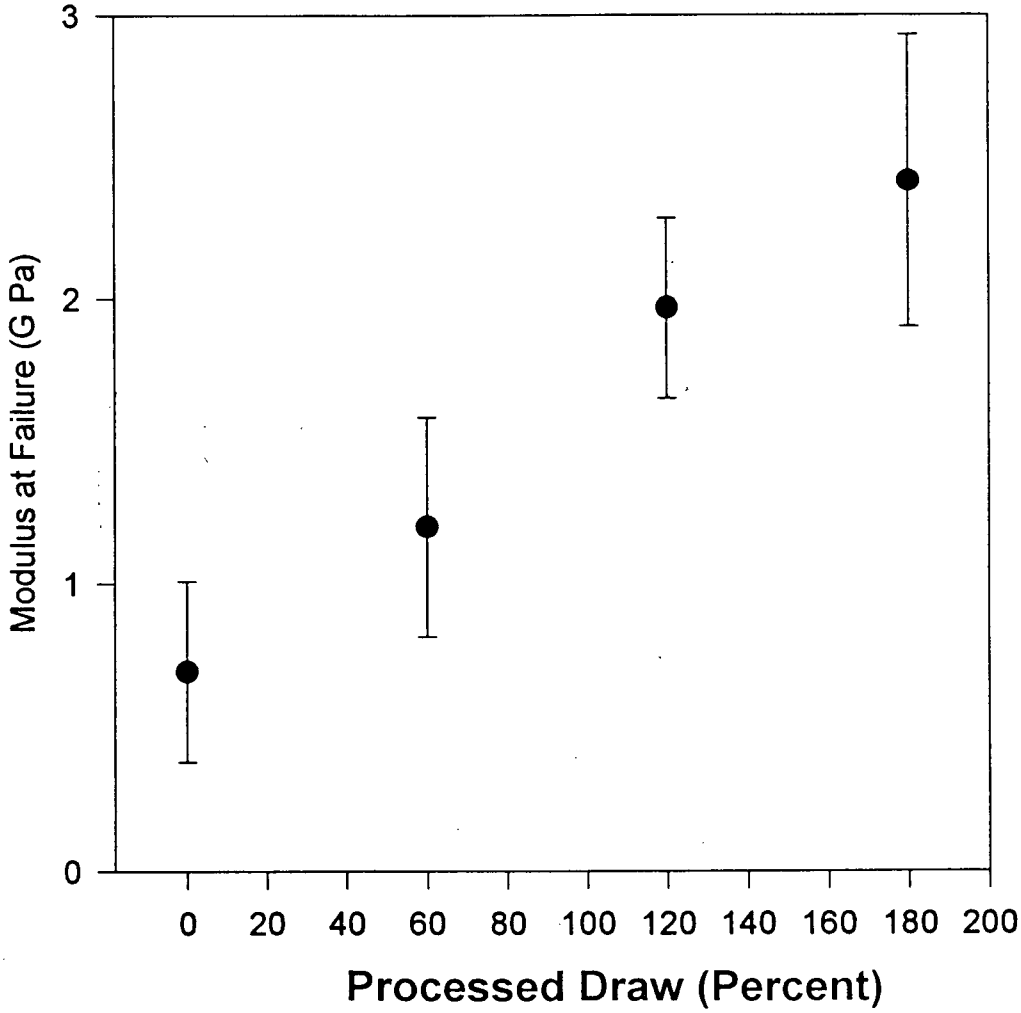
Modulus at Failure (G Pa)
3
2
1
0
0
20
40
60
80
100
120
140
160
180
200
Processed Draw (Percent)

Figure 4.15.

Plot of mean toughness ± 95 % C.I. vs. processed draw percent for processed FL silk.

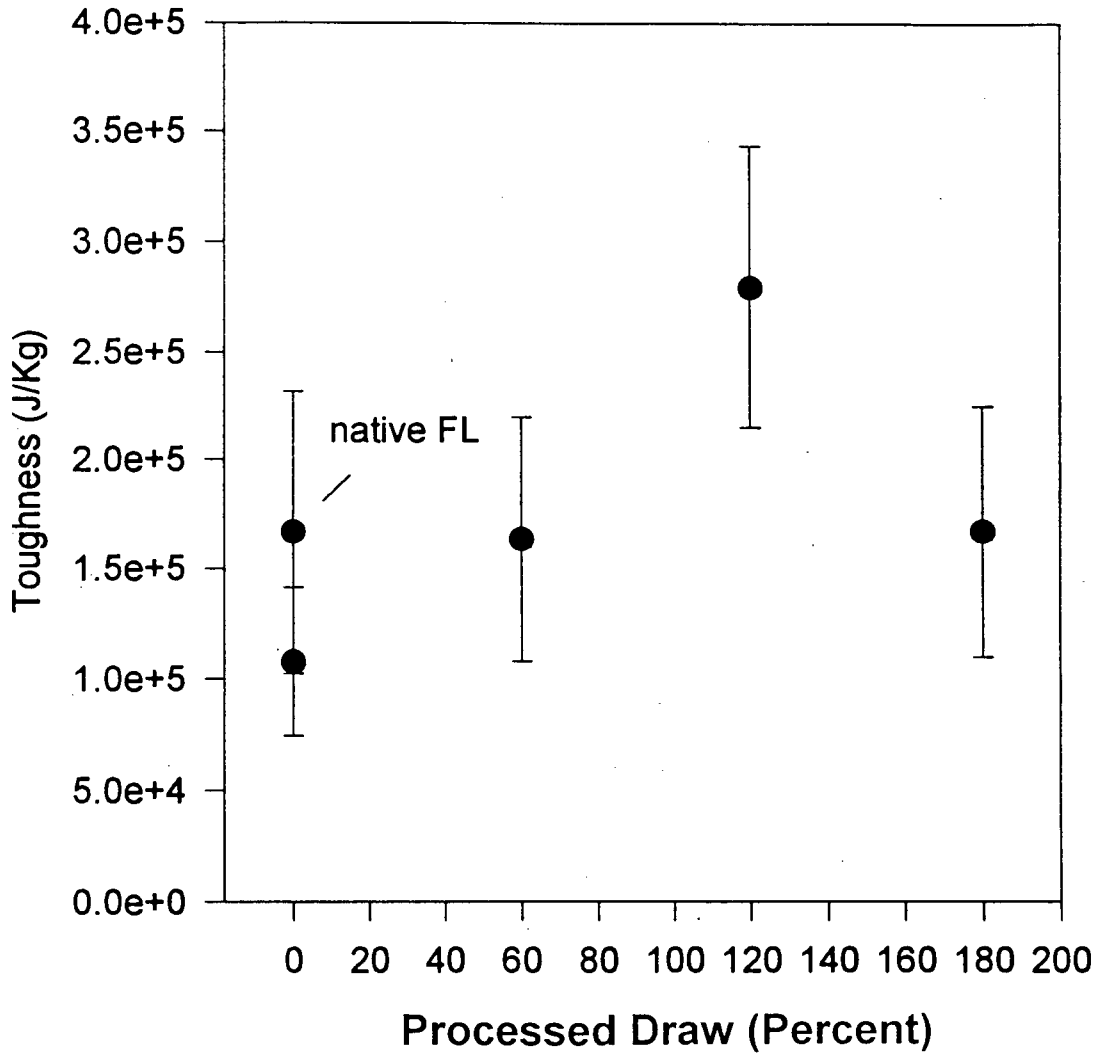
4.0e+5
3.5e+5
3.0e+5
2.5e+5
2.0e+5
1.5e+5
1.0e+5
5.0e+4
0.0e+0
Toughness (J/Kg)
native FL
0
20
40
60
80
100
120
140
160
180
200
Processed Draw (Percent)

these same processed fibers. The 120 % and 180 % processed fibers exhibit remarkable true ultimate stresses of 1.92 G Pa and 1.49 G Pa respectively.

Figure 4.10 shows that engineering yield stress increased asymptotically up to 120 % processed draw. ANOVA indicated significant differences between the mean yield stresses from the different draw treatments ($P < 0.0001$, $F = 29$, $DF = 38$), and the SNK method showed that only the mean yield stresses from 120 % and 180 % draw treatments were statistically similar ($P > 0.05$).

Figure 4.11 shows that failure strain decreased linearly with an increase in draw. ANOVA indicated significant differences between mean failure strains for fibers from the different treatments ($P < 0.0005$, $F = 7.60$, $DF = 38$), and the SNK method showed that the mean failure strain pairs at 60 % and 120 % draw, and 120 % and 180 % draw were statistically similar to each other alone ($P > 0.05$). The mean failure strains for 60 % and 180 % draw were statistically distinct (SNK $P < 0.05$) as were all other pair-wise combinations.

Figure 4.12 shows that yield strain increased moderately and linearly with processing draw. ANOVA indicated significant differences between the mean yield strains from the different treatments ($P = 0.0172$, $F = 3.87$, $DF = 38$). The SNK method showed that the differences only occur between the 120 % and 0 %, and 180 % and 0 % treatment pairs ($P < 0.05$).

Figure 4.13 shows that the initial modulus increased linearly with increased processing draw up to 120 %. ANOVA indicated significant differences between mean initial moduli from the different draw treatments ($P < 0.0001$, $F = 14.2$, $DF = 36$), and the SNK method revealed that only the mean initial moduli from the 120 % and 180 % draw treatments are statistically similar ($P > 0.05$). The mean initial moduli at 120 % and 180 % draw are extremely high, 7.15 G Pa and 7.59 G Pa respectively, and these values approach the initial moduli reported for MA silk (Table 4.1).

Figure 4.14 shows that the final modulus increased linearly with draw processing. ANOVA

indicated significant differences between mean final moduli from the different draw treatments ($P < 0.0001$, $F = 20.5$, $DF = 38$), and the SNK method revealed that only the mean final moduli from 120 % and 180 % processed draws are statistically similar ($P > 0.05$). The 180 % drawn fibers had exceptionally high mean final modulus of 2.40 G Pa, and this value approaches that reported for MA silk. (Table 4.1).

Figure 4.15 shows that toughness increased up to 120 % processing draw and then decreased again at 180 % draw. ANOVA indicated significant differences between mean toughness values from the different treatments ($P < 0.0001$, $F = 19.2$, $DF = 38$), and the SNK method showed that the mean toughness at 120 % draw was significantly different from all other treatments ($P > 0.05$). All other treatments were statistically similar ($P < 0.05$). The toughness of the 120 % draw processed fiber was truly exceptional. With a mean value of 2.79×10^5 J $Kg^{-1,}$ it is tougher than any biological material, and approaches the toughest materials known.

DISCUSSION

The results have demonstrated that, as is the case for high property, flexible chain based polymers like Spectra and Nylon, the supra-molecular organization and physical properties of FL silk are manipulable over a broad range using specific processing regimes. It is important to recognize that the optical data only indicate that an increase in molecular organization occurs with processing and that elucidation of the precise supra-molecular structure adopted by the processed FL network awaits characterization using techniques in solid-state chemistry. Several chemical and physical mechanisms that may underlie the changes in supra-molecular organization and physical properties of the FL network are discussed.

1. The mechanical properties of the native FL silk.

Table 4.1 documented the only published data available on the mechanical properties of orb-spider native FL silk. As a starting point, the mechanical properties of *A. diadematus* silk were again determined in this study. These data were summarized in Table 4.4. Several discrepancies were found to exist between the published mechanical data and that collected in this study. The mean ultimate engineering stress of native FL silk was found to be 0.44 G Pa, which was significantly lower than the values of 1.34 G Pa reported by Kohler and Vollrath (1995) and 0.76 G Pa reported by Denny 1976 for *A. sericatus* FL silk. In addition, while the mean failure strain estimate of 2.48 corroborates well with Denny's estimate of 2.03, Kohler and Vollrath report a mean failure strain of nearly double this value, at 4.76. There are several possible explanations for these differences. First, this study used native FL fiber diameter measurements obtained from the light microscope, while Vollrath and Kohler used diameter measurements obtained from the SEM. Although there is a relatively large error involved in using light microscopy to measure silk fiber diameters because the

fibers are barely the size of the wavelength of light, SEM measurements are done under vacuum, and as such all the water in the sample is likely lost, resulting in a large decrease in fiber diameter. This may explain the fact that Kohler and Vollrath's mean ultimate stress estimates were about 2.3 times greater than that obtained during the course of this study. Also, Denny's measurements of the mechanics of *A. sericatus* FL silk were obtained from force extension records using an Instron tensile testing apparatus. Since the load cell of this apparatus is relatively insensitive, Denny had to test FL silk bundles of 5 to 10 fibers. With this approach problems can arise in terms of differential loading and premature failure of individual fibers in the test bundle. It is unclear why the failure strain reported for *A. diadematus* by Kohler and Vollrath is so much larger than the mean value obtained in this study. If the FL fibers were allowed to reel into the glue droplets before testing, the measured extensibility of the fiber would undoubtedly be greater, since the a large portion of the observed extension would simply reflect the unreeling of the fibers from the glue droplets and not the actual tensile properties of the fiber. However, Kohler and Vollrath appear to have begun their tensile tests at the same resting slack length used in this study. A failure extension of close to 500 % would result in a fiber with a an enormous true ultimate stress of 7.76 G Pa. This value is much higher than that obtained from any known polymeric fiber. The results presented here predict a true ultimate stress for native FL silk that is somewhat more conservative at 1.53 G Pa.

2. The influence of micro-environment on the supra-molecular organization and mechanical properties of FL silk.

2.1. *Optical properties of the wash\dry FL silk.*

The results showed that the wash\dry manipulation of the FL fibers induced an increase in optical anisotropy of the FL network, where the retardation increased by about 10 nm. This

observation indicates that new supra-molecular order develops in the FL network, however, it remains unclear what type of molecular structure develops or what molecular events underlie this increase in optical anisotropy. Several possibilities are discussed here.

First, when the native FL fibers were wash\dried, their diameter decreased from about 2 μm to close to 1μm, while their length was held constant. The removal of water and/or water soluble compounds with processing likely gives way for inward collapse of the FL network that could result in the alignment of amorphous sequences and/or pre-existing crystals along the fiber axis, and thus explain, in whole or in part, the increase in anisotropy of the network. Second, when the FL network is allowed to dry, some sequences must enter a low mobility glassy state. Perturbations in the polarizability of glassy structure are known to result from unbalanced stress on a material, stresses that may develop when the fiber is pulled through the water meniscus and air dried. Finally, the increase in optical anisotropy of the fiber may result from the crystallization of sequences that previously existed in an amorphous conformation. Crystallization may take place as the network collapses and amorphous fibroin sequences are permitted to associate inter-molecularly.

2.2. Mechanical properties of the wash\dry FL fiber.

The mechanical properties of the wash\dry FL fiber may provide additional clues regarding the nature of its new supra-molecular organization. The mechanical signature of the wash\dry processed FL silk was highlighted by very high initial modulus, followed by a sharp yield into a long low modulus plateau and finally a small increase in modulus to failure. The high initial modulus of the processed fibers may indicate that amorphous FL sequences have undergone a drastic reduction in orientational and translation mobility, achieving a glassy state when they are allowed to dry. Amorphous polymers locked in the glassy state create high initial modulus materials that develop

stress concentrations at low strains. When these sequences rupture, the material either fails, or a yield point appears where a low modulus plateau develops as a result of polymer chain slippage. While a plateau was in fact observed for the wash\dry FL fiber, when it is stretched through several discrete extension cycles it maintains its high initial modulus (preliminary data not shown). If a polymer glass alone were ruptured, it likely would not show high initial modulus behavior on subsequent extension cycles. Another possibility is that the high initial modulus behavior is derived from relatively unstable crystal structures created in the wash\dry process. The yield may develop when these crystals unfold at greater strains, giving rise to the observed low modulus plateau. In both cases, the subsequent rise in modulus to failure could result from alignment of pre-existing crystals that begin to bear load on further extension or possibly from stain induced crystallization processes.

Regardless of the precise supra-molecular structure of the wash\dry processed FL silk, the dramatic change in both optical and physical the properties must implicate water and/or water soluble LMW compounds known to be present in whole web water wash offs as 'plasticizers' of the FL silk network, and indicate that a specific micro-environment is key to determining the physical properties of the native FL silk in the orb-web.

3. The influence of plasticizers on supra-molecular organization and fiber properties.

3.1 Plasticizers of the FL fibroin network.

Plasticizers are chemical compounds that are incorporated into materials to increase workability and extensibility. The addition of a plasticizer to a material can decrease its ultimate strength and modulus while increasing extensibility. Four separate theories have emerged to account for the effects that plasticizing compounds have on polymers (Sears and Touchette, 1988). The *Lubricity* theory stipulates that the stiffness of a material results from inter-macromolecular friction

and that the plasticizer provides internal lubrication to facilitate movement of polymer chains across one another. The *Gel* theory, devised for amorphous polymers, predicts that these materials resist deformation because they are connected by loose inter-molecular attachments along the length of the polymer chains. In this case, the plasticizer is believed to mask centers of force by selectively solvating the polymer at the attachment points, producing the same result as if the polymer were cross-linked to a lesser degree. *The Mechanistic Theory* is similar to the *Gel Theory*, but it predicts that plasticizers are never permanently bound to centers of force and are in a dynamic equilibrium between solvation and desolvation. As a result, a certain fraction of force centers is continually masked by the plasticizer. The *Free Volume Theory* predicts that spaces in a polymeric network provide for freedom of movement of polymer chains under the appropriate time, temperature, or pressure conditions. The polymer can be 'internally' plasticized by increasing chain ends (ie. decreasing molecular weight of the polymer), or by adding flexible side chains to the main chain backbone of the polymer. The addition of a LMW 'external' plasticiser can also increase free volume and freedom of movement of the polymer chains by creating spaces in the network for the polymer chains to move into. For semi-crystalline polymers this mechanism operates primarily on amorphous and imperfect crystal structure (Sears and Touchette, 1988).

In the polymers industry, the most commonly used plasticizers are organic, and are esters of carboxylic acids or phosphoric acid, hydrocarbons, halogenated hydrocarbons, ethers, poly-glycols and sulfonamides. Even some LMW elastomeric polymers have shown plasticizing effects. Water is *the* biological plasticiser. Wool, cellulose, silk, and elastin are examples of polymers known to be plasticized by water, and in its absence amorphous polymer sequences can become crystalline and/or glassy. Water plasticizes biolpolymers because it is polar and can disrupt non-covalent hydrogen bonds. For example, water can plasticize some crystalline structure in Cellulose by disrupting inter-

chain hydrogen bonds, and this phenomenon results in a dramatic decrease in the initial modulus of cellulose (Vincent, 1980). The amorphous sequences of MA silk and elastin are also plasticized by water, where water disrupts hydrogen bonds that stabilize amorphous sequences, thus imparting mobility to the amorphous chains. It is reasonable to suspect that amorphous FL sequences are plasticized by water, but because the fiber is so thin, water alone would most definitely evaporate from the FL silk as soon as it is spun. However, of the LMW compounds contained in whole-web water wash-offs, Choline, N-acetyl taurine, N-acetyl putrescine, Isethionic acid and GABamide are all hygroscopic at high relative humidities (RH's). In fact, above 50 % RH, these compounds can attract enough water to give a 70 % weight increase from their dry sample weight (Vollrath et al. 1990). Only Choline, and to a lesser degree N-acetyl taurine are hygroscopic in the physiological 20-30 % RH range (see Figure 2b in Vollrath et al. 1990). (N-acetyl putrescine is also mildly water absorptive in this range). These compounds appear to be small enough to interpenetrate the FL fibroin network, and if they do, they may function as osmoregulators, recruiting water molecules from the atmosphere to plasticize the FL network. Vollrath et al. (1990) and Townley et al. (1991) note that the organic LMW compounds listed in Table 4.2 are similar to those which occur in eubacteria, plants and animals which are subject to osmotic stress that arises from variable intracellular osmotic concentrations. Since the orb-web must be subject to large humidity fluctuations in the field, solute concentration must also vary regularly within the adhesive glue. High or variable inorganic salt concentrations could have disruptive effects on fibroin structure or could result in salt crystallization. Therefore, salts may have been avoided during selection in favor of the hygroscopic organic LMW compounds that remain miscible in the aqueous glue (Vollrath et al. 1990). The LMW compounds are either organic amines that carry a net positive charge, or anions of strong acids. Together, these compounds may maintain a concentrated hygroscopic solution with a stable vapor pressure that could

also minimize their own interaction with the AG or FL fibroins. Townley et al. (1991) and Vollrath et. al. (1990) indicate that Betaine, Taurine, GABA and glycine are all considered compatible solutes for proteins, so even at high concentrations they may minimally perturb protein structure. They also note that some of the charged side groups of these compounds resemble ions known to have stabilizing effects on macromolecules.

Some of the LMW compounds present in the FL silk glue coating may act as plasticizers by directly interacting with the FL fibroin network during spinning and in the orb-web. Figure 4.16 shows the molecular structure of three of the high concentration LMW compounds present in the FL silk glue coating along with one of Nylons plasticizers, N-ethyl toluene sulfonamide. (Recall that Nylon 6,6 chains bear likeness to natural protein sequences). Though not identical, note the structural similarities between these compounds. N-acetyl taurine, Isethionic acid and N-ethyl toluene sulfonamide all contain sulfonyl groups, and N-acetyl taurine and N-ethyl toluene sulfonamide both also contain a single amide attached to an ether. Unlike Nylon's plasticizer, N-acetyl taurine, Isethionic acid and GABamide are all polar and as such they may have an affinity for the mildly hydrophilic amorphous sequences of ADF-5 and ADF-3. In this case, the *Gel* or *Mechanistic* theory would best describe the plasticizing mechanism. On the other hand, the polar LMW compounds should also have an affinity for water which could mask the charge of the compound in question. If this is the case, the Free Volume theory may best describe the 'external' plasticizing effects of a LMW compounds. Any excess 'unbound' water could directly plasticize the network as well.

3.2. Dialysis experiments.

The dialysis experiments were designed to assay for the presence of a plasticizer in the FL

Figure 4.16.

Chemical structure of a) N-acetyl taurine b) Isethionic acid c) GABamide, d) Nylons plasticiser, N-toluene sulfonamide and e) the sulfa drug sulfanylamide.

a)

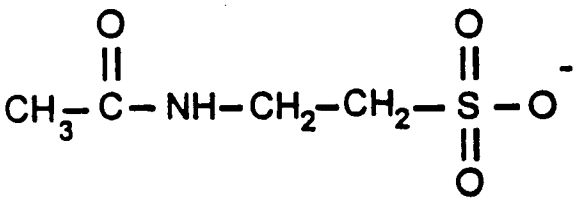

b)

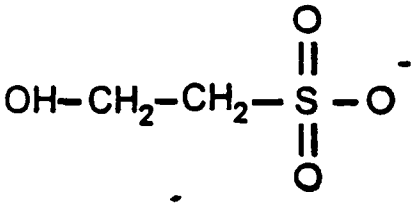

c)

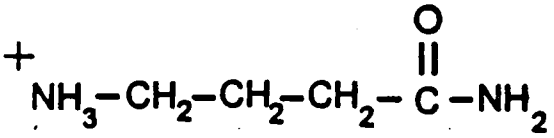

d)

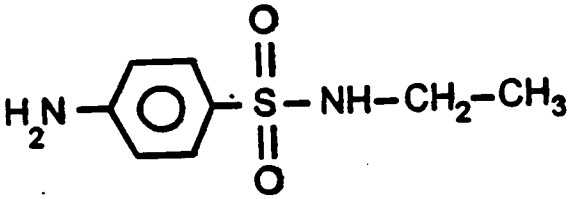

e)

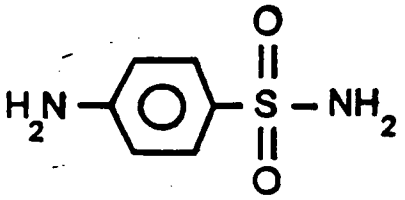

secretion and to determine if any LMW compound present could inhibit crystallization in other silk secretion types. A small amount of fine crystal structure appeared in the dialyzed\sheared FL secretion that was not seen in the control dialized FL shear product. This result suggests that at least one water soluble LMW plasticiser is present in the FL gland. The dialysate from the FL secretion was also shown to have an inhibitory effect on the MA secretion when it was allowed to dry, but no difference was seen between MA secretion sheared in the presence of a dialysate compared to that sheared in a drop of water. These results suggest that a water soluble LMW plasticiser exists in the FL gland, but that some MA fibroin sequences have a large tendency to crystallize even when sheared in its presence.

An attempt was made to determine which, if any, of the LMW compounds listed in Table 4.2 had plasticizing effects on the MA, MI, FL and CY secretions by testing several of the LMW compounds obtained in synthetic form. All of the compounds tested failed to show crystal inhibiting effects on dried or sheared MA, MI, FL or CY secretions whether these compounds were assayed individually or together at physiological concentrations (data not shown). It is noted that GABamide and N-acetyl taurine were not commercially available and that GABA and Taurine were used in their place. It is possible that the side groups that are absent from these compounds are essential to their plasticizing capacity.

At this time it is not possible to forward any direct conclusions regarding the identity of the LMW plasticizer or its specific mode of action. Future investigations should include testing the plasticizing action of GABamide and N-acetyl taurine and determining if the aqueous AG glue has plasticizing effects on other silk secretions and fiber types. It would be interesting to forcibly silk the MA fiber from the orb-spider after having injected the aqueous glue, individual LMW compounds, or plasticizers used in industry directly into the silk gland, to determine if the physical properties of

fibroin secretions with a high propensity to crystallize can be controlled when they are spun in the presence of a plasticizer.

3.3. Additional functions of the LMW compounds.

Choline, Isethionic acid , N-acetyl taurine, GABamide and Glycine are all biochemically related to inhibitory neurotransmitters. It is therefore possible that the FL silk glue is neurotoxic to prey, making escape from the web even more unlikely. These LMW molecules may have been derived over an evolutionary time scale from the neurons known to innervate some silk glands (Vollrath et al. 1990). Some of the LMW compounds may also act in an anti-fungal or anti-microbial capacity. Figure 4.16 includes the chemical structure of the synthetic anti-microbial agent sulfanilamide. Note the similarities between the LMW compounds and Sulfanilamide. Sulfanilamide is known to mimic the chemical structure of p-Aminobenzoic acid which many bacteria require to synthesize Folic acid (Solomons, 1990). It may therefore be hypothesized that some of FL silks LMW compounds combat microbial attack in addition to acting as plasticizers. Finally, the hygroscopic nature of the LMW compounds is believed to be important in the spiders regular uptake of water, as it consumes its web every 1 or 2 days (Vollrath and Edmons, 1992).

4. The effect of draw processing on the supra-molecular order and physical properties of the FL silk.

4.1. Optical properties of the wash\draw\dry processed FL silk.

Table 4.3 and Figure 4.7 showed that the birefringence of the draw processed FL silk increased asymptotically with increased draw ratio. These results indicate that draw processing increases supra-molecular orientation, but it is again not clear weather this increase results from

alignment of amorphous sequences and/or pre-existing crystals along the fiber axis or from the formation of new crystal structure.

In order that the reader may appreciate the relative magnitudes of increase in anisotropy with strain for differentially crystalline fibers, the birefringence-strain plots a random polymer network (predicted from network theory, Pollak (1993)), hydrated MA and FL silks, draw processed FL silk and draw processed Nylon are included in Figure 4.17. When the random network is aligned, a small increase in birefringence is observed that results from alignment of amorphous sequences along the fiber axis. The hydrated FL silk exhibits a somewhat greater rise in birefringence with strain since it contains a small proportion of crystal structure that originally had little preferred orientation, but that becomes aligned at greater extensions. The hydrated MA fiber exhibits an initial Birefringence slightly lower than the wash\dry processed FL fiber. Recall that when MA silk is hydrated its amorphous MA sequences become mobile, and they retract, resulting in a decrease in alignment of crystal structure along the fiber axis and a concomitant reduction in fiber length. The crystals are, however, stable in water so that when the fiber re-extended, birefringence rises rapidly, resulting from the re-alignment of the large proportion of crystal structure known to be present. (Note that the dashed line for the MA Birefringence represents my own extrapolation since birefringence data above 0.6 strain were not available for the hydrated MA fiber). The idealized curve for the draw processed FL silk was inferred from the incremental values of birefringence obtained from the 0, 60, 120 and 180 % draw processed fiber. Note that 0% strain birefringence is substantially greater than that of the random network or hydrated FL fiber. The birefringence rises asymptotically with increased strain (actually incremental draw ratio) and approaches the birefringence of the dry native MA fiber. The idealized curve for Nylon was inferred from incremental birefringence values for cold drawn Nylon provided by (Zimmerman, 1988). Nylon shows a rapid increase in birefringence with processing

Figure 4.17.

Birefringence-strain plots for a random network, hydrated MA and FL silk, and draw processed Nylon and FL silk.

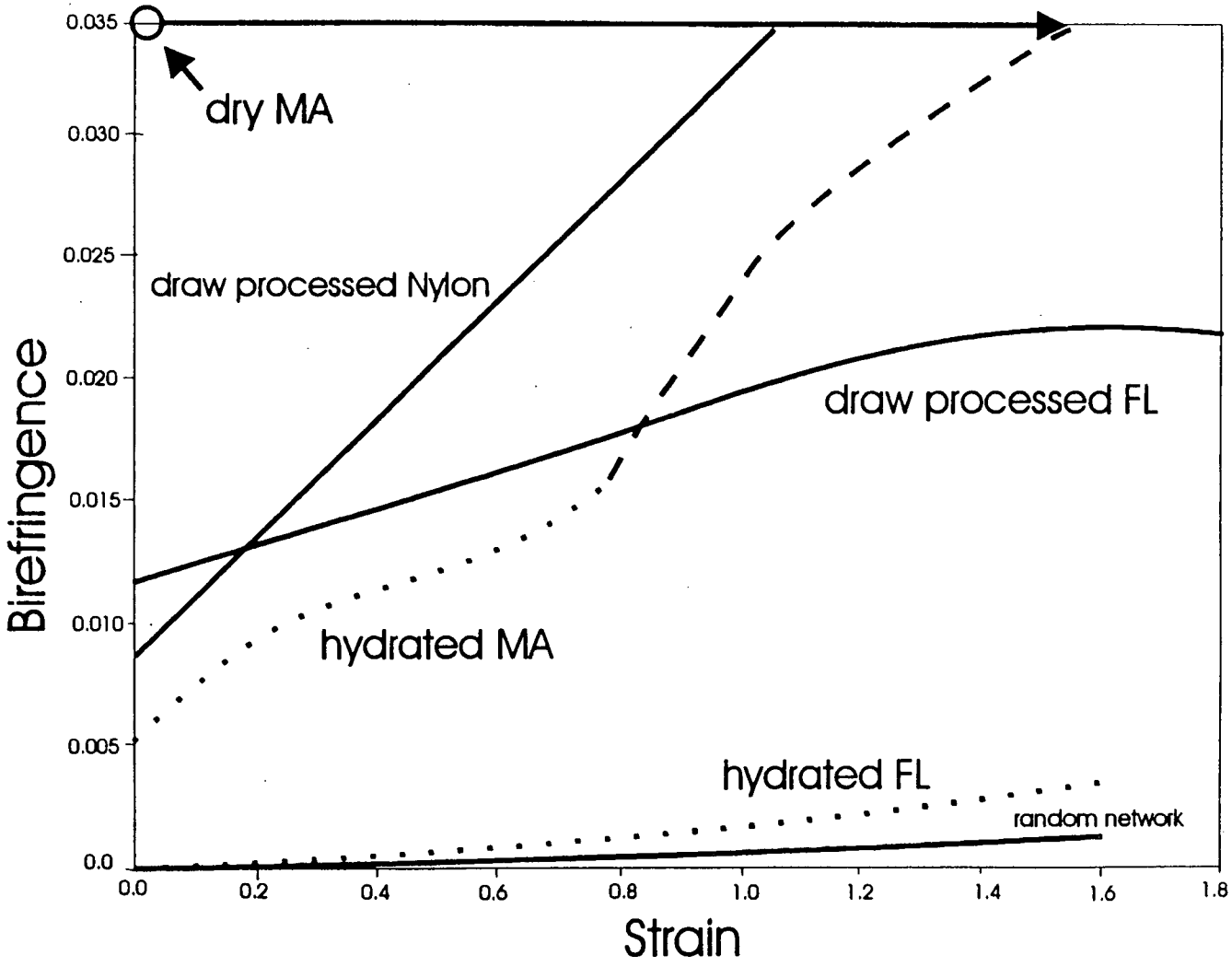
0.035
0.030
0.025
0.020
0.015
0.010
0.005
0.0
Birefringence
dry MA
draw processed Nylon
draw processed FL
hydrated MA
hydrated FL
random network
0.0
0.2
0.4
0.6
0.8
1.0
1.2
1.4
1.6
1.8
Strain

draw, and this is known to result from the creation of new extended chain crystal structure. Figure 4.17 provides only a conceptual picture of the change in birefringence with strain for these differentially crystalline materials. It is important to note that the hydrated FL fibers are roughly twice the diameter of the dry processed silk, and the dimensions of the crystal structures present in FL silk are not known, so that a direct inference of the proportion of crystal structure present from these data is not possible. Also, it would be unwise to generate quantitative comparissons between the different fiber types based on these data since compositionaly distinct polymer chains may exhibit differential polarizabilities.

It is of particular interest to determine if draw processing actually induces the formation of new crystal structure within the FL network. Therefore an attempt was made to tease out the contribution of alignment of amorphous and/or pre-existing crystal sequences to the retardation of the processed fibers by subtracting mean retardation values obtained from the hydrated native FL silk from those of the processed FL fibers at equivalent extensions. (Recall that retardation is used rather than birefringence because the fiber diameters in the hydrated and processed dry states were not equivalent). In order to do so, it must be assumed that 1) the hydrated native FL fiber does not undergo strain induced crystallization and that an increase in retardation of the extended native FL silk is solely a reflection alignement of amorphous and/or pre-existing crystals, and 2) local stress distortions in glassy structure contribute minimally to the polarizability of processed fibers.

Table 4.5 shows the mean retardation values obtained from the processed fiber as they were presented in Table 4.3, but also includes mean retardation values for the hydrated native FL silk at equivalent extensions (inferred from Pollack, 1993). In all cases retardation increased by ~ 10 nm. The 60 % draw processed fiber had a retardation of 9.78 nm greater than the native strand at an equivalent extension, and the 120% processed fiber had a mean retardation of 10.94 nm greater than

Table 4.5.

Retardation (Γ) difference between wash\draw\dry processed FL fibers and hydrated FL silk at equivanlent extensions. Numbers in brackets are sample sizes. Reference : 1. Pollack, 1993.

% extension	Γ pocessed FL silk	Γ hydrated FL silk [1]	Γ processed - Γ native
0	12.78 (10)	3.10 (4)	9.68
60	14.33 (10)	4.62 (2)	9.71
120	16.82 (10)	5.88 (2)	10.94

the native strand at the same extension. These observations, coupled with the preliminary comparisons of birefringence-strain behaviour of the hydrated and draw processed FL silk presented in figure 4.17, indicate that draw processing induces the formation of new supra-molecular organization in addition to amorphous sequence and/or pre-existing crystal alignment. The data therefore suggests that new crystalline structure develops with draw processing, however the quantity or morphology of these new crystals is not known.

4.2. Possible supra-molecular crystal morphology in draw processed FL fibers.

It may be predicted that draw processing aligns formerly amorphous ADF-5 and ADF-3 sequences, encouraging crystallization in the extended chain conformation on drying. However, ADF-5 contains a predominance of proline residues whose side chains link back to the peptide main chain, and these likely introduce a kink in the peptide backbone, making the chain non-linear. Also, because the prolines are irregularly spaced, ADF-5 sequences may not align, pack and crystallize as readily as the regular glycine and proline-rich sequences of collagen, regardless of the processing regime. X-ray diffraction data from synthetic poly (G-G-P) peptides indicates that these sequences can form a hybrid PGII-PPII extended chain crystal structure. The PG-II structure is that referred to in Chapter 1 which has already been observed on a local scale in *N. madagascarensis* MA silk. PP-II structure develops in synthetic poly(proline) sequences from anti-parallel, left-handed helices containing three proline residues per unit cell (Fig. 4.18a). PG-II-PP-II hybrid chains also form a left-handed helix, but because the proline residues occur directly above one another, the complete chain is highly asymmetric. Figure 4.18b shows that these chains can pack together in antiparallel configuration where sheets are stabilized by inter-chain hydrogen bonds. Separate PG-II-PP-II sheets pack in a slightly staggered manner to accommodate the proline side chain. Because of the similarity

Figure 4.18.

a) Structural model of the poly(proline) PP-II helices in crystal form. b) Structural model of the PGII-PPII hybrid crystal. Both views are down the chain axis.

a)

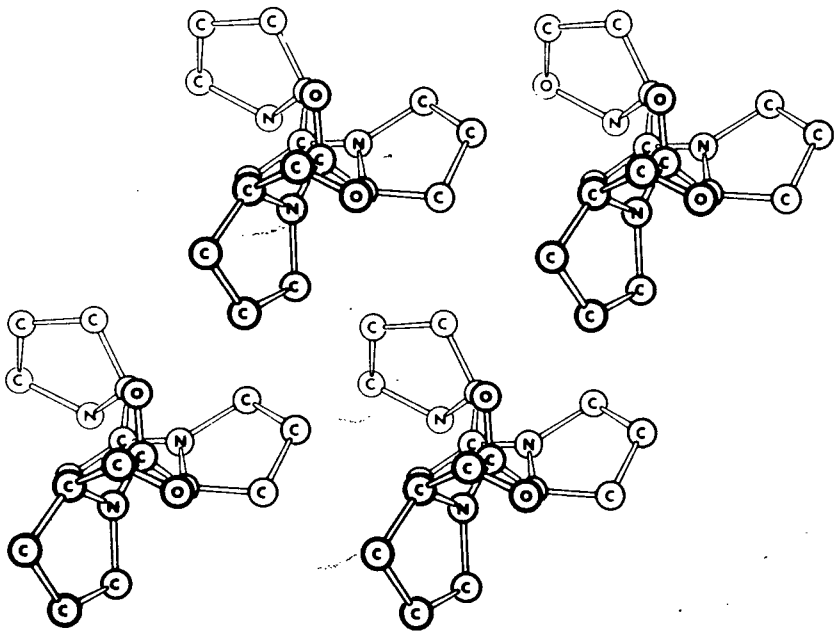

b)

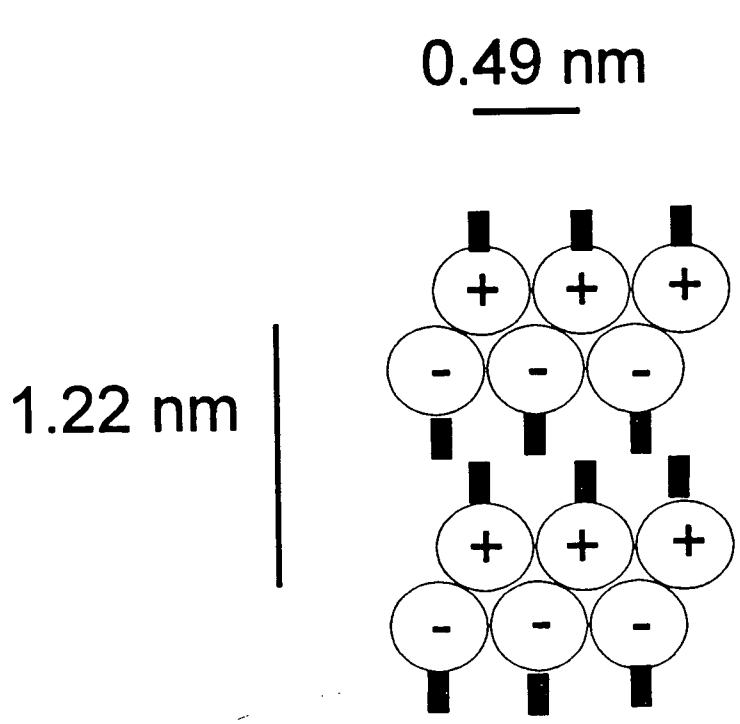

between the ADF-5 and poly(G-G-P) sequences, it may be hypothesized that the new crystal structure suggested to be present from the optical and mechanical data in this study is in the PG-II-PP-II form. It is noted, however, that the irregular placement of proline residues along the length of ADF-5 may actually impede the assembly of such structure. It is conceivable that new crystal structure may also arise through the alignment of amorphous ADF-3 glycine rich amorphous sequences into the PG-II conformation, or from the creation of many other possible crystal morphologies from amorphous ADF-3, ADF-5 and as yet unknown FL fibroin sequences.

The true identity of the new supra-molecular order of processed FL silk remains to be elucidated. In 1994 I attempted to generate x-ray diffraction patterns from bundles of 100 wash\dry and wash\draw\dry FL fibers at DuPont's Pioneering Experimental Research station in Wilmington Delaware. Unfortunately, these bundles were too small to provide a sufficient diffraction pattern. In the future, much larger sample sizes will be needed, in the range of 5000 to 10000 processed strands, to generate interpretable diffraction patterns. Another option would be to use electron diffraction or synchrotron radiation which can provide x-ray patterns from a single fiber.

5. The mechanical properties of the wash\draw\dry processed FL fibers.

The mechanical properties of the FL silk were shown to be manipulable over a broad range with the water wash\draw\dry protocol. The physical property-draw dependence of the FL fiber is remarkably similar to that observed in other synthetic flexible chain polymers including Spectra and Nylon. Figure 4.19 shows that the changes in mechanical properties that poly(ethylene) exhibits with increase processing draw ratio are quite similar to those observed for FL silk. Figure 4.19a shows that, like FL silk (see Fig. 4.9), increased processing draw ratio results in an asymptotic increase in ultimate stress. Figure 4.19b shows that poly(ethylene) also exhibits a linear increase in initial

Figure 4.19.

The influence of draw processing on a) tensile strength, b) modulus and c) failure strain of poly(ethylene).

a)

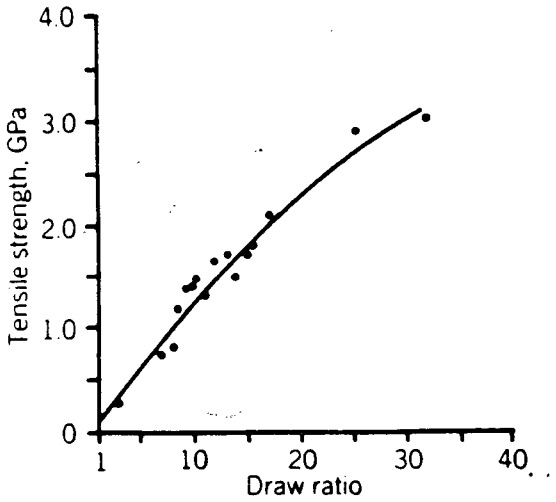
Tensile strength, GPa
4.0
3.0
2.0
1.0
0
1
10
20
30
40
Draw ratio

b)

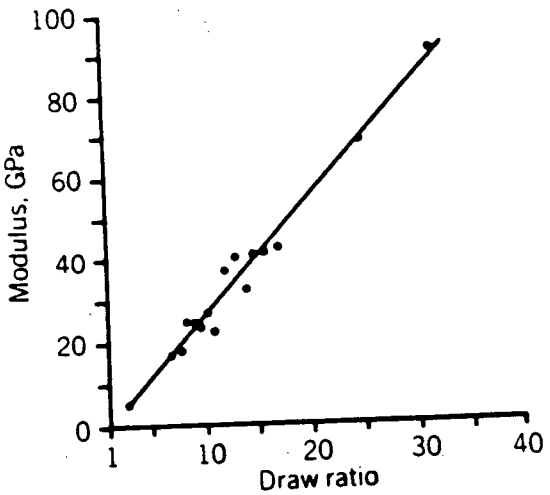
Modulus, GPa
100
80
60
40
20
0
1
10
20
30
40
Draw ratio

c)

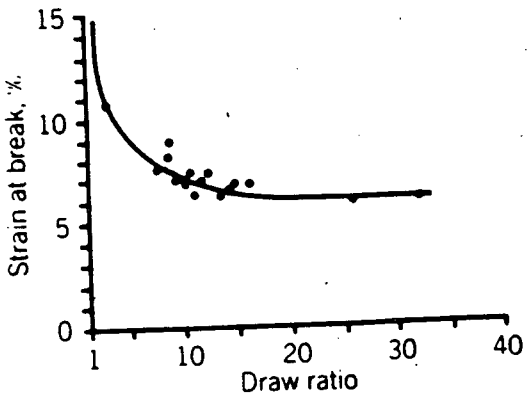
Strain at break, %
15
10
5
0
1
10
20
30
40
Draw ratio

modulus with increased draw, as is the case for the FL silk (Fig. 4.13). Finally, Figure 4.19c shows that poly(ethylene) exhibits an exponential decrease in failure strain as a result of increased processing draw, while the processed FL silk showed a linear decrease (Fig. 4.11). The physical properties of flexible chain polymers evidently depends intimately on the degree of alignment imparted to the chains during processing, and the results of this study show for the first time for any biopolymer that such is the case for spider FL silk. In addition, since the results indicate that ADF-5 may have the capacity to crystallize on extension, it may be suggested that the exceptional ultimate strength of the native FL fiber is explained by strain crystallization phenomena at high extensions. It may also be suggested that the orb-spider may take advantage of specific draw processing regimes during spinning to tune the properties of the FL and its other silks in the wild.

The FL fiber processed to 120 % draw exhibits truly remarkable properties. It is as strong as the MA silk and almost as stiff, but because of its greater extensibility, it about doubles MA silk's toughness at 2.79×10^5 J Kg^{-1}. This is tougher than any biopolymer known, and this value approaches that of some of the toughest man made materials. Table 4.6 compares the toughness MA silk and 120 % draw processed FL silk with the toughest materials known. Processed FL silk ranks only to second in toughness to Fused Silica, a ceramic-glass used in the construction of spacecraft windows, and it is even tougher than Beryllium Oxide, a super-tough material used to construct electronic heat sink substrates. Naturally, in considering how competitive a material is, there are many parameters that can be considered, including thermal stability and resistance to UV bombardment, but because there is little data available on these parameters for silks this discussion is restricted to mechanical properties. Table 4.6 also includes ultimate strength and moduli for the same materials. Both MA silk and the processed FL silk are inferior the best man made fibers and materials. However, the fact that some orb-spider silks are in the same 'ball park' with man made

Table 4.6.

Mechanical properties of some of the highest performance materials known. References : 1. Denny 1976, 2. Jaffee 1988, 3; Gilman, 1996.

Material	**Strength G Pa**	**Modulus G Pa**	**Extensibility %**	**Toughness × 10^5 J Kg^{-1}**	**Ref**
MA silk	1.42	10	27	1.40	1
FL silk, 120 % draw	1.21	7.15	59	2.79	pers.
Kevlar	4	124	2.5	0.24	2
Spectra	5	119	5.2	1.22	2
Fused Silica	14	73	19.2	6.05	3
Berylium Oxide	25	380	6.5	2.88	3

super-materials is striking.

6. Native FL silk's mechanical properties are important for efficient vibrational signal transmission in the orb-web.

FL silk evidently has the potential to be processed into a fiber with greater strength and toughness than what is observed for the native FL strands retrieved from the orb-web. The question arises as to why orb-spiders do not make superior property FL fibers during web construction. One main reason may be the requirement for efficient transmission of vibrational signals generated by entrapped prey in one part of the web to the spiders location at the central hub or nearby retreat.

Orb-spiders detect both the presence and location of entangled prey from vibrations that are transmitted along radial MA strands to lyriform organs located in their tarsal-metatarsal joints. Three types of vibration occur along the MA fiber radii; longitudinal (along the axis of the fiber), transverse (perpendicular to the fiber axis and the web plane) and lateral (perpendicular to the fiber axis and parallel to web plane). Masters (1984) has examined the efficiency of transmission from a vibration source in the catching portion of the web to the central hub using vibration frequencies in the physiological range, between 1 and 10 kHz. Longitudinal vibrations are considered the major signal source and are transmitted along the MA radial fibers with the least amount of attenuation, with a loss of only 1-2 decibels (dB) at vibration frequencies ranging from 1 Hz to 1 kHz (Masters, 1984). There was no correlation between longitudinal attenuation and distance from the vibrator to the central hub, indicating that attenuation due to viscous losses in the stimulated radial strand is not significant over the distances tested (63 ± 11mm). In addition, longitudinal vibrations were found to be directional, where the amplitude of the adjacent non-stimulated radius is about 6 dB less that the stimulated radius up to 1 kHz, and 15 to 20 dB lower above this frequency.

As the longitudinal wave travels along the MA radial strand it will encounter, on average, twelve FL fiber junctions. The cross-strand interactions, if viewed as a simplified infinite string model, will result in the conversion of the MA radial fibers longitudinal waves into lateral vibrations in the cross FL strands, and the lateral impedance of the FL strands will determine the efficiency of transmission of the longitudinal vibration along the MA radius (Masters 1984). The transmission of the MA radial vibration's longitudinal pathway is expressed as:

$$T=2Z_1/Z_{1+}Z_2 \qquad (2)$$

where Z_1 is the longitudinal impedance of the input strand and Z_2 is the sum of the lateral impedances of the output strands, and impedance is defined as the stress force velocity per unit velocity at any point along the string in a traveling wave, or

$$Z=a(E\rho)^{½} \qquad (3)$$

where a is the cross sectional area of the string, E is Young's modulus, and ρ is the linear density of the string. Apparently, if the lateral impedance of the FL fibers were greater or equivalent to the longitudinal impedence radial MA fiber, transmission of the longitudinal wave would be drastically reduced, as would be the case for the high initial modulus processed FL fiber. In the web, the lateral impedance of the native FL strand is at least two orders of magnitude lower than the longitudinal impedance of the MA radial fiber because the native FL silk retains a much lower initial modulus. As result, longitudinal transmission is not drastically reduced by the FL cross strands, and the dinner bell sounds without a hitch.

Concluding remarks.

The results presented in this chapter indicate that specific chemical and physical processing conditions can influence the supra-molecular organization and mechanical properties of orb-spider

FL silk. The wash\dry experiments indicate that a water soluble LMW plasticizer is present in FL silks aqueous glue coating that acts by either recruiting water molecules from the atmosphere, which in turn plasticize the fibroin network, or by interacting directly with the silk network. The processing draw experiments indicate that like other synthetic flexible chain polymers, physical draw processing aligns the FL silks constituent fibroin chains and possibly encourages the formation of new crystal structure on drying. The precise morphology of any new crystal structure remains to be elucidated using solid-state chemistry. At this time it is unclear if the orb-spider takes advantage of specific draw regimes to modulate the supra-molecular crystallinity and mechanical properties of its many silks in the wild.

CHAPTER 5

GENERAL CONCLUSION

INTRODUCTION

The previous chapters described the experimental elucidation of several mechanisms that the orb-spider *A. diadematus* employs to modulate the supra-molecular crystallinity and ultimately the physical properties of its variety of mechanically distinct silks. While spider silk is a natural protein fiber, this work was presented within the context of the supra-molecular morphology and mechanics of many fibrous polymers, both biological and synthetic, since decades of industrial polymers research undoubtedly provide a solid foundation to study factors that govern supra-molecular organization in biopolymers. Biopolymer science offers the additional advantage that its materials can be studied in their natural, functional context, where manufacturing constraints are imposed by the processes of natural selection rather than monetary directives. As such, there is great potential for basic design principles to emerge from biopolymers research that may not only be of basic interest to life scientists but that might also be used to engineer new materials with physical properties suited to a specific function required by man. The first part of this chapter briefly summarizes the results of this thesis work. The discussion section is then used to highlight questions of major import for the advancement of silk science. The final part of this chapter relates to the field of biomimetics, or the design and construction of machines or materials based on biological design principles. The design and manufacture of synthetic spider silk will likely be a research field of great activity in the coming years that will hopefully lead to new insights regarding basic principles of polymer supra-molecular structure\physical property relationships, as well as provide a host of new materials with innumerable potential applications.

SUMMARY OF RESULTS AND CONCLUSIONS.

A detailed examination of the chemical structure and processing conditions of biological and synthetic fibrous polymers in the introductory chapter of this thesis showed that polymer supra-molecular morphology depends intimately on both the chemical sequence design of the material's constituent polymer chains and the conditions that these chains are subjected to when they are spun into fibers. The orb-spider *A. diadematus* has the capacity to produce at least seven mechanically distinct silk types, and it was hypothesized that the factors that determine fiber properties were also related to polymer chain chemistry and/or conditions of fiber spinning. The results and major conclusions of this investigation are summarized here.

1. Silk supra-molecular crystallization depends on the chemical sequence design of its constituent fibroins.

1.1. The orb-spider genome was found to contain members of at least one fibroin gene family.

3 cDNA libraries were constructed with mRNA purified from the MA, FL and CY glands of the orb-spider *A. diadematus*. Library screens using oligonucleotide probes designed to contain 'silk-like' sequences uncovered 5 novel fibroin cDNAs. 6 of the 8 spider silk gene sequences known (adf-1 to 4, adf-6, ncf-1 and 2) were found to encode reiterated modules of similar size and internal structure (note that silk-like sequence was not available for abf-1, but it will likely be found to be part of this group). In addition, 7 of the 8 genes (adf-1 to 4, abf-1 and ncf-1 and 2) were found to encode a highly conserved 78-88 amino acid COOH-terminal domain. Based on these similarities, it was deduced that these genes are part of a fibroin gene family that is likely to have been assembled over time from one or several ancestral spider fibroin gene sequences.

adf-5, 1 of the 7 spider fibroin genes cloned in this study, was found to encode glycine, proline

and valine rich reiterated sequences that are similar to the sequences of the elastic protein elastin. The very limited sequence data suggests that this fibroin is devoid of poly(alanine) sequence runs that are known to assemble into β-sheet crystals in other insect and arachnid silks. In addition, this fibroin contains a COOH-terminal domain that is distinctly different in charge and sequence from all the other known spider fibroins. Based on these differences it was suggested that adf-5 is a member of a second 'elastomeric' spider fibroin gene family.

1.2. Gland-specific expression of members of at least one spider fibroin gene family offers the orb-spider the potential to modulate the supra-molecular crystallinity and physical properties of its variety of mechanically distinct silks.

The reiterated peptide modules encoded by orb-spider fibroin genes contain variable proportions of crystal forming poly(alanine) and/or poly(glycine-alanine) domains and amorphous glycine rich sequence blocks. It was hypothesized that tissue specific expression of these genes would allow *A. diadematus* to produce a variety of gland-specific secretion types, each with different crystal domain content and hence differential potential for supra-molecular crystallization. The gland tissue expression localities of adf-1 to 5 were assayed by Northern analysis, and in all cases gland specific expression patterns were observed. Chemical or mechanical stimulation of MA and CY glands is known to result in a transient accumulation of fibroin mRNAs rather than translational activation of pre-existing stable fibroin mRNAs (Candelas et al. 1988). The Northern analysis, therefore, indicates that transcriptional regulation of the fibroin genes allows the orb-spider to produce a variety of gland-specific compositionaly distinct secretions.

By combining data on the tissue specific expression localities of the adf genes, the amino acid composition of the 'silk-like' sequences they encode, and the published data available on the amino

acid composition of *A. diadematus*, silks it was possible to predict the fibroin composition and crystal domain content of the MA, MI and FL silks and to partially predict the fibroin composition of the AG and CY silks. It was hypothesized that silks of different crystal domain content should maintain different crystallization potentials.

1.3. The MA, MI, FL and CY secretions were found to exhibit differential shear crystallization potentials.

The shear crystallization sensitivity of the MA, MI, FL and CY glandular secretions were evaluated qualitatively using polarized light microscopy to test the hypothesis that different orb-spider glandular secretions of have differential crystallization potentials. The crystallinity of the shear products from each glandular secretion were distinct and corresponded roughly with the predicted crystal domain content of each secretion type, indicating that each glandular secretion does, in fact, maintain a differential supra-molecular crystallization potential that likely relates to its fibroin composition.

2. FL silk supra-molecular crystallization depends on conditions of fiber processing.

Ecribillate orb-spider FL silk is a unique material that has allowed for the investigation of the importance of processing conditions in determining supra-molecular crystallinity and mechanical properties of spider silk.

2.1. FL fibroin network supra-molecular morphology and mobility are determined by a specific chemical micro-environment in the orb-web.

The native FL fiber exhibits a low initial modulus, high extensibility, and quite exceptional

ultimate strength. In the orb-web, the FL fibroin network is subject to a distinct chemical micro-environment provided by an inter-penetrating aqueous glue coating that contains water, glycoproteins, free amino acids and several water soluble Low Molecular Weight (LMW) hygroscopic compounds. To test the hypothesis that the FL network micro-environment influences supra-molecular morphology and mechanics, the glue coating was removed by a simple water wash\dry process in the lab. The processed FL fibers exhibited a change in optical properties that indicated an increase in molecular order of the FL network and possibly an increase in supra-molecular crystallinity. The mechanical properties of the native FL silk were also dramatically altered by the wash\dry process, to a material with a high initial modulus, lower extensibility and roughly equivalent ultimate strength. The high initial modulus indicated either that the mobility of amorphous FL fibroin sequences were dramatically reduced as they underwent a glass-phase transition on drying, and/or that new crystal structure developed with the processing manipulation.

The amorphous sequences present in the major fibroin constituents of the FL silk, ADF-5 and ADF-3, were predicted to maintain a degree of mobility in the native FL strand because of the presence of a micro-environmental 'plasticizer' that may function either by 1) recruiting water molecules from the atmosphere which in turn hydrate the FL fibroin network 2) by interacting directly with the FL network, and/or 3) by creating free volume to allow for additional mobility of the FL fibroin chains.

2.2. Physical draw increased supra-molecular organization and altered the physical properties of the FL silk.

It was hypothesized that like many other flexible chain fibrous polymers, supra-molecular crystallinity and mechanical properties of orb-spider silk depends on specific physical draw conditions

during fiber spinning. The effects of draw processing on supra-molecular crystallization and mechanical properties of the FL silk were therefore examined in the laboratory. A simple water wash\draw\dry protocol was found to dramatically alter the optical and mechanical properties of the FL fiber.

Birefringence of the processed FL fiber increased asymptotically with increased draw, reaching a plateau at 120 % draw. This result implied that an increase in supra-molecular order develops with draw processing, however, optical data alone fail to reveal whether the new supra-molecular order developed from alignment of amorphous and pre-existing network components and/or from the creation of new crystal structure. A rudimentary comparison of retardation values of processed FL fibers with published data for the hydrated FL silk at equivalent extensions suggested that draw processing imparted new crystal structure to the FL network.

The mechanical properties of the native FL silk were also dramatically altered by draw processing, following the general trend of increased ultimate strength, increased stiffness and decreased extensibility with increased draw. Similar trends in changes of mechanical properties are known to occur for flexible chain based polymers like poly(ethylene) Spectra and Nylon, materials whose polymer chains are known to adopt additional extended chain crystal structure with increased draw. It was suggested that the orb-spider uses specific draw processing regimes in the wild to tune the supra-molecular crystallinity and mechanics of its variety of silks.

3. Future Directions.

While this work has uncovered some of the basic principles of spider silk fiber property control, silk research is in many respects, still in its fledgling stages. There is much to be learned about spider silks in the areas of genetics and cell biology, fibroin design, fibroin folding, supra-molecular

structure, fiber processing, fiber mechanics and web architectural design. Some of the major, as yet unresolved issues of spider silk biology are outlined in this section. These topics may form the basis for future research initiatives.

3.1. Genetics and cell Biology.

3.1.1. Silk gene evolution.

The abundance of gc and gg rich codons in fibroin gene coding sequence has led to the suggestion that *B. mori* silk genes evolved by the placement non-coding micro-satellite sequences into a functional reading frame, and it was offered in Chapter 2 that a similar process may have lead to the formation of the first spider fibroin gene. The molecular processes that have lead to the modular organization of the fibroin genes observed in present day orb-weavers remain to be elucidated. However, when full length genomic DNA sequence becomes available from several spider fibroin genes, it may be possible to delineate intron-exon boundaries and to make predictions about the gene expansion, gene duplication and/or exon shuffling events that may have taken place since the appearance of the first spider silk, close to 400 million years ago. Since erosion of the original intron-exon organization of a gene occurs over time, gene sequences from amber preserved fossils and more primitive spider species may be required to properly reveal the molecular mechanisms important in fibroin gene evolution.

The chromosomal location of the fibroin gene family members may provide additional clues regarding their evolutionary origins. It may be predicted, for example, that these genes are clustered, (as is the case for reiterated genes that encode other structural proteins, like the collagen genes) and that the fibroin genes expanded because their reiterated sequences contain many recombination hot spots where continuous unequal crossing over of similar reiterated sequences may have lead to the

expansion of the progenitor fibroin gene and possibly the creation of additional fibroin gene family members. The location of fibroin genes could be determined by probing chromosome squashes with gene specific oligonucleotide probes. If the genes appear to be clustered, it may then be of interest to generate a P1 phage genomic DNA library that can accommodate huge genomic DNA fragements of up to 100 Kb in length. If a single P1 phage plaque hybridizes to more than one unique fibroin gene family member probe, it will then be possible to isolate and sequence the P1 fragement and to begin to spatially map the location of the fibroin genes relative to each other.

3.1.2. Transcriptional regulation of the fibroin genes.

Synthesis, cellular processing and cellular export of nascent fibroin molecules takes about 90 minutes in the orb-spider *N. clavipes*, and is preceded by at least three rounds of RNA synthesis (Candelas et al. 1988). The first round of RNA synthesis peaks about 15 minutes after mechanical stimulation (forcible silking), with the accumulation of the small nuclear RNA U1 that are probably involved in fibroin gene splicing. Fibroin mRNA synthesis peaks at about 30 minutes post-stimulation. The third round of RNA synthesis peaks at around 45 minutes post-stimulation and results in the accumulation of silk-gland specific tRNA isoacceptor pools.

The molecular pathways important for gland specific transcriptional enhancement or derepression of specific orb-spider fibroin gene family members and their complementary tRNA genes remain to be elucidated. In order to trace out these pathways it will first be necessary to obtain 5' end genomic DNA sequence from one or several orb-spider fibroin genes. These data will provide gene promotor sequence that may contain binding sites for both ubiquitous and tissue specific transcription factors. The Yeast-2-Hybrid system may then be used to identify factors from that bind these sequences *in vitro*. Differential display PCR analysis could also reveal genes that are expressed

in gland tissues and not in other spider tissues. This brute force approach could potentially reveal a suite of proteins including those important for transcription initiation of both fibroin and complementary tRNA genes, as well those important for fibroin folding and cellular export of fibroin secretory granules into the glandular lumen.

While it may be predicted that fibroin production is enhanced by the presence of multiple copies of individual fibroin gene family members within the orb-spider genome, it is noted that the silkworm genome contains only a single copy of the heavy chain fibroin gene. (Gage and Manning, 1975). The P1 phage genome mapping experiments proposed in section 3.1.1 of this chapter should also reveal the copy number of individual fibroin gene family members.

The genome of the orb-weaver *N.clavipes* is known to contain a cluster of alanine tRNA isoaccepetor genes that are expressed constitutively in silk gland tissue (Candelas et al. 1996). It will be of interest to determine where these gene clusters are located with respect to the fibrion genes, and to determine the physical or chemical means by which their transcription is coupled to fibroin gene expression.

3.1.4. Differential splicing of the fibroin genes.

Northern analysis indicates that some of the orb-spider fibroin genes may be differentially spliced. This is intriguing because tissue specific splicing could offer the orb-spider yet another mechanism to adjust fiber properties. Once intron-exon boundaries are delineated through genomic DNA sequencing, comparisons with full length cDNA sequence data will allow for the determination of which exons are preferentially spliced in which tissues. It may then be possible to make predictions regarding the contribution of specific sequences to the supra-molecular morphology of mechanically distinct silk types.

3.1.5. Translation and fibroin folding.

It has been suggested that translational pauses observed during the synthesis of *B. mori* heavy chain fibroin and orb-spider MA and CY fibroins are important for proper folding of the nascent fibroin molecule (Candelas et al. 1983 and see Appendix 2). Precise folding of may prevent pre-mature crystallization of the fibroin molecules or inter-molecular association with other proteins or fibroins, and it may also provide time for the formation of the fibroin conformations necessary for export into the glandular lumen and the subsequent secondary structural transitions necessary for fiber spinning. Eukaryotic cells are known to contain a whole host of binding proteins that are required for proper protein folding, for example, the immunopholins, a class of chaperons, play key roles in the intermediate folding stages of many proteins. It may be predicted that fibroin folding is assisted by the intermediate binding of chaperons during the translational pause.

3.1.6. Cellular processing of nascent fibroins.

Orb-spider silk-gland cells undergo the following ultrastructural changes during fibroin synthesis: First, the cellular nuclei become distorted, and an enlargement of nuclei and nucleoli occurs. Second, transient synchronous movements of the ribosomes within the cells are observed, and an increase in the nucleolar distention in the rough endoplasmic reticulum (RER) cisternae occurs. Thirdly, a re-configuration of RER into whorls with nascent fibroin in the centre occurs. Fourthly, proliferation and enlargement of the Golgi elements is observed. Next, Golgi elements bud off secretory vesicles, and microtubules move the vesicles to the apical cell surface where mature fibroin molecules are exported into the glandular lumen through spaces in the apical cell surface (Tillinghast and Townley, 1994; Kovoor, 1987).

There is no information available on chemical and structural modifications that the fibroins

undergo as they move through the ER and Golgi bodies and are packaged as vesicles for cellular export. While it appears unlikely that the fibroins are glycosylated, specific folds and linkages may be introduced along the secretory pathway. The fact that the 3' COOH-terminal sequence contains a highly conserved cysteine, a residue that appears to be virtually absent from the remainder of the known silk-like sequences, may indicate that this is a disulfide linkage site. The sequences flanking this residue may be BIP or disulfide isomerase binding sites, enzymes that are known to encourage the formation disulfide linkages. The Yeast-2-Hybrid system could help to identify which proteins bind to the COOH-terminal domain sequence *in vitro*.

3.1.7. Silk gland cellular regionalization.

The results from the present study indicate that more than one fibroin species is produced in the MA and FL glands and possibly in the MI and CY glands. Histochemical and ultrastructural studies have also shown that spiders from the sub-orders Liphistomorpha, Mygolomorpha and Araneomorpha are all capable of producing silks composed of more than one protein (Kovoor, 1987). These studies show that some glands are cellularly regionalized, and that the different protein products are produced in the distinct regions of the gland, while other glands contain individual cell types that are capable of producing at least two distinct secretory products (Kovoor et al. 1987). The tail and the distal most 1/4 of the *A. diadematus* MA gland storage sac is composed of one cell type, while the remaining 3/4 of the sac, the region closest to the duct, is composed of another cell type. These two regions were found to discharge histochemically and ultrastructurally distinct secretory granules (Kovoor, 1987). It may be hypothesised that each regionalised cell type produces a single major MA fibroin constituent, such as ADF-3 or 4, although histochemical data from another orb-weaver, *Agiope bruennichi*, demonstrate that changes in size and histochemical affinities of secretory

granules can also occur gradually accross glandular regions that are presently considered to contain the same cell type. The MI, FL and PY glands of *A. diadematus* are all composed of two sharply delineated cell types that synthesize histochemically distinct secretory products, and it has been demonstrated that the two distinct secretory products of the PY gland remain separate even within the glandular duct and after spinning. On the other hand, the secretory tail and sac regions of the AG, CY and AC glands are all composed of what is believed to be a single cell type, although some degree of regionalisation may also occur (Kovoor, 1987).

While some fibroins may self-associate within the cellular cytoplasm, others may remain distinct within the gland and while they are spun into fibres. Work (1984) proposed a sheath core morphology for fibrous orb-spider MA silk. This prediction was based on the observation that a skin dissociates from the outside of the *A. diadematus* MA fiber when it is hydrated, extended, and subsequently relaxed. Li et al. (1994) used Atomic Force Microscopy (AFM) to study the nanometer scale strcuture of *N. clavipes* MA silk, and their results suggest this silk is comprised of three layers; skin, tube and core. Finally, based on timed super-contraction experiments of *N. clavipes*, *N. madagascarensis* and *N. edulis* MA silks in variable concentrations of urea, Vollrath et al. (1996) have proposed that this silk consists of an outer coating, a structured fibril based tube and a thin core. At this stage it is not clear if the different components of this apparent hierarchical organization arise from different fibroin products produced in different regions of the MA glands or if variations in fibroin secondary structure occur through the fiber diameter during spinning. An examination of the profile of shear rates through the fiber diameter will surely reveal a greater shear rate at the outside of the fiber, and this could lead to greater alignment (ie. increased β-sheet crystallisation) at the edge compared to the inner core. *In situ* hybridization of the silk glands with fibroin specific probes should reveal the precise location of synthesis of individual fibroin species and provide clues regarding the

association of distinct fibroins within individual cell types or within the glandular lumen.

3.2. Processing and Spinning.

The silk spinning process is presently poorly understood. It is of interest to determine the factors that dictate the amorphous→cholesteric→nematic liquid-crystalline phase changes that likely occur within all orb-spider silk glands, and to learn about the secondary structure that the fibroin molecules adopt as they assemble into nematic mesogens and are subsequently spun into highly ordered semi-crystalline fibers. The factors that determine molecular organization in the gland may be both chemical and physical.

In chapter 1 it was explained that a pH gradient occurs along the length of the *B. mori* silk gland. Such a gradient may also exist in spider silk glands, and this specific micro-environment, coupled with a specific charge distribution of amino acids in silk-like or non-silk-like fibroin domains may govern fibroin folding and inter-fibroin interactions as well as the orientation of nematic mesogens. If such a gradient exists, it should be possible to isolate glandular secretions on a microscope slide and subject them to chemical or electrical charge gradients while viewing them under polarized light, to learn more about the factors that induce phase changes. It will also be of interest to determine if, as is the case for the micro-environment within the *B. mori* silk gland ions like Ca^{+2} are present, that could encourage inter-fibroin assembly. Finally, it will be necessary to confirm if LMW plasticisers exist in fiber forming glands, as was suggested by preliminary dialysis/shear crystallization experiments in Chapter 4 of this thesis.

Physical restrictions imparted by glandular morphology may also dictate the fibroin conformation and mesogenic alignment. All silk glands appear to have a drastic reduction in diameter moving from the storage sac to the spinning duct. This constriction may physically align secretion mesogens and must result in increased shear rates during spinning, factors which likely ensure global

molecular alignment and crystallization during spinning. The spinning duct of the MA gland is also known to contain a muscular valve that is believed to constrict during spinning and which likely results in an increase in shear rate during spinning (Foelix, 1982).

3.2.3. Spinning shear rates.

The precise forces necessary to induce the liquid crystalline to solid phase semi-crystalline silk fiber transition are not known. Viscometry may be used to determine the shear crystallization threshold of the nematic liquid crystalline secretion. By attaching the spider to a mobile stage and a leading edge of its MA silk to a transducer and moving the stage away from the transducer, it should also be possible to measure the force needed to spin an MA fiber (MA silk is the only orb-spider silk that is reasonably amenable to the forcible silking process). The properties of the fiber could subsequently be evaluated using the standard methods outlined in Chapter 4.

3.3. Fibroin design and structure.

Supra-molecular organization of silks depends intimately on the sequence design of their constituent fibroin chains. It was explained in Chapter 1 that x-ray diffraction and NMR experiments clearly demonstrate that crystal structure in the orb-spider silks studied to date arises from reiterated poly(alanine)sequences, while amorphous structure develops from glycine-proline rich sequences. Naturally, there are countless other peptide sequence designs that can give rise to crystal structure, and some of these have already been observed in insect silks, as was explained Chapter 1. With advances in the power and availability of synchrotron x-ray sources, it will soon be possible to characterize the supra-molecular structure of silks much more readily, hopefully lending to a rapid advancement of our limited knowledge of the precise organization of fibroins in their fibrous form in many more insect and spider silks. Advances in this area will allow us to refine our view on the

composition, shape, size, proportion and orientation of crystal domains, and to better understand the relation between supra-molecular organization and physical properties. The NMR studies of Kummerlen et al. (1996) show that orb-spider fibroins may adopt order on a local scale as well, and the nature of this organization may not be accessible by x-ray diffraction. 2-dimentional NMR techniques that reveal the proximity of specifically labeled amino residues to one another may therefore also be required properly elucidate the supra-molecular organization of silks.

3.4. Physical properties of spider silks.

The mechanical properties of some spider silks are superior to all other biological fibers, and rival some of the best man made materials in terms of ultimate strength, stiffness and toughness. A comparative study of the mechanical properties of silks from a variety of diverse spiders species may reveal silks with physical properties that are superior or unique. The mechanical signature of a silk can also provide clues about its supra-molecular organization, as was eluded to in Chapter 4

3.5 Web design.

With the invention of silk, spiders have been able to move into and dominate a previously unexploited areal niche. Some researchers have deemed the evolution of the spiders web an event of comparable importance to the invention of wings in insects or warm bloodedness in mammals (Foelix, 1982). The physical properties of several silks contribute to the trapping mechanism that is the spiders web. Researchers have begun modeling the design of webs to attempt to evaluate the contribution of different silk types to energy dissipation. One recent finding suggests that aerodynamic damping of the very thin fibers is important in the energy dissipation of *A. diadematus* orb-web silks (Lin et al. 1995). Orb-spider webs appear to be designed to maximize trapping surface area with minimal protein usages (Denny, 1976). The macrobiotic factors that influence web

structural design must include, gravity, wind loading, substrate attachment sites, prey size, humidity, the weight of the spider, and efficiency of signal transmission to the source.

3.6. Production of synthetic silk.

It is now possible to express fibroin sequences in prokaryotic and eukaryotic cell lines and to purify the protein products in large enough quantities to initiate laboratory scale spinning efforts (Fahnstock and Irwin, 1996; Fahnstock and Bedzyk, 1996). There are several major goals for this direction, some of which apply to basic science and others which are obviously of import to industry and the development of inexpensive, biodegradable fibers with a huge potential range of physical properties.

It is of basic importance to refine our understanding of the relationships between primary peptide sequence design, supra-molecular structure and the mechanical properties of fibroin based fibers. Expression of fibroin genes with precisely engineered sequence designs will allow for the synthesis of proteins with precise molecular weights and amino acid sequence designs, offering a level of control over supra-molecular structure and physical properties not yet available to synthetic polymers technology. One of the next steps of my experimental work will involve expressing specific fibroin gene fragments and chimeric constructs thereof in bacteria, yeast and/or insect cell lines, purifying the fibroin product, and subsequently spinning these products into fibers whose supra-molecular and mechanical properties can subsequently be evaluated.

Once the sequence design/supra-molecular structure/physical property relationships are better understood, it should be possible to bio-engineer a suite of mechanically distinct fiber types, possibly with properties that are superior to spider silks. There are, however, several obstacles that must be overcome in expressing, purifying and spinning synthetic silk proteins based on orb-spider fibroin sequences.

3.6.1. Fibroin gene stability.

Reiterated fibroin gene sequences maintained in procaryotic vectors can be unstable, suffering rearrangements and deletions over multiple cell division cycles. However, Fahnstock and Irwin (1996) have shown that synthetic fibroin gene sequences designed to minimize repetetiveness help to alleviate this problem.

3.6.2. Codon bias.

The accumulation of specific tRNA isoaccpetor pools in silk gland tissues are known to be required to accommodate the fibroin codon usage biases (Candelas et al. 1990). Therefore, it will probably be necessary to use one of several possible strategies to ensure efficient translation. One option would be to create synthetic fibroin genes that lack the codon bias. While this approach may reduce rearrangement events and allow the expression system to accommodate translation of codon biased sequences, the pattern of codon bias observed in the present study may be essential for proper processing of the protein in the cellular cytoplasm. Another option would involve engineering tRNA gene clusters into a pre-existing cell lines to ensure that adequate tRNA pools are available. Finally, it should be possible to use an expression system that can deal with the codon bias inherently, such as silkworm gland tissue or orb-spider gland tissue cell lines. I have been able to grow *A. diadematus* silk gland cells in culture over what appear to be several cell division cycles, but naturally the development of an immortalized cell line from scratch would take time. It should also be possible to create a spider silk spinning silkworm transgene, with the advantage that the silkworms spinning apparatus could help circumvent the problems that will arise in developing purification and spinning protocols. In this case however, it would probably be necessary to knock out the pre-existing *B. mori* fibroin genes. Unfortunately this type of project would be very long term and appears unreasonable considering the immediacy of results required by funding agencies today. The idea of having whole

warehouses containing various strains silkworms capable of producing spider or specifically engineered fibers may have to remain an unachievable goal.

3.6.3. Cellular processing.

There is nothing known about the cellular processing steps that occur in silk gland cells. It may therefore be an advantage to use a eucaryotic expression system that has the capacity to impart the required post-translational modifications.

3.6.4. Protein purification.

Synthetic fibroins produced in bacteria have been purified using silica spin columns (Fahnstock and Irwin 1996) and reverse phase High Pressure Liquid Chromatography (HPLC) (Prince et al. 1995), while fibroin based gene products produced in yeast have been purified by dialysis against NAOAc pH 4, following cell sonication in the presence of glass beads (Fahnstock and Bedzyk, 1996). In the future, it will be of interest to develop strategies that allow large quantities of fibroin to be purified while inhibiting crystallization prior to spinning.

3.6.5. Processing purified synthetic fibroins.

A major problem in the commercial manufacturing of fibers from polymers that have a strong tendency to crystallize is preventing crystal formation prior to spinning and encouraging crystallization during spinning. To date, synthetic silk spinning has required potent and expensive chaotropic agents such as 8M LiBr or hexafluoroisopropanol to dissolve the proteins prior to spinning (Capello and Macgrath, 1994). It may be of interest to develop and use the LMW crystal inhibitors that may be produced in the FL and/or AG glands or plasticizers already used in industry to assist in the spinning process.

While it is possible to draw the liquid secretion retrieved directly from the MA gland into a fiber, these fibers exhibit a banded micro-structure that indicates imperfections in molecular sub-structure that are not seen in the natural fiber (Kerkam et al. 1991). It will therefore be important to learn the precise solvent type, fibroin concentration, fibroin molecular weight and shear rate used by the spider, in order that the combination of presumably optimized conditions may be mimicked in the lab to spin smooth, molecularly regular fibers .

Spinning of synthetic fibroin secretions in the lab may be accomplished by placing the secretion in thin a glass micro-capillary tube and drawing the fiber out through a fine orifice. Following spinning it should also be possible to use the specific wash\dry and wash\draw\dry processing regimes developed in Chapter 4 of this thesis to precisely tailor the supra-molecular organization and physical properties of the synthetic spider fibers. Finally, it may be of interest to introduce cross-linking cites, such as lysine residues, into synthetic fibroin gene constructs, or to chemically cross-link synthetic and natural silks using tanning agents, or radiation. Cross-linking may impart greater ultimate strength and stiffness to the fibers, and it may prevent super-contraction, a phenomenon that may be undesirable if these materials are to be used in man-made structures or fabrics of the future.

APPENDIX 1.

TWO ADDITIONAL PUTATIVE *ARANEUS DIADEMATUS* FIBROINS

INTRODUCTION

The CY gland cDNA library was screened with two oligonucleotidde probes simultaneously to target sequences encoding silklike poly(alanine) domains and a small conserved sequence block known to be present in present the COOH-terminal domain of 7 of the 8 known orb-spider fibroins. Preliminary sequencing of putative silk clones revealed two additional cDNAs that encode silklike sequences. The very limited predicted amino acid sequence data presently available for these two additional putative silk genes is presented here. Sequencing of the 3' end of these cDNAs remained to be done. The gland tissue expression locality of each these two genes also remains to be determined. This will be achieved through Northern analysis at a future date.

MATERIALS AND METHODS

The CY library was screened to the secondary level at low stringency (42 °C, 0.01 × SSC, 0.01 % SDS) according Maniatis et al. (1983) using two synthetic oligonucleotide probes simultaneously. One of these was the same probe that was designed based on NCF-1 to target sequences encoding silk-like poly(alanine) crystal domains (see Table 2.1) . The second probe was designed to target sequences encoding an 8 amino acid sequence block that surrounds the highly conserved cysteine residue present in the COOH-terminal domain of ADF-2, 3 and 4, and NCF-1 and 2. Putative silk clones were isolated and sequenced according to the Methods outlined in Chapter 2.

RESULTS AND DISCUSSION

Two cDNAs encoding reiterated alanine and glycine rich sequences were uncovered during the CY cDNA library screens; these were named adf-6 and 7. Figure A1.1 shows the shows the predicted silklike amino acid sequences that these genes encode. ADF-6 is alanine, glycine, serine and arginine rich. It is not entirely like clear where the limits of individual crystal domains fall because poly(alanine) sequences are interspersed with glycine and serine. It may be proposed that the crystal forming sequence for ADF-6 is AAAGSGAGAAS, which appears to be a hybrid of spider poly(alanine) and poly(glycine-alanine) sequences and the serine rich silkworm crystal forming sequence GAGAGS. If the sequence predicted to be a crystal forming domain is correct then as much as 65 % of the entire ADF-6 sequence available may have the capacity to adopt the β-sheet conformation. It may be predicted that the intervening GGRGG sequence has the capacity to form β-turns which could bring crystal forming domains from the same fibroin molecule into an anti-parallel β-sheet arrangement, although when ADF-6 is drawn during spinning these sequences may crystallise inter-molecularly in the extended chain conformation.

While ADF-6 was cloned from the CY cDNA library an examination of the amino acid composition of the CY silk (see Table 1.3) indicates that it contains 28 % serine, a much greater proportion that the 6 % found in ADF-6. Therefore, while ADF-6 remains a candidate for a constituent of the CY silk, there must be other as yet uncloned fibroins that contain greater proportions of serine residues to account for the composition of the CY silk. In the future, Northern blot analysis will reveal the expression locality of ADF-6. It may also be of interest to design probes containing serine, and serine alanine repeats to attempt to isolate the major constituent of the CY silk.

ADF-7, encodes reiterations of a single amino acid, glycine. This reiterated sequence design has also not yet been documented for spider silks, although some insect silks are known to contain

Figure A1.1.
Predicted amino acid sequeces of two putative A. diadematus fibroins.

ADF-6

SARGGGGAAA
GSGAGAASGGRGGG-AAA
GSGAGAASGGRGGG-AAA
GSGAGAASGGRGGG-AAA
GSGAGAASGGRGGG-AAA
GSGAGAASGGRGG-AAAA
GSGAGAASGGR

ADF-7

RGGGGGGNAGYGAGGGGGGGG

reiterated poly(glycine) sequences. It was shown, for example, in Chapter 1 that the cadis fly silk is comprised of as much as 57 % glycine and that glycine rich sequences could conceivably crystallize in the PG-II form if properly aligned. The Genbank DNA sequence database reveals that many genes that are unrelated to structural proteins encode glycine rich stretches, so until Northern expression analysis is done to confirm that this gene is expressed in silk gland tissue, adf-7 must be classified candidate fibroin gene.

In conclusion, two novel putative spider silk cDNAs were retrieved by screening a cDNA library constructed from *A. diadematus* Cylindrical glands. Additional sequencing, Northern expression analysis and solid state chemistry will, in the future, reveal the macromolecular design of orb-spider Cocoon silk and thus the basis for its observed mechanical properties.

APPENDIX 2.

THE SPIDER FIBROIN GENES CONTAIN PATTERNS OF CODON USAGE

INTRODUCTION

This study's main purpose was to investigate mechanisms of fiber property modulation employed the orb-spider *A. diadematus*. Some of the data acquired was not directly related to this main theme, but was predicted to provide rational clues related to the molecular efficiency of fibroin production. A detailed understanding of transcriptional and translational regulation as well as post-translational processing of the spider fibroins may allow us to engineer expression systems tailored to production of properly processed synthetic spider silk proteins in large volumes.

The silk gland tissues of silkworm and orb-spiders are responsible for the specialized synthesis of relatively enormous quantities of protein. For example, each cell in the posterior region of the *B. mori* larval silk gland produces close to 300 μg of the heavy chain fibroin during the 4 days prior to the initiation of spinning behaviour (Tashiro et al. 1968). The silk glands of adult female orb-spiders also generate massive quantities of protein, which in most cases are available to the spider over the course of several months.

A clear correlation has previously been established between *B. mori* fibroin mRNA codon usage and a heavily skewed tRNA population in the cells that comprise the posterior region of the silk glands (Mita et al. 1988). In both *B. mori* and *N. clavipes* MA silk glands, large amounts of tRNA's cognate to the alanine codon ($tRNA^{ala}$) in the fibroins are known to appear prior to the transient production of fibroin mRNA. In both tissue types, the $tRNA^{ala}$'s are present in two isoaccepting forms; one which is constitutive, the other gland specific (Susuki et al. 1986; Candelas et al.1990). While *B. mori* and *N. clavipes* are likely to have diverged over 400 million years ago, they have apparently arrived at the common molecular strategy of accumulating tissue specific tRNA isoacceptors to deal with biosynthesis of proteins that are heavily biased in their amino acid compositions.

In an evolutionary context, a correlation between fibroin gene sequence and compatible tRNA pools could reflect either a selective constraint imposed by tRNA availability on codon choice or contrarily an adjustment of the tRNA content to the codon spectrum of the gene. Mita et al. (1988) have examined codon usage preferences in the *B. mori* heavy chain fibroin mRNA. They found that the reiterated 248 nucleotide unit structure of the this fibroin encodes two distinct peptide modules. The first sequence module consists of eight consecutive GAGAGS repeats. This region is followed by a 24 residue 'spacer' region which is also alanine, glycine and serine rich but does not contain the signature hexapeptide present in the first 48 amino acid module. An examination of codon usage in these two different regions shows that the codon usage is heavily skewed for glycine (codon=GGU), alanine (codon=GCG) and serine (codon=UCA) in the repetitive region, but in the spacer region codon usage is skewed in a different sense: glycine (codon:GGA), alanine (homogenous distribution), serine (codons=AGC and UCU). In addition, there is no codon usage skew in the 5' end coding region of that gene. The fact that mRNA codon usage preferences are distinct in each of the three regions strongly suggests that codon usage is determined by chromatin or mRNA structure rather than the availability of tRNAs (Mita et al. 1988). Precise gene structure may be necessary to maintain stability over generations or for transcriptional efficiency. On the other hand, a properly folded transcript may be required to prevent degradation or to permit for efficient translation of the message.

Western blots of fibroin produced both *in vivo* and *in vitro* for B. mori and *in vitro* for *N. clavipes* exhibit distinctive molecular weight 'ladders' indicative of the occurrence of step-wise pausing during translation. It has therefore been hypothesised that precise codon placement determines fibroin mRNA structure which in turn dictates pausing. Pausing may be essential for proper folding of the enormous fibroin molecules (Mita et al. 1988 and Candelas et al. 1990).

The study of codon usage preferences in *B. mori* Heavy chain fibroin has provided c l u e s regarding fibroin synthesis and processing. Using those studies as a precedent, I chose to examine gene structure and codon preference in the spider fibroins.

RESULTS

1. Codon usage biases.

Tables A2.1 to A2.7 show the codon usage distributions (expressed as percent of total) for adf-1 to 5 and ncf-1 and 2. In general, there is no discernable codon bias for low abundance fibroin amino acids. Conversely, the codons corresponding to high abundance residues like serine, tyrosine, proline, arginine, alanine and glycine all exhibit very heavy biases. In all Tables A2.1 to A2.7, the residues which exhibit heavy codon bias are stippled and those codons used which exhibit the heaviest positive bias are denoted with an asterisk.

adf-1 exhibits a heavy codon bias for the residues serine, tyrosine, alanine and glycine (Table A2.1). For adf-2 the codon usage is skewed for serine, tyrosine, glutamine, alanine and glycine (Table A2.2). The codon usage bias in adf-3 occurs for serine, tyrosine, proline , glutamine, alanine and glycine (Table A2.3). adf-4 exhibits a codon usage bias for serine, tyrosine, glutamine, alanine and glycine (Table A2.4). There is a positive codon usage bias for proline and glycine for adf-5 (Table A2.5). ncf-1 exhibits heavy positive codon biases for serine, tyrosine, leucine, arginine, glutamine, alanine and glycine (Table A2.6). ncf-2 exhibits a positive codon skewness for serine, tyrosine, proline, glutamine, alanine and glycine (Table A2.7).

2. Codon usage pattern biases.

Interestingly, there are very specific patterns of codon usage within all of the known spider fibroin genes. The sequence of codon usage for adf-1 to 5 and ncf-1 and 2 are presented in figures A2.1 to A2.7. The codon numbering scheme used is included in Table A2.1 as subscripts (For example, the four codons for glycine were numbered as gct: 1; gcc: 2; gca: 3 and gcg: 4.). I will not point out every permutation in the patterns of codon usage since they are too numerous, however,

Table A2.1.

Codon usage for adf-1. Codons that exhibit biases are stippled. Those that exhibit the heaviest positive bias are indicated with *. The subscript numbers are used to annotate individual codons to reveal the pattern of codon usage within the spider fibroin genes.

TTT (F_1)	1.3	TCT(S_1)	4.0	TAT(Y_1)	4.3	TGT (C_1)	0.3
TTC (F_2)	0.3	TCC(S_2)	0.5	TAC(Y_2)	1.5	TGC(C_2)	0.0
TTA (L_1)	0.5	TCA(S_3)	1.8	TAA (*)	0.8	TGA (*)	0.3
TTG (L_2)	1.3	TCG(S_4)	0.8	TAG (*)	0.0	TGG(W)	0.3
CTT (L_3)	0.8	CCT(P_1)	0.3	CAT(H_1)	0.5	CGT(R_1)	0.0
CTC (L_4)	0.3	CCC(P_2)	0.3	CAC(H_2)	0.3	CGC(R_2)	0.3
CTA (L_5)	0.3	CCA(P_3)	0.0	CAA(Q_1)	1.5	CGA(R_3)	0.3
CTG (L_6)	1.0	CCG(P_4)	0.0	CAG(Q_2)	0.3	CGG(R_4)	0.0
ATT (I_1)	2.3	ACT(T_1)	1.0	AAT(N_1)	3.0	AGT(S_5)	3.5
ATC (I_2)	1.0	ACC(T_2)	0.3	AAC(N_2)	0.5	AGC(S_6)	0.5
ATA (I_3)	0.5	ACA(T_3)	0.3	AAA(K_1)	1.5	AGA(R_1)	1.8
ATGM$_1$	0.8	ACG(T_4)	0.3	AAG(K_2)	0.3	AGG(R_2)	0.0
GTT(V_1)	1.3	GCT(A_1)	12.0	GAT(E_1)	0.0	GGT(G_1)	7.5
GTC(V_2)	1.0	GCC(A_2)	3.8	GAC(E_2)	0.3	GGC(G_2)	4.8
GTA(V_3)	2.0	GCA(A_3)	8.5	GAA(D_1)	1.3	GGA(G_3)	13.5
GTG(V_4)	0.5	GCG(A_4)	1.8	GAG(D_2)	0.3	GGG(G_4)	1.0

Table A2.2.

Codon usage for adf-2. Codons that exhibit biases are stippled. Those that exhibit the heaviest positive bias are indicated with *.

TTT (F)	0.3	TCT (S)	5.5*	TAT (Y)	2.1	TGT (C)	0.3
TTC (F)	0.3	TCC (S)	0.9	TAC (Y)	0.9	TGC (C)	0.0
TTA (L)	2.4	TCA (S)	1.5	TAA (*)	0.6	TGA (*)	0.3
TTG (L)	3.0	TCG (S)	0.9	TAG (*)	0.0	TGG(W)	0.0
CTT (L)	1.8	CCT (P)	0.6	CAT (H)	0.0	CGT (R)	0.0
CTC (L)	0.0	CCC (P)	0.3	CAC (H)	0.3	CGC (R)	0.3
CTA (L)	0.0	CCA (P)	0.9	CAA (Q)	7.6	CGA (R)	0.3
CTG (L)	0.0	CCG (P)	0.0	CAG (Q)	0.9	CGG (R)	0.0
ATT (I)	3.4	ACT (T)	0.6	AAT (N)	1.2	AGT (S)	2.4
ATC (I)	0.3	ACC (T)	0.0	AAC (N)	0.6	AGC (S)	0.6
ATA (I)	0.3	ACA (T)	0.0	AAA (K)	1.8	AGA (R)	0.0
ATG (M)	0.6	ACG (T)	0.0	AAG (K)	0.0	AGG (R)	0.3
GTT (V)	1.2	GCT (A)	5.2	GAT (D)	0.0	GGT (G)	9.8
GTC (V)	0.6	GCC (A)	6.4	GAC (D)	0.3	GGC (G)	1.8
GTA (V)	1.5	GCA (A)	8.2*	GAA (E)	0.9	GGA (G)	18.9*
GTG (V)	0.0	GCG (A)	0.6	GAG (E)	0.0	GGG (G)	0.3

Table A2.3.

Codon usage for adf-3. Codons that exhibit biases are stippled. Those that exhibit the heaviest positive bias are indicated with *.

TTT (F)	0.4	TCT (S)	4.0	TAT (Y)	3.3	TGT (C)	0.0
TTC (F)	0.1	TCC (S)	2.1	TAC (Y)	0.9	TGC (C)	0.3
TTA (L)	0.3	TCA (S)	0.9	TAA ( )	0.3	TGA ()	0.4
TTG (L)	0.4	TCG (S)	0.6	TAG ( )	0.0	TGG(W)	0.0
CTT (L)	0.9	CCT (P)	2.7	CAT (H)	0.3	CGT (R)	0.1
CTC (L)	0.3	CCC (P)	6.8	CAC (H)	0.0	CGC (R)	0.1
CTA (L)	0.0	CCA (P)	2.8	CAA (Q)	15.9	CGA (R)	0.1
CTG (L)	0.1	CCG (P)	0.0	CAG (Q)	0.3	CGG (R)	0.0
ATT (I)	0.4	ACT (T)	0.3	AAT (N)	0.6	AGT (S)	0.9
ATC (I)	0.6	ACC (T)	0.1	AAC (N)	0.1	AGC (S)	0.6
ATA (I)	0.6	ACA (T)	0.0	AAA (K)	1.2	AGA (R)	0.1
ATG (M)	0.3	ACG (T)	0.0	AAG (K)	0.1	AGG (R)	0.0
GTT (V)	0.0	GCT (A)	3.3	GAT (D)	0.1	GGT (G)	7.7
GTC (V)	1.2	GCC (A)	4.9	GAC (D)	0.0	GGC (G)	0.7
GTA (V)	0.1	GCA (A)	7.0	GAA (E)	0.1	GGA (G)	21.7
GTG (V)	1.5	GCG (A)	0.3	GAG (E)	0.0	GGG (G)	0.4

Table A2.4.

Codon usage for adf-4. Codons that exhibit biases are stippled. Those that exhibit the heaviest positive bias are indicated with *.

TTT (F)	0.4	TCT (S)	7.3	TAT (Y)	3.1	TGT (C)	0.7
TTC (F)	0.4	TCC (S)	1.5	TAC (Y)	0.7	TGC (C)	0.0
TTA (L)	1.3	TCA (S)	2.2	TAA (*)	0.4	TGA (*)	0.4
TTG (L)	1.1	TCG (S)	0.7	TAG (*)	0.2	TGG(W)	0.0
CTT (L)	1.3	CCT (P)	7.5	CAT (H)	0.0	CGT (R)	0.2
CTC (L)	0.0	CCC (P)	1.5	CAC (H)	0.0	CGC (R)	0.2
CTA (L)	0.2	CCA (P)	2.4	CAA (Q)	3.3	CGA (R)	0.0
CTG (L)	0.2	CCG (P)	0.0	CAG (Q)	0.9	CGG (R)	0.0
ATT (I)	0.9	ACT (T)	0.2	AAT (N)	1.8	AGT (S)	3.3
ATC (I)	0.0	ACC (T)	0.0	AAC (N)	0.9	AGC (S)	2.2
ATA (I)	0.4	ACA (T)	0.2	AAA (K)	1.5	AGA (R)	0.0
ATG (M)	0.4	ACG (T)	0.2	AAG (K)	0.0	AGG (R)	0.0
GTT (V)	1.1	GCT (A)	4.0	GAT (D)	0.2	GGT (G)	4.4
GTC (V)	0.4	GCC (A)	2.0	GAC (D)	0.0	GGC (G)	0.7
GTA (V)	1.8	GCA (A)	11.9	GAA (E)	0.9	GGA (G)	19.3
GTG (V)	1.1	GCG (A)	0.9	GAG (E)	0.4	GGG (G)	0.7

Table A2.5.

Codon usage for adf-5. Codons that exhibit biases are stippled. Those that exhibit the heaviest positive bias are indicated with *.

TTT (F)	1.0	TCT (S)	1.6	TAT (Y)	3.9	TGT (C)	1.0
TTC (F)	1.0	TCC (S)	1.3	TAC (Y)	1.0	TGC (C)	0.6
TTA (L)	1.3	TCA (S)	1.6	TAA (*)	0.3	TGA (*)	0.3
TTG (L)	0.6	TCG (S)	0.3	TAG (*)	0.3	TGG(W)	0.3
CTT (L)	1.0	CCT (P)	2.6	CAT (H)	0.3	CGT (R)	0.3
CTC (L)	0.6	CCC (P)	0.6	CAC (H)	0.6	CGC (R)	0.6
CTA (L)	1.3	CCA (P)	7.1	CAA (Q)	1.0	CGA (R)	0.3
CTG (L)	1.0	CCG (P)	1.3	CAG (Q)	0.0	CGG (R)	1.9
ATT (I)	0.3	ACT (T)	0.6	AAT (N)	1.9	AGT (S)	0.0
ATC (I)	1.6	ACC (T)	0.3	AAC (N)	0.6	AGC (S)	0.6
ATA (I)	1.6	ACA (T)	1.0	AAA (K)	2.3	AGA (R)	0.3
ATG (M)	0.3	ACG (T)	0.3	AAG (K)	0.0	AGG (R)	0.3
GTT (V)	1.0	GCT (A)	2.3	GAT (D)	2.6	GGT (G)	7.4
GTC (V)	1.6	GCC (A)	1.3	GAC (D)	0.3	GGC (G)	5.2
GTA (V)	2.3	GCA (A)	2.3	GAA (E)	2.6	GGA (G)	17.2
GTG (V)	1.6	GCG (A)	1.3	GAG (E)	0.6	GGG (G)	0.3

Table A2.6.

Codon usage for ncf-1. Codons that exhibit biases are stippled. Those that exhibit the heaviest positive bias are indicated with *.

TTT (F)	0.8	TCT (S)	1.0	TAT (Y)	2.3*	TGT (C)	0.3
TTC (F)	0.3	TCC (S)	0.6	TAC (Y)	0.3	TGC (C)	0.3
TTA (L)	1.8	TCA (S)	0.9	TAA (*)	0.1	TGA (*)	0.0
TTG (L)	0.6	TCG (S)	0.5	TAG (*)	0.3	TGG(W)	0.0
CTT (L)	2.7	CCT (P)	0.3	CAT (H)	0.1	CGT (R)	0.1
CTC (L)	0.4	CCC (P)	0.1	CAC (H)	0.0	CGC (R)	0.0
CTA (L)	1.3	CCA (P)	0.3	CAA (Q)	8.6*	CGA (R)	1.9
CTG (L)	0.5	CCG (P)	0.1	CAG (Q)	0.3	CGG (R)	0.1
ATT (I)	0.3	ACT (T)	0.4	AAT (N)	0.5	AGT (S)	0.6
ATC (I)	0.5	ACC (T)	0.0	AAC (N)	0.8	AGC (S)	1.4
ATA (I)	0.4	ACA (T)	0.1	AAA (K)	0.4	AGA (R)	0.6
ATG (M)	0.5	ACG (T)	0.0	AAG (K)	0.6	AGG (R)	0.1
GTT (V)	1.2	GCT (A)	6.9	GAT (D)	0.1	GGT (G)	15.8
GTC (V)	0.3	GCC (A)	4.6	GAC (D)	0.1	GGC (G)	1.7
GTA (V)	0.3	GCA (A)	12.3*	GAA (E)	0.3	GGA (G)	21.7*
GTG (V)	0.4	GCG (A)	0.5	GAG (E)	0.0	GGG (G)	0.8

Table A2.7.

Codon usage for ncf-2. Codons that exhibit biases are stippled. Those that exhibit the heaviest positive bias are indicated with *.

TTT (F)	0.6	TCT (S)	4.5	TAT (Y)	4.7*	TGT (C)	0.2
TTC (F)	0.5	TCC (S)	0.5	TAC (Y)	0.0	TGC (C)	0.3
TTA (L)	0.6	TCA (S)	1.5	TAA (*)	0.5	TGA (*)	0.0
TTG (L)	0.6	TCG (S)	0.0	TAG (*)	0.2	TGG(W)	0.2
CTT (L)	0.3	CCT (P)	3.3	CAT (H)	0.0	CGT (R)	0.5
CTC (L)	0.5	CCC (P)	0.8	CAC (H)	0.0	CGC (R)	0.0
CTA (L)	0.3	CCA (P)	8.9	CAA (Q)	11.1*	CGA (R)	0.0
CTG (L)	0.2	CCG (P)	0.0	CAG (Q)	0.3	CGG (R)	0.0
ATT (I)	0.9	ACT (T)	0.3	AAT (N)	0.5	AGT (S)	2.6
ATC (I)	0.6	ACC (T)	0.2	AAC (N)	0.5	AGC (S)	0.5
ATA (I)	0.0	ACA (T)	0.0	AAA (K)	0.5	AGA (R)	0.3
ATG (M)	0.2	ACG (T)	0.0	AAG (K)	0.0	AGG (R)	0.0
GTT (V)	1.1	GCT (A)	3.6	GAT (D)	0.3	GGT (G)	4.5
GTC (V)	0.3	GCC (A)	4.8	GAC (D)	0.0	GGC (G)	2.9
GTA (V)	0.5	GCA (A)	11.5*	GAA (E)	0.3	GGA (G)	21.7*
GTG (V)	0.2	GCG (A)	0.3	GAG (E)	0.0	GGG (G)	0.5

Figure A2.1.

Codon usage pattern for ADF-1. The numbers in bold type in the first module indicate codon choices that are relatively well conserved in subsequent modules of the silklike sequence.

[1]GGYGQGYGAGAGAGAGAGAGGA[24]
2323122413111431313331111
[25]GGYGQGYGAGAAAAAGAGAGAA[46]
331212112313**341**1131313
[47]GGYGGGSGAGAGGA[60]
33132251131312
[61]GGYGQGYGAGSGAGAGAAAAAGASAGAA[88]
131212221313323311**341**1151313
[89]GGYGGGAGVGAGAGAA[104]
3313331132433331
[105]GGYGQSYGSGAGAGAGAGAAAAAGAGARAA[134]
131216221313133124131**341**2333113
[135]GGYGGGYGAGAGAGAGAAASAGAS[158]
131332211311331**341**51313
[159]GGYGGGYGGGAGAGAVAGASAGSYGGAVN[187]
331333133311312233132131311121

Figure A2.2.

Codon usage pattern for ADF-2. The numbers in bold type in the first module indicate codon choices that are relatively well conserved in subsequent modules of the silklike sequence.

```
[1]GGAGQGGYGA--------GG-GGAAAAAAAAVGAGG-GGQ---GGLGS[35]
  132311313133 2332343233332 331   32211
[36]GGAGQ-G------YGAGLGGQGGASAAAAAAGGQGGQGGQGGYGGLGSQGA[79]
  11231 3      212311311311323332131311311123133112131
[80]GGAGQLGYGAGQE---------SAAAAAAAAGGAGG-GGQ---GGLGA[114]
  1333113131313          52332343233332 331   32211
[115]GGAGQ-GYGAAGLGGQGGAGQGGGSGAAAAAGGQGGQ---GGYGGLGPQGA[161]
  11231 32122321313333113113233321313 31   23133112131
[162]GGAGQGGYGGGSLQYGGQGQA-QAAAASAAAS[192]
  1323133133152111311131133212334
```

Figure A2.3.

Codon usage pattern for ADF-3. The numbers in bold type in the first module indicate codon choices that are relatively well conserved in subsequent modules of the silklike sequence.

[1]GPGQQGPYGPGASAAAAAAGGYGPGSGQQGPSQQGPGQQ[39]
3231133132132233321311323131132611312 11
[40]GPGGQGPYGPGASAAAAAAGGYGPGSGQQ[68]
32111331321322233211313212311
[69]GPGGQGPYGPGSSAAAAAAGGNGPGSGQQGAGQQGPGQQ[107]
33311331311321233213113231311421111 1311
------[108]GPGASAAAAAAGGYGPGSGQQGPGQQ[133]
3213222332133232313113231 1
[134]GPGGQGPYGPGASAAAAAAGGYGPGSGQ-GPGQQ[166]
33311331311322133213323231 31 32311
[167]GPGGQGPYGPGASAAAAAAGGYGPGSGQQGPGQQGPGQQ[205]
33311331321321333213113231311323113131 1
[206]GPGGQGPYGPGASAAAAAAGGYGPGYGQQGPGQQ[239]
32111331321322233213323211321331 1
[240]GPGGQGPYGPGASAASAASGGYGPGSGQQGPGQQ[273]
33311331311322233213323231311323 11
[274]GPGGQGPYGPGASAAAAAAGGYGPGSGQQGPGQQGPGQQGPGQQGPGQQ[319]
31311331311322333213113231311332113211131311
[320]GPGGQGPYGPGASAAAAAAGGYGPGSGQQGPGQQGPGQQGPGQQGPGQQGPGQQGPGQQGPGQQGPGQQGPGQQ[388]
32111131311322333213113231311321113211132111322113211132211311111
[389]GPGGQGAYGPGASAAAGAAGGYGPGSGQQGPGQQGPGQQGPGQQGPGQQGPGQQGPGQQGPGQQGPGQQ[452]
12111431311322333213113231311323113231132311323113231132311323113231132311
[453]GP-----YGPGASAAAAAAGGYGPGSGQQGPGQQGPGQQ[486]
33 1311322333213113231313221131311
[487]GPGGQGPYGPGAASAAVSVGGYGPQS[512]
32111331311411313113313316

Figure A2.4.

Codon usage pattern for ADF-4. The numbers in bold type in the first module indicate codon choices that are relatively well conserved in subsequent modules of the silklike sequence.

```
[1]GSSAAAAAAAA--SGSGGYGPENQGPSGPVAYGPGGP[35]
  33133342433  5313323112133131331131132
[36]VSSAAAAAAA--GSGPGGYGPENQGPSGPGGYGPGGS[70]
  3131333213  353113231121331323313112
[71]GSSAAAAAAAA--SGPGGYGPGSQGPSGPGGSGGYGPGSQGASGPGGP[116]
  31333332133  5313313136133131132331123614313114l
[117]GASAAAAAAAAAAASGPGGYGPGSQGPSGPGAYGPGGP[153]
  131433333213353133131361331313313113l132
[154]GSSAAAAAAAA--SGPGGYGPGSQGPSGPGVYGPGGP[188]
  31313332133  531331313613313133131132
[189]GSSAAAAAAA--GSGPGGYGPENQGPSGPGGYGPGGS[223]
  3131333213  353113231121331323313112
[224]GSSAAAAAAAA--SGPGGYGPGSQGPSGPGGSGGYGPGSQGGSGP[266]
  31333332133  5313313136133131132331123214313l
[267]GASAAAAAAAA--SGPGGYGPGSQGPSGPGYQGPSGP[301]
  13143332133  531331313613313131121511
```

Figure A2.5.

Codon usage pattern for ADF-5. The numbers in bold type in the first module indicate codon choices that are relatively well conserved in subsequent modules of the silklike sequence.

```
---GAGPY----------------
   11311
GPGGAGPY----------------
33134311
GPGGAGPY----------------
33134311
GPGGAGPYGPGGV-----------
3313231133233
GPGGAGPY----------------
33112311
GPGGAGPYGPGGV-----------
3311221133213
GPGGAGPY----------------
33132311
GPGGEGGA----------------
33331123
GPGGAGPY----------------
33132311
GPGGA------GV-----------
33233      31
GPGGAPGSPGGPGGPGGPG------
1333313133131333332
GPGGAGPY----------------
33331411
GPGGV-------------------
33233
GPGGAGTY----------------
32132311
GPGGV-------------------
33233
GPGGAGPF----------------
33131311
GPGGPG------------------
333331
GPGGAGPE----------------
33123341
EGEGPVTVDVEVNVGGSPGGGPVGV
1121233322131131333333123
--------GPGGV-----------
        33233
--------GPGGV-----------
        33333
GPGGAGPYGPGGV-----------
3313131133213
GPGGAGPY----------------
33332311
GPGGA-------------------
33233
```

Figure A2.6.

Codon usage pattern for NCF-1. The numbers in bold type in the first module indicate codon choices that are relatively well conserved in subsequent modules of the silklike sequence.

NCF-1

```
----------------------QGAGAAAAAA-
                       1431333331
GGAGQGGYGGLGGQG------------------
312313313131313
--AGQGGYGGLGGQG------AGQGAGAAAAAAA
  1111313131311      2313113223331
GGAGQGGYGGLGSQGAGR---GGQGAGAAAAAA-
112313313113611133   131313321314
GGAGQGGYGGLGSQGAGRGGLGGQGAGAAAAAAA
1123131131335113331131431332133l
GGAGQGGYGGLGNQGAGR---GGQ--GAAAAAA-
312313313233211133   131  1333331
GGAGQGGYGGLGSQGAGRGGLGGQGAGAAAAAA-
311313313133611333131131131333332
GGAGQGGYGGLGGQG------------------
311312321131311
--AGQGGYGGLGSQGAGRGGLGGQGAGAAAAAAA
  2313213333611133331131131333331
GGAGQ---GGLGGQG------AGQGAGASAAAA-
31231   3351311      131313321331
GGAGQGGYGGLGSQGAGR---GGEGAGAAAAAA-
113313313133611133   131132323332
GGAGQGGYGGLGGQG------------------
311313321131311
--AGQGGYGGLGSQGAGRGGLGGQGAGAAAA---
  231321333361113333113113133331
GGAGQ---GGLGGQG------AGQGAGAAAAAA-
31241   3351311      131313321331
GGAGQGGYGGLGSQGAGRGGLGGQGAGVAAAAAA
112313313133611333131131431332133l
GGAGQGGYGGLGSQGAGR---GGQGAGAAAAAA-
312313313133611133   131313321331
GGAGQRGYGGLGNQGAGRGGLGGQGAGAAAAAAA
112315113133111333131131431332133l
GGAGQGGYGGLGNQGAGR---GGQ--GAAAAA--
312313313233211133   131  133331
GGAGQGGYGGLGSQGAGR---GGQGAGAAAAAA-
312313313133611133   131132323332
VGAGQEGIR---GQG------------------
311311331   311
--AGQGGYGGLGSQGSGRGGLGGQGAGAAAAAA-
  2313213333611113331131131333331
GGAGQ---GGLGGQG------AGQGAGAAAAAA-
31131   3311311      131311121331
GGVRQGGYGGLGSQGAGR---GGEGAGAAAAAA-
111513313133611133   131132323332
GGAGQGGYGGLGGQGVGRGGLGGQGAGAAAA---
311313311131311231311321323431
GGAGQGGYGGV-GSG----------ASAASAAA-
11131331111 114           41121313
```

Figure A2.7.

Codon usage pattern for NCF-2. The numbers in bold type in the first module indicate codon choices that are relatively well conserved in subsequent modules of the silklike sequence.

NCF-2

```
-----------------PGGYGPGQQGPGGYGPGQQGP--SGPGSAAAAAAAAAA
                 133133311233312131133  131252133332233
------GPGGYGPGQQGPGGYGPGQQGPGGYGPGQQGP--SGPGSAAAAAA----
      3133121311323313331123513331133  13125213233
-----------GSGQQGPGGYGPRQQGPGGYGPGQQGP--SGPGSAAAASAAASA
           3131123331331111331131311 33  133253232323233
-ESGQQGPGGYGPGQQGPGGYGPGQQGPGGYGPGQQGP--SGPGSAAAAAAAAS-
 113112331133111233113311111133133311 33  13315213322233
-----------GPGQQGPGGYGPGQQGPGGYGPGQQGP--SGPGSAAAAAAAAS-
           3131133331331111133133311 33  13315213222233
-----------GPGQQGPGGYGPGQQGPGGYGPGQQGL--SGPGSAAAAAAA---
           313113333133111133113331135  133253133233
----------------------GPGQQGPGGYGPGQQGP--SGPGSAAAAAAAAA-
                       31311323313331133  13215213332233
----------------GPGGYGPGQQGPGGYGPGQQGP--SGAGSAAAAAAA---
                 31331213113233133311 33  133253333233
-----------GPGQQGLGGYGPGQQGPGGYGPGQQGPGGYGPGSASAAAAAA--
           3131131311333111333133311133313313311333233
----------------------GPGQQGPGGYGPGQQGP--SGPGSASAAAAAAAA
                       31311333313131133  133253133323233
----------------GPGGYGPGQQGPGGYAPGQQGP--SGPGSASAAAAAAAA
                 333133331113331331133  133213133323233
----------------GPGGYGPGQQGPGGYAPGQQGP--SGPGSAAAAAAAAA-
                 333133331113331331133  13325333331133
--------------------------GPGGYGPAQQGP--SGPGIAASAASA---
                           311313341233  111323131133
----------------GPGGYGPAQQGPAGY----------GPGSAVAASAGA--
                 313113331131 31          413633321213
--------------------------GSAGY----------GPGSQASAAA----
                           31311          4311112131
```

in the first module of each spider fibroin gene, codons which appear to recur at the same location within subsequent modules of the same fibroin are highlighted in **bold**. The conserved codon pattern can be seen simply by following the line directly below the highlighted codons for all the subsequent modules of each individual fibroin. It appears as though the codon usage patterns are conserved within fibroins but not between them, for example the conserved codon pattern for the poly(alanine) block of adf-3 is AB3321, (where A is usually 2 and B is usually 2 or 3), while the poly(alanine) block for adf-4 is usually A3332133 (where A is usually 1 or 4).

adf-1 has the lowest proportion of conserved codon pattern usage and adf-3 is enormously conserved. adf-2 contains a biphasic codon usage pattern which matches the biphasic modular organisation of this protein. Specifically, the lines beginning with residue 1 and 80 have very similar codon usage patterns and those beginning with residues 36 and 115 share similar codon usage patterns.

DISCUSSION

1. Codon usage bias and pattern bias.

The fact that very specific patterns of codon usage exist within 6 of the 7 spider fibroin genes examined suggests that spider fibroin gene structure evolved to govern gene or transcript structure rather than to strictly complement the availability in tRNAs. Because the fibroin genes are highly repetitive, there is an increased likelihood of gene slippage during recombination that could result in polymorphisms detrimental to gene and protein structure. It has previously been demonstrated that the *B. mori* heavy chain fibroin is polymorphic between closely related species but it is not clear if these are based on functional differences or a reflection of the instability of the gene. Specifically conserved codon placements may ensure that gene slippage is minimised by reducing redundancy in recombination sites on sister chromatids. The specific codon usage pattern may otherwise be important to maintain chromatin conformation important for efficient transcription. On the other hand, specific codon usage patterns may determine mRNA secondary structure important for transcript stability or translational efficiency. An mRNA transcript which is stable and not susceptible to the rapid degradation processes common to other RNA messages could enhance fibroin production efficiently simply because more fibroin templates would be continuously available for translation. But Candelas et. al (1988) have presented evidence that the fibroin mRNAs accumulate rapidly and transiently following mechanical or chemical stimulation, indicating that a stable fibroin mRNA is not essential for voluminous silk production. Specific mRNA secondary structure may otherwise be important for rapid and efficient translation. A structure which is too rigid would be unfavourable for most active messages and a specific nucleotide substitution may be avoided. A template with a large amount of strong codon-anticodon pairing (g-c pairs) may also be energetically unfavourable for efficient rapid translation (Mita et al. 1988). Finally, as has been proposed for *B.*

mori translation, I predict that the codon pattern biases determine fibroin mRNA secondary structure which somehow dictates translational pausing; a phenomenon which may be essential for the proper folding and processing of the enormous nascent fibroin chains in the cell. Further experimentation is obviously required to fully elucidate the molecular mechanics which underlie the efficient high volume production of fibroin molecules by silk gland tissues.

If a future industry is to be based on the production of bulk synthetic protein polymers it will need to compete with the already low cost production of synthetic polymers. To do so, efforts will need to be made to enhance transnational efficiency in host micro-organism or plant based expression systems. A detailed understanding of the molecular mechanics of fibroin production used by the orb-weavers may provide clues leading to the development of such expression systems.

BIBLIOGRAPHY

Anderson, S.O. (1970). Amino acid composition of spider silks. *Comp. Biochem. Physiol.* **35**:705-711.

Andrews G.D. and R.L. Dawson. (1988). Ethylene polymers. In: Encyclopedia of Polymer Science and Engineering. Edited by H.F. Mark, N.M. Bikales, C.G. Overbeger, G. Menges and J.I. Kroschwitz. **6**:383-522.

Beckwitt, R. and S. Arcidiacono. (1994). Sequence conservation in the C-terminal region of spider silk proteins (spidroin) from *Nephila clavipes* (Tetragnathidae) and *Araneus bicentenarius* (Araneidae). *The Journal of Biological Chemistry.* **269**: 6661-6663.

Bonthrone, K.M., F. Vollrath, B.K. Hunter and J.K.M. Sanders. (1992). The elasticity of spiders' webs is due to water induced mobility at a molecular level. *Proceedings of the Royal Society of London.* **248**:141-144.

Candelas, G.C., G. Arroyo, C. Carrasco and R. Dompenciel. (1990). Spider silkglands contain a tissue-specific alanine tRNA that accumulates *in vitro* in response to the stimulus for silk protein synthesis. *Developmental Biology.* **140**:215-220.

Candelas, G.C., T. Candelas, A. Ortiz and O. Rodriguez. (1983). Translational pauses during spider fibroin synthesis. *Biochemical and Biophysical Research Communications.* **116**: 1033-1038.

Candelas, G.C. and E. Luciano. (1996). An alanine tRNA gene cluster from *Nephila clavipes. Gene.* **171(2)**:301-302.

Candelas, G.C., A. Ortiz and N. Ortiz. (1988). Features of cell-free translation of a spider fibroin mRNA. *Cell Biol.* **67**:173-176.

Candelas, G.C., A. Ortiz and C. Molina. (1986). The cylindrical or tubilliform glands of *Nephila clavipes. The Journal of experimental zoology.* **237**:281-285.

Cappello J. and K.P. McGrath. (1994). Spinning protein polymeer fibers. In: Silk polymers. Material science and biotechnology. Edited by D. Kaplan, W.W. Adams, B. Farmer and C. Viney. Washington: American Chemical Society. pp. 311-327.

Chomczynski P. and Sacchi. (1986). *Anal. Biochem.* **162**: 156-158.

Cunniff, P.M et al. (1994). Mechanical and thermal properties of dragline silk from the spider *Nephila clavipes. Polymers for Advanced Technologies.* **5**:401-410.

Denny, M.W. (1980). Silks-their properties and functions. In: The mechanical properties of biological materials. Edited by J.F.V. Vincent and J.D. Currey. Society of Experimental Biology, Symposium 34. Cambridge University Press. pp. 245-272.

Denny, M.W. (1976). The physical properties of spider's silk and their role in the design orb-webs. *Journal of Experimental Biology.* **65**:483-506.

Fahnstock, S.R. and L.A. Bedzyk. (1996). Production of synthetic spider dragline silk protein in *Pichia pastoris*. *Appl. Microbiol. Biotechnol.* In press.

Fahnstock, S.R. and S.L. Irwin. (1996). Synthetic spider dragline silk proteins and their production in *Escherichia coli*. *Appl. Micobiol. And Biotechnol.* In press.

Foelix. R.F. (1982). Biology of Spiders. Harvard University Press. 306p.

Fraser, R.D.B. and T.P. MacRae. (1973). Conformation in fibrous proteins and related synthetic polypeptides. Academic press, New York. 628 p.

Gage, P.L. and R.F. Manning. (1975). Determination of the multiplicity of the silk fibroin gene and detection of fibroin gene-related DNA in the genome of *B. mori*. *Journal of Molecular Biology.* **101**:327-348.

Gilman, J.J. (1996). Strength of spider silk. *Science*. **272**:17.

Gosline, J. M., M.E. DeMont and M.W. Denny. (1986). The structure and properties of spider silk. *Endeavour*. **10**:37-43.

Gosline, J.M., M.W. Denny and M.E. DeMont. (1984). Spider silk as rubber. *Nature*. **309**:551-552.

Gosline, J.M., C.C. Pollack, P.A. Guerette, A. Cheng, M.E. DeMont and M.W. Denny. (1993). Elastomeric network models for the frame and viscid silks from the orb web of the spider *Araneus diadematus*. In: Silk polymers. Material science and biotechnology. Edited by D. Kaplan, W.W. Adams, B. Farmer and C. Viney. Washington: American Chemical Society. pp. 328-341.

Guerette, P.A., D.G. Ginzinger, B.H.F. Weber and J.M. Gosline. (1996). Silk properties determined by gland-specific expression of a spider fibroin gene family. *Science*. **272**:112-115.

Hepburn, H.R., H.D. Chandler, and M.R. Davidoff. (1979). Extensomeric properties of insect fibroins: The green lacewing cross β, Honey bee helical and greater waxmoth parallel β conformations. *Insect Biochemistry.* **9**:69-77.

Hinman, M.B. and R.V. Lewis. (1992). Isolation of a clone encoding a second dragline silk fibroin. *The Journal of Biological Chemistry.* **267 no. 27**:19320-19323.

Iizuka, E. (1985). Silk thread: mechanisms of spinning and its mechanical properties. *Journal of applied polymer science:applied polymer symposium.* **41**:173-185.

Jaffe, M. (1988). High modulus polymers. In: Encyclopedia of Polymer Science and Engineering. Edited by H.F. Mark, N.M. Bikales, C.G. Overbeger, G. Menges and J.I. Kroschwitz. 7:699-723.

Kerkham, K., C. Viney, D. Kaplan and S. Lombardi. (1991). Liquid crystallinity of natural silk secretions. *Nature.* **349**:596-598.

Kohler, T. and F. Vollrath. (1995). Thread biomechanics in the two orb-weaving spiders *Araneus diadematus* (Araneae, Araneidae) and *Uloborus walckenaerius* (Araneus, Uloboridae). *The Journal of Experimental Zoology.* **271**:1-17.

Kovoor, J. (1987). Ecophysiology of spiders. Edited by W. Nentwig. Springer Verlag, Berlin. 320 pp.

Kummerlen, J., J.D. van Beek, F. Vollrath, and B.H. Meier. (1996). Local structure in spider dragline silk investigated by two-dimentional spin-diffusion nuclear magnetic resonance. *Macromolecules.* **29**:2920-2928.

Lewis, R.V. (1992). Spider silk: The unraveling of a mystery. *Acc.Chem. Res.* **25**:392-398.

Pauling, L. and R.B. Corey. (1953a). *Proc. Nat. Acad. Sci.* **39**:253-256.

Labeit S. and B. Kolmerer. (1995). Titins: giant proteins in charge of muscle ultrastructure and elasticity. *Science.* **270**:293-296.

Li, S.F.Y., A.J. MacGhie and S.L. Tang. (1994). New internal structure of spider dragline silk revealed by atomic force microscopy. *Biophys. J.* **66**:1209-1212.

Lin, H.F., D.T. Edmonds and F. Vollrath. (1995). Structural engineering of an orb-spider's web.

Lucas, F. and K.M. Rudall. (1968). Extracellular fibrous proteins: the silks. In: Comparative Biochemistry. Edited by M. Florkin and E.H. Stotz, Amterdam Elsevier. pp. 247-272.

Lucas, F. (1964). Spiders and their silk. *Discovery.* **25**:20-26.

Luciano, E., and G. Candelas. (1996). An alanine tRNA gene cluster from *Nephila clavipes. Gene.* **171**:301-302.

MacDonald, M.E. (1993). A novel gene containing a trinucleotide repeat that is expanded and unstable on Huntington's disease chromosomes. *Cell.* **72**:971-983.

Magoshi, J., Y. Magoshi and S. Nakamura. (1994). Mechanism of fiber formation of silkworm. In: *Silk polymers. Material science and biotechnology.* Edited by D. Kaplan, W.W. Adams, B. Farmer and C. Viney. Washington: American Chemical Society. pp. 292-310.

Magoshi, J. (1985). Liquid crystal and fiber formation of silk. *Proceedings of the 7th International Wool Textile Research Conference, Tokyo.* **1**:329-336.

Maniatis T. (1983). *Molecular Cloning a Laboratory Manual.* Cold Spring Harbour, New York. 545 pp.

Marsh, R.E., R.B. Corey and L. Pauling. (1955a). An investigation of the structure of silk fibroin. *Biochimica et Biophysica Acta.* **16**:1-34.

Masters, M.W. (1984). Vibrations in the orbwebs of *Nuctenea sclopetaria. Behavioral Biology and Sociobiology.* **15**:207-215.

Mita, K., S. Ichimura and M. Zama. (1988). Specific codon usage pattern and its implications on the secondary structure of silk fibroin mRNA. *Journal of Molecular Biology.* **203**:917-925.

Nguyen, A.N., A.M.F. Moore and S.A.C. Gould. (1994). High-resolution images of cobweb threads of black widow spider *Lactradectus mactans* by atomic-force microscopy. In: Proc. 52nd Annual Meeting of the Microscopy Society of America. Edited by G.W. Bailey and A.J. Garratt-Reed. San Francisco Press. pp.1056-1057.

Northolt, M.G. and J.J. van Aartsen. (1973). On the crystal and molecular structure of poly-(p-phenylene terephthalamide). *Polymer Letters Edition.* **11**:333-337.

Patthy, L. (1995). *Protein Evolution by Exon Shuffling.* Springer Verlag, Austin Texas U.S.A. 136 pp.

Pollack, C.C. (1993). Mechanical and optical analysis provide a network model for spiral silk from the orb web of the spider *Araneus diadematus.* Masters thesis, University of British Columbia.

Prince, J.T., K.P. McGrath, C.M. DiGirolamo and D.L. Kaplan. (1995). Construction, cloning and expression of synthetic genes encoding spider dragline silk. *Biochemistry.* **34**:10879-10885.

Rich, A. and Crick F.H.C. (1955). *Nature.* **176**:915.

Rosenbloom, J., W.R. Abrams, R. Mecham. (1993). *FASEB.* 7:1208.

Robson, P. et al. (1993). *Journal of Biological Chemistry.* **268**:1440.

Rudall, K.M. and W. Kenchington. (1971). *Annual Review of Entomology.* **16**:73.

Saltman, W.M. (1977). The Stereo Rubbers. John Wiley & Sons, U.S.A. 897p.

Sears, J.K. and N.W. Touchette. (1988). Plasticizers. In: Encyclopedia of Polymer Science and Engineering. Edited by H.F. Mark, N.M. Bikales, C.G. Overbeger, G. Menges and J.I. Kroschwitz. **5**:568-647.

Seldon, P.A.. (1989). Orb-web weaving spiders in the early Cretaceous. *Nature.* **340**:711-713.

Shaeffgen, J.R. (1983). Aramid fibers:structure, properties and applications. In: Biopolymers. Edited by A.G. Walton and J. Blackwell. Academic Press Inc. London. 604p.

Shear, W.A., J.M. Palmer, J.A. Coddington, P.M. Bonamo. (1989). A Devionian spinneret : early evidence of spiders and silk use. *Science.* **246**:479-481.

Simmons, A.H., C.A. Michal and L.W. Jelinski. (1996). Molecular orientation and two-component

nature of the crystalline fraction of spider dragline silk. *Science*. **271**:84-87.

Sprague, K.U., O. Hagenbuchle and M.C. Zuniga. (1977). The nucleotide sequence of two silk gland alanine tRNAs: Implications for fibroin synthesis and for initiator tRNA structure. *Cell*. **11**:561-570.

Susuki, Y., T. Masaaki, S. Takiya *et al.* (1986). Tissue specific transcription enhancement of the fibroin gene characterized by cell free systems. *Proc. Natl. Acad. Sci.* **83**:9522-9526.

Susuki et al. (1991). Purification and characterization of an Enhancer-binding protein of the fibroin gene. *The Journal of Biological Chemistry*. **266**:16942-16947.

Tashiro, Y., M. Takahashi, S. Matsuura and S. Nagata. (1968). Studies on the posterior silk gland of the silkworm, *Bombyx mori. The Journal of Cell Biology*. **38**:574-588.

Thiel, B.L., K.B. Guess and C. Viney. (1997). Non-periodic Lattice crystals in the hierarchical microstructure of spider (major ampullate) silk. *Biopolymers*. **42**:703-719.

Tillinghast, E.K. and M.A. Towlnley. (1994). Silk glands of Araneid spiders: selected morphological and physiological aspects. In: Silk polymers. Material science and biotechnology. Edited by D. Kaplan, W.W. adams, B. Farmer and C. Viney. Washington: American Chemical Society. pp. 29-44.

Tillinghast, E.K. and M.A. Towlnley. (1986). The independent regulation of protein synthesis in the major ampullate glands of *Araneus cavaticus. J. Insect Physiol.* **32 No. 2**:117-123.

Tillinghast, E.K. and M.A. Townley. (1984). Water extraction by the major ampullate duct during silk formation in the spider *Argiope aurantia. J. insect physiol.* **30**:591-596.

Townley, M.A., D.T. Bernstein, K.S. Gallagher and E.K. Tillinghast. Comparative study of orb web hygroscopicity and adhesive spiral composition in three Araneid spiders. *The Journal of Experimental Zoology*. **259**: 154-165.

Treloar, L.R.G. (1975). The physics of rubber elasticity. Oxford University Press, Oxford. pp. 1-303.

Tsujimoto, Y. and Y. Susuki. (1979). The DNA sequence of *Bombyx mori* fibroin gene including the 5' flanking, mRNA coding, entire intervening and fibroin protein coding regions. *Cell*. **18**:591-600.

Tsujimoto, Y., S. Hirose, M. Tsuda and Y. Suzuki. (1981). Promoter sequence of fibroin gene assigned by *in vitro* transcription system. *Proceeding of the National Academy of Science*. **78 No. 8**:4838-4842.

Vincent, J. (1982). *Structural Biomaterials*. Princeton University Press, Princeton New Jersey. 204 pp.

Vollrath, F. and D. Edmonds. (1989). Modulation of normal spider silk by coating with water.

Nature **340**:305-307.

Vollrath, F., W.J. Fairbrother, R.J.P. Williams *et al.* (1990). Compounds in the droplets of the orb spider's viscid spiral. *Nature* **345**: 526-528.

Vollrath, F., T. Holtet, H.C. Thogersen and S. Frische. (1996). Structural organization of spider silk. *Proceedings of the Royal Academy of Sciences London B.* **298**:147-151.

Vollrath, F. (1992). Spider webs and silks. *Scientific American.* **266** :70-76.

Vollrath, F. (1994). General properties of some spider silks. In: Silk polymers. Material science and biotechnology. Edited by D. Kaplan, W.W. Adams, B. Farmer and C. Viney. Washington: American Chemical Society. pp. 17-28.

Vollrath, F. and E.K. Tillinghast. (1991). Glycoprotein glue beneath a spider web's aqueous coat. *Naturwissenschaften.* **78**:557-559.

Wainright, S. A., W. D. Biggs, J.D. Currey and J.M. Gosline. (1976). Mechanical Design in Organisms. Edited by Edward Arnold Ltd, London. 423p.

Warwicker, J.O. (1960a). Comparative studies of fibroins II. The crystal structure of various fibroins. *Journal of Molecular Biology.* **2**:350-362.

Willcox, P.J., S.P. Gido, W. Muller, D.L. Kaplan. (1996). Evidence of a cholesteric liquid crystalline phase in natural silk spinning processes. *Macromolecules.* **29**:5106-5110.

Kummerlen J., J.D. van Beek, F. Vollrath and B.H. Meier. (1996). Local structure in spider dragline silk investigated by two-dimentional spin diffusion nuclear magnetic resonance. **29**:2920-2928.

Work, R.W. and P.D. Emerson. (1982). An apparatus and technique for the forcible silking of spiders. *J. Arachnol.* **10**:1-10.

Work, R.W. (1977). Dimensions, birefringence, and force-elongation behaviour of major and minor ampullate silk fibers from orb-web-spinning spiders- the effects of wetting on these properties. *Textile Research Journal.* **47**:650-662.

Work, R.W. and N. Morosoff. (1982). A physico-chemical study of the supercontraction of spider major ampullate fibers. *Textile research journal.* **59**:349-356.

Work, R.W. (1984). Duality in major ampullate silk and precursive material from orb-web building spiders (Araneae). *Trans. Am. Micros. Soc.* **103**:113-121.

Xu, M. and R.V. Lewis. (1990). Structure of a protein superfiber: Spider dragline silk. *Proc. Natl. Acad. Sci.* **87**:7120-7124.

Zimmerman R. (1988). Polyamides. In: Encyclopedia of Polymer Science and Engineering. Edited

by H.F. Mark, N.M. Bikales, C.G. Overbeger, G. Menges and J.I. Kroschwitz. **11**:315-381.